ARL 75-0224

12

Aerospace Research Laboratories

THRUST AUGMENTING EJECTORS

Hermann Viets

Energy Conversion Research Laboratory (LE)

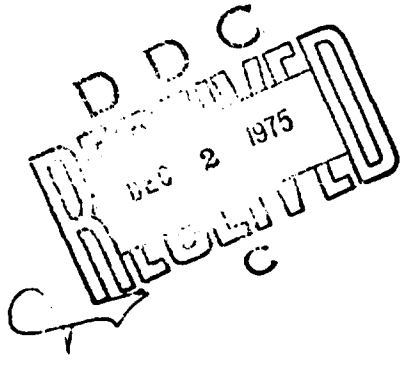

JUNE 1975

AIR FORCE SYSTEMS COMMAND
United States Air Force

147

UNCLASSIFIED

SECURITY CLASSIFICATION OF THIS PAGE *(When Data Entered)*

REPORT DOCUMENTATION PAGE

READ INSTRUCTIONS BEFORE COMPLETING FORM

1. REPORT NUMBER: ARL-75-0224	2. GOVT ACCESSION NO.
3. RECIPIENT'S CATALOG NUMBER	
4. TITLE *(and Subtitle)*: THRUST AUGMENTING EJECTORS	5. TYPE OF REPORT & PERIOD COVERED: Technical Interim Jan 75 – Jun 75
	6. PERFORMING ORG. REPORT NUMBER
7. AUTHOR(s): HERMANN/VIETS	8. CONTRACT OR GRANT NUMBER(s)
9. PERFORMING ORGANIZATION NAME AND ADDRESS: Energy Conversion Research Laboratory (LE), Aerospace Research Laboratories (AFSC), Wright-Patterson AF Base, Ohio 45433	10. PROGRAM ELEMENT, PROJECT, TASK AREA & WORK UNIT NUMBERS: AF-7116-03-06
11. CONTROLLING OFFICE NAME AND ADDRESS: 7116	12. REPORT DATE: June 1975
	13. NUMBER OF PAGES: 108
14. MONITORING AGENCY NAME & ADDRESS *(if different from Controlling Office)*	15. SECURITY CLASS. *(of this report)*: Unclassified
	15a. DECLASSIFICATION DOWNGRADING SCHEDULE

16. DISTRIBUTION STATEMENT *(of this Report)*

Approved for public release; distribution unlimited.

17. DISTRIBUTION STATEMENT *(of the abstract entered in Block 20, if different from Report)*

18. SUPPLEMENTARY NOTES

19. KEY WORDS *(Continue on reverse side if necessary and identify by block number)*

thrust augmentors
ejectors
jets
unsteady flow
aircraft
V/STOL

20. ABSTRACT *(Continue on reverse side if necessary and identify by block number)*

An overview of ejectors as thrust augmentors is presented including the motivation for and operation of thrust augmenting ejectors. Background studies involving jet mixing and diffusion studies are included as well as the state of the art in unsteady jet interactions. Examples of V/STOL aircraft designs incorporating thrust augmenting ejectors are shown and their advantages discussed.

DD FORM 1 JAN 73 1473 EDITION OF 1 NOV 65 IS OBSOLETE

UNCLASSIFIED

SECURITY CLASSIFICATION OF THIS PAGE *(When Data Entered)*

THRUST AUGMENTING EJECTORS

Hermann Viets

Energy Conversion Research Laboratory

JUNE 1975

Aerospace Research Laboratories
Air Force Systems Command
United States Air Force
Wright-Patterson Air Force Base, Ohio 45433

PREFACE

The following notes are an attempt to cover a substantial and very rapidly growing field of knowledge in a rather limited space. Therefore, the required reductions in the amount of material to be presented have been made. The presentation is aimed primarily at a physical view of thrust augmentors and the included analyses are designed to strengthen that view and provide basic design insights. For more analytical material, the reader is referred to the notes of two previous lecture series on ejectors held at the von Karman Institute in 1968-69 as well as the other references noted.

The material presented here relies heavily on the experience of those individuals directly involved in the thrust augmentation program at the Aerospace Research Laboratories, Wright-Patterson Air Force Base, Ohio. Many of the basic concepts involved in augmentors as described here are due to Dr. Hans J. P. von Ohain, Chief Scientist of ARL. The major successes of the program were attained while Dr. Brian Quinn was in the position of Group Leader of this effort. Captain Paul Bevilaqua, Lt Thomas Rosfjord and Mr. Howard Toms are present members of the research group and have made important contributions to these notes. Other significant accomplishments were due to the former Group Leader, Captain W. [illegible] Campbell, and former members Captain Richard Fancher, Mr. Charles Eastlake II, and Captains David Campbell, Gary Johnson and Roy Stern.

TABLE OF CONTENTS

LIST OF FIGURES

I. Ejectors as Thrust Augmentors[1-6]

A. Operation of a Thrust Augmenting Ejector

The basic purpose of a thrust augmenting ejector is the transfer of energy from a high velocity, low mass flow stream to a lower velocity, high mass flow exhaust. As a consequence of this process the momentum flux exiting the ejector is greater than that produced by the primary nozzle and therefore the thrust of the primary nozzle system is increased or augmented.

The basic operation of an ejector as a thrust augmentor may be described by reference to Figure 1. In general, the ejector consists of a primary nozzle injection system which is mounted in the inlet region of a shroud. The arrangement of the primary nozzles varies in particular designs and may resemble the centerbody injector shown in the schematic, a Coanda jet type of injection system on the walls of the inlet or various combinations and permutations of the two.

In general, air from a high stagnation pressure source is expelled from the primary nozzle system into the shroud. Due to viscous mixing about the periphery of the jet, air is entrained into the jet from the surrounding fluid. The entrained air is replaced by air from further upstream in the inlet of the shroud and consequently a steady motion is set up in the secondary as indicated by V_1 in the figure. This fluid enters through the inlet of the shroud, mixes with the jet in the mixing region of length L_m and the mixed flow may be diffused as indicated.

The secondary air is entrained into the ejector from the ambient external condition and thus has a stagnation pressure equal to the ambient pressure. Since the flow of the secondary air is isentropic until the air is actually entrained into the primary jet flow, the Bernoulli equation

applies and indicates that the static pressure at station 1 is reduced below the ambient pressure by an amount equal to $1/2\ \rho\ V_1^2$.

That the thrust produced by an ejector device is equal to the efflux of momentum from it may be seen from the control surface illustration in Figure 2. Sides 1, 2, and 3 of the control surface are allowed to recede to an infinite distance from the ejector device while side 4 remains coincident with the exit plane of the ejector. As the three sides move farther away from the ejector, their length increases linearly with the distance from the ejector h. When viewed from far away, the inflow into the inlet of the ejector appears as a sink flow and the velocity distribution induced by such a flow decays with distance from the inlet as $\frac{1}{h}$.

Now the force on the control surface is equal to the net outflow of momentum and so

$$T_A = \lim_{\substack{h_1 \to \infty \\ h_2 \to -\infty \\ h_3 \to -\infty}} \int_{① + ② + ③ + ④} \rho u^2 \, dA \qquad \text{(I.A.1)}$$

$$= \lim_{h \to \infty} \int_{① + ② + ③} \rho \left(\frac{K_1}{h}\right)^2 d(K_2 h) + \int_{A_2} \rho V_2^2 \, dA$$

$$= \rho V_2^2 A_2$$

Therefore, the entrained inlet flow need not be taken into account in the determination of the thrust produced by an ejector.

Now in order to develop some insight into the important parameters involved in the optimization of thrust augmenting ejectors, the following

simplified analysis is proposed. Consider the diffuserless ejector illustrated in Figure 3. The velocity profile at position 1 at the primary nozzle exit has been idealized as a top hat profile, the walls are assumed inviscid; the flow at the ejector exit, position 2, is assumed to be fully mixed; i.e., the velocity profile is flat and the primary nozzle is assumed to have no losses.

Applying the conservation of momentum between positions 1 and 2:

$$p_1 (A_0 + A_1) + \rho \int_{①} v^2 dA = p_a A_2 + \rho \int_{②} v^2 dA \qquad (1.A.2)$$

Evaluating the integrals and solving for the velocity integral at position 2

$$\rho V_2^2 A_2 = \rho V_0^2 A_0 + \rho V_1^2 A_1 - (p_a - p_1) A_1 \qquad (1.A.3)$$

The flow in the inlet is defined to be isentropic so the Bernoulli equation holds

$$p_a - p_1 = \frac{1}{2} \rho V_1^2 \qquad (1.A.4)$$

The flow in the nozzle incurs losses due to viscosity defined by a nozzle efficiency η_N and

$$P_T - p_1 = \frac{1}{2} \rho V_N^2 = \frac{1}{2} \frac{1}{\eta_N} \rho V_0^2 \qquad (1.A.5)$$

then

$$\rho V_2^2 A_2 = \rho \eta_N V_N^2 A_0 + \rho V_1^2 A_1 - \frac{1}{2} \rho V_1^2 (A_1 + A_0)$$

$$= \rho \eta_N V_N^2 A_0 + \frac{1}{2} \rho V_1^2 (A_1 - A_0) \qquad (1.A.6)$$

where $\rho V_2^2 A_2$ is the thrust produced by the ejector configuration while $\rho \eta_N V_N^2 A_o$ is the thrust produced by the primary nozzle alone, operating in the reduced pressure environment within the ejector. The ratio of these two forces is one possible definition of thrust augmentation.

Another definition of thrust augmentation is the ratio of the thrust produced by the ejector device to the thrust developed by the same primary nozzle system, without a shroud, exhausting to ambient conditions. For the primary configuration nozzle alone, exhausting to ambient (with an efficiency η_N)

$$P_T - p_a = \frac{1}{\eta_N} \frac{1}{2} \rho V_o'^2 = \frac{1}{2} \rho V_N'^2 \qquad \text{(I.A.7)}$$

while the same nozzle configuration operating within the ejector shroud has been defined by Eq. (I.A.5).

Subtracting (I.A.7) from (I.A.5) and combining with (I.A.4),

$$V_N^2 - V_N'^2 = V_1^2 \qquad \text{(I.A.8)}$$

Then Eq. (I.A.6) may be rewritten

$$\rho V_2^2 A_2 = \rho \eta_N V_N'^2 A_o + \rho V_1^2 \left[A_o \left(\eta_N - \frac{1}{2} \right) + \frac{A_1}{2} \right] \qquad \text{(I.A.9)}$$

or

$$\frac{T_A}{T_N} = 1 + \left(\frac{V_1}{V_N'} \right)^2 \left[1 + \frac{1}{\eta_N} \frac{1}{2} \left(\frac{A_1}{A_o} - 1 \right) \right] \qquad \text{(I.A.10)}$$

where T_A is the augmentor thrust while T_N is the thrust of the nozzle configurations without the shroud. Even from this simple analysis, several trends are indicated. The inlet area ratio A_1/A_o should be maximized. This is also true of the entrained velocity, which can be improved to a significant degree by the use of a diffuser as indicated in Figure 1.

There is, however, a disturbing implication in Eq. (I.A.10) and that is the indication that the thrust ratio is inversely proportional to the primary nozzle efficiency. This is not very intuitively appealing and points out one problem with this definition, the fact that the denominator T_N is also dependent upon the nozzle efficiency. Therefore, as η_N decreases, T_N decreases and the thrust ratio by this definition increases although the actual augmentor thrust output has decreased.

An additional problem with the thrust definition in Eq. (I.A.10) is especially important in mass and energy limited systems such as aircraft. If the stagnation pressure available to the primary nozzle system is held constant and the comparison made between the thrust produced by the nozzle system flowing into the ambient and the same nozzle mounted in an ejector, the nozzles within the ejector shroud experience a lower static pressure at their exit and hence pass more mass flow (and energy) than the nozzles exhausting to ambient, for the subsonic nozzle flow considered here.

A definition which overcomes these objections and which will be used exclusively in the remainder of these notes is

$$\Phi = \frac{\text{Thrust produced by ejector device}}{\text{Calculated thrust due to an isentropic expansion of the same mass flow rate to ambient conditions}}$$

$$= \frac{T_A}{(\rho V_N) V_N'} \qquad \text{(I.A.11)}$$

The definition compares the thrust obtained to the total thrust available from the same mass flow.

The following sections will discuss the reasons behind the pursuit of ejector performance and the type of ejectors of interest and will in turn be followed by a more detailed analysis of ejector flow fields.

B. An Ejector Analogy *

In order to clarify the basic operation of the thrust augmenting ejector, consider the analogy of the inelastic collision of two railroad cars shown in Figure 4. Two cars of mass M_0 and M_1 with velocities V_0 and V_1 respectively, collide inelastically so that the result is a combined mass of $(M_0 + M_1)$ moving at a velocity V_2. The governing equations are:

$$M_0 + M_1 = M_2 \tag{I.B.1}$$

$$M_0 V_0 + M_1 V_1 = M_2 V_2 \tag{I.B.2}$$

$$\frac{1}{2} M_0 V_0^2 + \frac{1}{2} M_1 V_1^2 = H + \frac{1}{2} M_2 V_2^2 \tag{I.B.3}$$

where H is the amount of energy dissipated to heat during the inelastic collision process. The dissipation H is required since the only way the three equations can be simultaneously satisfied with H = 0 (i.e. no impact loss) is in the trivial case $V_0 = V_1 = V_2$. Therefore, even in cases where there are no other losses, the impact loss is inescapable.

*Suggested by H.J.P. von Ohain

Now consider the inelastic collision to take place after both cars have been accelerated down an incline as illustrated in Figure 5. The impact takes place at a lower elevation, with both cars at higher velocity, and the two cars together are decelerated as they return to the same initial level. Coming down the incline, assuming no resistance to the motion of the cars, the total energy is conserved

$$V_o^2 = V_o'^2 + 2gh$$
$$V_1^2 = V_1'^2 + 2gh \qquad \text{(I.B.4)}$$

Conserving total energy (i.e. no resistance) coming back up the hill,

$$V_3^2 = V_2^2 - 2gh \qquad \text{(I.B.5)}$$

Relating the energy after the collision to that prior to the collision, the ratio is the efficiency of the energy transfer

$$\eta = \frac{\bar{m}^2 + (1-\bar{m})^2\bar{V}^2 + 2\bar{m}(1-\bar{m})\left[(1+S^2)^{1/2}(\bar{V}^2+S^2)^{1/2} - S^2\right]}{\bar{m}^2 + (1-\bar{m})^2\bar{V}^2 + \bar{m}(1-\bar{m})(1+\bar{V}^2)}$$

where $\bar{m} = \frac{M_o}{M_o + M_1}$; $S^2 = \frac{2gh}{V_o'^2}$; $\bar{V} = \frac{V_1'}{V_o'}$ (I.B.6)

It may be seen from Equation (I.B.6) that the efficiency is maximized at unity when the initial velocity ratio $\bar{V}$ is unity. This implies that for unequal initial velocities, the transfer efficiency may be improved by lowering

the depression h, as is verified by the computations in Figure 6, for $\bar{m} = .1$ and various velocity ratios.

Now the ratio of the momentum at position 3 in Figure 5 to that at position 0 is

$$\Phi = \frac{M_3 V_3}{M_0 V_0'} = \frac{V_3}{\bar{m} V_0} \qquad \text{(I.B.7)}$$

but $$\eta = \frac{V_3^2}{\bar{m} V_0^2} \qquad \text{(I.B.8)}$$

so $$\Phi = \frac{1}{\bar{m}} \left[\bar{m} \eta \right]^{1/2} \qquad \text{(I.B.9)}$$

Now for the simplest case of a moving body striking a stationary body ($\bar{V} = 0$) on level ground ($S = 0$), Equations (I.B.6) and (I.B.9) reduce to

$$\eta = \bar{m} \qquad \Phi = \sqrt{\frac{\eta}{\bar{m}}} \qquad \text{(I.B.10)}$$

so the momentum is, of course, conserved. However, if the same collision occurs after the cars have been accelerated down the incline $S = 1$, (one car starting from rest) then

$$\eta = \frac{\bar{m}^2 + 2\bar{m}(1-\bar{m})\left[(1+S^2)^{1/2} S - S^2\right]}{\bar{m}^2 + \bar{m}(1-\bar{m})}$$

The resulting variation in ϕ with the speed ratio S is shown in Figure 7. Thus, it may be seen that the resultant momentum at position 3 is greater than that at 1 and a thrust augmentation has been affected.

The analogy to thrust augmenting ejectors is this: The primary mass flow M_o collides with the secondary mass flow M_1. The efficiency with which this process can be undertaken can be improved if the flows are accelerated so that the velocity difference between them at collision, is minimized. This is precisely the role of the ejector shroud; to lower the static pressure within the mixing region and thereby accelerate the ambient air into the device. Thus the elevation is analogous to the pressure within the ejector, the decrease occurring in the inlet and the increase in the diffuser.

Of course in the real case, there are losses due to friction both for the case of the cars and the ejector. In the case of the colliding masses, the track friction and drag losses make it more difficult for the combined cars, after the collision, to make it back up the hill. If the cars have insufficient energy to reach the top of the diffuser incline, they fall back. This is analogous to diffuser stall where the flow near the wall has insufficient energy to overcome the pressure gradient in the diffuser.

Since the momentum at position 3 is greater than that at 0 , there must be a net force to the left on the earth supporting the track arrangement. This is analogous to that force transmitted to the ejector shroud by the pressure distribution which becomes the useable force on the aircraft.

The relative effect of inlet area ratio may be seen in the mass ratio $\bar{m}$. A small $\bar{m}$ corresponds to a high inlet area ratio and leads, (in the ideal, no loss case) to improved performance. The analogy to the primary nozzle thrust efficiency is the ratio of the velocity of mass M_o at position 0 to it velocity at a position 0' further up the line where the motion originated. The losses

between these positions are analogous to the flow losses within the primary nozzle system.

Thus, in this analogy, the basic mechanism responsible for thrust augmentation may be identified. This is the improved transfer efficiency from the primary to the secondary through the presence of the shroud which accelerates the secondary. However, the optimization of this process in the presence of various loss mechanisms is not straightforward due to the many parametric interactions involved.

C. Motivation for the Study of Thrust Augmenting Ejectors

The potential application to V/STOL aircraft propulsion systems is the overriding motivation for the study of ejectors as thrust augmenters. The advantage of ejectors for such an application is that they offer a mechanism to allow the useable thrust of the aircraft to be increased during take-off and landing and hence allow the propulsion system to be sized for cruise or combat conditions or other considerations[6].

The basic concept for an ejector wing as applied to a vertical take-off aircraft is shown in Figure 8. Three modes of operation are illustrated; VTOL, transition and cruise. The circular ducts shown in the figure serve a dual purpose. They act as the main structural elements of the wing and also serve to bring the primary air from the turbofan engines out to the ejectors mounted in the wings. The primary air is injected into the ejector bays (two in this case) from the circular ducts through a primary nozzle system. In the VTOL case, the ejector efflux is directed toward the ground and the inlet doors on top of the wing are completely open.

When the aircraft has attained sufficient altitude, the ejector efflux is directed rearward and the aircraft begins a transition from hover

to foreward flight. The inlet doors are simultaneously inclined foreward to offer a minimum of resistance to the ambient air being entrained into the ejector bays. Finally, in the cruise mode, the engine air is directed out through a more conventional tailpipe and the ejector wing is closed to resemble a conventional wing cross section.

The conceptual application for ejectors to STOL aircraft is shown in Figure 9. During take off and landing, the ejector flap unfolds near the trailing edge of the wing. The operation of the ejector flap results in high entrainment of air from above the wing. This, in turn, leads to higher velocities on the upper surface of the wing and hence increased lift is generated as well as increased thrust.

For the ejector configurations described above, there are several advantages in addition to the fact that they allow the sizing of the propulsion system to other considerations besides take off and landing. One of these is that there are no moving parts in the ejector. There are, of course, geometric changes which must be undertaken but these are no more involved than the usual flap and slot motions on conventional aircraft. In addition, the ejectors could potentially be used in flight to achieve a superior inflight maneuvering capability. The low downwash velocities produced by the ejector efflux are also advantageous since they reduce the problem of the reingestion of expelled gases and hence debris. This is also reflected in lower temperatures in the ejector efflux as compared to vectored thrust, for example. The temperature footprint is especially important for ship landings and areas of combustible ground cover.

The ejector as applied to aircraft also offers a smooth transition mode between VTOL and cruise flight as illustrated in Figure 8. Many VTOL devices (fan in wing, vectored thrust, helicopter) which incline the thrust vector to achieve foreward flight, experience a decrease in altitude during this

phase because the vertical component of the thrust (or lift in this case) has been decreased. However, since the ejector entrains air from above the wing during this phase, a "supercirculation" results due to the increased velocity on the upper surface and a lift is produced in excess of the expected component of the ejector thrust. This effect can be seen in the experiments of Thornhill[7] and has been discussed by Quinn[1].

Ejector thrust augmentors also offer the potential for reducing the aircraft noise level by the use of acoustic liners on the internal surfaces of the ejector. The reduction in noise level has been investigated by O'Keefe and Kelly[8]. A suppression of radiated noise level was achieved by applying an augmentor as opposed to a slot nozzle while further suppression was achieved by lining the augmentor with a sound absorbing material.

As may be seen above, the ejector has the potential for significant advantages over some other V/STOL devices. However, to achieve that potential two important objectives must be met, high performance and compactness. The latter is especially important for aircraft application since the devices must fit into an aerodynamically smooth exterior. These two objectives are often conflicting and it is the pursuit of their simultaneous attainment which is the subject of most of the following material.

D. Ejector Geometries

The ejector illustrated schematically in Figure 1 is one of several ejector concepts which have been and are being investigated for application as thrust augmentors. The single centerbody design is simple and allows the integration of the ejector into the aircraft design with a minimum complexity. This device has been investigated primarily for application as an ejector flap as illustrated in Figure 9. The inlet area ratios of interest, A_i/A_e,

are generally less than 10 for such a device.

A higher area ratio ejector, investigated primarily at ARL and intended for application to VTOL aircraft is illustrated in Figure 10. In this case the primary air is injected through a family of nozzles of a shape resembling a shark fin and attached to the circular ducts serving as the primary air reservoir. Between the primary nozzles are located root nozzles whose function it is to inject a blanket of high energy air near the walls to overcome the wall friction and thereby avoid separation which is detrimental to ejector performance.

The bulk of the work at ARL has concerned the two ejector designs described briefly above. The majority of the present material will likewise be discussed in relation to these concepts. However, the basic insight into the flow processes involved is a necessary ingredient for any ejector design.

Other ejector concepts have been proposed and some are currently under investigation. One of these, the Coanda ejector[9] was examined theoretically by von Karman[5] and is illustrated in Figure 11. The distinguishing feature of the Coanda ejector is the position of the primary nozzles on the inlet scroll for the ejector. The jets remain attached to the rounded walls by the effect made famous by Coanda. Therefore, by the time the jets reach the injection planes advocated by the designs illustrated in Figures 1 and 10, they are more intimately mixed with the entrained fluid. As will be discussed in the ejector analysis in the following section, the rate of mixing between the primary and entrained flows is a major parameter governing ejector performance because of the overall length constraint imposed by the application to aircraft. A disadvantage to the Coanda approach is that the viscous losses on the walls of the ejector are increased due to the

presence of so much high energy air near the walls. In addition, penetration of the mixing to the centerline of the ejector is difficult. The Coanda ejector has been tested by Scott and the results are discussed in Section I-F. A combination of the centerbody ejector illustrated in Figure 1 and the Coanda ejector of Figure 11 is the device being investigated by the North American Aircraft Division of Rockwell International in Columbus, Ohio[11] and illustrated in Figure 12. This concept intends to take advantage of the increased mixing due to the Coanda jets and yet not suffer the full extent of the wall losses by injecting half of the air through the centerbody nozzle. This concept also improves the mixing, (as opposed to pure Coanda injection), near the centerline of the ejector by placing a primary nozzle in that position. This device will be further discussed in a later section on the aircraft integration of ejector devices.

Ejector devices employing active diffusers have been investigated by Haight and O'Donnell[12] and Alperin[13]. The former concept is shown in Figure 10 and involves the use of a driven trapped vortex to allow more rapid diffusion of the flow. Separation is postponed until larger diffuser area ratio because the effective diffuser wall is not solid and thus does not have the no-slip boundary condition. The remainder of the ejector system is schematically the same as that illustrated in Figure 10.

The concept investigated by Alperin[13] is shown in Figure 13 and involves the use of a jet near the solid diffuser exit as well as a louvered inlet. The jet is inclined at an angle to the mean streamwise direction. His intention is to take advantage of the pressure difference across the turning jet as it deflects to the mean stream direction and in this way allow the diffusion process to continue downstream of the diffuser walls.

The degree to which such an effect is useful is related to the amount of momentum injected near the end of the solid diffuser wall. If a substantial portion of the primary air is injected at that position, then the ejector is essentially the first step to a staged ejector, from which some improved performance is to be expected.

The improvement of ejector performance through the use of staged ejectors has been demonstrated experimentally by Morrison[14]. The axisymmetric staged ejector geometry used by Morrison is illustrated in Figure 15 alone with a representative experimental result. The conclusion that multistage ejectors offer an advantage over the single stage ejector has also been reached analytically by Nagaraja et al[15] and the computed results are shown in Figure 16. The potential offered by staging is indeed promising but experimental efforts in this direction are in a stage of relative infancy.

In addition to the ejector performance advantages to be gained from staging, a reduction of the duct losses could also be achieved. This could be accomplished by greatly increasing the pressure in the supply ducts carrying the primary air from the engine to the wing mounted ejectors. In this way, the flow velocity in these ducts is reduced and the duct losses correspondingly decreased. The first stage of the thrust augmentor then operates primarily as a mass augmentor. Such a system however requires some engine development work since a high pressure, high bypass ratio engine is not currently available.

Because of the potential for a superior mixing rate between the primary and secondary streams, ejectors maintaining an unsteady flow are of great interest. A recent paper by Binder and Favre-Marinet[16] has

demonstrated the increased performance of an unsteady primary nozzle. The unsteady component in the primary flow was introduced by a spinning butterfly valve. Other methods of introducing the unsteadiness into the flow are being investigated. A spinning primary nozzle which introduced an unsteady component was investigated by Foa[17]. More recently, a fluidically controlled unsteady nozzle with no moving parts was developed by Viets[18]. In addition, an acoustic interaction phenomenon between the screech tones emitted by a choked jet and the ejector geometry is currently the subject of an ongoing investigation[19, 20]. The subject of unsteady ejector flows will be treated more explicitly in Section III.

E. Ejector Analysis Including Losses

In order to identify those areas of ejector technology which are most likely to yield the maximum return (in terms of performance) when subjected to intense investigation, the following ejector analysis including loss mechanisms was performed by Quinn[4]. The analysis is based in principle upon the original von Karman[5] analysis of ejector performance.

Consider the ejector illustrated in Figure 1. Without the assumptions employed in the simplified analysis of Section IA, the continuity and momentum equations may be written as

$$\int \rho v \, dA_3 + \int \rho v \, dA_1 = \int \rho v \, dA_2 = \int \rho v \, dA_2 \tag{I.E.1}$$

$$\int (p + \rho v^2) \, dA_3 + \int (p + \rho v^2) \, dA_1 = f + \int (p + \rho v^2) \, dA_2 \tag{I.E.2}$$

where f is the streamwise component of the total skin friction force exerted by the ejector walls upon the fluid.

The velocity distributions across any of the streamwise stations are, in general, non-uniform. This non-uniformity may be lumped into a single parameter by the defintion of β_i;

$$\beta_i = \frac{\int \rho v^2 dA_i}{\frac{1}{A_i}\left[\int \rho v\, dA_i\right]^2} = \frac{\int \rho v^2 dA_i}{\rho V_i^2 A_i} \qquad \text{(I.E.3)}$$

$$= \frac{\text{Momentum Flux through } A_i}{\begin{array}{l}\text{Momentum Flux Due to a}\\ \text{Uniform Mass Average}\\ \text{Velocity Profile}\end{array}}$$

At the inlet position, the integration is over A_o and A_1.

Here V_i is the mass average velocity through area A_i. The skewness parameter β is an indication of the deviation of the velocity profile from an idealized uniform velocity. As the profile deviates further from the uniform velocity case, β increases from unity.

In addition, the friction force term may be written as

$$f = \xi_f \rho_2 \beta_2 V_2^2 A_2 \qquad \text{(I.E.4)}$$

where

$$\xi_f = \frac{1}{2} C_f \left(V_{ref}/V_2\right)^2 A_{ref}/A_2 \qquad \text{(I.E.5)}$$

For the type of ejector geometry shown in Figure 1, ξ_f would be rather small but for other types of ejectors, such as the Coanda ejector, the wall friction losses can become significant.

In order to keep the present analysis relatively simple, the pressure is assumed constant across any streamwise position and the fluid is assumed incompressible. These have been shown to be very realistic assumptions by the experiments described in later sections.

Besides the frictional losses on the internal walls of the ejector, there are several other loss mechanisms which detract from overall ejector performance. These include the loss, ξ_1, sustained by the entrained flow passing through the inlet. If the inlet had no losses, Bernoulli's equation would be sufficient to relate the external conditions to the entrained velocity. However, the inlet loss results in a modified Bernoulli relation:

$$P_1 = P_{T_\infty} - \frac{\rho}{2} V_1^2 (1 + \xi_1) \qquad \text{(I.E.5)}$$

The entrained flow is irrotational except in the limited regions which have been affected by the boundary layers on the inlet walls. Thus the entrained velocity is essentially uniform and a possible β_1 term in Eq. I.E.6 is treated as unity.

If the ejector configuration has a diffuser attached, then a loss due to the imperfect operation of the diffuser must be included. This may be accomplished by the use of the diffuser pressure coefficient

$$C_p = \frac{P_3 - P_2}{\frac{\rho}{2} \beta_2 V_2^2} \qquad \text{(I.E.7)}$$

where P_3 is the static pressure at the exit.

If the loss mechanisms described above are incorporated into the governing equations I.E.1 and 2, they may be manipulated into a

quadratic equation for the entrained to primary velocity ratio

$$\left(\frac{V}{V_1}\right)^2\left[2\frac{A_1}{A_0}\frac{A_2}{A_0}-(1+\xi_1)\left(\frac{A_2}{A_0}\right)^2-q\left(\frac{A_1}{A_0}\right)^2\right]$$

$$-2q\frac{A_1}{A_0}\frac{V_1}{V_0}+\left[2\beta_0\frac{A_2}{A_0}-q\right]=0 \qquad \text{(I.E.8)}$$

where the losses downstream of the injection plane have been lumped into the parameter q defined by

$$q=\beta_2\left[2\xi_f+2-C_p\right] \qquad \text{(I.E.9)}$$

Now consider a situation with perfect mixing, $\beta_2 = 1.0$, frictionless ejector walls, $\xi_f = 0$ and a perfect diffuser $C_p = 1 - \frac{A_2}{A_3}$. Then the function q is minimized and equal to

$$q_{IDEAL} = 1+\left(\frac{A_2}{A_3}\right)^2 \qquad \text{(I.E.10)}$$

Then for convenience

$$q = q_{IDEAL}\left(1+\frac{\Delta q}{q_{IDEAL}}\right) \qquad \text{(I.E.11)}$$

The fact that it is desirable to minimize the value of q in Eq. I.E.9 leads to some interesting, if not surprising, insight. The wall friction loss term ξ_f may be reduced by building the ejector as short and compact as possible.

However, a very short ejector makes it difficult to obtain a reasonably low value of β_2 because the mixing between the primary and secondary streams is not rapid enough. This trade-off between the conflicting objectives of compactness and complete mixing is one of the basic problems in ejector design. An additional complication is that any attempt to increase the mixing rate of the primary jet leads to either an increased inlet loss (i.e., perhaps by using more primary nozzles) or a reduced primary nozzle thrust efficiency (which will be considered in more detail) or both. Relatively straightforward is the meassage from Eq. I.E.9 to maximize the diffuser performance and hence maximize C_p.

Now to allow a numerical comparison of the loss terms, consider the thrust augmentation ratio as defined in Eq. I.A.11:

$$\Phi = \frac{\int \rho v^2 dA_3}{V_N' \int \rho v dA_o} = \frac{\beta_3 V_3^2 A_3}{V_N' V_o A_o} \qquad \text{(I.E.12)}$$

Now V_N^i is the velocity obtainable by a perfect expansion of the primary flow from its stagnation pressure P_{T_j} to the ambient conditions P_a so

$$P_{T_j} = P_{T_\infty} + \frac{\rho}{2} V_N'^2 \qquad \text{(I.E.13)}$$

Now solving for the ambient pressure from I.E.6 and combining:

$$P_{T_j} = p_1 + \frac{\rho}{2} V_1^2 (1 + \xi_1) + \frac{\rho}{2} V_N'^2 \qquad \text{(I.E.14)}$$

Now the primary thrust efficiency is the ratio of the thrust produced to the thrust available from the isentropic expansion across the same pressure difference, i.e.,

$$\eta_N = \frac{\frac{1}{2}\rho V_o^2}{P_{T_j} - P_1} = \frac{V_o^2}{V_1^2(1+\xi_1) + V_N'^2} \qquad \text{(I.E.15)}$$

Substituting into Eq. I.E.12 for V_N' and eliminating $V_3^2 A_3$ by continuity

$$\Phi = \beta_3 \frac{A_o}{A_3}\left(1 + \frac{A_1 V_1}{A_o V_o}\right)^2\left[\frac{1}{\eta_N} - (1+\xi_1)\left(\frac{V_1}{V_o}\right)^2\right]^{-1/2} \qquad \text{(I.E.16)}$$

Attempting to interpret the importance of various loss components directly from Eq. I.E.16 is a risky proposition since the parameters are still interrelated. However, the numerical solution of Eq. I.E.16 along with I.E.8 yields some interesting results as seen in Figure 17. For a particular ejector of $A_1/A_o = 20$ and $A_3/A_2 = 1.5$, the relative importance of the loss terms is shown. The basic message is that increased losses of one type are acceptable and even desirable if in so doing the loss of another type is reduced.

The degree to which the losses are critical to the ejector performance is shown in Figure 18, where computed thrust augmentation is plotted versus inlet area ratio for three loss combinations; no losses, reasonable and heavy losses. The labeling of the loss combinations as reasonable or heavy is certainly debatable but the conclusion is clear: successful ejectors for V/STOL application must have the losses held to a very tight

minimum since it is obvious from the figure that small percentage changes in the loss mechanisms can greatly affect the performance.

The theoretical performance limits for augmentors with no losses are shown in Figure 19. It is clear that performance increases with inlet area ratio and diffuser area ratio. The calculation assumes perfect (or complete) mixing as well as no losses. Physically, the actual reductions from the performance shown here are due in large part to the fact that the mixing attained in the ejector decreases as the inlet and/or diffuser ratios are increased and that the diffuser performance breaks down completely for larger area ratios as diffuser stalling occurs.

Not let us consider the q loss term in more detail. The q loss as defined by Eq. I.E.9 consists of three parts; skin friction, diffuser efficiency and degree of mixing. Now if an ejecotr configuration is being optimized for an aircraft application, tbe length is generally not very flexible and the diffuser efficiency in terms of area ratio is relatively well known. The optimization is likely to concentrate on the flow structure within the ejector. In particular the mixing rate should be optimized (i.e. β_2 minimized) in relation to the nozzle thrust efficiency η_N. A reduction in η_N is generally the price which must be paid to achieve increased mixing. An analysis which clearly shows the trade-off between nozzle thrust efficiency and performance as related to mixing was performed by Bevilaqua and Toms[21] and is shown in Figure 20. For a diffuser area ratio of 1.5, the results clearly show that taking a five percent loss in nozzle thrust efficiency to obtain a ten percent improvement in mixing at the exit (as measured by β) can lead to an improvement on the order of 25% in thrust augmentation ratio. The calculation is performed holding the remaining losses to zero.

The lower half of Figure 20 illustrates the effect of the above trade-off on the transfer efficiency defined as the ratio of the kinetic energy of the efflux to energy of the primary jet system.

Thus the enhancement of the mixing rate is one of the most important parts of the ejector optimization process, especially for V/STOL application, and will be considered in more detail in Section II.

F. Some Recent Ejector Results

The thrust augmenting ejector effort at the Aerospace Research Laboratories has concentrated on two devices -

- a high inlet area ratio (≃24) ejector to produce the high thrust augmentation values required for VTOL (See Figure 10) and

- a lower inlet area ratio (≃8) ejector to be applied as an ejector flap and to act mainly as a mass augmentor and increase the velocity over the upper wing surface of a STOL aircraft and thereby augment the lift produced and required for rapid conventional take-off.

The high area ratio device is schematically illustrated in Figure 10. The throat width is 10 inches (25.4 cm) while the endwall to endwall distance is 60 inches (1.52 m). A photographic view upstream into half the ejector exit is shown in Figure 21. The primary nozzles extend out from the round supply ducts and meet on the centerline of the device. In this way the primary air is distributed over the ejector cross section. Twelve small nozzles inject primary air on the end walls of the ejector. The design of the individual primary nozzles as well as the root nozzles which supply the boundary layer control air is shown in Figure 22. The primary nozzles are in the shpae of a "shark fin" to minimize the inlet loss to the entrained air which passes over them. The exit shape of the nozzles is cut back on

alternate sides in order to impart an alternately transverse velocity component to the flow, as illustrated in Figure 23. This particular exit shape is called the hypermixing nozzle and is the result of an extensive investigation of nozzle mixing versus efficiency which will be described in Section II. Both the primary nozzles and the root nozzles were injection molded from a Nyafil material.

The various configurations tested are indicated in Table 1, where L_m and L_D are the lengths of the mixing duct and the diffuser, respectively, as shown in the schematic of Figure 7, and W is the width of the mixing duct.

The highest values of thrust augmentation obtained to date with this device are shown in Figure 24 and correspond to configuration F from Table 1. The lower set of thrust augmentation values have been obtained with a much shorter diffuser and hence a shorter overall ejector. The reduction in performance can be attributed to the reduced degree of mixing achieved in the shorter ejector. This is evident in the fact that the velocity profiles at the exit of the shorter ejector are more highly skewed (or non-uniform) than in the case of the longer ejector. The difference in performance of these two cases illustrates the importance of complete mixing to the ejector process because the longer ejector requires that one accept an increase in wall friction losses (and hence in Δq) and yet the performance is improved.

The effect of the length of the mixing duct, L_M, on overall performance is shown in Figure 25. The comparison is for configurations D and F of Table 1, which are of equal overall length. It is clear from the data that a long mixing duct is not as important as a more gradual diffusion process. This is a somewhat unexpected result since it is a generally accepted fact that diffusion tends to accentuate the non-uniformites or skewness of a flow.

Evidently, there is a very significant amount of mixing occurring within the diffuser of the present ejector geometry. This effect is related to the sense of the diffusion relative to the skewness and will be discussed in detail in Section II. Unfortunately, the mechanics of the experimental device made it impossible to further shorten the mixing duct.

The optimization of the primary nozzle depends not only on the mixing rate of the jet produced, but also on the ejector geometry itself. Once the flow is fully mixed at any streamwise position within the ejector, any additional ejector length only contributes to skin friction and does not enhance performance but rather detracts from it.

Recent experiments by Bevilaqua[22], on the same apparatus described above, indicate the importance of designing the primary nozzles with regard to their application. By doubling the aspect ratio of the individual elements on the hypermixing nozzles (see Figures 22 and 23) from those of the previous tests, the thrust augmentation ratio obtained was held practically constant while the total length of the mixing and diffuser sections was more than halved as shown in Figure 26. The single low thrust augmentation value at a diffuser areas ratio of 2.1 was purposely produced by placing a small roughness element .025" (0.64 cm) wide and 0.50" (1.27 cm) high on the sidewall downstream of the primary jet injection plane. The sensitivity of the thrust augmentation to a small disturbance in the flowfield is apparent.

To insure a sufficient amount of boundary layer control, primary air is placed on the sidewalls by root nozzles of the kind illustrated in Figure 22 and on the endwalls by the twelve nozzle spray system shown in the lower part of Figure 21. Not only is it important to have the boundary layer blowing, but it must be accomplished in the proper manner as may be

seen in Figure 27. Not surprisingly, the poorest performance was obtained without endwall blowing. If a single nozzle using 9.1% of the primary mass flow is employed, the performance rises. However, using the 12 segment nozzle (Figure 21) to more successfully distribute the flow, the percentage of mass flow used for endwall blowing can be reduced to 4.7% and still the performance is increased dramatically.

The highest augmentation values achieved by Quinn[1,3,4] have been independently verified by Haight and O'Donnell[12]. In fact, Quinn's values appear to be conservative, being exceeded by 2-7% in Reference 12. This difference is attributed "to small design changes in inlet shape and differences in external laboratory flow constraints (walls, ceiling, etc.)". Haight and O'Donnell[12] are basically concerned with a reduction in the diffuser length by employing the trapped vortex diffuser, as illustrated in Figure 13. The basis of this device is the fact that the diffuser wall is replaced by the dividing streamline between the vortex and the diffuser flow. The vortex is driven by injection at the upstream lip and hence the separating boundary layer at that point is energized. In addition, boundary layer separation (and hence stall) can be avoided in principle, since there is a fluid (instead of solid) interface. The experimental results employing the vortex diffuser show a dependence of thrust augmentation on primary jet stagnation pressure that did not exist in the solid wall diffuser case. Reductions of pressure average peak thrust augmentation ratios to 1.91 and 1.88 were experienced with respective reductions in total length of 21 and 44%. The concept appears to require more optimization to make it a viable diffusion candidate.

The low area ratio ejector, shown schematically in Figure 1 was tested by Fancher[23] including the hypermixing nozzles mentioned above and described in more detail in Section II. A cutaway of the ejector on the test stand is illustrated in Figure 28. The maximum measured performance for an inlet area ratio (A_1/A_o) of 8.6 was ϕ = 1.35. A small increase in this value of thrust augmentation was reported by Bevilaqua and Toms[21, 24] by the use of higher aspect ratio individual elements in the hypermixing nozzles and subsequent improved mixing.

II. Mixing Studies

A. Parameters Affecting Jet Mixing

The importance of the rate of mixing between the primary and secondary streams on the overall ejector performance has been pointed out in Section I. A dramatic quantitative estimate of this effect has been made by Quinn[1,25] and is shown in Figure 29. Doubling the assumed mixing rate leads to very substantial improvements in thrust augmentation, especially for the short (length/width) ejectors of interest for aircraft application. Therefore, various methods of increasing the mixing rate of a primary jet have been attempted and some of these are presented below. Of course, the enhanced mixing rate must be achieved at the cost of reduced nozzle thrust efficiency and therefore a trade-off between these effects must be negotiated. In addition, several other mixing problems arise in application including three dimensional effects, and the concurrent processes of diffusion and turning. The results discussed here are all steady state. The time dependent methods are delayed until the following section.

A study of several methods which directly affect jet mixing rates was performed by Fejer et al[26,27,28] at the Illinois Institute of Technology. This study included the mixing effects due to

a. A disturbance at the interface between the primary and secondary flows to produce turbulence.

b. A density difference between the jet and secondary flows.

c. The addition of a gross swirl component to the primary flow.

The turbulence production at the flow interface was accomplished by mounting a ring of spheres around the outside of the primary jet nozzle at the exit plane. In this way, the turbulence increase is in the secondary flow and one

might expect that the effect on the mixing process is proportional to the secondary flow velocity. This is indeed the case as may be seen in Figure 30. The effect on both velocity decay and the concentration decay of the argon tracer gas in the primary flow is significant for secondary streams of 200 ft/sec (60.96 m/sec). However, the effect is slight for a secondary stream of half that velocity. Of course, the disturbance could be applied to the primary stream instead and the mixing rate further enhanced. However the losses involved in such a procedure would increase accordingly. Since the ejector is very sensitive to primary nozzle losses any disturbance of the flow interface must be viewed with a critical eye.

The effect of a density difference between the primary and secondary flows has been studied by various investigators[29-34]. The basic conclusion is that as the density of the primary decreases relative to the secondary, the velocity decay (or mixing) rate increases. This is true whether the density difference is due to composition and/or temperature differences. Thus, it would appear that a low density primary (perhaps hot engine air) would be desirable for thrust augmenting ejector applications to aircraft. However, passing the same mass flow in the lower density case requires higher primary velocities which in turn yield lower transfer efficiencies. The advantages (if any) of a lower density primary therefore depend upon the ejector configuration and constitute another design tradeoff.

For very short ejector configurations, the effective increase in viscosity due to higher temperature primaries may offset the reduced transfer efficiency. This is a basic result of an axisymmetric heated ejector study by Quinn and Toms[19]. For the relatively long ejector (L/D = 10.18) shown in Figure 31, the effect of primary temperature on the ratio of entrained

to primary mass flow (reduced by the temperature ratio) is significant. Since the eiector is so long anyway, the flows are relatively well mixed, even in the cold jet case, so a mixing improvement provides no increase in performance. To the contrary, the increased wall losses cause the performance to suffer. However, for a short ejector configuration (L/D = 4.36, Figure D) the elevated primary temperature produces an increase in mixing rate which compensates for the reduced transfer efficiency and hence the performance (in terms of entrainment ratio) is not compromised. The change in the shpae of the curves will be discussed in the following section on unsteady effects.

The significant mixing advantages to be gained by the introduction of a swirl component into the jet flow may be seen in the experimental results of Rose[35] in Figure 33. In this case, the swirl is produced by a rotating pipe, although there are alternate methods available including guide vanes upstream of the jet exit. Again the problem arises of the cost in performance required to produce the disturbance in the jet. This led to an investigation of the possibility of producing interactions outside the primary nozzle which will be discussed.

The influence of the state of the boundary layer on the inside of the primary jet is currently being investigated by Hill and Jenkens[36]. Initial results indicate that the state of the boundary layer, laminar, transitional or turbulent, has a significant effect on the jet mixing rate.

B. Three Dimensional Effects

In a series of pioneering papers, Sforza and Trentecoste[37-39] have experimentally clarified the three dimensional structure of jets emanating from orifices of bilaterally symmetric shape. From the point of view of

ejector application, an important result of their experiments is illustrated in Figure 34. Here the half widths in the major and minor axis directions of an aspect ratio ten orifice are plotted versus distance downstream. The half width are a gross indication of the transverse dimensions of the jet since they contain a majority of the jet's momentum within their bounds and are defined as the distance between the jet centerline and the point on the transverse velocity profile where the velocity is equal to the average of the jet centerline velocity and the free stream velocity. For three dimensional jets, the half width furthest from the centerline (i.e. on the short side) initially decreases and then grows while that on the near side of the jet grows monotonically. The importance of this fact may be seen in relation to the schematic of the area ratio 24 ejector discussed in Section I and shown in Figure 10. In order for the primary jet mixing to penetrate to the center of the mixing duct, the high aspect ratio jet must grow rapidly on its short side. However, according to the aforementioned 3-D results, this is not possible. Therefore, Quinn[40] extended the "shark fin" nozzles out to the center of the ejector channel and obtained improved mixing on the ejector centerline which (along with other changes) resulted in substantially improved performance.

An analytical treatment of the flow from a finite aspect ratio nozzle has been produced by Viets[41] for a laminar jet issuing from an elliptical nozzle. The treatment is based on the assumption that the jet isovels are elliptical, a fact observed at a short distance downstream in the turbulent case, even for a rectangular orifice[38]. This fact allows the separation of the three dimensional problem into two 2-D problems, only coupled by the aspect ratio of the elliptical orifices. The results

of a numerical solution of the resulting equations is shown in Figure 35 for an aspect ratio three ellipse and two different coflowing stream ratios. The qualitative agreement with the experimental results of Figure 34 may be seen. In order to obtain a quantitative comparison, an eddy viscosity model applicable to a 3-D flowfield is required.

The above discussion concerns the interaction between a finite aspect ratio jet and the coflowing stream. In most cases, however, there is also an interaction between the primary jet and an ejector wall. This situation has been examined experimentally by Foss and Jones[42] and Eastlake[43]. The latter finds that confining the jet with endwalls (walls aligned with the edges of the jet parallel to the minor axis) results in a decrease of the minor axis half width growth. This is due to the fact that the endwalls prevent entrainment through that side and therefore prevent the decrease in the half width dimension observed by Sforza and Tretacoste[37-39] and predicted by Vites[41]. This forces the jet momentum to fill to the endwalls and hence reduces the momentum available to the minor axis and results in a reduced half width growth there.

Foss and Jones[42] found unexpected secondary flows in the viscinity of the walls of a slot jet bounded as that above. The secondary flow causes a more rapid spreading of the jet near the walls. According to the proposed flow model, the secondary flow is caused by vortex rings which are shed by the jet orifice or nozzle and then deformed by the flow field, being retarded near the walls and blown downstream in the center of the channel. This model is similar to that proposed by Van Der Hegge Zijnen[44] and employed by Sforza and Trentacoste[38] to explain the velocity irregularities found in some jet flows. These irregularities involve situations where the maximum

jet velocity does not appear on the jet centerline as expected but rather appears off center resulting in a saddle-shaped velocity profile. Viets and Sforza[45] have computed the motion of a finite aspect ratio vortex ring and confirmed the calculations with flow visualization experiments. The vortex ring deforms in much the same manner as the jet cross-section (as seen in the half width growths of Figures 34 and 35) and thus lends credibility to the vortex model of jet dynamics. This structure also fits well with the latest model of turbulent entrainment which pictures the flow field as consisting of a large scale eddy structure which is responsible for the majority of the jet entrainment. This model will be discussed further below.

C. Nozzle Studies - Origin of Hypermixing

A comprehensive investigation of the effect of primary nozzle exit geometry in the mixing rate and the nozzle efficiency has been performed by Eastlake[46]. The principle aim of the investigation was to identify nozzle configurations which yielded substantial improvements in spreading rate at a reasonable cost in nozzle velocity efficiency, defined as the ratio of the actual nozzle velocity to the isentropic velocity due to the same nozzle pressure ratio.

Some examples of the types of nozzle geometries tested are shown in the following Figures. The nozzles tested included:

a. Straight cone nozzle - producing a line of axisymmetric jets.

b. Alternating cone nozzle - producing axisymmetric jets alternately inclined at ±10° to the nominal centerline. (See Figure 36)

c. Alternating exit nozzle - alternate segments of a converging slot nozzle cut back to produce rectangular jet elements inclined to the centerline. The

aspect ratio of each element is approximately four. Presently referred to as the hypermixing nozzle (See Figure 37).

d. Alternating exit nozzle - same as c, but the elemental aspect ratio is approximately equal to eight.

e. Simplified fin nozzle - producing a line of parallel slot jets.

f-j Scalloped exit nozzle - the nozzle exit is cut back in an alternating fashion illustrated in Figure 38 to produce inclined jets of nonuniform shape. This was accomplished to varying degrees with five different nozzles.

The major result of this nozzle study is shown in Figure 39, where the nozzle spreading rates are plotted against their price, the nozzle efficiency. In this case the efficiency is defined as the ratio of the actual to isentropic exit velocity. This is equivalent to the nozzle thrust efficiency defined earlier since

$$\frac{T_{Actual}}{T_{isen(same\ mass\ flow)}} = \frac{\rho V^2_{Actual}}{\rho V_{Actual} V_{isen}} = \frac{V_{Actual}}{V_{isen}}$$

That the price of rapid mixing is reduced nozzle efficiency is clear from the Figure. The particular nozzle chosen for further testing based on these tests is the .8 alternating exit nozzle having a half width spreading rate of approximately .17 and an efficiency slightly below 98%. It was this basic nozzle exit design which was employed in the successful test program described by Quinn[3].

Further evidence of the three dimensional effect discussed above may be seen in Figure 40, where the half width growths of the two alternating exit (now referred to as hypermixing nozzles) are compared to those of a slot jet of the same overall aspect ratio. Certainly the improved performance

in the minor axis direction is clear. However, the decrease in the major axis half width is exaggerated as the performance is improved in the opposite direction. Thus, as discussed in relation to 3-D effects, penetration of the jet in the major axis direction becomes more and more difficult as minor axis penetration (or spreading improves).

The performance of the hypermixing nozzle geometry has been further investigated in detail by Bevilaqua[21, 22, 24], both experimentally and analytically, based on the early work of Quinn[40]. Since the question of the mechanism of turbulent entrainment is still a point of controversy in the technical community, there is no surprise in the fact that the mechanism of enhanced entrainment in hypermixing jets is not completely clear. There is little doubt, however, that the increased spreading is related to the production of streamwise vorticity by the jet as shown in the schematic of Figure 23.

Recent results[47-50] in the general area of turbulent entrainment have pointed out the existence of a large scale vortex structure in the entrainment process and have attributed the bulk of the entrainment process to the action of this structure. This point of view is consistent with the concept that the increase in mixing rate in the hypermixing nozzles is due to the large scale streamwise vortices produced. A logical mechanism for the production of these vortices is the discontinuity in the transverse velocity which exists between elements at the exit of the hypermixing nozzle. Another possible mechanism[51], however, is the realization that each element of the hypermixing jet may be viewed as an airfoil with a jet flap at the trailing edge. Thus alternate elements of the hypermixing jet have different amounts of effective camber and the resultant lift on each element alternates in direction opposite to the alternating jet deflection. Then the streamwise

vorticity may be viewed as the downstream legs of a horseshoe vortex bound to each element of the nozzle. An analytical description of hypermixing is included in the following subsection.

D. Eddy Viscosity Models

1. Modified Prandtl Model

Eddy viscosity models have proven to be a very popular technique in the mathematical treatment of turbulent flows. Their popularity stems from the fact that their use laminarizes the problem in the sense that it allows the use of laminar methods of solution. The effect of turbulence is then to complicate the otherwise simple evaluation of the viscosity. The purpose here is certainly not to examine the usefulness of various proposed models but rather to present two methods of attack pursued at ARL and which indicate some promise and are applicable to thrust augmenting ejectors. A very comprehensive review of eddy viscosity models has been performed by Harsha[52].

From the present point of view, a desirable eddy viscosity model would have the simultaneous features of performance and simplicity. One of the simplest (and earliest) models is due to Prandtl[53] and is valid for free jets.

Prandtl's model of the eddy viscosity ε, is

$$\varepsilon = K\, b\, (U_{max} - U_{min}) \tag{II.D.1}$$

where K is an empirical constant, b is proportional to the width of the mixing region and U_{max} and U_{min} are the maximum and minimum values of streamwise velocity at a given streamwise position.

The ability of the Prandtl model to predict the axis velocity decay of jet into stationary surrounding has been demonstrated[52]. However, with the addition of a coflowing stream the model's performance deteriorates. This may be seen in Figure 41 where the centerline velocity u and the coflowing stream velocity U_e, are equivalent to U_{max} and U_{min} respectively. The initial velocity of the jet is V, while the velocity ratio is $m = U_e/V$. The constant in the Prandtl model is chosen as k = .007 in the region $u \geq .99V$ and k = .011 downstream of that region. The halfwidth b is defined as above.

A reasonable fit of the available data[52] at m = .67 is indicated by the heavy line decaying at X^{-1} (i.e. 45° slope). It may be seen that the agreement of the Prandtl model, which was designed for a jet into ambient air, is not very successful for the case of a substantial coflowing stream. Also indicated are the results employing a model due to Ferri, Libby and Zakkay[54] which was formulated to account for the effect of variable density in the jet flow. This model depends upon the difference in mass fluxes rather than the velocity difference;

$$\rho \varepsilon = K_f \, r_{1/2} \left(\rho_c u_c - \rho_e u_e \right) \qquad \text{(II.D.2)}$$

where $r_{1/2}$ is defined at any streamwise station as the distance between the centerline and the position at which the mass flux is equal to the average of the centerline value $\rho_c u_c$ and the coflowing stream value, $\rho_e u_e$. In addition, the constant K_f was chosen to be equal to .025.

When reduced to the incompressible case, the Ferri model is simply the Prandtl model with a different constant. Therefore, the results as in Figure 41, are merely shifted rather than improved. A correction factor to the Prandtl model to account for the coflowing stream can be developed by the following argument[55]:

The original development of the Prandtl model assumed that the dimensions of the lumps of fluid which are transported across the jet are of the same order of magnitude as the width of the mean shear layer. That this assumption is affected by the addition of a coflowing stream may be seen in the limit where the coflowing stream velocity is equal to the jet velocity and the width of the mean shear layer is zero. The flow is, however, still turbulent and the lumps of fluid transported by the turbulence are of finite size. Thus as the coflowing stream velocity increases, the size of the fluid lumps can be substantially larger than the width of the shear layer. Increasing the dimensions of the fluid lumps is equivalent to increasing the magnitude of the effective viscosity. To incorporate this effect into the Prandtl model, the eddy viscosity is increased by a term inversely proportional to the local velocity difference between the jet and freestream $(U - u_e)/(u - u_e)$.

The denominator of the preceding term is equivalent to the $(u_{max} - u_{min})$ term in the Prandtl model, so if the Prandtl model were simply multiplied by the coflowing stream modification, the local velocity difference terms, $(u - u_e)$, would cancel out and the resulting eddy viscosity would be proportional to the halfwidth alone. To avoid this, the modification factor is raised to a power characteristic of the flow situation, the ratio of the coflowing stream velocity to the jet velocity, m.

The use of the velocity ratio as the exponent in the modification term may be viewed as follows. The shortcoming of the Prandtl model in the coflowing stream case is its inability to match the exponential decay rate of the jet. The experimental decay rate exponent is dependent upon the velocity ratio, while the Prandtl model exponent is equal to unity. The present

modification improves the model by making the exponential decay rate dependent upon the initial velocity ratio. The resulting modified Prandtl eddy viscosity model is

$$\varepsilon = k\, b\, (u - u_e) \left[(U - u_e)/(u - u_e) \right]^m \qquad \text{(II.D.3)}$$

Thus the Prandtl model is simply multiplied by the inverse of the quantity usually plotted as the ordinate of the velocity decay plots, raised to the power of the velocity ratio. In the case of the absence of a coflowing stream, the modified Prandtl model reduces identically to the classical Prandtl model.

The ability of the modified Prandtl model to predict the far field decay of coaxial jet is shown in Figure 41. The new model successfully predicts the centerline velocity decay from approximately $\bar{x} = 20$ downstream.

It is appropriate to point out here that Maczynski[56] has shown that the effective mixing length in the far field of the jet is <u>not</u> proportional to the width, b, of the jet as the basic Prandtl model assumes. Rather the effective mixing length is proportional the the distance from the jet nozzle, which grows more rapidly than the jet width upon the addition of a coflowing stream. Thus the bracketed term in Equation (II.D.3) may be viewed as a modification of the jet width, b, to make it more compatible with the results of Maczynski. The effective mixing length thus obtained,

$$b \left[\frac{U - u_e}{u_c - u_e} \right]^{\frac{u_e}{U}}$$

is larger than b, and the difference becomes most pronounced in the far field.

Now analogous to the Ferri model, Boyle and Viets[57] rewrote the modified Prandtl model of Equation (II.D.3) in terms of mass ratio,

$$\rho \varepsilon = K(\lambda)\, b\, (\rho_c u_c - \rho_e u_e) \left[\frac{\rho_o U - \rho_e u_e}{\rho_c u_c - \rho_e u_e} \right]^{\lambda} \qquad \text{(II.D.4)}$$

where $\lambda = \rho_e u_e / \rho_o U$ is dependent only upon the initial conditions and the constant has been freed to vary with λ. In addition, an examination of the available literature indicates that the density ratio to the half power has a significant effect on both the entrainment[58] and axis velocity decay[59] rates of variable density jet flows. The inclusion of this factor leads to the model,

$$\rho \varepsilon = K(\lambda)\, b\, (\rho_c u_c - \rho_e u_e) \left(\frac{\rho_e}{\rho_o} \right)^{1/2} \left[\frac{\rho_o U - \rho_e u_e}{\rho_c u_c - \rho_e u_e} \right]^{\lambda} \qquad \text{(II.D.5)}$$

It now remains to determine the variation of $K(\lambda)$ empirically and thereby illustrate the applicability of the model. In an effort to retain the simplicity of the model, the constant in the second region of the flow (i.e., $U_c < .99\ U$) is specified as equal to the second constant in the Prandtl model, $K = .022$. The constant in the first region of the flow is chosen empirically and depends upon the mass flux ratio, λ. The choice of $K(\lambda)$ is essentially equivalent to specifying the length of the potential core as a function of mass flux ratio, λ, and is presented in Figure 42.

The empirical variation of K with λ was obtained by producing the best match of centerline decay of velocity, temperature and concentration of axisymmetric jet experiments from ten different sources. The axisymmetric geometry was chosen because of the relative abundance of data. A similar curve could be produced for two-dimensional results.

The success of the simple model in the case of a heated jet is shown in Figure 43 and Figure 44 for the case of a heated jet of nonuniform composition. The experimental results are due to Landis and Shapiro[60] and the general agreement is good.

2. Hypermixing Eddy Viscosity

The hypermixing nozzle development has been discussed above and the general flowfield produced is illustrated in Figure 23. It is desirable to develop an eddy viscosity for the hypermixing nozzle in order to facilitate design studies. The basic difficulty is that the hypermixing flowfield is fully three dimensional. This difficulty was overcome by Bevilaqua[22], who smeared the changes in the spanwise direction while retaining the essential feature of hypermixing, the streamwise vorticity. Thus, instead of treating individual streamwise vortices, the analysis treats a distribution of vorticity.

The governing equation for the streamwise vorticity Ω is

$$\frac{D\Omega}{Dt} = \alpha\Omega + \varepsilon\nabla^2\Omega \qquad \text{(II.D.6)}$$

where $\alpha\Omega$ can be interpreted as the straining of the vorticity by the main flow and $\varepsilon\nabla^2\Omega$ as its diffusion by the turbulence. As the jet moves downstream, spreads and decelerates, the characteristic streamwise dimension decreases and thus the streamwise vortex is compressed, so

$$\alpha = \frac{\partial U_c}{\partial x} \tag{II.D.7}$$

Then, if the vorticity is not a function of time but merely convected downstream, the resulting vorticity equation is,

$$U_c \frac{\partial \Omega}{\partial x} = \frac{\partial U_c}{\partial x} \Omega + \varepsilon \nabla^2 \Omega \tag{II.D.8}$$

If the vorticity is written as the product of two terms, turbulent diffusion diffusion Ω_t and the rate of strain due to compression, then (II.D.8) becomes,

$$U_c \frac{\partial \Omega_t}{\partial x} = \varepsilon \nabla^2 \Omega_t \tag{II.D.9}$$

This equation may be transformed and solved for the velocity distribution within the vortex as well as the size of the vortex (defined as the radius at which the maximum velocity occurs) and the maximum velocity. Employing the size of the vortex and its maximum velocity as the mixing length and velocity scales, the vortex induced stress can be determined. The detail for these operations are presented in Reference 22.

The governing equations for the jet flow containing the vorticity may be solved for the case of a self preserving jet, to within two constants. One can be determined by the magnitude of the jet spreading rate far from the nozzle while the second is determined from the near field of the jet by matching the initial spreading rate (which is indicative of the strength of the hypermixing vortices).

The comparison between analysis and experiment is shown in Figure 45. Since there are two free constants in the model the quantitative

comparison is not the most important thing, but rather the qualitative shape of the jet growth. Work is currently underway on an improved analysis based on the concept of approximating the various elements of the hypermixing nozzle by jet flaps[51] and thereby to define the free constants in the above model.

E. Simultaneous Mixing and Diffusion

Ejectors for aircraft application are constrained to be rather short. This leads to situations where, in spite of the rapidly mixing primary nozzles described above, the velocity profile at the inlet to the diffuser is not fully mixed (i.e. not flat). Therefore, superior performance demands that as much mixing as possible take place within the diffuser. However, Prandtl[61] contended that diffusers tend to accentuate the flow nonuniformaties (or skewness). During some early experiments at ARL, it appeared that this was true in one sense relative to the velocity profile and not the other and that the difference between the two is due to the direction of the diffusion process relative to the mixing process. Consider an unmixed velocity profile at the inlet to the diffuser. The question then arises: Is there a preferred direction of diffusion? That is, is it more effective to diffuse the flow in the plane of the velocity profile (Figure 46) or in the plane normal to that of the velocity profile (Figure 47)? The schematics in Figures 46 and 47 show a square inlet in order to separate the directional effect from that of aspect ratio.

1. Theory[62]

For diffusers of moderate expansion angles, the character of the flow is that the cross flow velocities v and w are small compared to the streamwise velocity component u. Therefore, as in Reference 63, the

boundary layer assumptions are applied in both the y and z directions. The resulting non-dimensionalized boundary layer equations are

$$u\frac{\partial u}{\partial x} + v\frac{\partial u}{\partial y} + w\frac{\partial u}{\partial z} = -\frac{\partial p}{\partial x} + \frac{1}{R}\left[\frac{\partial^2 u}{\partial y^2} + \frac{\partial^2 u}{\partial z^2}\right]$$

$$\frac{\partial p}{\partial y} = 0 \qquad \text{(II.E.1)}$$

$$\frac{\partial p}{\partial z} = 0$$

and continuity

$$\int u\, dA = 1$$

The velocities are non-dimensionalized with respect to the average velocity at the diffuser inlet U_o; the distances with half the initial wall separation L_o; and the pressures with the dynamic head ρU_o^2. Thus R is the Reynolds number, defined as $R = \frac{\rho U_o L_o}{\mu}$. In addition, due to the double symmetry about the y and z axes, the analysis will treat only one quadrant of the yz coordinate system. Therefore, the area A(x) is one fourth the total area distribution.

Now U(x) is defined as the average non-dimensional velocity in the duct of diffuser. Then from the conservation of mass

$$U(x) = \frac{U(0)\,A(0)}{A(x)} = \frac{1}{A(x)} \qquad \text{(II.E.2)}$$

where $A(x) = g(x)\,H(x)$ is the streamwise area distribution in one quadrant.

Consider the initial velocity profiles (at x = 0) such that the deviation of the velocity from the average velocity, $[u(o,y) - U_o]$, is small. If, in addition, the diffuser angles are small, the transverse velocities,

v and w, are small. Then the streamwise momentum equation (1a) may be linearized about U(x) by introducing u' = u - U(x), noting that u', v, w, and $\frac{\partial U}{\partial x}$ are small and neglecting terms of higher than first order in these variables.

The resulting streamwise momentum equation is (including Equation (II.E2)):

$$\frac{1}{A(x)}\left[\frac{d}{dx}\left(\frac{1}{A(x)}\right)+\frac{\partial u'}{\partial x}\right]=-\frac{dp}{dx}+\frac{1}{R}\left[\frac{\partial^2 u'}{\partial y^2}+\frac{\partial^2 u'}{\partial z^2}\right] \qquad \text{(II.E.3)}$$

Also, due to the definition of u' as the deviation from the average velocity,

$$\int_0^g\int_0^h u'\,dy\,dz = 0 \qquad \text{(II.E.4)}$$

Now, in neither diffuser flow situation is the velocity a function of z, so $\partial u'/\partial z = 0$ and Equation (II.E.3)

$$\frac{1}{A}\frac{\partial u'}{\partial x}+\left[\frac{1}{A}\frac{d}{dx}\left(\frac{1}{A}\right)+\frac{dp}{dx}\right]=\frac{1}{R}\frac{\partial^2 u'}{\partial y^2} \qquad \text{(II.E.5)}$$

Integrating over the quadrant area, A(x);

$$\frac{1}{A}\frac{\partial}{\partial x}\int_A u'\,dy\,dz+\frac{d}{dx}\left(\frac{1}{A}\right)+A\frac{dp}{dx}=\frac{1}{R}\int_0^h dz\left.\frac{\partial u'}{\partial y}\right|_0^g \qquad \text{(II.E.6)}$$

In diffuser analyses, it is not uncommon for the core flow to be treated separately from the boundary layer flow on the diffuser walls. Thus the

core flow has an inviscid boundary condition and this, along with the condition of symmetry on the diffuser centerline, means $\partial u'/\partial y\Big|_0^g = 0$ in Equation (II.E.6). The integral term on the lefthand side is zero from Equation (II.E.4). Then

$$\frac{d}{dx}\left(\frac{1}{A}\right) + A\,\frac{dp}{dx} = 0 \qquad \text{(II.E.7)}$$

or Equation (II.E.3) simplifies to:

$$\frac{1}{A}\,\frac{\partial u'}{\partial x} = \frac{1}{R}\,\frac{\partial^2 u'}{\partial y^2} \qquad \text{(II.E.8)}$$

Let (II.E.9)

$$\eta = \frac{y}{g(x)} \qquad \text{and} \qquad \xi = \int_0^x \frac{h}{g}\,ds$$

then Equation (II.E.7) becomes

$$\frac{\partial u'}{\partial \xi} = \frac{1}{R}\,\frac{\partial^2 u'}{\partial \eta} \qquad \text{(II.E.10)}$$

with (II.E.11)

$$\frac{\partial u'}{\partial \eta} = 0 \quad \text{at} \quad \eta = 0, 1$$

and

$$u' = F(\eta) \quad \text{at} \quad \xi = 0$$

The solution to Equation (II.E.10) with boundary conditions (II.E.11) is,

$$u'(\xi, \eta) = 2\sum_{n=1}^{\infty} e^{-\frac{n^2\pi^2\xi}{R}} \left[\int_0^1 F(\eta)\cos n\pi\eta\, d\eta\right]\cos n\pi\eta \qquad \text{(II.E.12)}$$

In order to illustrate the effect of direction on the diffusion process, consider the simplest case of a straight walled diffuser. Then, the equation of the expanding walls for diffusion in the plane of the velocity profile, Figure 46 is $g(x) = ax + 1$ where a is the slope of the expanding walls. The transformed streamwise coordinate is

$$\xi_1 = \int_0^x \frac{1}{as+1}\, ds = \frac{1}{a} \ln(ax+1) \qquad \text{(II.E.13)}$$

Now for diffusion in a direction normal to the plane of the velocity profile, Figure 47, the equation of the expanding walls (for the same area ratio between exit and inlet) is the same as above, $h(x) = ax + 1$.

Then the transformed streamwise coordinate is

$$\xi_2 = \int_0^x (as+1)\, ds = \frac{ax^2}{2} + x \qquad \text{(II.E.14)}$$

Now consider two diffusers of equal length but different sets of diverging walls, as illustrated in Figures 46 and 47. what is the difference between their exit velocity profiles? The simplest way to examine this question is to compare the two streamwise coordinate transformations, as shown in Figure 48. The two transformed coordinates are plotted versus non-dimensionalized physical distance downstream for the case of the wall slope a = 0.1. Then at any x position downstream, the corresponding value ξ is directly related to the amount of mixing having taken place up to that streamwise position. Thus it may be seen from the figure that diffusion normal to the plane of the velocity profile always leads to improved mixing in contrast to diffusion in the plane of the velocity profile, since $\xi_2 > \xi_1$ everywhere.

The difference in the degree of mixing indicated above can be substantial. Defining a variable D as the difference between the transformed coordinates at any x position divided by that x position, the value of D is 19% at an x location of two. The difference D grows very rapidly, reaching values of 28% and 44% at x locations of three and five, respectively.

Some insight into the problem of concurrent mixing and diffusion may be obtained by noting that for no diffusion the transformation of the streamwise coordinate degenerates to $\xi = x$. (It should be kept in mind that the walls are assumed inviscid). This situation is depicted in Figure 48 by the dashed line. Then it can be clearly seen from the figure that diffusion in the plane of the velocity profile (ξ_1) inhibits the mixing process while diffusion normal to the plane of the velocity profile (ξ_2) enhances the mixing process.

A physical explanation of this process may be the following. For diffusion in the plane of the velocity profile, the diffusion process tends to accentuate the nonuniformity of the velocity profile while the mixing process tends to reduce the nonuniformity. Thus the two processes oppose each other. For the case of diffusion normal to the plane of the velocity profile, the mixing tends to smooth out the nonuniformities while the diffusion process works in a different direction. Therefore, the two processes do not oppose each other.

As a simple example, consider the deviation from uniformity of the velocity profile at the entrance to the diffuser to be $F(\eta) = b \cos \pi\eta$. Then the coefficient of the Fourier series solution, Equation (II.E.12), is

$$b \int_0^1 \cos \pi\eta \cos n\pi\eta \, d\eta = \begin{cases} b/2 & n=1 \\ 0 & n \neq 1 \end{cases} \qquad \text{(II.E.15)}$$

and the solution for u' reduces to

$$u'(\xi,\eta) = b\, e^{-\frac{\pi^2}{R}\xi} \cos \pi\eta \qquad \text{(II.E.16)}$$

Thus the shape of the velocity profile remains qualitatively unchanged while the deviation of the velocity from uniform flow decays as the exponential

$$e^{-\frac{\pi^2}{R}\xi}$$

Now suppose a = 0.1, R = 100, and the diffuser length is $x_e = 4$ (here R may be viewed as the inverse of an eddy viscosity term). Then the transformed streamwise coordinate is $\xi_1 = 3.36$ for diffusion in the plane of the profile and $\xi_2 = 4.80$ for diffusion normal to the plane. The ratio of the magnitudes of u' at the exit of the diffuser in the two cases is

$$e^{-\frac{\pi^2}{R}\xi_1} \Big/ e^{-\frac{\pi^2}{R}\xi_2} = 1.153$$

Thus the mixing rate has been improved by approximately 15% by diffusing the flow normal to the plane of the velocity profile rather than in the plane.

An independent treatment of the same problem was presented by Quinn[64], who was able to predict the concurrent mixing and diffusion in an ejector configuration by modeling the flow as a series of large scale transverse vortices. These vortices have been found to persist several hundred characteristic lengths downstream in the wake of a cylinder[48]. Others have found this large scale phenomenon in jet flows.

Depending upon the orientation of the diffsuion process relative to the velocity profile, the transverse vortices may be either stretched or contracted. For example, the vortex filaments contained in the shear flow of Figure 46 are aligned parallel to the z axis. Thus, during the diffusion process, the length of the vortices remains unchanged. The vortices in Figure 47 are aligned in the same direction but the diffusion process takes place in a direction 90° removed from that in the previous figure. During the diffusion process, the vortices are stretched by a ratio equivalent to the area ratio through the diffuser.

According to the Helmholtz vortex theorems, when a vortex filament is stretched, its angular velocity and induced linear velocity are increased by an amount specified by the conservation of angular momentum.

Quinn[64] defined the velocity at any point to consist of the sum of the local mean velocity V and a not necessarily small perturbation u'

$$u = V + u'(x,y) \tag{II.E.17}$$

where u' varies inversely with the length of the vortex, λ;

$$\frac{u'}{\lambda} = \frac{u'_r}{\lambda_r} \tag{II.E.18}$$

Here $(\ )_r$ indicates reference values.

Employing the analytical form for the perturbation component due to strained line vortices suggested by Keffer[65,66] the skewness factor β (defined by Equation I.E.3) may be written,

$$\frac{\beta - 1}{\beta_r - 1} = \left(\frac{\lambda}{\lambda_r}\right)^2 \left(\frac{A}{A_r}\right) \left[F^2 \frac{I}{I_r}\right] \tag{II.E.19}$$

where F is the decay function of the local perturbation velocity,

$$F = \left(\frac{u'}{u'_r}\right)_{local} \tag{II.E.20}$$

and I is the integration of the induced velocity due to the vortices.

With this vortex decay model, Quinn produced expressions for the pressure coefficient

$$K_p = \frac{P_{amb} - p(x)}{P_{amb} - P_r} \tag{II.E.21}$$

in a highly skewed flow for the case where the vortices end on walls of constant separation,

$$K_p = 1 + \left(\frac{V_r}{V_i}\right)^2 \left\{ 2(\beta_r - 1)(G - 1) + 2C_f\left(\frac{W_r}{H} + 1\right)\frac{x}{W_r} \right\} \tag{II.E.22}$$

and for the flow situation where the vortices end on diverging walls,

$$K_p = 1 + \left(\frac{V_r}{V_i}\right)^2 \left\{ \left(\frac{A_r}{A}\right)^2 - 1 + 2(\beta_r - 1)\left[\frac{A}{A_r} G - 1 + 2 \tan\theta \frac{K}{R} \ln\left(\frac{G(x)}{G(L_m)}\right)\right] + 2C_f\left(\frac{W_r}{H} + 1\right)\frac{x}{W_r} \right\} \tag{II.E.23}$$

where

$$G = 1 + 2K\left(\frac{1 - V_i/V_o}{1 + V_i/V_o}\right)\frac{x}{W_r} \tag{II.E.24}$$

c_f = coefficient of friction

W = width of duct

X = streamwise distance

H = ejector height

L_m = length of constant wall separation preceding the diffuser

K = empirical constant determined to be = 1.5

Mixing experiments were performed in the large area ratio ejector described in section I.D and illustrated in Figure 10 and 21. The data within the ejector were obtained by pitot-static tubes and sphere probes. The excellent comparison between the predictions of Equations II.E.22 and 23 and the experimental data is shown in Figure 49. Configuration I consisted of a 5 in (12.7 cm) constant area mixing section followed by a 45 in (114.3 cm) diffuser while configuration II had a 16 in (40.64 cm) mixing section and a 34 in (80.36 cm) diffuser. In each case the diffusion was out of the plane of the velocity profile and therefore the vortices were stretched. An increase in the decay rate of K_p is evident at the end of the constant area mixing section, at which position the straining of the transverse vortices begins.

Thus, by the results of Quinn's model, the vortices in the case of the traditional diffusion method shown in Figure 46 would remain of constant length while the vortices in the case of diffusion out of the plane of the velocity profile (Figure 47) would be stretched and thus lead to more rapid mixing and hence lower skewness.

In order to more clearly define the effect of direction on the process of concurrent mixing and diffusion, an experiment was performed[67] on a diffuser of unit aspect ratio, much the same as shown schematically in Figures 46 and

47. The skewed velocity profile at the inlet to the diffuser was created by 1, 2 or 3 primary slot nozzles. The secondary flow consisted of the entrained ambient air brought into the device.

A gross indication of the relative performance of the two methods of diffusion may be obtained by measuring the secondary flow entrained into the diffuser. If indeed one diffusion method is superior to the other, it should result in greater entrainment into the device. A number of static pressure probes were mounted in the diffuser inlet and the results are shown in Figure 50. The total pressure of the secondary flow is the ambient pressure, so the ordinate of the graph, by Bernoulli's equation, is proportional to the entrained velocity squared. Thus the level of entrainment is plotted versus the diffuser angle for two different diffusion methods, the traditional diffuser (□) and the diffusion out of the plane of the velocity profile (X) as well as for two levels of primary nozzle total gauge pressure P_{T_p}. Boundary layer control air is injected about the periphery of the injection plane so that premature separation of the flow is avoid and the effect of direction on the diffusion of the core flow can be identified.

It may be seen that the entrained velocity into the ejector configurations is consistently superior for the case of diffusion out of the plane of the velocity profile than for the more traditional diffuser.

In addition, the skewness of the velocity profile at the diffuser exit has been measured for each of the diffuser configuration described above. A three dimensional version of the skewness parameter δ, defined by Equation (I.E.3) is employed,

$$\hat{R}_{3\text{-}D} = \frac{\iint u^2\,dx\,dy}{\frac{1}{\iint dx\,dy}\left[\iint u\,dx\,dy\right]^2}$$

$$= \frac{\int\left[\int u^2\,dx\right]dy \cdot \int\left[\int dx\right]dy}{\left[\int\left[\int u\,dx\right]dy\right]^2}$$

The effect of direction on the skewness of the exit profile is shown in Figure 51. For the case of diffusion out of the plane of the velocity profile, the skewness of the exit profiles is considerably lower, especially for higher diffusion angles. This is true for both the three nozzle inlet velocity profile and the single peak inlet profile produced by a single nozzle.

Thus the effect of the diffusion direction on the diffuser performance must be considered, especially in cases (such as aircraft applications) where relatively highly skewed velocity profiles must be effectively diffused. As shown above, the effect can be demonstrated by both analysis and experiment. This directional effect is also likely to be of importance in other applications, one possibility being in the case of dump combustors[68].

III. Unsteady Flow Effects

A. Background

The concept of the introduction of unsteady components into a jet flow to increase the mixing rate has been examined for some time. From a physical point of view, each of the methods to cause a time dependency in the jet results in a lengthening of the interface between the jet and its surroundings. The interaction between the two is thereby enhanced and the mixing rate improved. However, in some cases the lengthening of the interface is accomplished by a gross disturbance of the jet while in others it is tne result of the amplification of existing instabilities in the jet structure.

In addition to lengthening the interface, unsteady primary jets present the possibility of transferring momentum from the primary to the secondary by pressure waves rather than viscous phenomena. This is an inherently more efficient transfer and is therefore very desirable for ejector applications.

The mechanics of the pressure transfer may be thought of in terms of a slug of fluid passing through the ambient air. A higher pressure results on the front of the traveling slug than the rear. The slug therefore imparts some momentum to the ambient fluid ahead of it by means of a pressure transfer process.

Two of the earlier studies on unsteady flows were performed by Lin[69] and Lighthill[70], although for unsteady flow effects on the boundary layer rather than the free shear layer. Lin's analysis involves an order of magnitude argument by which the governing equation is reduced to a linear form and the overall solution may be obtained in closed form.

Lin's analysis has been adapted by McCormack[71] et al, who applied it to the problem of a free jet which is subjected to a very high frequency transverse oscillation as illustrated in Figure 10. In terms of the analysis, this is viewed as a periodic high frequency source of vorticity at the nozzle exit. The computed results of the analysis do indeed show an increase in the spreading rate with an increase in the amplitude of the transverse oscillation. An experiment performed on the device schematically illustrated in Figure 52, found a significant increase in the mixing rate as illustrated in the streamwise velocity profiles shown in Figure 53. The two cases of the vibrating jet were conducted at the same frequency, but at different acceleration or G loadings. It may be seen that the simple theory predicts the effect of the time dependency quite well.

An analysis which examines the effect of an unsteady primary jet in an ejector configuration has been performed by Johnson and Yang[72] by the method of characteristics. The specific solution involves the case where the primary flow (when it is on) completely fills the ejector. The analysis makes reasonable predictions of the performance of an accompanying experiment. An interesting point brought out by this experiment is the existence of an optimum frequency (in terms of performance) of the pulse jet. The measure of performance is the ratio of the total mass flow through the ejector device to the primary mass flow rate. Thus, for this type of ejector, as the frequency of the intermittent primary flow increases past the optimum, the flow within the ejector becomes closer to the steady state condition and the advantage of the intermittency is lost.

In the device examined by Johnson and Yang the intermittent flow was produced by a "chopper" type of device. Two plates with the same slot pattern machined into them were placed in the primary air line upstream of the ejector. One was held stationary and the other rotated, producing

an intermittent frequency proportional to the speed of rotation. Such a valving device would be unlikely in application due to the very substantial losses entailed.

The investigation described above was based on an extensive study of intermittent flow on a thrust augmentor device by Lockwood[73].

The time dependent primary flow in this device was supplied by the pulse jet, illustrated schematically in Figure 54. The operation of the pulse jet is as follows: Rapid combustion takes place in the chamber indicated. The hot gases so produced expand and travel down the tubes toward both exits. Once the momentum in the tubes is set up, the slugs of fluid travel out of the nozzles leaving a lower than ambient pressure in the combustion chamber. Thus ambient air is entrained into the combustion chamber, mixes with fuel and the remaining hot gases there and the combustion cycle begins again. As far as the augmentor shrouds are concerned, they see an unsteady pulsating jet, each pulse of which completely fills the shroud. Therefore the slug of air acts somewhat in the manner of a piston traveling through the shroud.

An alternate method of producing the unsteady flow is the location of a valving arrangement on the inlet to the combusion chamber. Such a concept was employed in German aircraft as early as the mid-forties. In Lockwood's investigation, the embodiment consisted of a one-way airflow valve at the inlet.

The advantage of the systems described above is the pocential improvement in performance. However, a major drawback is the fact that the time dependency is evidenced by an unsteady thrust component, not just unsteady flow in the augmentor. Then one must be concerned with the

interaction between this variation in thrust and the rest of the system, especially in terms of performance, noise and metal fatigue.

One of the basic results of Lockwood's work were achieved by high speed flow visualization. He found that the mechanism of the energy transfer from the unsteady primary to the entrained fluid within the augmentor occurs as "a combination of a jet-piston-like action coupled with relatively high energy compression and rarefaction waves".

An unsteady flow ejector device which has received substantial attention in the past and is still being investigated, has been proposed by Foa[17,74,75]. The basic device is illustrated in Figure 55 and consists of a rotating nozzle mounted in an ejector shroud. The rotation is due to either the action of the incoming primary flow on some turning vanes (or nozzles) or to a power source external to the device. Analysis of the device by Foa[75] indicates high values for thrust augmentation, but here ϕ is defined as the ratio of the thrust of the device to the thrust of the primary nozzle system without the shroud. Therefore comparison with the augmentation values of Section I is unclear since the efficiency of the primary nozzle system and the increased primary mass flow in the ejector geometry must be taken into account.

A detailed analysis of the flow in a rotary jet ejector has been performed by Hohenemser[76] and Hohenemser and Porter[77]. From the point of view of aircraft application, the most important analytical results of these studies are:

a. For a given geometry, there exists an optimum rotational speed for the primary nozzle.

b. For equal total temperatures of the primary and secondary flows, the predicted thrust augmentation ratio is moderately greater. For elevated primary temperatures, the predicted performance is substnatially greater.

c. Mixing reduces the maximum thrust augmentation, especially for elevated primary total temperatures. Therefore, the results are inconclusive because of the trade-off indicated by (b) and (c).

Two recent tests of rotary flow thrust augmentors have been performed by Maise and Dunn[78] and Maise[79]. The observed temperature dependence[78] was, contrary to the predictions discussed above, that the rotary ejector performance decreased with increasing primary jet temperature. In the nonrotating configuration, the performance improved slightly with primary temperature.

By improving the shroud design, the performance of the rotary flow augmentor was substantially improved, reaching levels in excess of 1.5 for an inlet area ratio of 19.6 and a length to diameter ratio of 3.9. The improved performance also decreased the sensitivity of the device to primary temperature.

There are, however, inherent disadvantages to the rotary augmentor as described above. Foremost is the added complexity involved in incorporating a moving part into the ejector design. This is dramatically pointed out by the high temperature test[78,79] where it was necessary to cool the bearings to avoid a failure. In addition, the integration of an axisymmetric ejector into an aircraft wing presents some difficulties as will be discussed in Section IV. Therefore, the rotary flow augmentor, although intuitively appealing, is as yet unproven and includes important drawbacks for aircraft application.

Because of the potential advantages of time dependent jets as discussed above, they have attracted considerable attention in the past several years. A pair of stimulating papers on unsteady jets were prepared by Binder and Favre - Marinet[16] and Curtet and Girard[80]. The former illustrates the improved rate of mixing achieved by pulsating the flow at the jet exit as opposed to a steady jet. The increase in the rate of halfwidth growth may be seen in Figure 56, where S indicates the strouhal number. Clearly, the inclusion of an unsteady component in the jet flow is highly desirable. However, an important consideration is the method by which the time dependency is introduced. In the case of reference 16, a spinning butterfly valve was located upstream of the jet exit and produced the pulsation. Such a device, although excellent for laboratory tests, has large losses associated with its operation and therefore is unlikely to be applied in practice.

The flow visualization results of Curtet and Girard[80] dramatically illustrate the fact that the pulsating jet consists of a series of vortex rings expelled periodically from the jet exit. In this case the unsteady jet is produced by a piston driven by an eccentric cam and operating in a stand-pipe configuration as illustrated in Figure 57. Again, such a device is ideal for a laboratory, but unlikely to be of great use in practice due to its complexity and the requirement for an external power source.

Another indication of the advantage of the use of unsteady flows may be seen in the results of Williams, et al[81], who employed a pulsating wall jet to study its effect on boundary layer attachment. The conclusion was reached that the unsteady nozzle did lead to increased mixing and entrainment. Compared to a steady wall jet, the unsteady jet mass flow could be reduced by more than half without affecting the performance.

Again, the time dependent jet was produced by a device which was unlikely to be employed in practice, a sliding valve plate which is opened and closed by an eccentric cam.

A device which overcomes the practical disadvantages of the unsteady jets described above was proposed by Hill and Greene[82]. The operation of this nozzle is based on the instability of the flow in a very rapidly expanding pipe section. The flow oscillates rapidly from one attached position to another and thereby produces a rapidly mixing unsteady jet. The mixing advantages to be gained by such a device is shown in Figure 58 by the growth of the "full width" which is equal to twice the halfwidth defined above. The mixing effect is substantial and the mechanism is simple with no moving parts. The missing piece of information is the nozzle thrust efficiency; the price which must be paid to obtain the increased mixing.

In addition to the mechanical or large scale jet stimulation described above, an important area of investigation is the stimulation of the jet structure by acoustic means, produced either from within or without the jet. This phenomenon was known to musicians who noted that the flame in a gas lantern flickered when bombarded by certain notes produced by a violin. That the acoustic stimulation caused a change in the vortex structure of the jet was shown by Brown[83], who employed a two dimensional smokeseeded air jet exposed to external acoustic waves. The fact that a free jet developed a distinguishable vortex structure at low Reynolds numbers had been demonstrated for the axisymmetric case by Johansen[84].

Becker and Massaro[85] and Roffman and Toda[86] found that external acoustic stimulation increased the spreading rate of the jet, although they do not agree on the frequency dependence to which the jet is most sensitive.

Very interesting results, from the point of view of recent turbulence research, were obtained by Vlasov and Ginevskiy[87] for turbulent jet of Reynolds numbers up to 520,000. They found that low frequency acoustic signals had a positive effect on the turbulence intensities and spreading rates of the jets, i.e., increased turbulence intensitives and jet spreading. However, high frequency acoustical bombardment resulted in both lower turbulence intensities and lower spreading rates. This result is completely consistent with some of the latest models of jet mixing[47-50,88], specifically that it is the large scale structure of the jet which is responsible for the mixing and entrainment process rather than a small scale viscous "nibbling" at the jet interface.

Thus the relatively low frequency acoustic waves could stimulate the large sclae jet structure and hence increase the mixing rate while the high frequency stimulation could enhance the small scale turbulence structure and result in an increase in viscous dissipation and a decrease in mixing rate.

A theoretical treatment of the effect of acoustic stimulation on the turbulence structure of the jet has been performed by Simcox and Hoglund[89]. Their results concur with the discussion above since they found "significant changes in the time-averaged vorticity can occur when the wave number which characterizes the vorticity fluctuation in the direction of travel of the acoustic wave equals the wave number of applied sound". Thus the applied signal and the vorticity structure must be tuned. In terms of the intensity, "it is apparent that the relative location in the energy spectrum of the eddies with which the direct interaction occurs will determine whether there is an increase or decrease of mean intensity".

The definitive work on acoustic stimulation from within the jet has been performed by Crow and Champagne[90], who mounted a loudspeaker upstream of the nozzle exit. By operating the loudspeaker at certain frequencies, they were able to stimulate the jet structure and increase the rate of mixing.

This is especially significant since a rather small variation in the exit velocity (less than 5%) resulted in a substantial increase in the mixing rate. In addition, they found that the jet was especially sensitive to disturbing frequencies characterized by the Strouhal numbers $st = \frac{fd}{v} = 0.3$ and 0.6.

B. The Flip-Flop Nozzle

In response to the potential performance advantages of unsteady jets discussed above, a nozzle development program was undertaken at the Aerospace Research Laboratories[18,91] to produce a time dependent flow at the nozzle exit. Since the unsteady jet was desired for ejector application and a basic advantage of ejectors is their simplicity, a requirement of no moving parts was imposed on the unsteady nozzle development.

Due to the earlier work on unsteady flows discussed above as well as the jet mixing investigations related in the preceding section, two facts were relatively clear at the outset of the unsteady nozzle study:

(1) Inclining the nozzle exit flow at a moderate angle to the streamwise direction can cause a substantial increase in the jet mixing rate, especially if the angle is alternately positive and negative.

(2) Introducing an unsteady component into the jet flow can likewise cause an increase in the mixing rate. However, the unsteadiness must be produced without a large efficiency loss or a great increase in complexity. In addition, the method should be self contained and not require an external driver.

1. Concept and Preliminary Experiments

In principle, the unsteady nozzle development is based on the simple fluid amplifier in general and the fluidic oscillator in particular. The operation of the fluid amplifier is dependent upon the fact that a jet exiting into a space between two sufficiently near walls is bistable (i.e., may attach to either wall). In addition, a rather small pressure gradient across the jet at its exit may cause the jet to detach from one wall and attach to the opposite one[92]. A simple bistable fluidic element, showing the effect of the more important parameters, has been examined by Warren[93].

A fluidic amplifier with the two control ports connected to each other was investigated by Spyropoulos[94]. In this way, it was possible to cause the jet to oscillate from one channel to the other. The basic principle of operation is as follows. Consider the jet to be attached to wall A in Figure 59. Then, due to the large amount of entrainment into the jet, the pressure at the control port A' is relatively low while the pressure at the control port B' is relatively high. Since the ports are attached to each other, a compression wave travels from port B' to port A', tending to raise the pressure there and push the jet off the wall. Simultaneously, an expansion wave originates at port A' and travels to port B', tending to lower the pressure there and pull the jet onto wall B. Thus, if the element is well designed, the jet will separate from wall A and attach to wall B, at which time the process begins anew.

At this point the question arises: Can this oscillation phenomenon be applied at the exit of a primary nozzle? If so, it offers a combination of the hypermixing nozzle concept of inclining the flow to the streamwise direction and the concept of an unsteady flow component introduced to accelerate the mixing process.

Three basic necessary changes from the device tested by Spyropoulos[94] present themselves immediately:

(1) To avoid large losses, the proposed nozzle exit must be far shorter than the conventional fluidic elements.

(2) The splitter plate (Figure 15) must be removed entirely. This is due to the fact that the splitter plate is exposed to the high velocity stream at the nozzle exit and would cause substantial losses.

(3) The nozzle exterior must be aerodynamically smooth to avoid large losses when exposed to the entrained flow.

In order to test the oscillation potential of a short element without a splitter, a variable geometry nozzle was constructed. The nozzle was built of plexiglas, and a wide range of geometrical changes could be combined. These included the variation of the powder jet exit size, the size of the control ports, the angle of the diffuser, the length of the device, and the location of the splitter, if any.

The observations made during the initial experimental runs were simply to see if the oscillation occurred and, if so, the sensitivity of that oscillation to other perturbations such as pressure variations or blockage at the exit. The basic result of the experiments was clearly that the nozzle could be made to oscillate in spite of its short length and the absence of the splitter. Further, more detailed tests utilizing new nozzles were then pursued.

2. Small Scale Nozzle Tests

Based upon the insight gained from the tests of the adjustable plexiglas nozzle model, a series of brass nozzles was constructed. The objective of this portion of the program was to do a limited parametric

study of the effect of the geometry on the nozzle thrust efficiency as well as the basic ability of the nozzle to oscillate. The designs for the nozzles employed in this portion of the investigation are shown in Figure 60 along with a schematic of nozzle number one with its mounting plate.

The oscillating design basically consists of a contraction section and a straight section, followed by a sudden diffusion (see Figure 60). At the point of diffusion,control ports are attached and connected to each other. As in usual fluidic devices, the jet leaving the contraction section attaches to one wall. The static pressure on this wall is then lower than the static pressure on the opposite wall, and the flipping of the jet from one wall to the other occurs as described above.

For each of the nozzles shown in Figure 60, the depth is one inch, yielding an aspect ratio at the throat of ten. The contour of the walls immediately downstream of the sudden diffusion varies from the more than 8° half angle diffuser through the parallel walls of series number 3 to the contraction section in series number 4. In addition, series number 5 employs a curved wall contour. The x dimension referred to in nozzle series 2 through 5 is due to the fact that, after each nozzle was adequately tested, its length was reduced in order to obtain further data. The x dimension will be referred to in the following descriptions as the diffuser section of the nozzle, whether or not its actual shape is that of a subsonic diffuser.

The aspect ratio at the nozzle throat, referred to above, was found to be a parameter critical to the operation of the nozzle. If the aspect ratio is too low, the endwall effects dominate the flow in the nozzle, and the oscillation is destroyed. In the case of a very large aspect ratio, various parts of the oscillating flow are out of phase with each other. This

results in a cancellation of the compression waves from one part of the nozzle by the expansion waves from another part. In this way, no coherent wave pattern is set up in the connecting tube between the two control ports, and the oscillation is destroyed.

As in any physical process, a price must be paid in terms of efficiency in order to cause the jet to oscillate from side to side. A nozzle thrust efficiency is defined as the measured thrust divided by the isentropic thrust of the mass flow through the nozzle. Thus

$$\eta = \frac{T}{\dot{m} V_i}$$

where η is the nozzle thrust efficiency, T is the measured thrust, $\dot{m}$ is the rate of mass flow, and V_i is the isentropic velocity which would be obtained at the nozzle exit if the flow were expanded from the stagnation plenum pressure to the ambient pressure with no losses.

The measured thrust efficiencies of the nozzle configurations depicted in Figure 60 are shown in Figure 61. The nozzle identification refers to the nozzle series as well as the particular "x" dimension as noted in Figure 60. The encircled data points are those taken at a plenum stagnation pressure of 1 psig, the lowest plenum reading taken. Since the pressure is relatively low, the errors involved are relatively high, and these points should be considered suspect. The remaining data are taken in the pressure range between 2 psig and 15 psig. It may be seen from the Figure that the most efficient nozzle tested is number 3D, followed closely by nozzle 4D. Both of these nozzles have parallel wall diffusers. That is, the diffusion process is very abrupt (as in all the nozzle designs) and is then followed by a parallel wall section.

Contraction sections on the nozzle apparently destroy the oscillation, as indicated by nozzle series #4. No oscillation occurs while a substantial contraction section exists on the nozzle. However, when the nozzle is cut back toward the 0.10" parallel wall segment so that the contraction is essentially gone, the jet not only oscillates but also operates relatively efficiently. When the nozzle is cut back even farther, the efficiency increases slightly. With respect to the contraction, a probable explanation is that in order to maintain a sufficient pressure difference across the jet and thereby control the flows, the static pressure in the control ports must be less than the ambient value. With the presence of the contraction section at the nozzle exit, keeping the pressure below ambient is not possible, and the oscillations do not occur.

In terms of nozzle thrust efficiency, the effect of decreasing the total nozzle length is to increase the efficiency. This may be seen in series two and three and, to a lesser extent, series four and five. In series three, in particular, the increase in efficiency with decreasing nozzle length is rather dramatic.

Nozzle thrust efficiency is not the complete answer, since nozzles with high thrust efficiencies generally possess relatively poor mixing qualities. Thus there must be a trade-off between the two basic parameters, nozzle thrust efficiency and the mixing rate.

The time average halfwidth growth, as defined in the mixing section was chosen to indicate the mixing rate and obtained by employing a constant temperature hot wire anemometer.

The halfwidth growth is presented in Figure 62. The various nozzles tested are the last members of each nozzle series and therefore each

is the most efficient nozzle in its series (see Figure 61). The dashed line in Figure 62 indicates the halfwidth growth of a two dimensional slot nozzle. The increase in mixing rate is dramatic but must be tempered by the attendant reduction in nozzle thrust efficiency.

By comparison of the halfwidth growth data with the thrust efficiency, some general observations can be made. As might be expected, the spreading rate decreases as the nozzle thrust efficiency rises. This is most clearly illustrated by a comparison of nozzle 1 with nozzle 2A. The two nozzles are of similar geometry, differing only in diffusion angle and length. In terms of nozzle thrust efficiency, nozzle 2A is clearly superior, while in terms of jet mixing, nozzle 1 is the better. Thus the penalty in thrust efficiency must be accepted in order to accelerate the mixing of the jet.

In addition to the rapid halfwidth growths of the flip-flop nozzles, they also offer the potential of an energy transfer from the primary to the secondary through pressure waves as opposed to the transfer by shear forces. This is similar to the performance potential of the Foa designs as discussed above. However, in this case there are no moving parts and no external stimulation is required.

The time dependent character of the flow may be seen in oscilliscope traces taken near the exit of nozzle 3D and shown in Figure 63. The magnitude of the velocity is plotted as a function of time at the nozzle centerline (b) and at the two halfwidth positions (a,c). The flow at the halfwidth position may be seen to have almost a square wave shape; so the jet is either "on" or "off" at any particular time. It is interesting to note, however, that even in the "off" configuration the velocity at the

halfwidth position is not zero. This indicates that the oscillating jet has set up a steady motion in the entrained flow in addition to the time dependent fluctuations. Thus the jet cannot be treated as quasi-steady. That is the entrainment pattern is not the same orientation. This induced steady motion is what leads to the increased entrainment and mixing rates which distinguish the unsteady jet.

3. Scaled-up Nozzle Tests

A scaled up version of nozzle 3D (see Figure 64) was constructed to further investigate the phenomenon. The throad dimension is 0.3 in (7.62 cm), the width is 4 in (10.16 cm), while the separation of the parallel wall diffuser section is 0.55 in (1.40 cm).

The parallel wall geometry was chosen due to a favorable combination of nozzle thrust efficiency and spreading rate. The scale of the throat dimension was chosen to match approximately the exit dimension of some previous low area ratio thrust augmenting ejector tests run ar ART[23, 24].

In addition, this nozzle demonstrated that the control ports could be swept back on the nozzle surface to present a smooth aerodynamic nozzle exterior. This is a requirement for thrust augmenting ejector applications since the entrained air must pass over the primary nozzles and any nonaerodynamic shape will lead to intolerable losses in the ejector inlet.

In order to indicate visually the enhanced spreading rate of the oscillating jet and also to show that the jet is indeed flapping from side to side rather than existing as a smeared jet across the entire exit plane, a schlieren experiment was performed. Helium was added to the jet flow to increase the photographic contrast. The results are shown in Figure 65, with the jet flowing from left to right.

The quantitative effects of stagnation pressure and feedback length on oscillation frequency of the flip-flop nozzle in Figure 64 are shown in Figures 66 and 67. The former figure indicates that frequency rises with stagnation pressure. A likely explanation is that, as the stagnation pressure increases, the velocity within the nozzle increases and therefore the rate of mass entrainment within the nozzle increases. The production frequency of the pressure waves in the feedback loops is proportional to the entrainment rate of the deflected jet within the nozzle and therefore oscillation frequency rises with stagnation pressure.

At first glance it is evident that the oscillation frequency must be inversely proportional to the length of the feedback loop from one control port to the other. This is due to fact that the pressure waves which pass through these tubes move at the speed of sound. Thus, if the actual time required for the pressure waves to cause the jet to flip is ignored, the frequency is simply inversely proportional to the time required for the waves to pass through the tube or, equivalently, the length of the tube. For such a situation, the data will fall on the minus one slope line indicated in Figure 67, where the frequency is plotted as a function of feedback tube length.

The experimental results shown in the figure confirm the expectation that for long tube lengths the frequency does, indeed, vary inversely with feedback length. Thus, in this regime, the switching time required for the jet actually to flip from one wall to another is negligible in comparison with the time required for the waves to pass through the feedback tube.

For shorter lengths (and correspondingly higher frequencies), the data diverge from the minus one slope. In particular, the frequency is not as high as would be predicted by extension of the inverse proportionality.

This is due to the fact that, as the tube lengths become shorter, the time required for the actual flipping of the jet from one wall to the other becomes a significant fraction of the time required for the waves to travel through the feedback tube.

4. Multi-element Nozzle

A nine element nozzle, each of whose elements has approximately the same geometry as the single element nozzle has been constructed and operated and is shown in Figure 68. Each nozzle element has in independent feedback loop and therefore each one oscillates with no specific phase relationship with the elements on either side of it. Although the oscillation frequency of the elements is nominally equal, there are small variations due to construction and thus any existing phase relationship is constantly changing. The nine element nozzle has been tested in low area ratio ejector corresponding to some earlier hypermixing nozzle tests[23,24] and the initial results indicate that the flip-flop nozzle lacks the overall performance of the best hypermixing nozzles. Further development work is required to match the nozzle mixing rate to the particular ejector application. In addition, the feedback loops on the nine element nozzle do not present an aerodynamically smooth exterior (although they are swept back toward the nozzle body) and present a significant inlet drag which can be improved.

Further studies on unsteady fluidically controlled jets have been performed by Platzer and Deal[95] and include frequency measurement to higher stagnation pressures and confirm the trend of the data in Figure 66 that the frequency levels out for higher pressures.

Additional unsteady nozzle tests have been performed employing a different feedback mechanism and will be discussed in part D of this section.

Curtet and Patural[88c] have produced a similar flowfield by a purely mechanical method and studied it by visual observation. The jet was flipped from side to side by mechanically bringing a circular rod in from one side until the jet attached to it and was deflected by the Coanda effect. The rod was then withdrawn and another simultaneously brought in from the other side to cause the slot jet to deflect in that direction. Therefore the resulting flow flip-flops from side to side in much the same manner as the fluidically controlled jet.

C. Acoustic Interaction

In order to clearly identify the effect of primary temperature on the ejector process, Quinn and Toms[19] performed an experiment with a heated primary and a simple axisymmetric ejector geometry. The inlet for the entrained flow was carefully calibrated to allow the accurate measurement of the secondary flow rate. The primary mass flow was measured by a renturi calibrated by the National Bureau of Standard. Thus the mass flow determinations were quite accurate.

A typical result for a long ejector length to diameter ratio, L/D, is shown in Figure 31. The reduced mass ratio, equal to the ratio of the primary to secondary mass flow (mi/mo) divided by the ratio of the absolute temperature ratio (θ) is plotted versus stagnation pressure ratio of the primary jet to ambient value. It may be seen that the mass flow ratio decreases with increasing pressure ratio. This is basically due to the reduced transfer efficiency of the energy from the higher pressure and hence higher velocity primary. The same kind of effect is evident with increasing primary temperature which results in increased primary velocity (for the same primary mass flow). Another factor involved in the reduction

in mass entrainment ratio with primary pressure and temperature is the fact that the frictional wall losses are increased since they are proportional to the entrained velocity and further downstream to the average velocity.

A more interesting variation appears in the case of a smaller length to diameter ratio of the ejector shroud, as shown in Figure 32. The mass flow ratio still generally decays with pressure but now the decay is not monotonic. Two peaks are evidently superimposed upon the decaying mass entrainment function. In addition, there appears to be no discernable trend in terms of primary temperature. The reason for this is due to two off-setting effect: (a) the flow in this shorter duct is not fully mixed at the exit and therefore increasing temperature (and hence increasing viscosity) improves the mixing process and thereby the mass ratio; (b) the degrading effect of temperature in terms of transfer efficiency and skin friction losses.

The line spacing of the data with pressure leads to the conclusion that the peaks reflect an actual flow condition and not data scatter. It was also observed that the appearance of these peaks coincided with a particular acoustical tone being emitted by the test apparatus. With this information, Quinn and Toms[19] were able to correlate the observed results with an acoustical interaction between the screech tones emitted by an overchoked primary jet and the geometry of the ejector shroud. Powell[96,97] empirically determined that an underexpanded primary jet produces identifiable screech tones of a frequency,

$$f_{screech} = K, \frac{a}{d\sqrt{FR - PR^*}}$$

where:

$f_{screech}$ = screech frequency

a = ambient speed of sound

d = Jet exit diameter

PR = ratio of jet stagnation pressure to the local static pressure at the jet exit

PR* = PR at the onset of choking

K_1 = empirical constant = 1/3 for axisymmetric jets

The interaction leading to the observed entrainment peaks occurs when the screech frequency is tuned to one of the transverse modes of the mixing duct, which are (from Morse[98]),

(symmetrical mode)

$$f_i = N_i \frac{a}{d} \quad ; \quad N_i = .766,\ 1.77,$$

(asymetric mode)

$$f_j = N_j \frac{a}{d} \quad ; \quad N_j = 1.2,\ 1.96,\ 2.23,$$

Thus the effect of the acoustic interaction is a dramatic increase in the mixing rate within the duct by a pressure transfer mechanism which is, as yet, not fully understood. The increased mixing is also evident in the exit velocity profiles obtained by Quinn and Toms, which are very uniform for the tuned cases and rather skewed for the untuned conditions.

The mechanism proposed by Powell for the existence of the screech tones proceeds as follows: Consider the structure of the overchoked jet, with its diamond shaped shock pattern. Assume that some sound sources are embedded within the flowfield. These emit signals which travel upstream outside the jet and disturbs the shear layer at the jet exit. These disturbances are carried downstream and amplified while passing through

the shock system and hence become the embedded sound sources assumed above. Not all embedded sources are amplified since they must be in tune with the disturbance of the shear layer at the jet exit. Therefore only those at certain positions in the clearly defined and repeatable shock structure lead to a screech tone. Another necessary condition imposed by Powell was that the amplification of the signals by the shock waves must be greater than the dissipation during signal generation and transmission, or else the signal would, of course, die out.

Powell's results were extended for higher pressure ratios by Merle[99], who found that an improved fit of the experimental frequency data is,

$$f = K_2 \frac{a}{d} + K_3 \frac{a/d}{\sqrt{PR - PR^*}}$$

where $K_2 = 7.7 \times 10^{-2}$; $K_3 = 0.38$

However, neither Powell nor Merle accounted for the observed discontinuities in the frequency versus pressure ratio curves in the axisymmetric case and the fact that they do not appear in the two dimensional case. A program to carefully examine the flow structure of the overchoked jet and to identify the temperature effect on the primary was undertaken by Rosfjord and Toms[100]. A basic result of their study is shown in Figure 69, screech frequency versus pressure ratio. The data indicate a jump in frequency at a pressure ratio of approximately 3.7 and is therefore consistant with the results of Powell[96,97] and Merle[99]. However, closer examination reveals some more structural details. When the frequency spectrum is displayed for a jet exhibiting a screech tone, that frequency appears as a dominant spike on another smooth and weaker distribution of frequencies. As the pressure ratio approaches the apparent discontinuity, the dominant spike decays and another spike appears

at another frequency. This is illustrated in the blow-up portion of the figure as two distinct frequency dependencies. This discontinuity or switch from one dominant frequency to another is defined by the arrows to take place at the pressure ratio where the two spikes are at equal strength. Thus there is no actual discontinuity but rather a rapid shift (in terms of pressure ratio) from one screech tone to another. As may be expected, Merle's curve fit with two constants gives abetter mean fit than the single constant of Powell's curve.

By obtaining the frequency dependence on pressure ratio for various primary temperatures, Rosfjord and Toms found that the frequency was indeed also dependent upon temperature. One possible mechanism to allow this dependence is a change of the shock structure with temperature. That this is not the case may be seen in Figure 70, where two of the characteristic lengths of the shock structure are plotted for various temperatures as a function of pressure ratio.

The mechanism proposed by Rosfjord and Toms[100] to correlate the temperature effect is based on the speed of the feedback signal traveling upstream. Powell and Merle had assumed a wave speed equal to the ambient speed of sound. However, for hot primaries, the waves are likely to be traveling in a heated layer about the outside of the jet. Then the speed of sound in that layer should also reflect the influence of the primary jet temperature. The method chosen is to base the speed of sound in this layer on the average of the ambient and jet exit temperatures,

$$c = \sqrt{\gamma R \left(\frac{T_{amb} + T_e}{2} \right)}$$

$$f = K_4 \frac{c}{d} + K_5 \frac{c/d}{\sqrt{PR - PR^*}}$$

The degree of success evidenced by this model is shown in Figure 71. The scatter is due mainly to the rapid jump in frequency discussed earlier and the only way to obtain further improvements is to incorporate the mechanism responsible for the jump into the theory.

D. Two Phase Flip-Flop Jet

The operation of the fluidically controlled Flip-Flop nozzle discussed in Section IIIB is consistent with basic requirements of rapid spreading and high reliability with moderate loss in efficiency. In order to widen the possible range of applications, the operation of the flip-flop jet was attempted in a two phase mode, i.e., a liquid jet exhausting into a gaseous environment. As may be seen in the schematic of Figure 59, when the jet is attached to either wall it entrains fluid from the feedback loops as well as the diffuser section of the nozzle. It is this entrainment from within the feedback loops which causes the pressure waves which in turn cause the oscillation.

In the two phase flow mode, as the liquid jet entrains liquid from the feedback loops, some of the ambient gas leaks into the loops to replace the entrained liquid. This gas pocket then acts as a damper, absorbing most of the energy in the pressure waves passing through the loop and causing the oscillation to cease.

There are important potential applications for a time dependent liquid jet. One is the fuel injector, since a majority of the fuels in use today are liquid as opposed to gaseous (especially in aircraft applications where storage volume is an important constraint). Another application is the generation of fire suppressing foam for sophisticated aircraft fire fighting. This process is undertaken in an ejector where the primary liquid

jet contains a foaming agent and entrains large amounts of ambient air to produce the required foam.

In order to pursue these applications, an alternate feedback method was attempted,[101,102], again based on fluidic switching experience (reference 92, page 65). A schematic of the two phase device is shown in Figure 72. The jet leaving the throat section is bistable due to the nearness of the walls and must attach to one wall. A portion of the jet is then scooped off at the nozzle exit and directed back upon the jet just downstream of the throat. This causes a pressure gradient across the bistable jet and it flips to the opposite wall and the process begins anew.

The process is a positive feedback and hence operates in both the single and dual phase modes. Since it does interrupt some of the jet flow by the scooping off process, it is inherently not as efficient as the acoustic method employed in the single phase flip-flop nozzle. This fact has been quantitatively determined by Platzer[103]. However, for the fuel injector application, and to a lesser extent the foam generator, the efficiency of the nozzle is not as critical a parameter as in the thrust augmentation application.

The advantages of the unsteady liquid jet may be seen in the high speed photograph of the flowfield shown in Figure 73. The flopping of the jet at the exit has produced a growing sinusoidal wave of liquid traveling downstream. The oscillation frequency is approximately 350 hertz and is not visible in real time. To the naked eye, only a smeared fan including the limits of the oscillation is visible. The two basic advantages of this jet are the spreading rate, which allows the very rapid entrainment of large quantities of air, and the intimate mixing between the liquid and gaseous

phases, which is ideal for either combustion or foam generation.

The actual geometry of the nozzle producing the above flowfield is shown in Figure 74 along with an isometric of the device. The actual performance in terms of spreading rate (defined as the half angle of the spreading fan) and oscillation frequency is illustrated in the following Figure 75 versus the stagnation pressure at the nozzle. After the onset of oscillation, the frequency rises monotonically with stagnation pressure while the spreading half angle increases by about a factor of two. It should be noted that the spreading rate, even without oscillation, is already greater than that produced by a slot nozzle.

The onset of oscillation is a very dramatic occurrence. As the stagnation pressure is raised, the jet begins to show some signs of unsteadiness with random, low frequency excursions from the streamwise direction. As the critical pressure is reached, the jet literally "pops" into the larger spreading fan mode. As the pressure is lowered, the process is reversed and the oscillation ceases just as abruptly. A movie film of this procedure is available on loan from the author.

An alternate geometry with longer feedback loops and with lips attached at the nozzle exit to encourage rapid reattachment is illustrated in Figure 76. In addition, the feedback loops are hinged to allow a variation of the percentage of the flow in the control ports. The results for two feedback settings are shown in Figure 77 (scoops account for 122% of the throat) and Figure 78 (scoops = 113% of the exit). The change does not have a significant effect on either frequency or spread. As in the tests in Figure 75, once the nozzle is oscillating, there is no strong effect of pressure ratio on spreading.

The results described above were achieved by the use of a very simple device which consisted of two pressurized water tanks and a motor driven valve. The data were obtained by the use of high speed photography. The devices themselves are really too large for fuel injector application, so a scaled down version of Figure 74 was constructed with a throat dimension of .059 in (.13 cm) and a depth of .250 in (.64 cm). The low mass flow requirements of this device allowed it to be tested by the use of the building water supply.

The flowfield of the small scale nozzle is shown in Figure 79. There is no clear sinusoidla flow pattern, in the sense of Figure 73, however, there are two facts which lead on to the conclusion that the device is oscillating. (1) The rapid popping of an increased spreading angle at a critical pressure as discussed above. (2) The appearance of crescent shaped filaments of fluid as seen in the figure. The origin of these shapes may be seen in Figure 73 where the outside of the spreading fan (and hence the tops and bottoms of the sinusoidal curve) are retarded by the ambient fluid and start to resemble crescent shapes. At the higher frequencies (on the order of 1000 hertz) on the small scale nozze, the appearance of the crescent shapes would therefore be expected.

The question of time dependent two phase nozzles is currently under further investigation. There are undoubtedly numerous industrial applications (perhaps in the area of material transport) for such devices in addition to those emphasized here.

IV. Aircraft Integration

The purpose of this sect'on is not to present design information but rather to illustrate some recent attempts to incorporate the ejector concept into an aircraft design as well as a present program to build two V/STOL prototypes.

The information presented here is due primarily to the cooperation of two organizations: The USAF Flight Dynamics Laboratory (J. M. Byrnes, R. D. Murphy, K. S. Nagaraja, D. L. Hammond) and the North American Division of Rockwell International (V. Hancock, P. Marshall, M. Schweiger). Their cooperation is much appreciated.

The probable aircraft applications for thrust augmenting ejectors are shown in Figure 80 in both a takeoff and cruise mode. One is the ejector flap system for STOL application and hence primarily for transports. The other is the ejector wing (shown here with two ejector bays) which is designed with VTOL capability. When possible, the ejector wing aircraft would also be operated in the STOL mode in order to increase its range and payload and reduce operating costs. However, in those situations where it is required, the VTOL capability would be available. This overload capability is an important plus for the ejector concept and is directly related to another important advantage, the performance during the transition from vertical to foreward flight. Both of these conditions are due to the creation of super circulation about the wing and a resultant increased lift.

A. Mating of the Engine - Thrust Augmentor System

Two basic questions which arise immediately in any consideration of the integration of thrust augmentors in aircraft are: Can the engine and augmentor be successfully mated without causing serious reductions in the

performance of one or the other? and, if so; can the performance of multi-channel engine driven ejectors be predicted by single channel, compressed air driven full scale laboratory ejectors?

The affirmative answers to these questions were supplied by Campbell and Quinn[104] who investigated a full scale, four channel ejector configuration driven by a turbo-fan engine. Temperature effects were not considered since only the bypass air was augmented. The engine inlet, as well as the ejector inlets on the top of each wing are shown in Figure 81.

The geometry of each of the channels is shown in Figure 82 and is generally the same design as the single channel test reported in reference 3. The geometrical differences between the center and outside ejector channels are evident although the nominal inlet area ratio for each of the channels is 23. As might be expected, the performance of the center ejectors is superior to that of the outer set. The data were obtained by a correlation of the performance with inlet static pressure as described by Quinn[3].

When the total mass averaged thrust augmentation is calculated from the data shown in Figure 83 and compared with the single channel data, the agreement is rather good, as seen in Figure 84. Therefore, cold multi-channel ejector performance can be predicted by single channel data and a turbo-fan engine (which operated stably and safely throughout the experiment) can be successfully mated to an ejector configuration.

B. Wind Tunnel Model Studies

A recent study of the performance of a thrust augmenting ejector device under foreward speed conditions has been conducted by Brown and Murphy[105]. Their basic configuration consists of a single channel augmentor as shown in Figure 85, located on the trailing edge of the wing. This

location simplifies the mechanical problems of varying the diffuser area ratio as well as folding up the ejector completely. The diffuser flaps could be adjusted independently while the primary nozzle orientation remained fixed. Thus one of the basic results of this investigation is the indication that significant augmentation can be achieved even if the primary flow is not aligned with the mean diffuser angle.

The augmentation levels achieved under static conditions exceeded values of 1.8. However, under forward speed conditions, additional lift is generated by the super circulation produced by the ejector itself. This effect is shown in Figure 86 where ΔC_L is defined as the difference between the lift coefficient generated by the device when the primary air is on and that generated with no primary flow. The theory is due to Spence's[106] jet flap theory and the fact it is not attained suggests possible improvement in the flap design. Since the thrust of the augmentor itself can exceed the nozzle thrust, it is possible for ΔC_L to exceed the 2-D theory.

An important observation made by Brown and Murphy from their data is that there is no evidence of stall, even at high angles of attack. This is also important to the transition problem and is reflected in the data of Figure 86.

C. Demonstrator Design Studies

Demonstrator vehicles, which are essentially scaled down versions of flight designs, have been proposed as one method to determine the operational potential of high technology advances in the state-of-the-art as they come out of the laboratory. In addition, the demonstrator itself may be designed for a particular remotely piloted vehicle (RPV) mission.

A design analysis of a demonstrator vehicle has been performed by the V/STOL Design Group[107] at the USAF Flight Dynamics Laboratory. The

basic areas of concentration were:

a. Ejector aerodynamic and mechanical design.

b. Exhaust gas ducting - aero and mechanical design.

c. Controls - analysis and mechanical design.

d. Turbo-fan engine installation.

These areas were judged to be of greatest importance to the proof of the thrust augmenting ejector concept. A design resulting from this study is shown in Figure 87 and includes a canard and a forward fuselage mounted ejector as well as a wing ejector.

The distinguishing attributes of this configuration, as presented by Reference 107 are:

ADVANTAGES

- STOL or high speed wing design
- Flexibility (engine flow to wing or forward ejector)
- VTOL balance and cruise stability/control are uncoupled
- Permits modulation of the ejector thrust for control
- Both thrust augmentation and lift supercirculation

DISADVANTAGES

- Two ejector types
- Fuselage ejector has center of pressure shift with velocity
- Fuselage volume used by forward ejector. An alternate RPV design is shown in Figure 88. In this case the ejectors are mounted in pods. Such a configuration does not allow the production of supercirculation and therefore is not a likely candidate for a full scale aircraft.

D. FDL Full Scale Preliminary Designs.

There preliminary designs are shown in Figures 89 - 91. The distinguishing features of Figure 89 are the fuselage mounted ejector and a trailing edge ejector, an auxillary inlet behind the cockpit, the ability to exhaust primary air through the vertical stabilizer section of the tail and a pitch/yaw control at the aft end.

The design of Figure 90 includes twin engines, a trailing edge ejector as well as a multi-channel forward canard ejector. Figure 91 is another twin engine design with a somewhat more conventional planform. In this case, the ejector is totally wing mounted.

E. Rockwell International Design[108]

As mentioned in an earlier section, Columbus Aircraft Division of Rockwell International is currently under contract to the US Navy to design and construct two prototypes of a V/STOL aircraft employing the thrust augmentation principles discussed above. The basic ejector design consists of a center body primary nozzle (passing half the primary air) and two wanda nozzles on the walls (contributing the other half of the primary flow) as shown in the schematic of Figure 12. An artists conception of the North American design, the XFV - 12A, is shown in Figure 92. The arrangement consists of a single channel wing mounted ejector as well as one in the forward canard. The vertical control surfaces are mounted at the wing tips and an auxiliary engine inlet for low speed flight is located behind the cockpit.

In order to minimize the construction costs, components of existing aircraft have been employed where possible. The fuselage, nose gear and main gear are from the McDonnell Douglas A-4, while the wing box and the inlets are from the F-4 by the same manufacturer. The engine is an F-401 developed for use on the F-14B.

The full engine flow is blocked by means of a diverter valve (developed by Pratt and Whitney[109]) and the flow passes radially into a dedicated ducting system which supplies the ejectors. The aircraft then sits on four posts of thrust, one at each ejector. The actual control is designed to be accomplished by modulating the ejector itself. As was seen in Figures 24-26, augmentation is a function of diffuser area ratio. Therefore, before takeoff the diffuser flaps are opened to the maximum augmentation position and the thrust to weight ratio becomes greater than unity resulting in takeoff.

Some Aircraft Statistics:

Length	43.16'
Height	9.25'
Width	28.0'
Thrust to Weight Ratio	
Engine Installed	0.72
Takeoff	1.12
Installed Engine Thrust	14,070 lb
Lift Thrust	21,800 lb
Takeoff Gross Weight	19,500 lb
Augmentation ratio	1.55

A typical VTOL flight sequence is shown in Figure 9 from left to right. At takeoff, the ejectors are set for maximum vertical thrust. During STOL/Conversion (or transition) the ejectors direct some of the thrust toward the aft end and the aircraft accelerates forward. At this point the diverter valve is released and the engine exhaust exploded through the tailpipe. The ejectors are simultaneously folded up to present a smooth, high performance airfoil section. This is especially important for a fighter application, as the XFV-12A is designed to exceed Mach 2.

The design of the flaps, which make up the ejector geometry, is accomplished with more than one purpose in mind, as seen in Figure 94. Besides forming the ejector during hover and transition and the airfoil section during cruise, the flaps can also be maneuvered to act as speed brakes. This, along with the vertical thrust ability of the aircraft results in the extreme agility desired for in-flight maneuvers.

The development of the ejector device has necessitated the development of a rotary test arm, dubbed the "whirley rig" and shown in Figure 95. The full scale ejector configuration is mounted at the end of the test arm, as shown in the top of the figure. The primary air is supplied by an F-401 engine mounted near the center of rotation. The primary mass flow into the ejector is measured by a venturi section shown in the blowup. The whirley rig has allowed the full scale hot testing of various ejector desires in forward flight as well as the investigation of the effect of modulating the ejector flow as a control mechanism.

An important testing result is the confirmation of one of the basic advantages of the ejector concept, that during transition from hover to forward flight, the lift does not decrease and hence there is no loss of altitude. This fact is shown in the test result of Figure 96. The total lift does not drop below the static value as the forward speed is increased. The augmented jet lift, consisting simply of the vertical component of the ejector efflux, does decrease but the loss is more than made up by the increase in the circulation lift caused by supercirculation. This is also the basis for the superior overloaded STOL performance of ejectors.

There are, of course, other problems which have not been treated in the space available here. However, in general, the thrust augmenting ejector

concept leads to unconventional designs for unconventional missions and the success of an aircraft of the type discussed above may revolutionize the aircraft industry.

Table 1. Dimensions of duct diffusers in inches

Configuration	L_M	L_D	$L = L_M + L_D$
A	13	32.35	45.25
B	13	15.25	28.25
C	5	23	28
D	16	34	50
F	5	45	50
H	5	45[a]	50

[a]Configuration H had a compound diffuser. The first 14 in. of L_D diverged at an included angle of 36°, the remainder used to obtain the required A_3/A_2.

THE EJECTOR PRINCIPLE

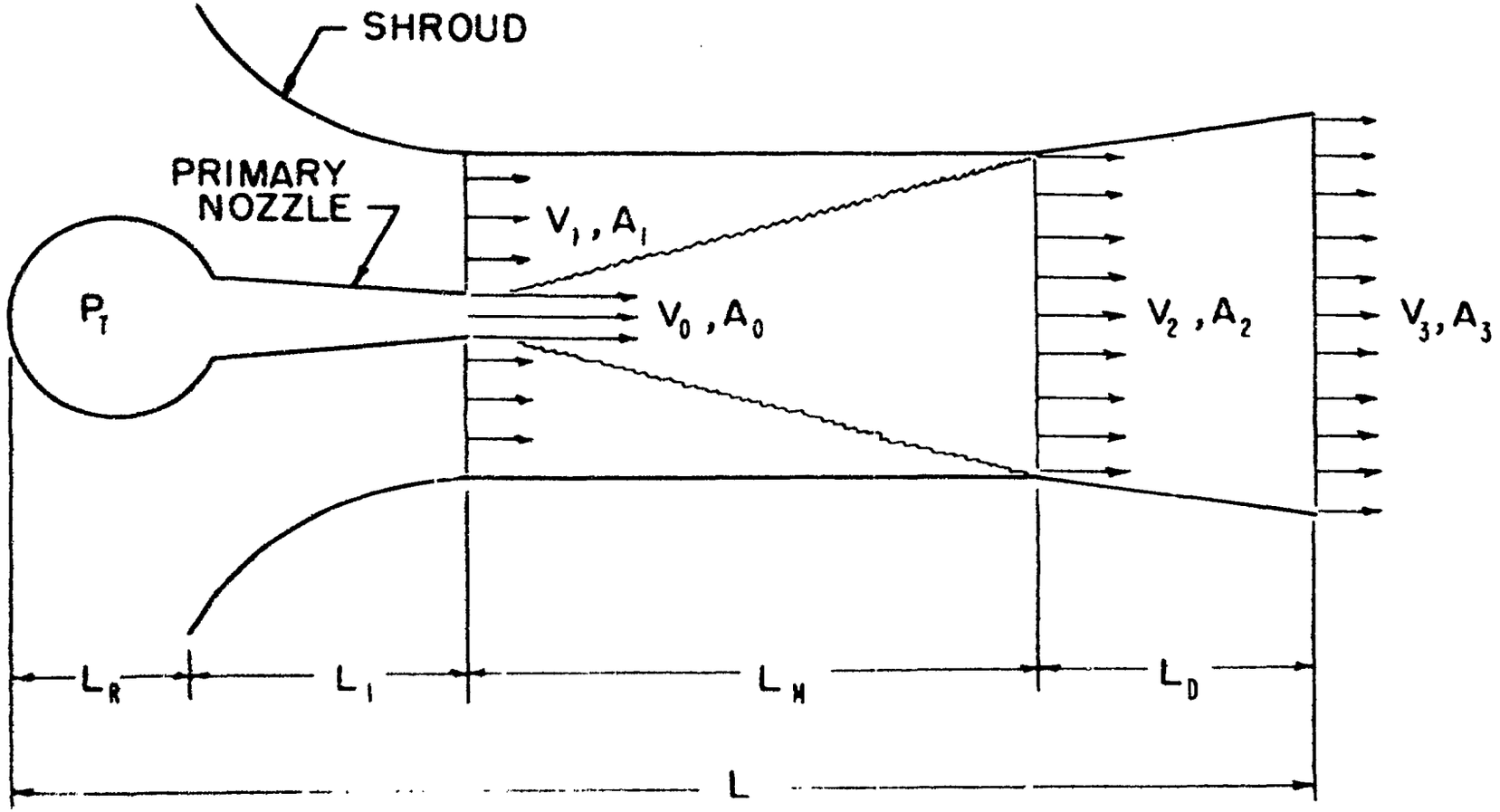

Figure 1. The ejector principle[1]

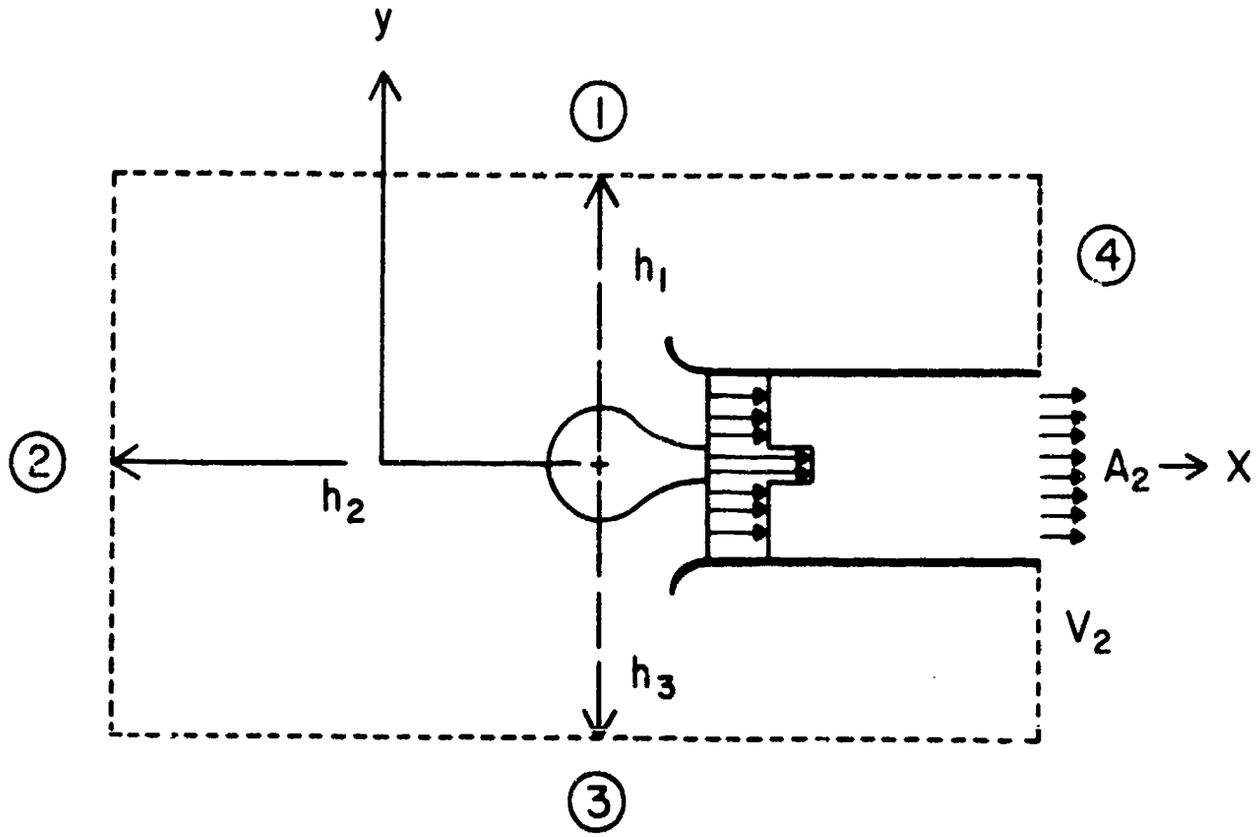

Figure 2. Control volume determination of the total thrust produced by the ejector device

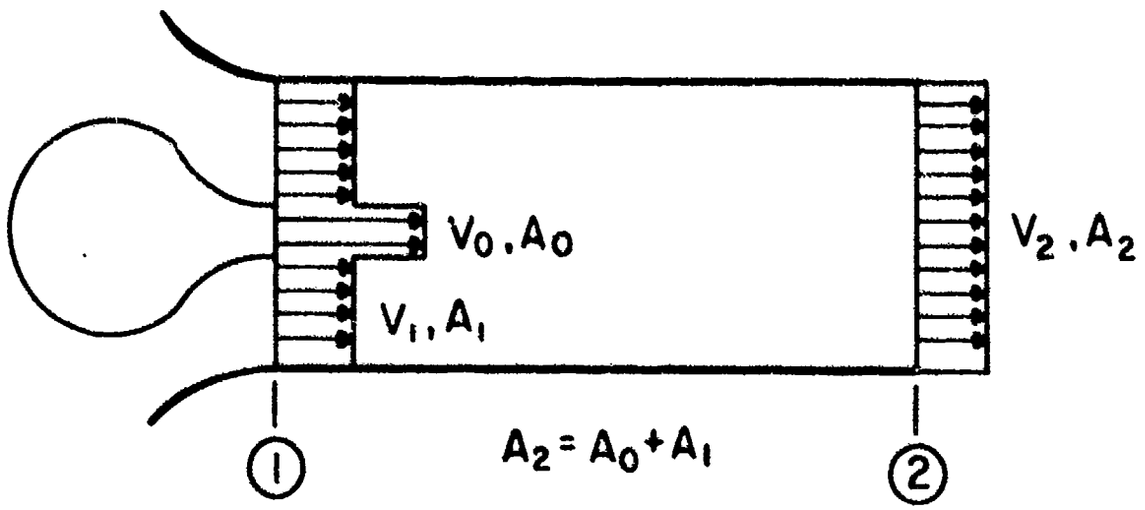

Figure 3. Simplified ejector

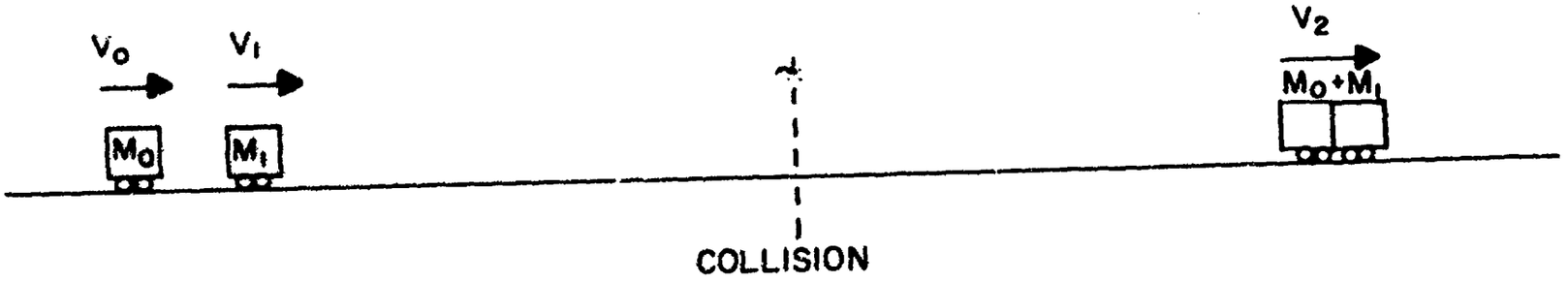

Figure 4. Analogy of colliding railroad cars

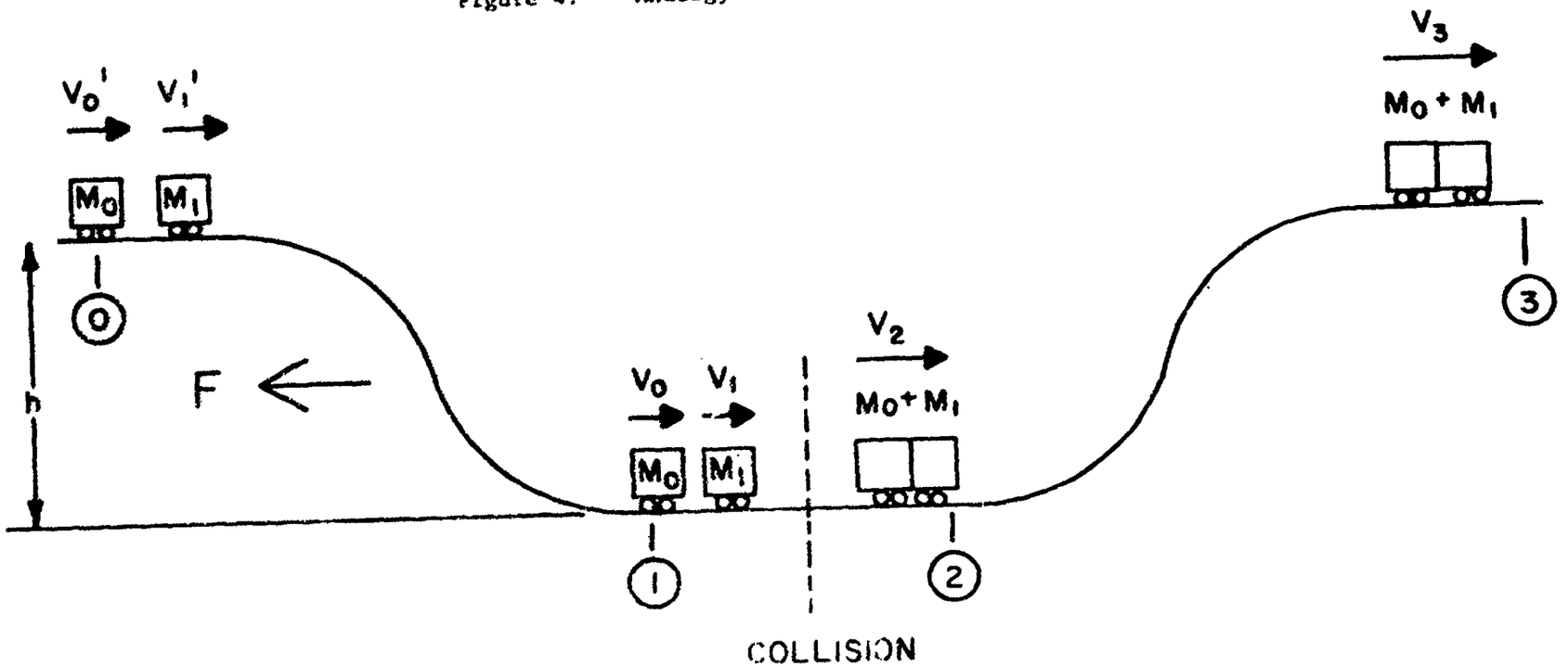

railroad car analogy including potential energy effect

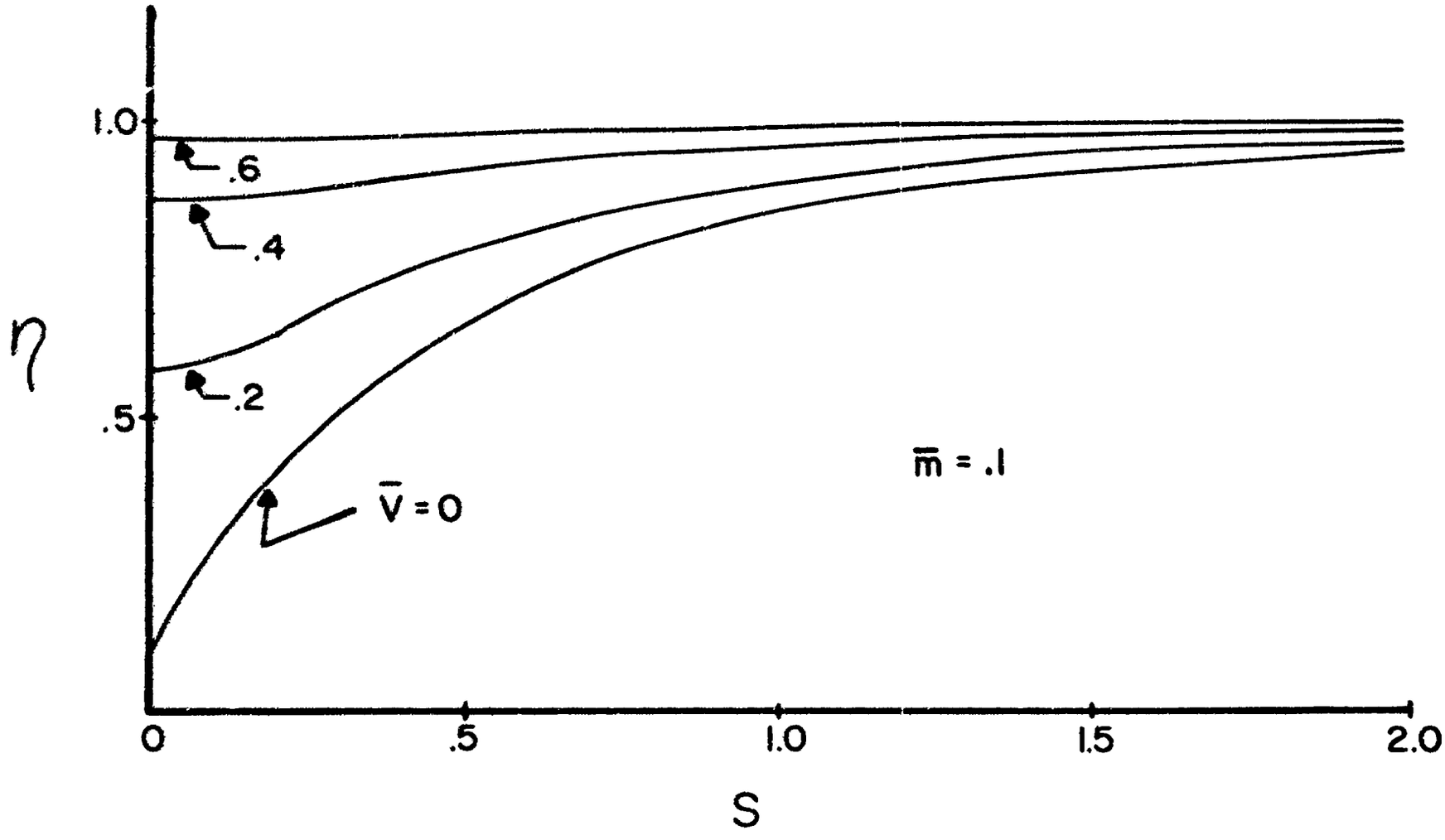

Figure 6. Variation of transfer efficiency with speed ratio

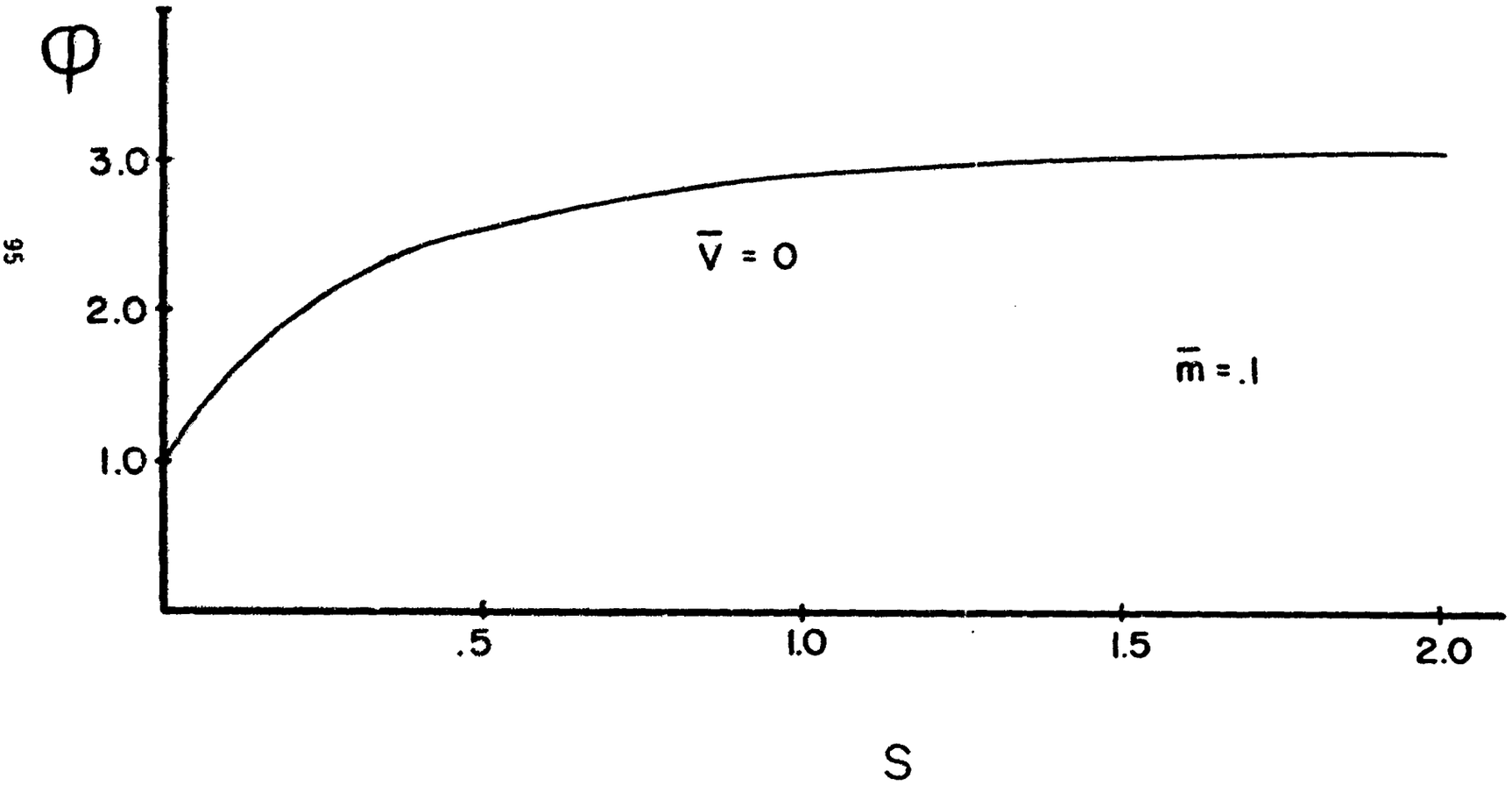

Figure 7. Variation of thrust (momentum) augmentation with speed ratio

CRUISE

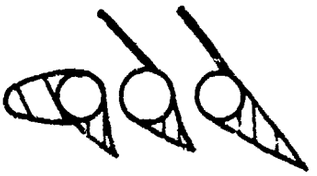

TRANSITION

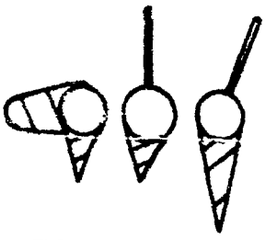

VTOL

Figure 8. Typical ejector flight sequence[1]

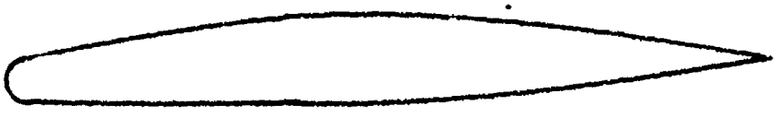

CRUISE

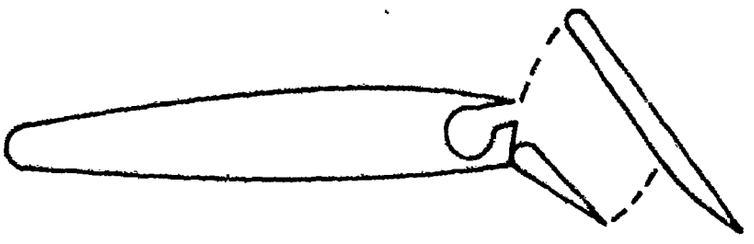

TAKE OFF & LANDING

Figure 9. Ejector flap configuration[1]

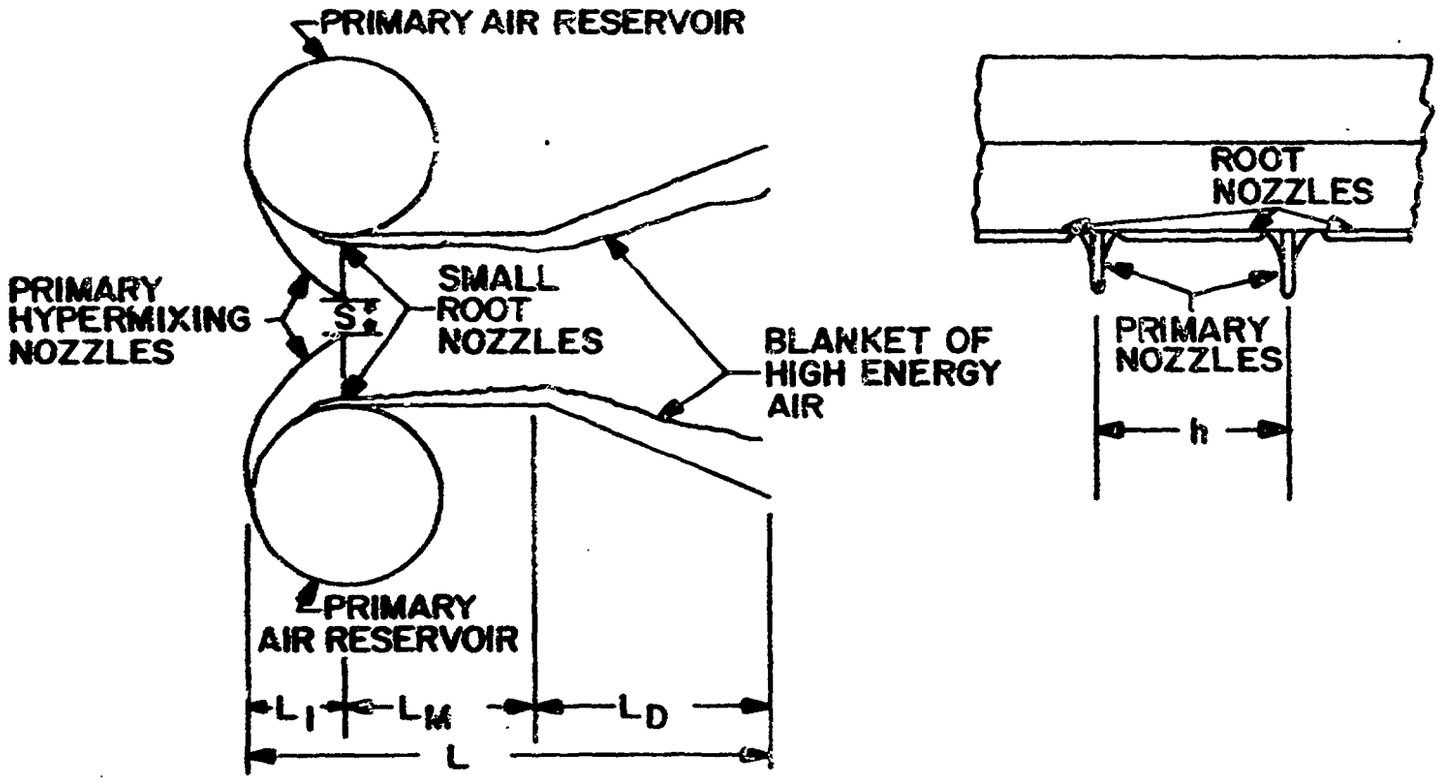

Figure 10. ARL high area ratio thrust augmenting ejector design[3]

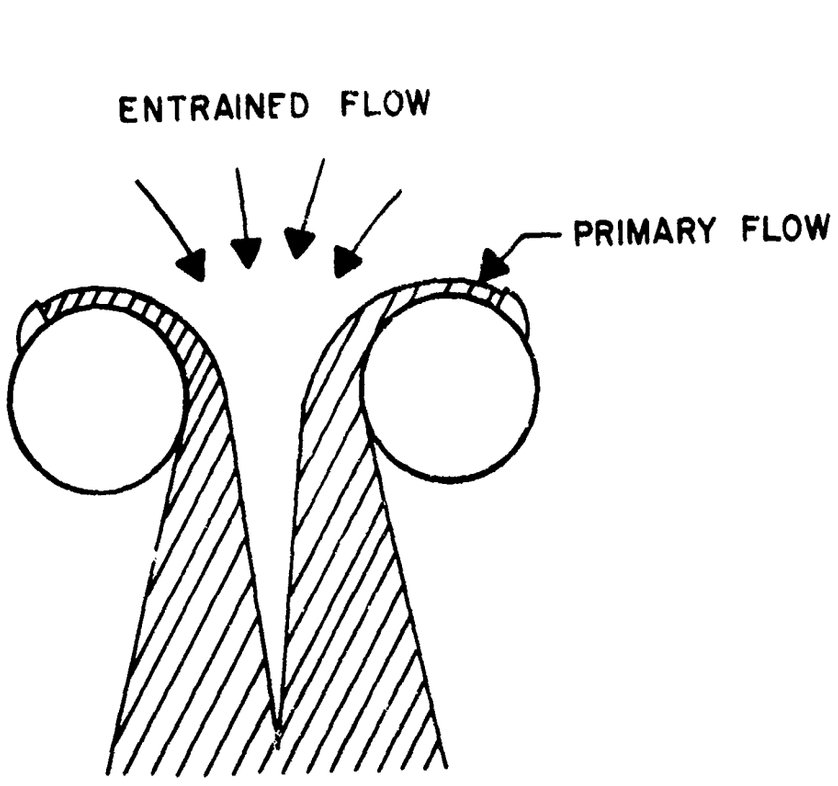

Figure 11 Coanda ejector

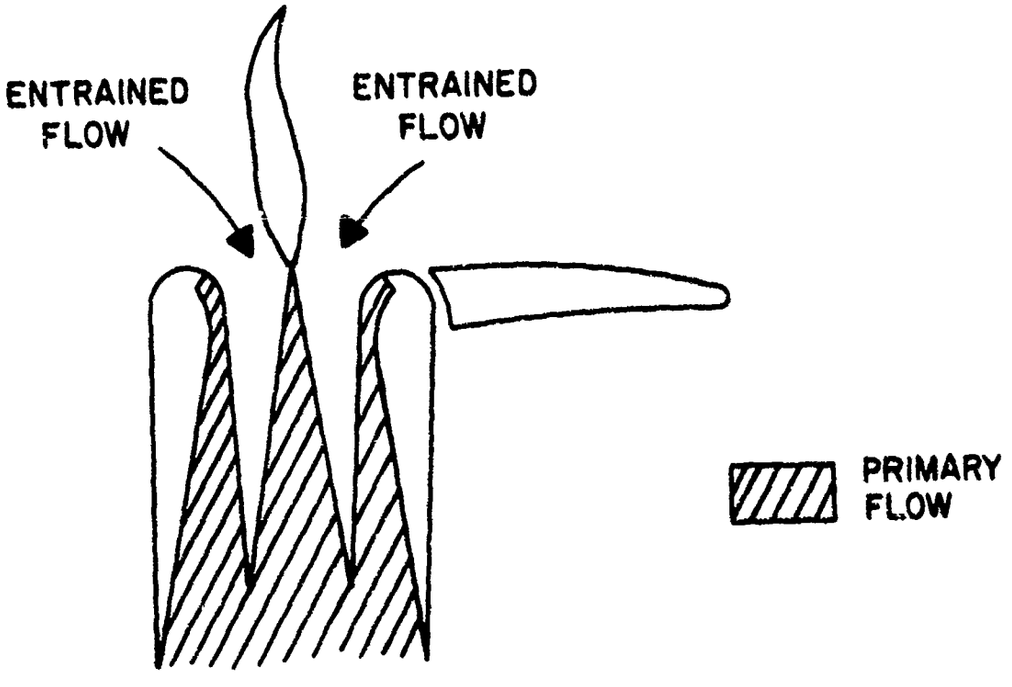

Figure 12. Rockwell International design - combination of centerbody and Coanda injection

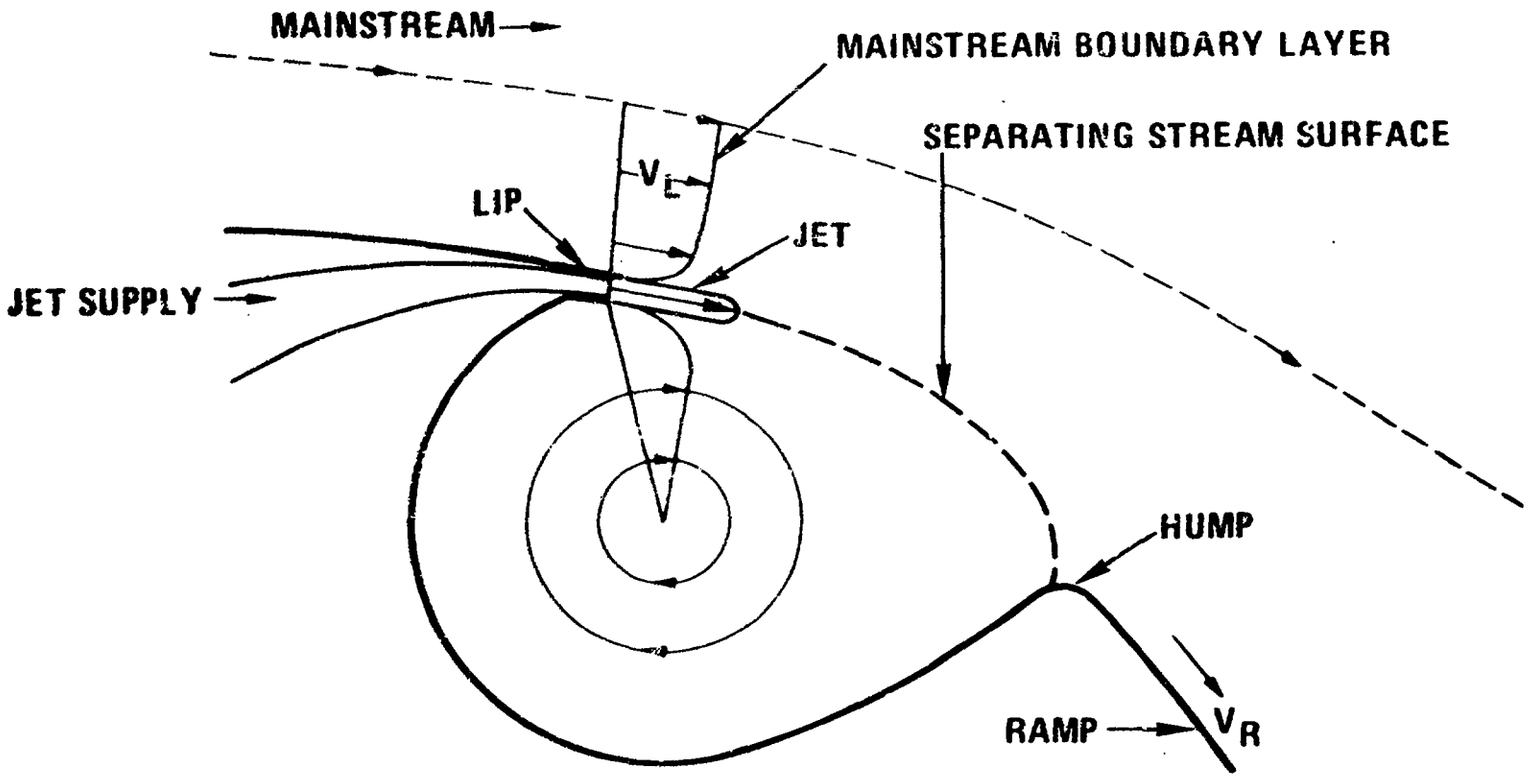

- o ALL OF THE PRESSURE RISE OCCURS ALONG THE SEPARATING STREAM SURFACE
- o THE BLOWING JET REENERGIZES THE LIP BOUNDARY LAYERS TO PREVENT FLOW SEPARATION
- o THE BLOWING JET POWER REQUIREMENT IS VERY LOW

Figure 13. Trapped vortex diffuser[12]

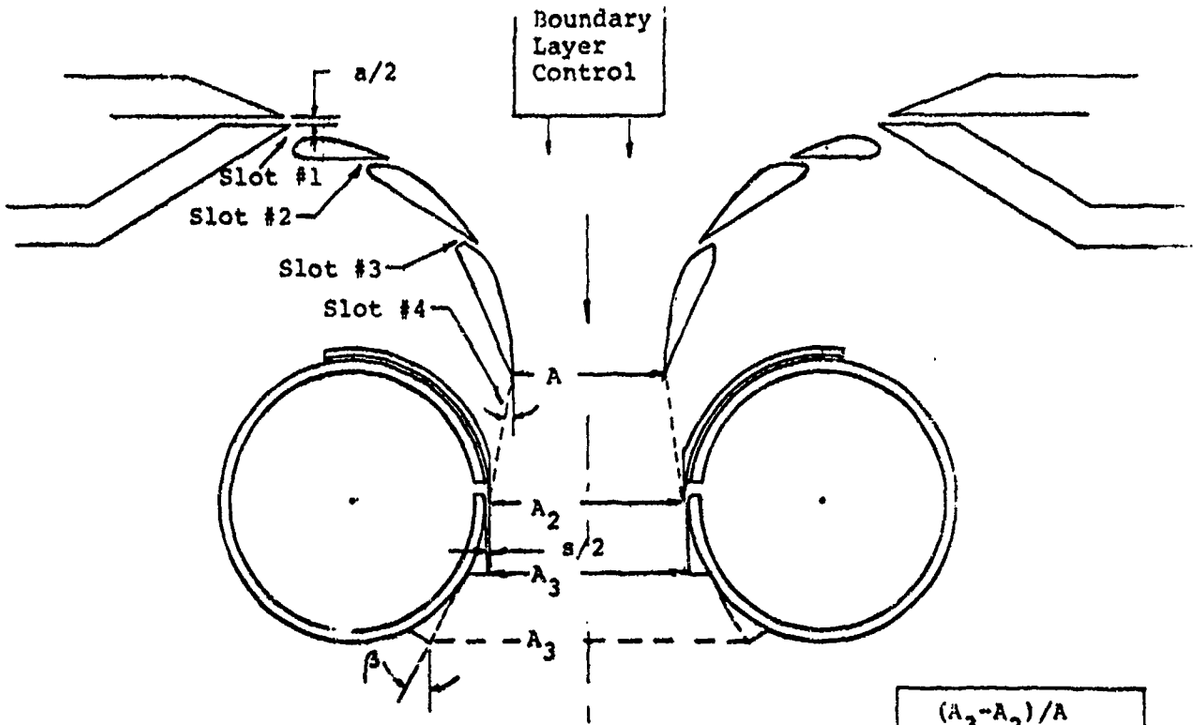

	$(A_3-A_2)/A$	
β deg.	s/a=1	s/a=3
0	0.0625	0.1875
10	0.2627	0.3877
20	0.5100	0.6350
30	0.7969	0.9219
40	1.1147	1.2397

Figure 14. Schematic of the Coanda/ Jet Flap Diffuser ejector[13]

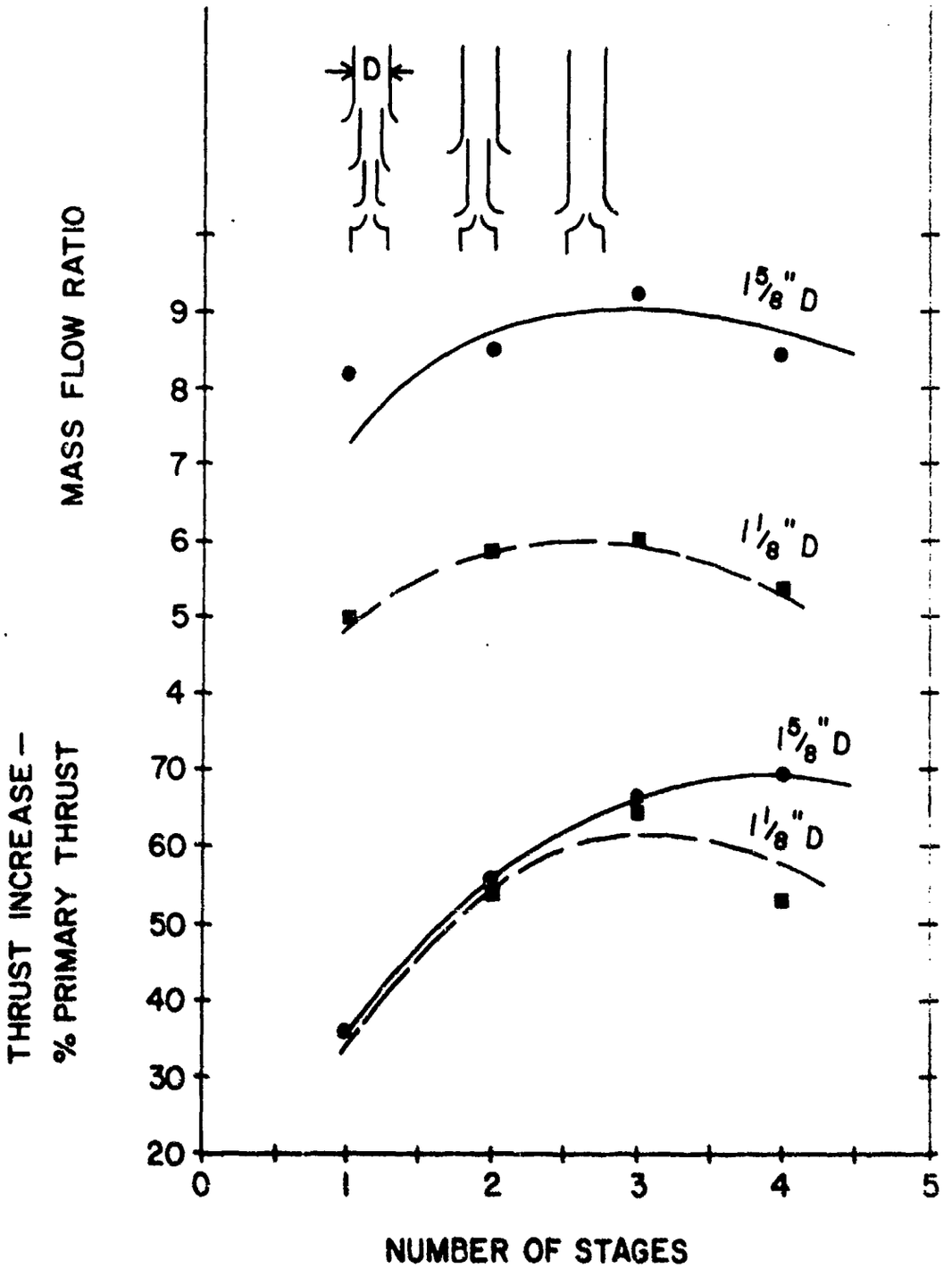

Figure 15. Effect of multi-staging on an axisymmetric ejector[14]

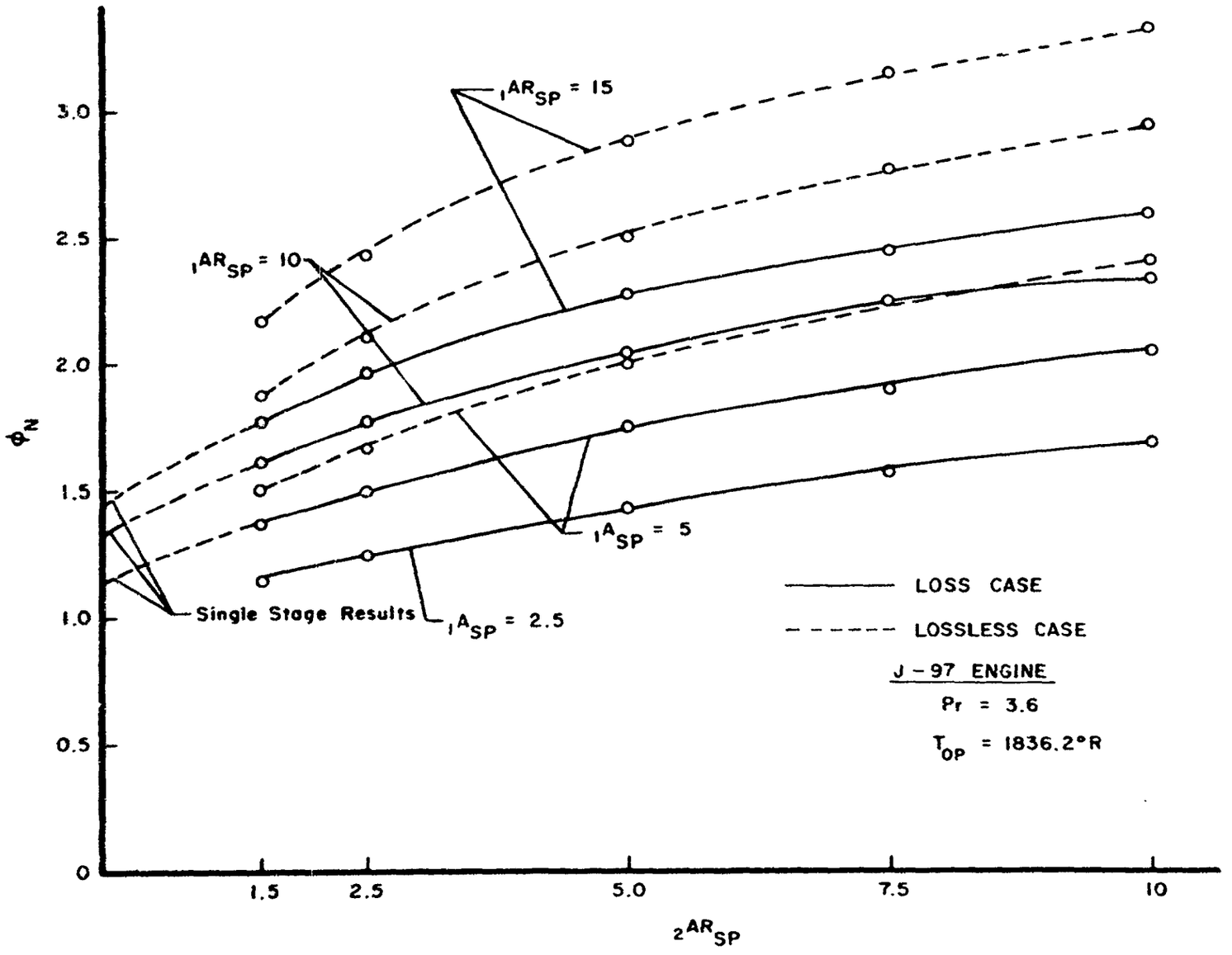

Figure 16. Analytical predictions of the effect of staging

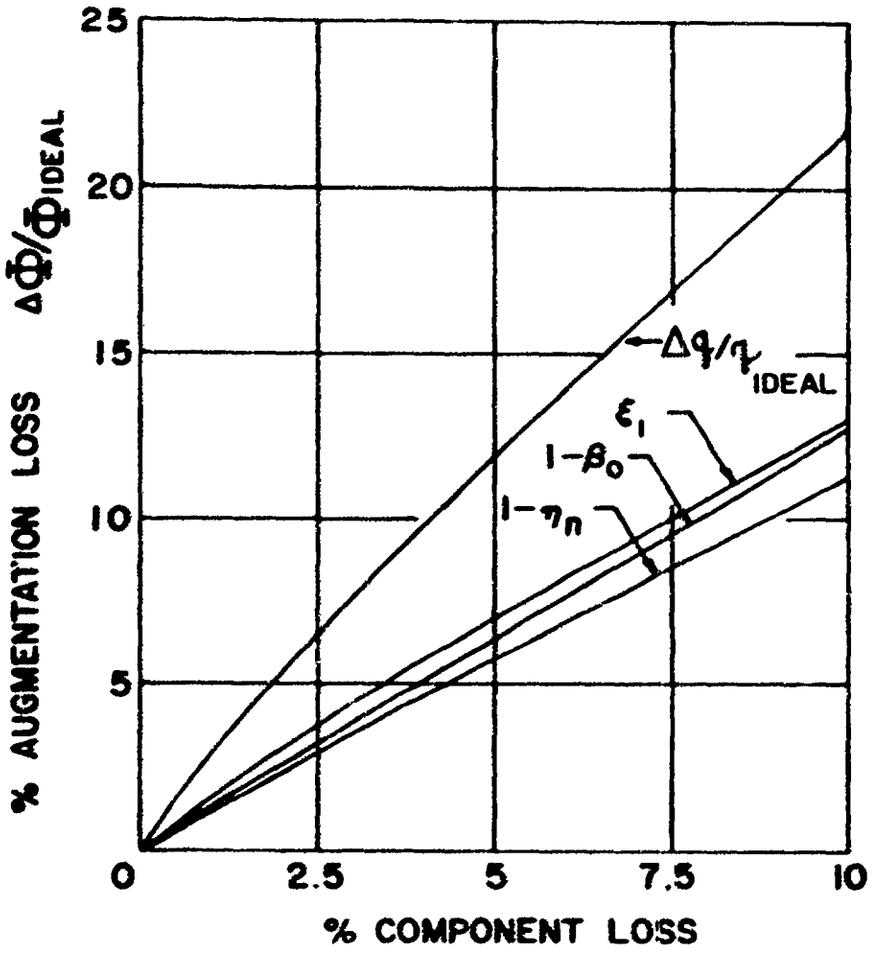

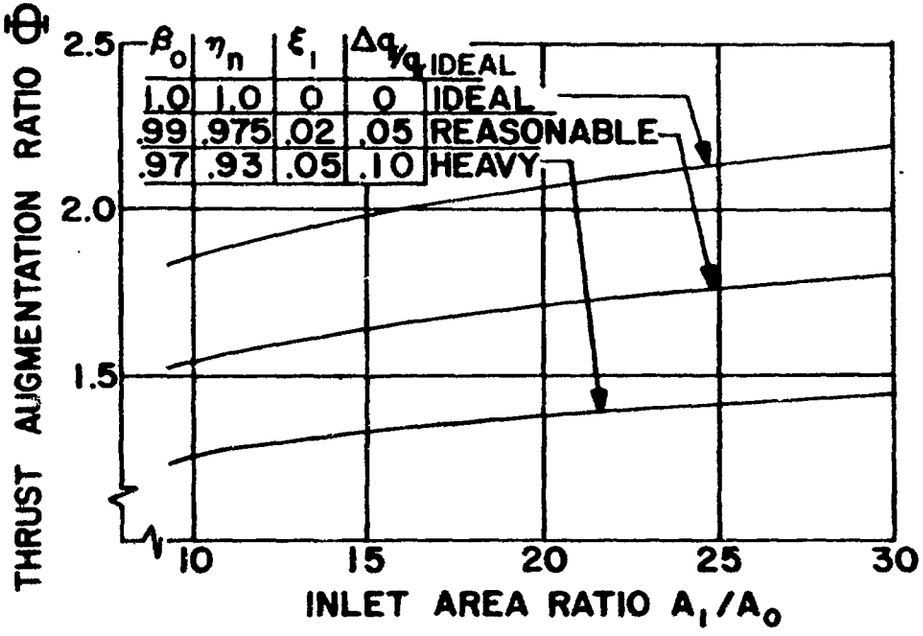

Figure 18. Estimates of ejector performance[3]

THEORETICAL AUGMENTATION RATIOS FOR LOSS-FREE EJECTORS

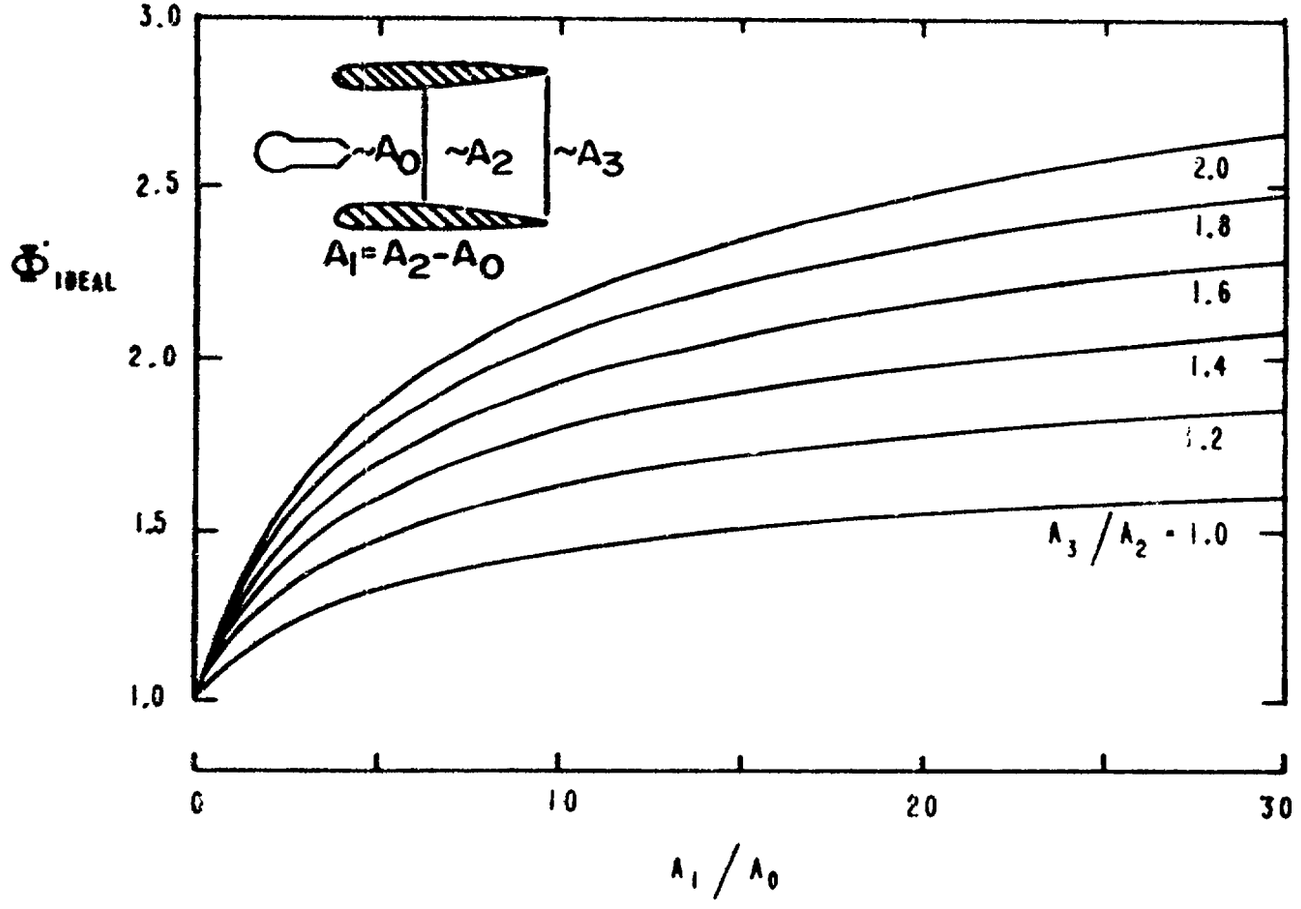

Figure 19. Theoretical augmentation ratios for loss free ejectors[1]

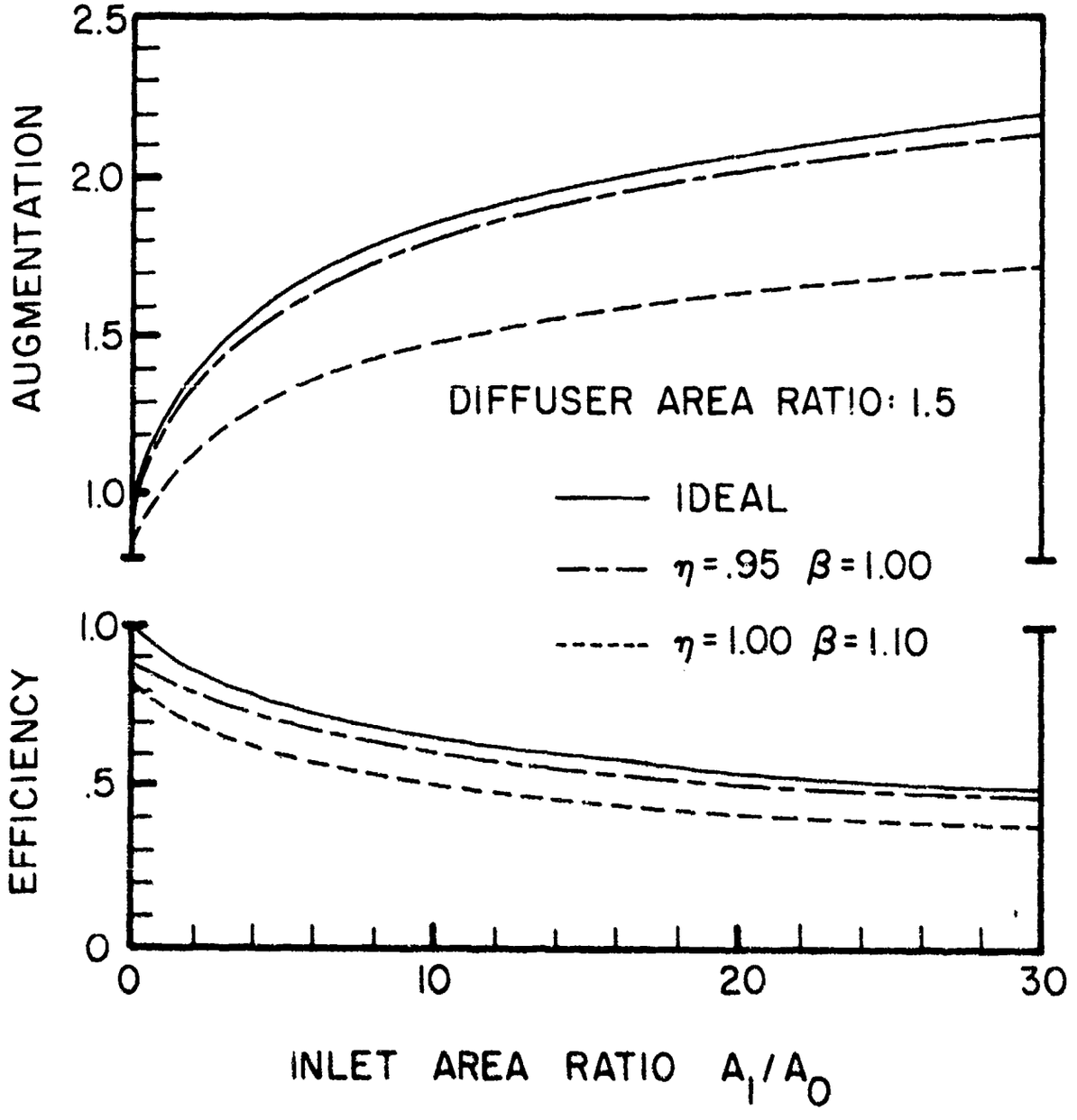

Figure 20. Tradeoff between nozzle thrust efficiency η_n and mixing[21]

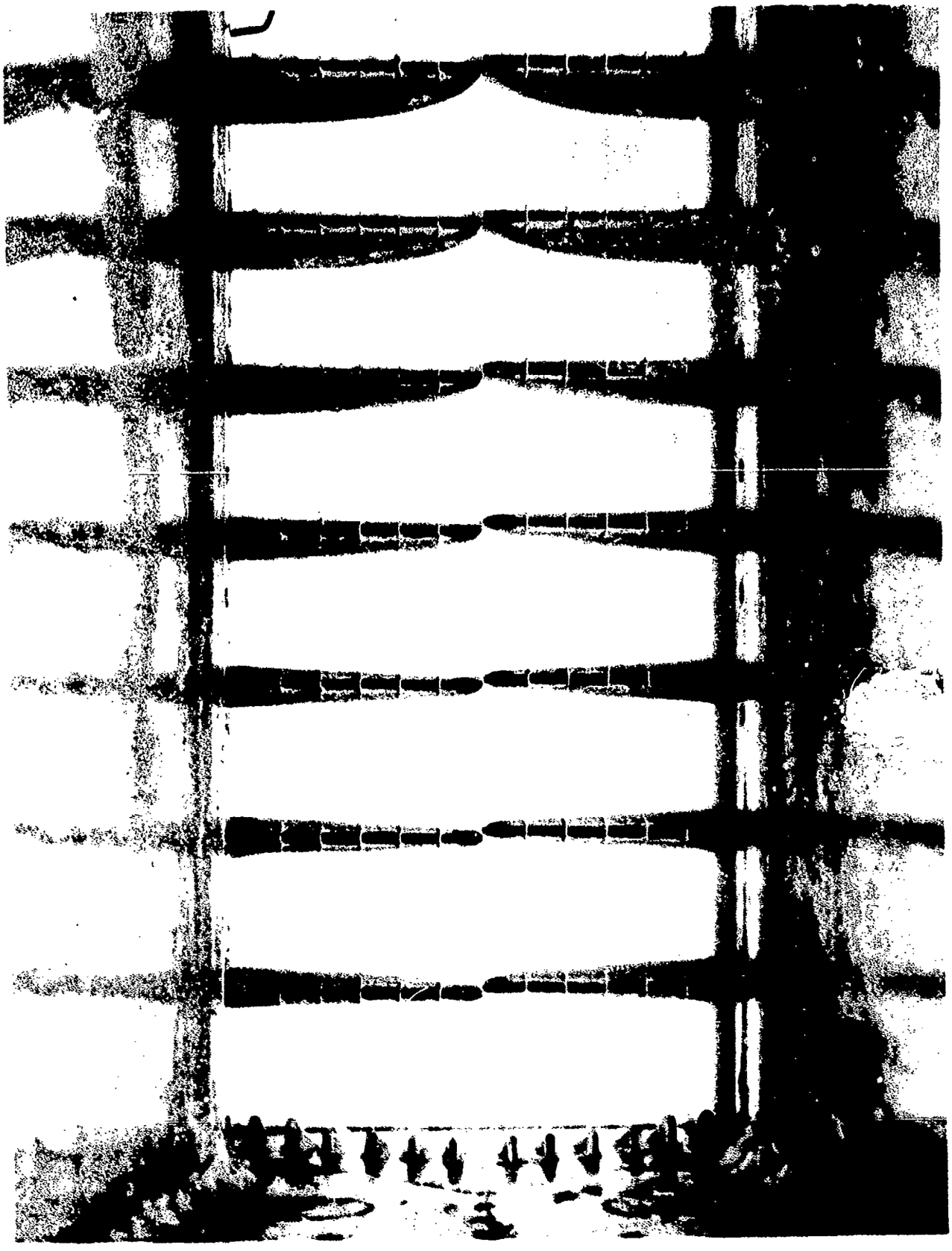

Figure 21. View upstream[3] into the exit of the ARL area ratio 24 ejector schematically illustrated in Figure 10

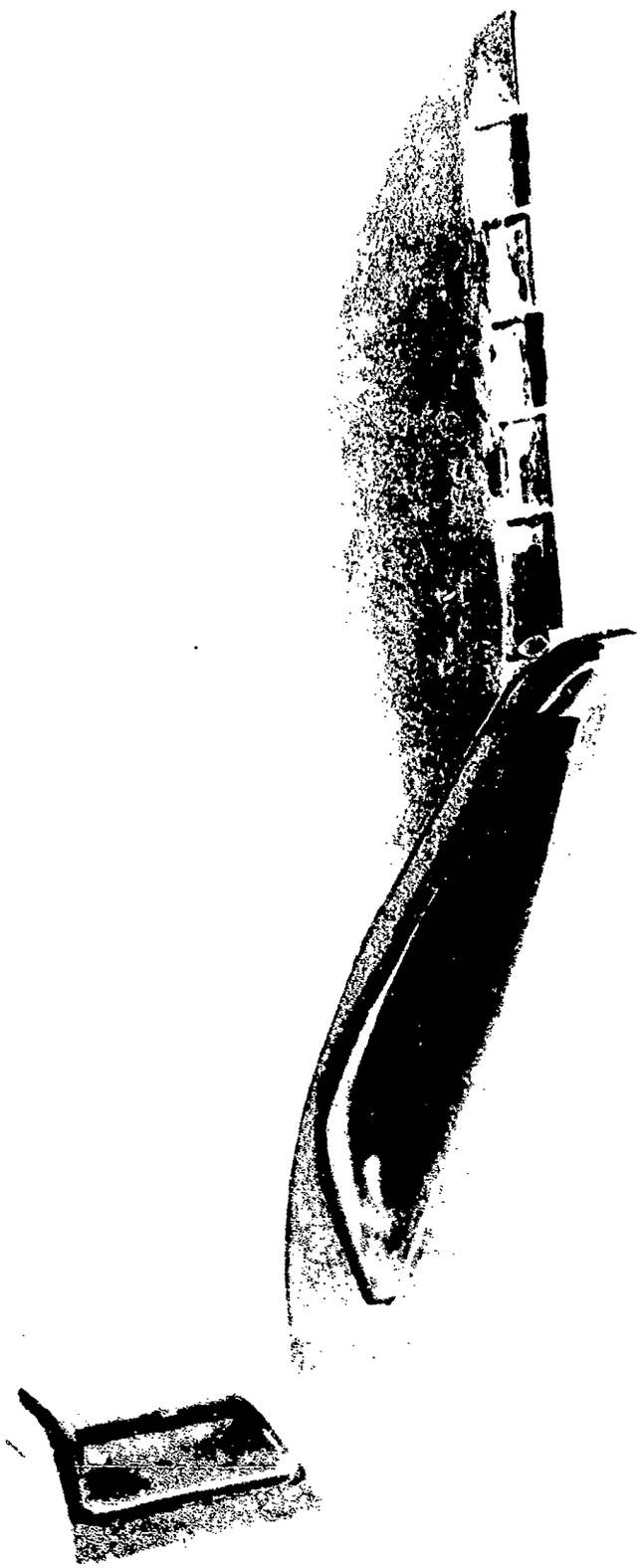

Figure 22. Primary and wall blowing nozzles from the area ratio 24 ejector[3]

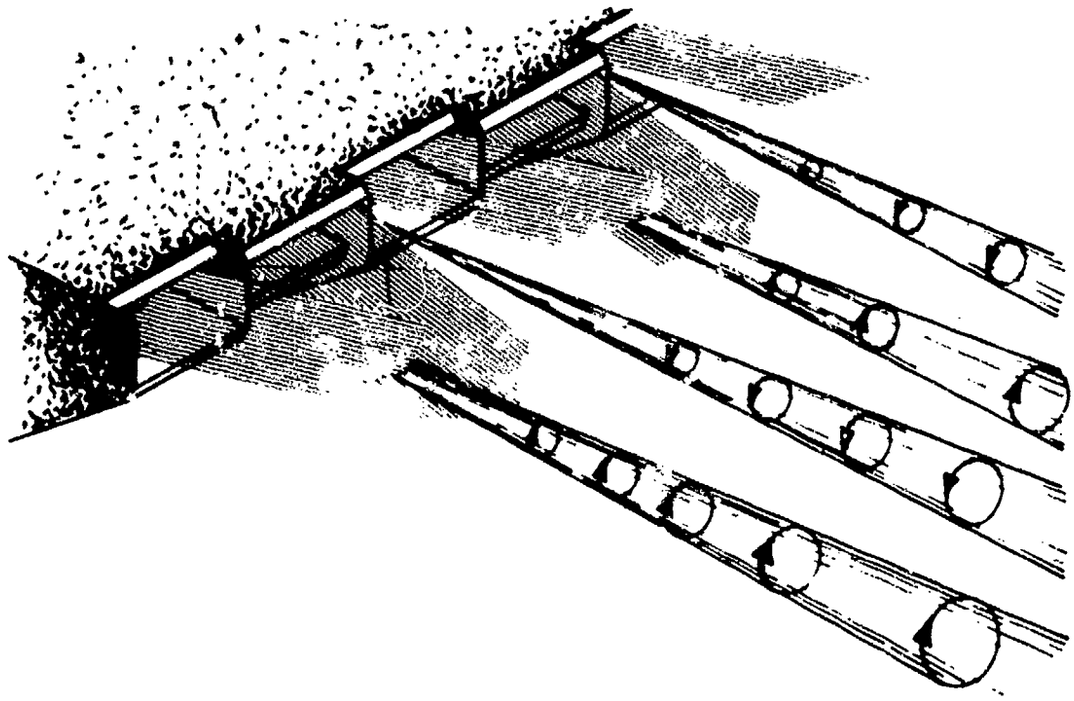

Figure 23. Schematic of the flow at the exit of a hypermixing nozzle[22]

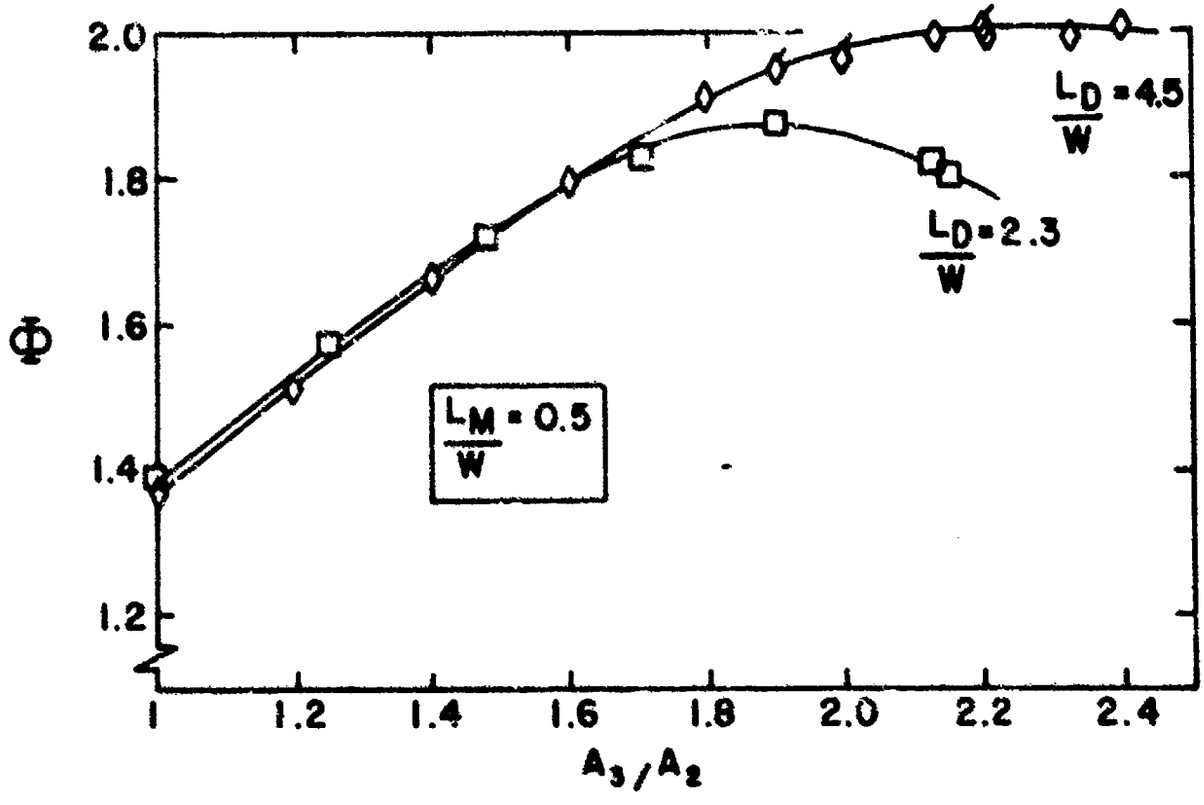

Figure 24. Performance of the area ratio 2.4 ejector[3], ◊ ,configuration F: □ , configuration C.

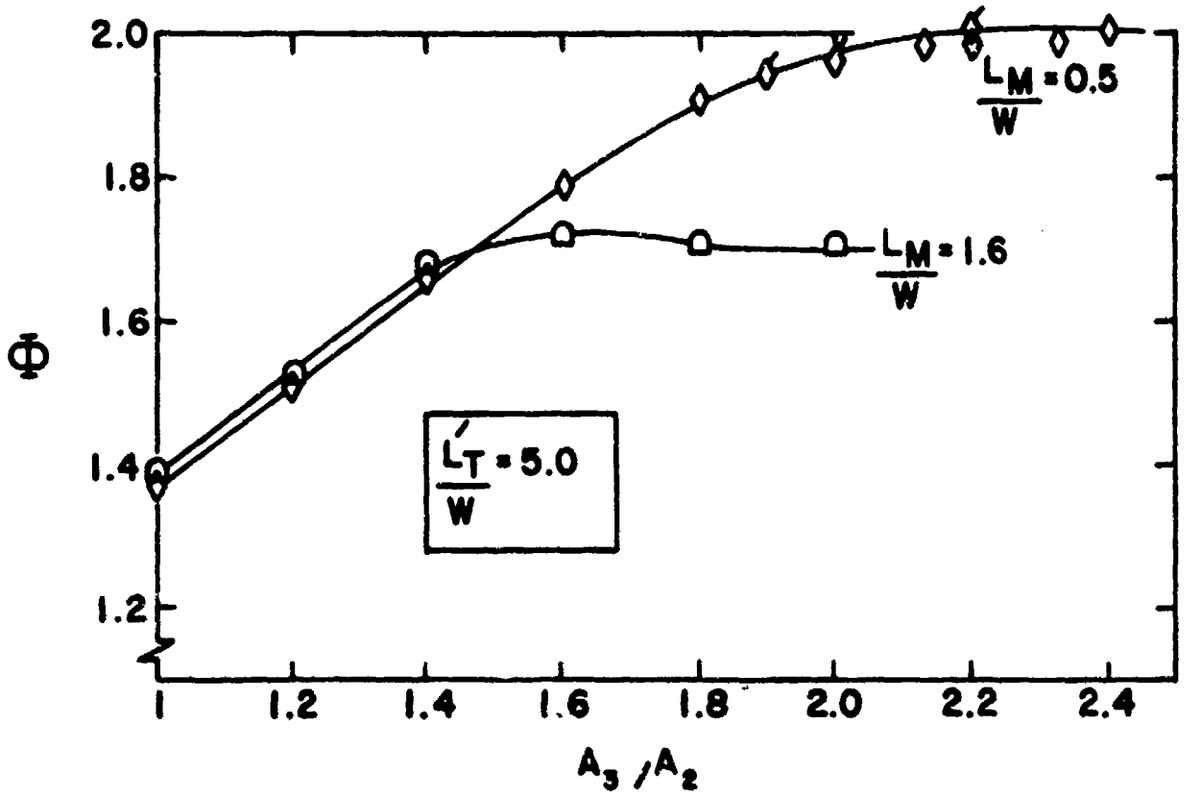

Figure 25. Performance of the area ratio 24 ejector[3], ◊, configuration F; ◻, configuration D.

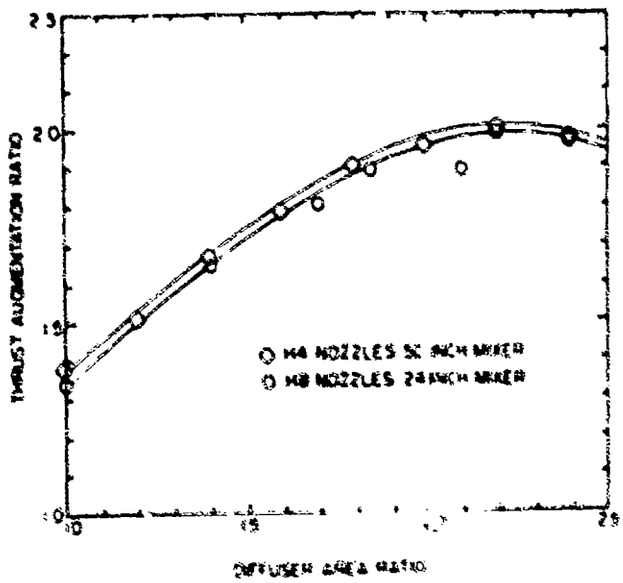

Figure 26. Performance of the area ratio 24 ejector[22], ◊, configuration F; ○, doubling the elemental aspect ratio of the hypermixing nozzle.

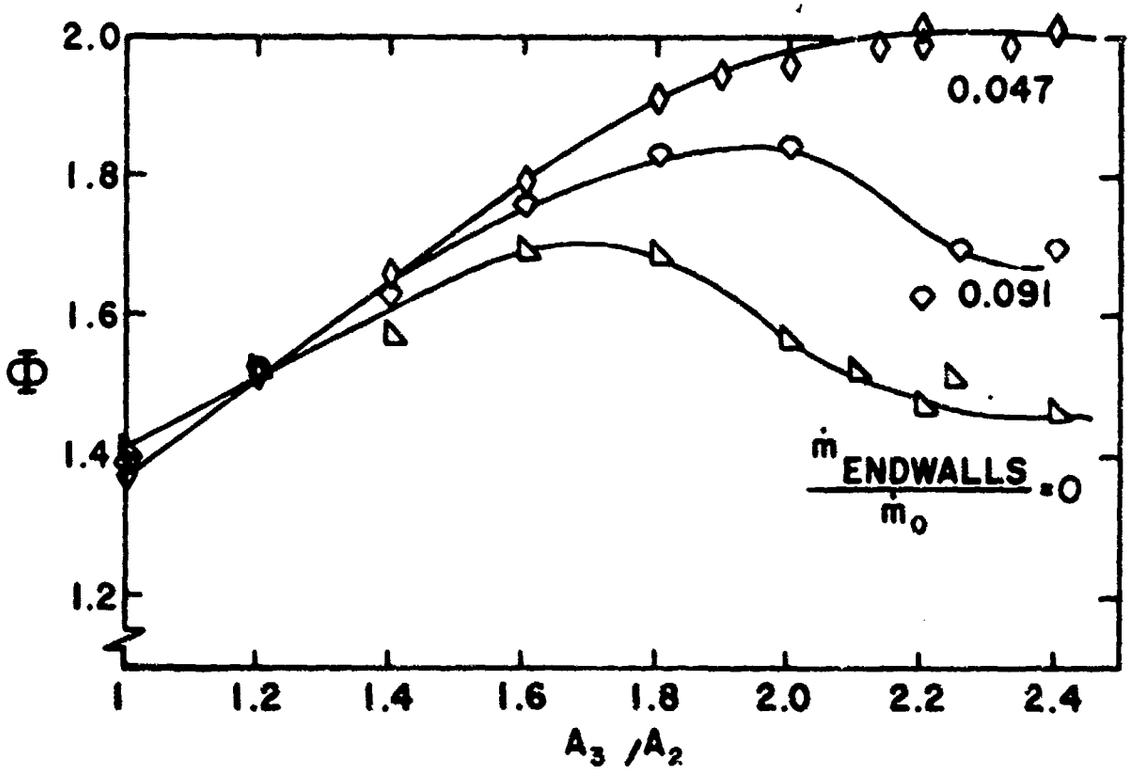

Figure 27. Effect of the manner and degree of endwall blowing on the performance of the area ratio 24 ejector[1]

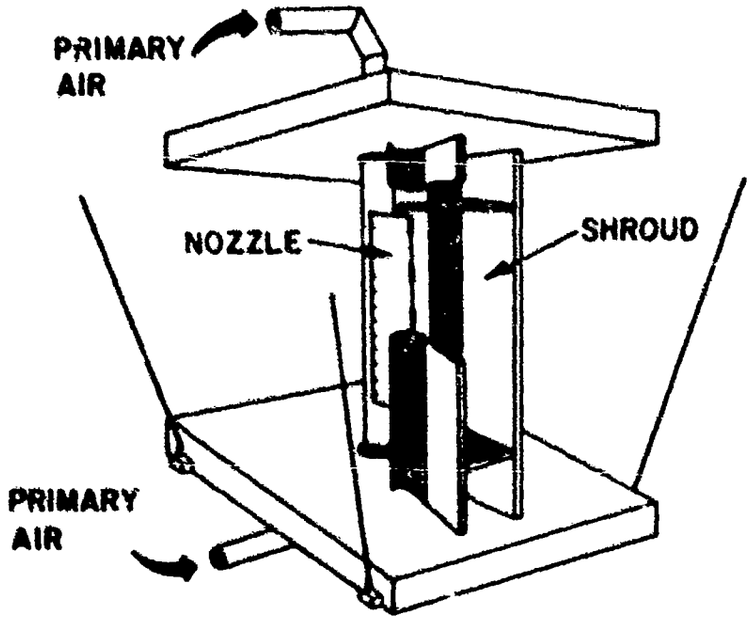

Figure 28. A cut-away view of the area ratio 8 ejector flap experiment[23].

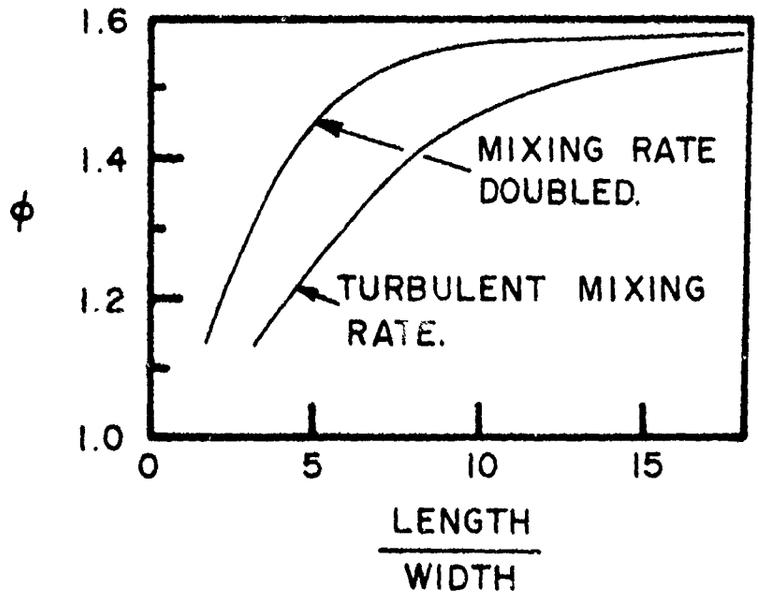

Figure 29. Estimate on performance of a doubling of the turbulent mixing rate[1]

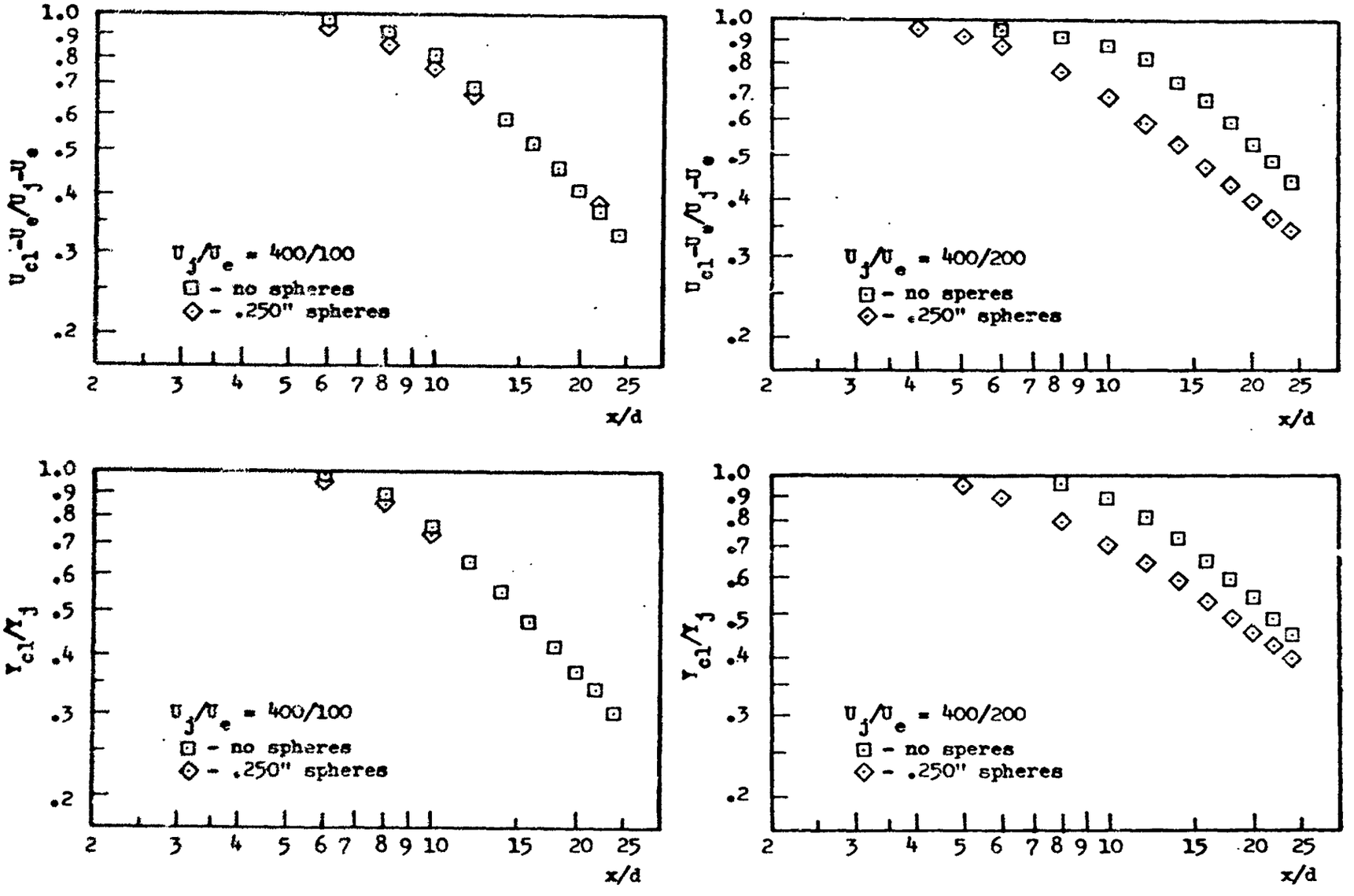

Figure 30. Effect of spherical turbulence generators on the velocity and concentration decays of axisymmetric jets in coflowing streams[28].

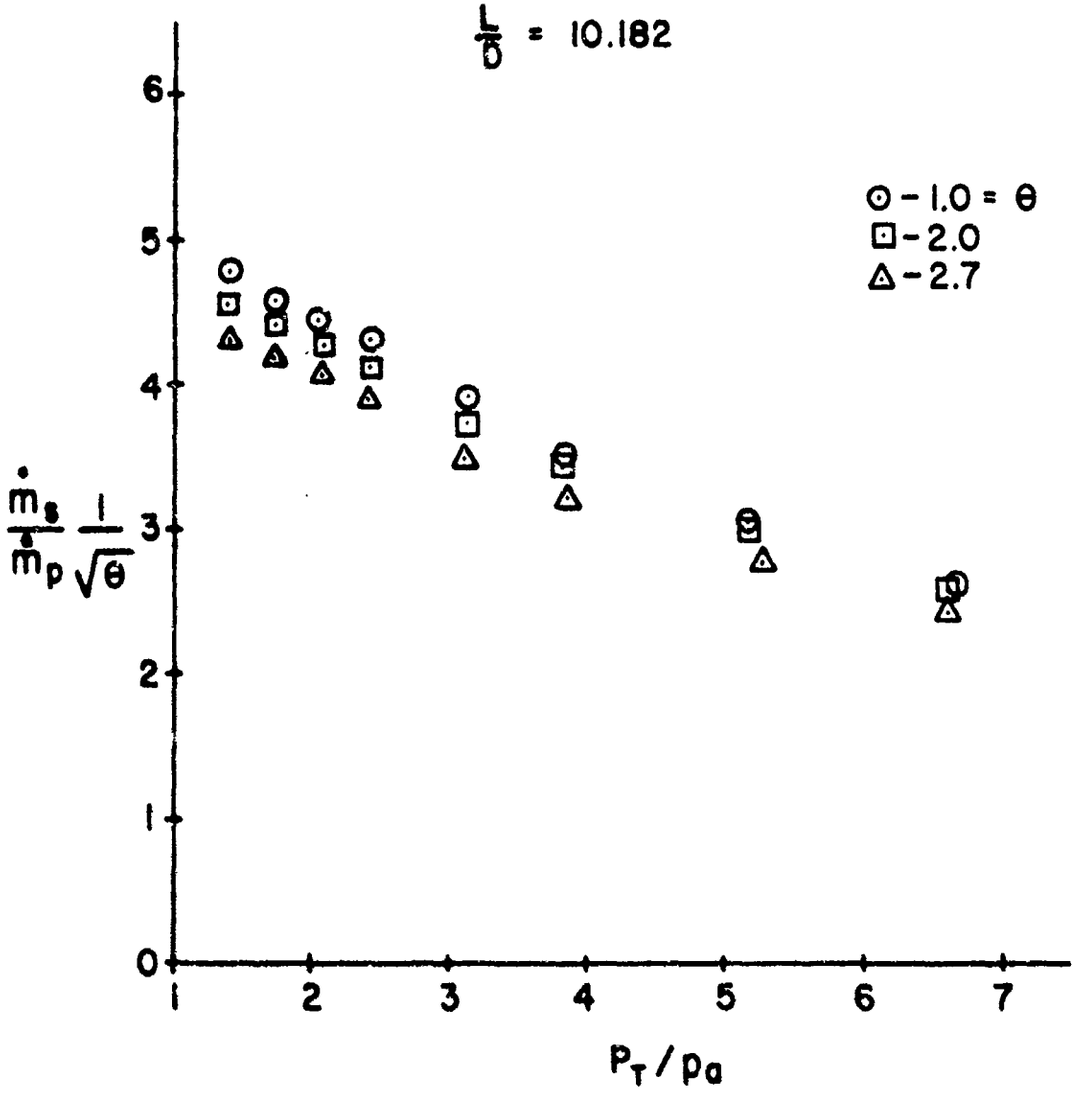

Figure 31. Effect of temperature on the mass flow through a long (L/D = 10.182) ejector[19]

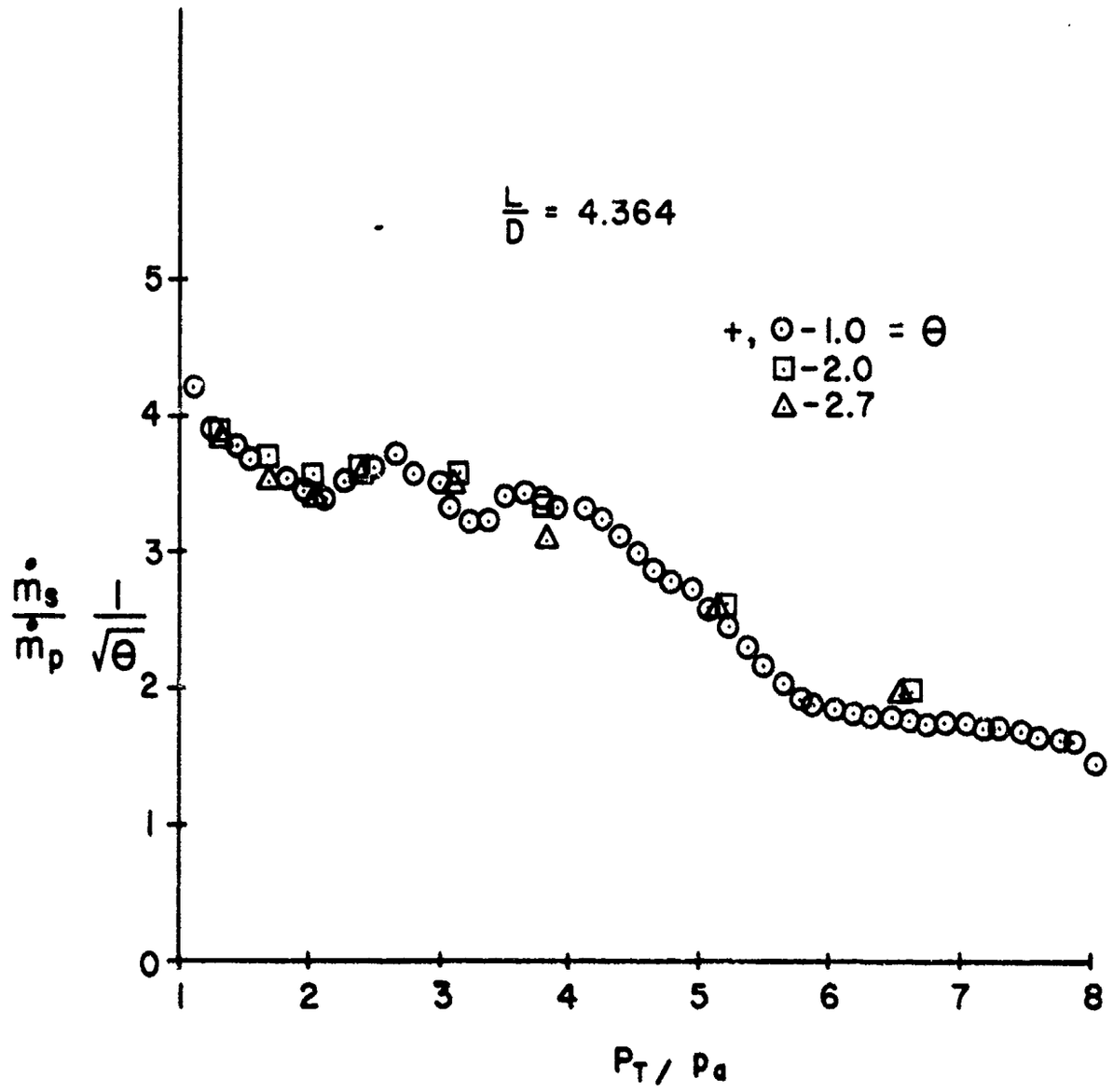

Figure 32. Effect of temperature on the mass flow through a short (L/D = 4.364) ejector[19]

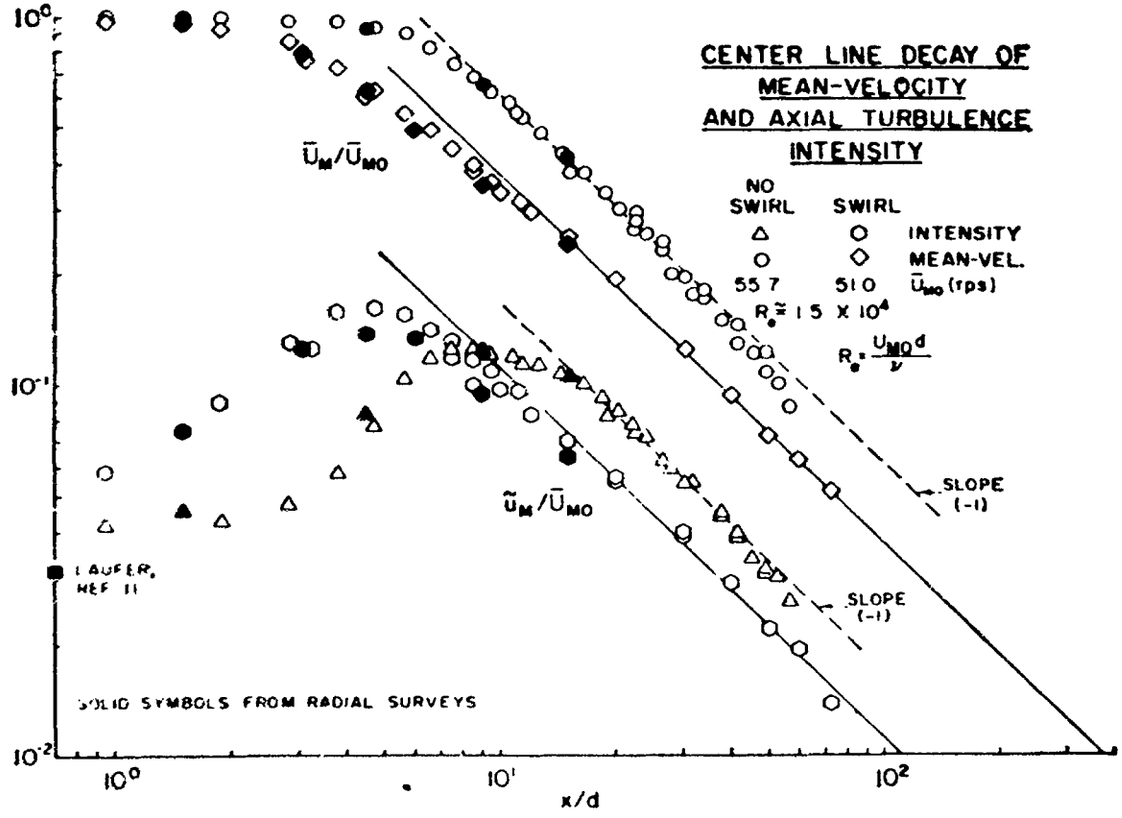

Figure 33. Effect of swirl on jet spread and decay of the maximum swirl velocity[35]

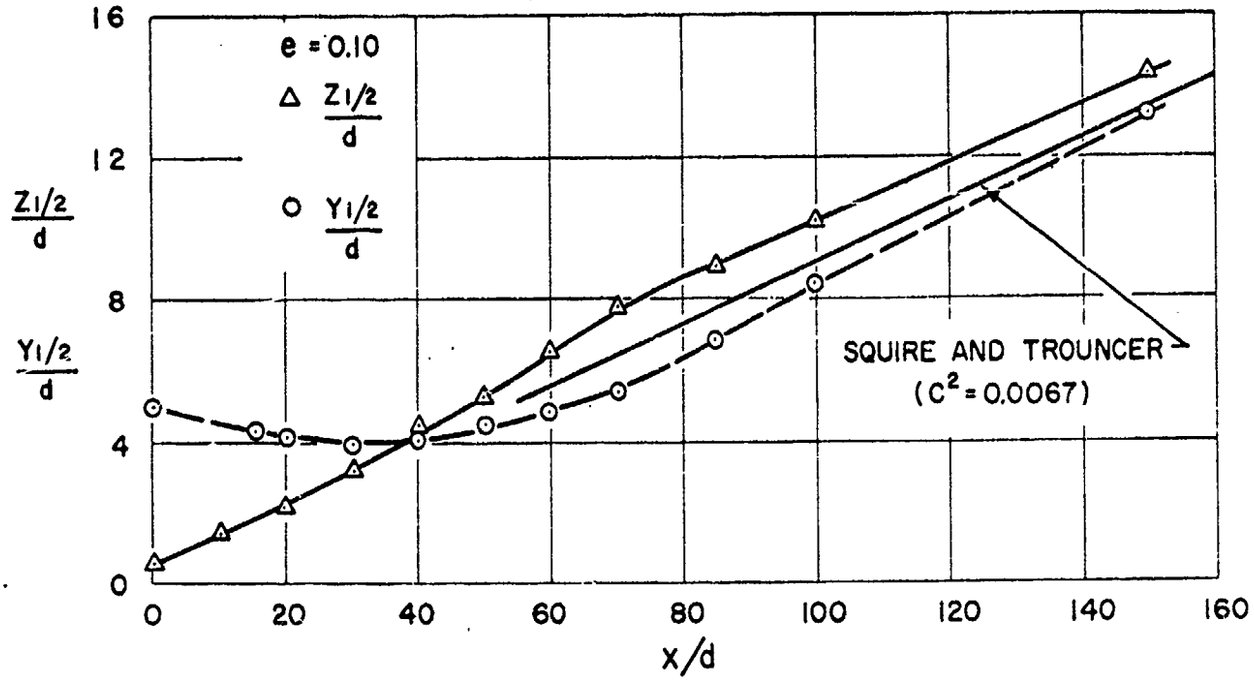

Figure 34. Halfwidth growths in major and minor axis directions for a rectangular slot of aspect ratio 10[37]

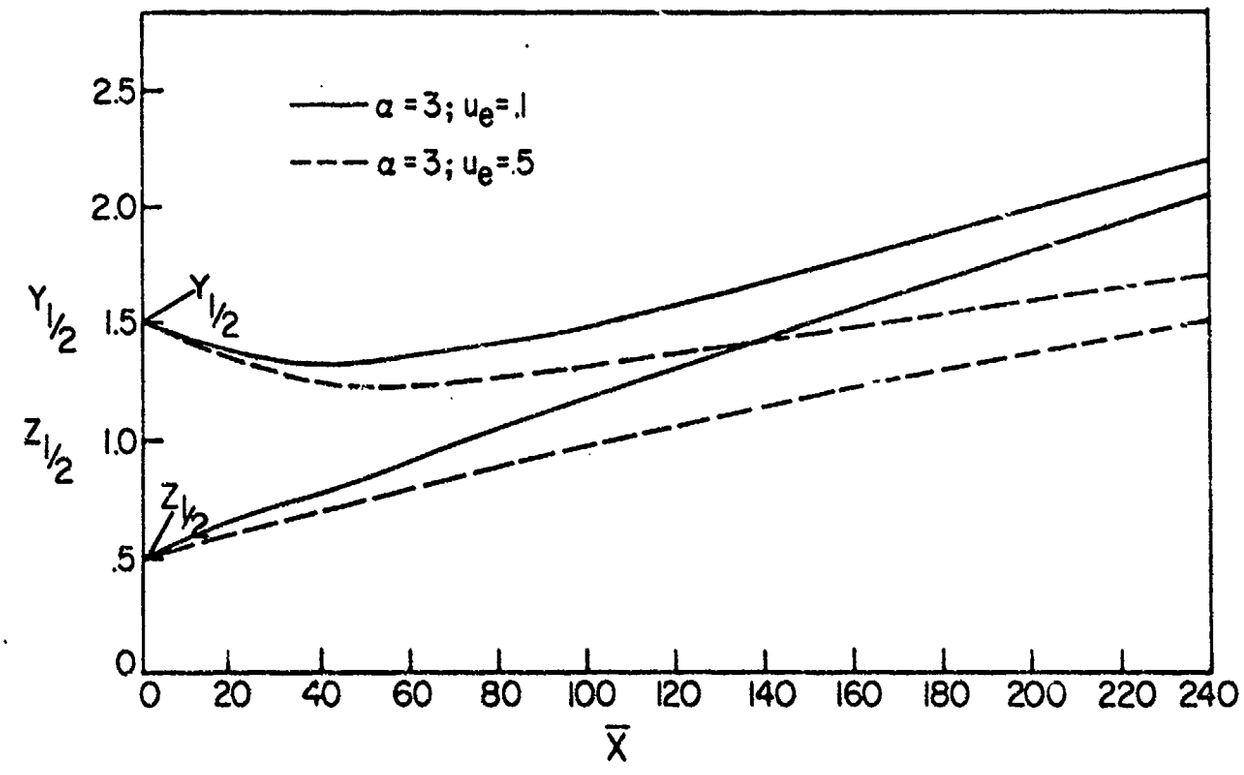

Figure 35. Effect of aspect ratio and coflowing stream on the growth of a laminar elliptical jet[38]

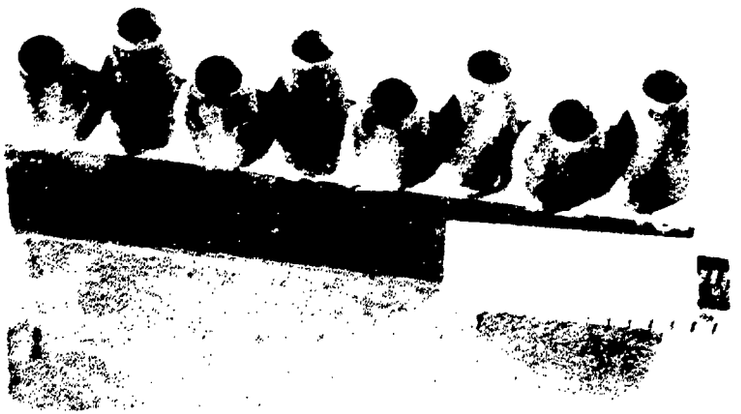

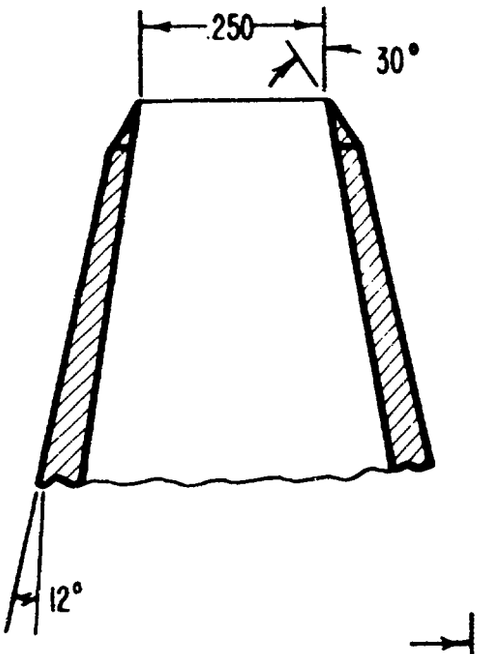

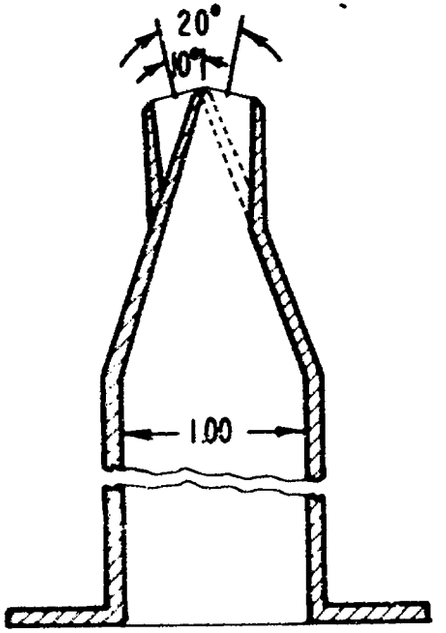

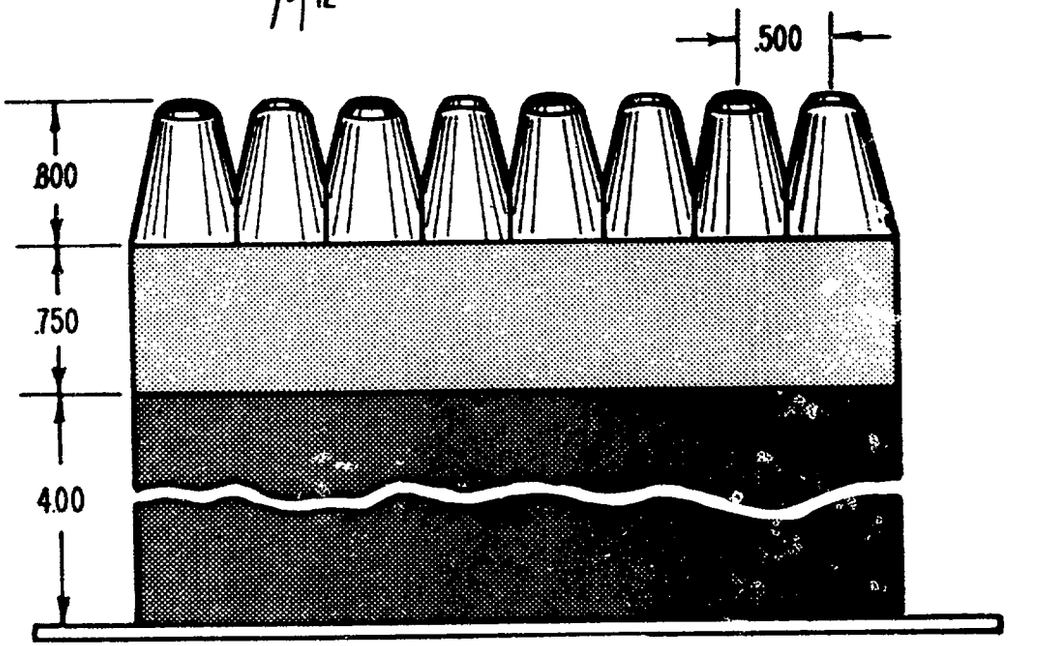

Figure 36. Alernating cone nozzle[46]

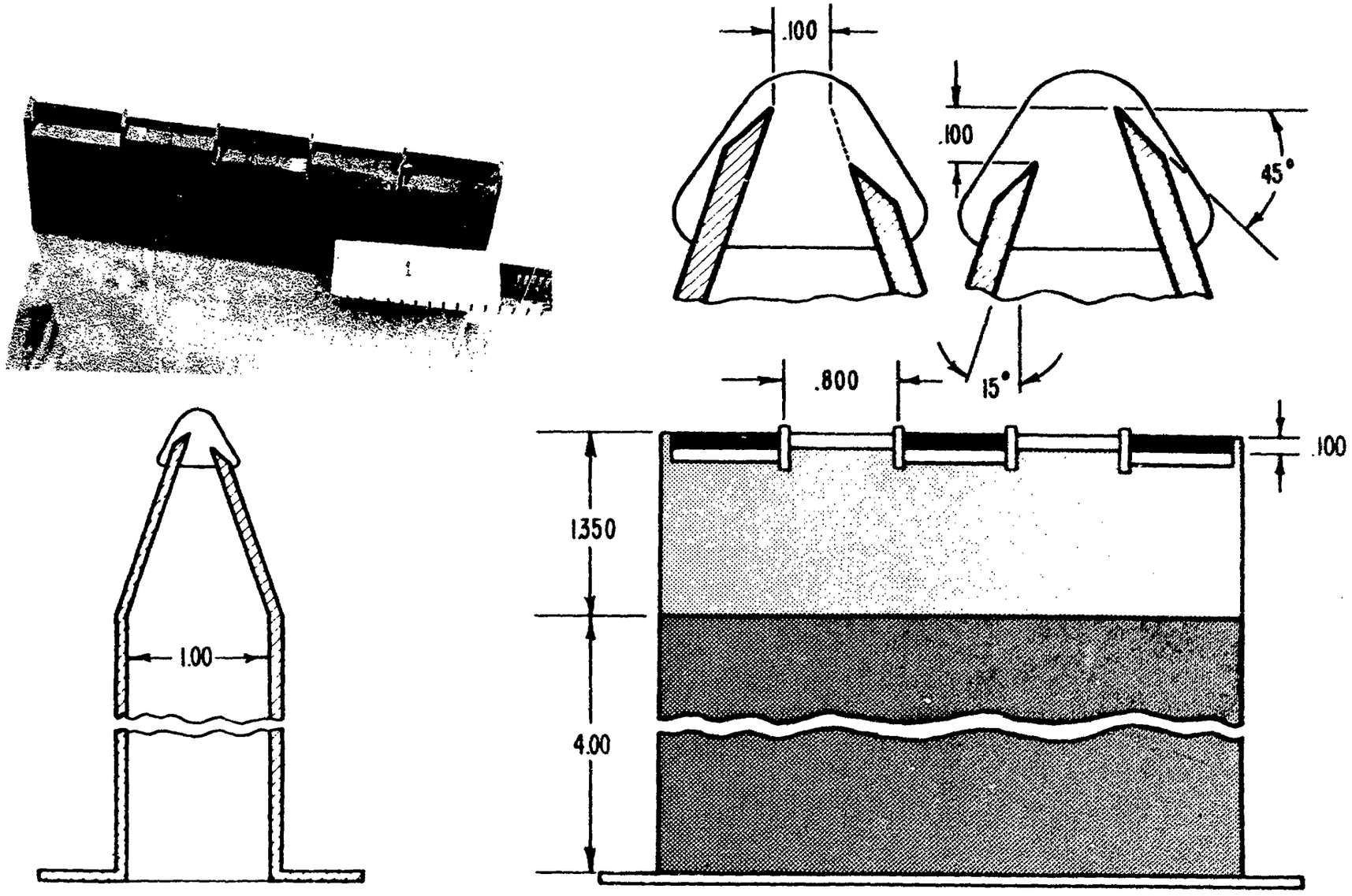

Figure 37. Alternating exit (hypermixing) nozzle[46]

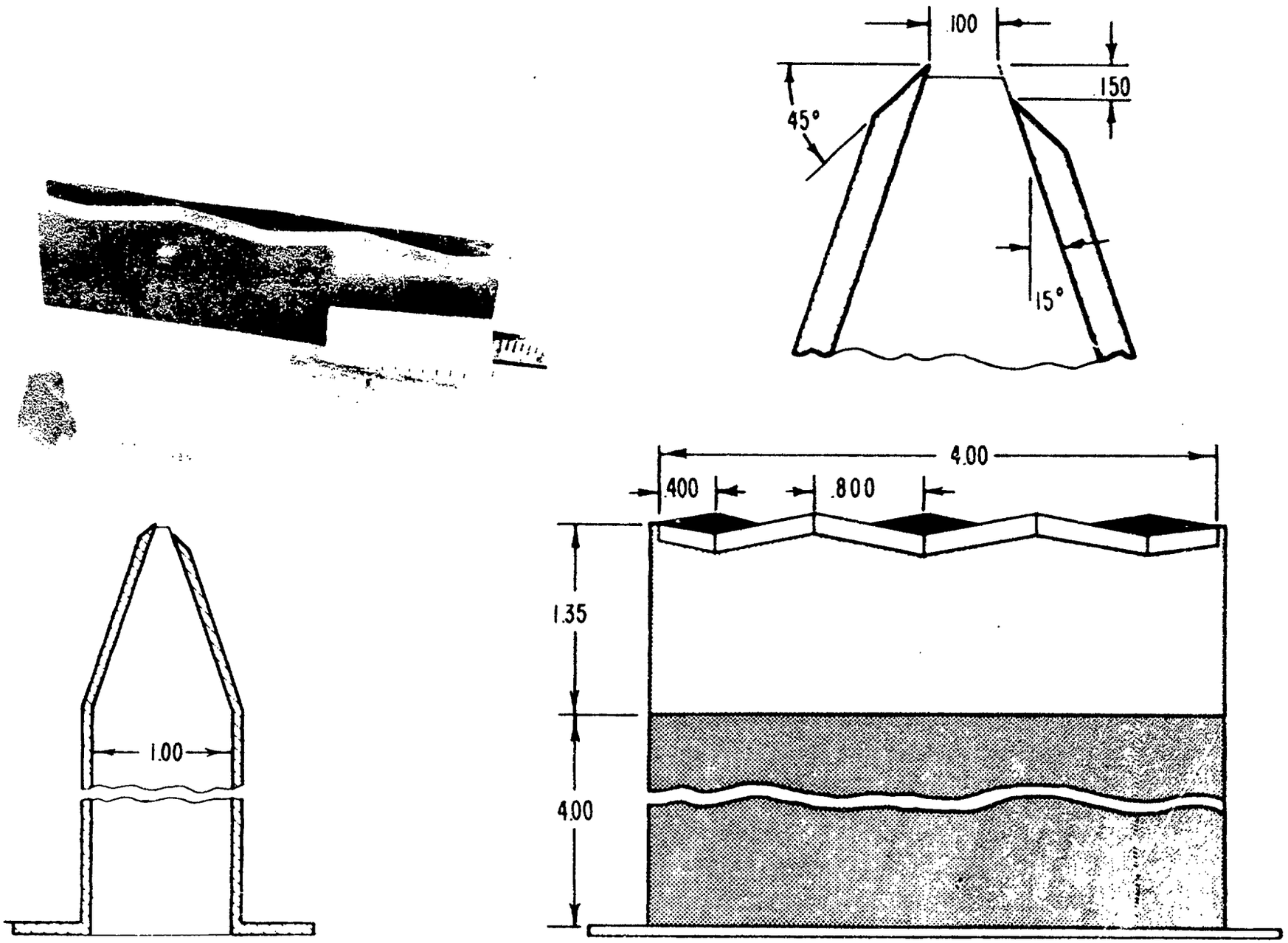

Figure 38. Scalloped exit nozzle[46]

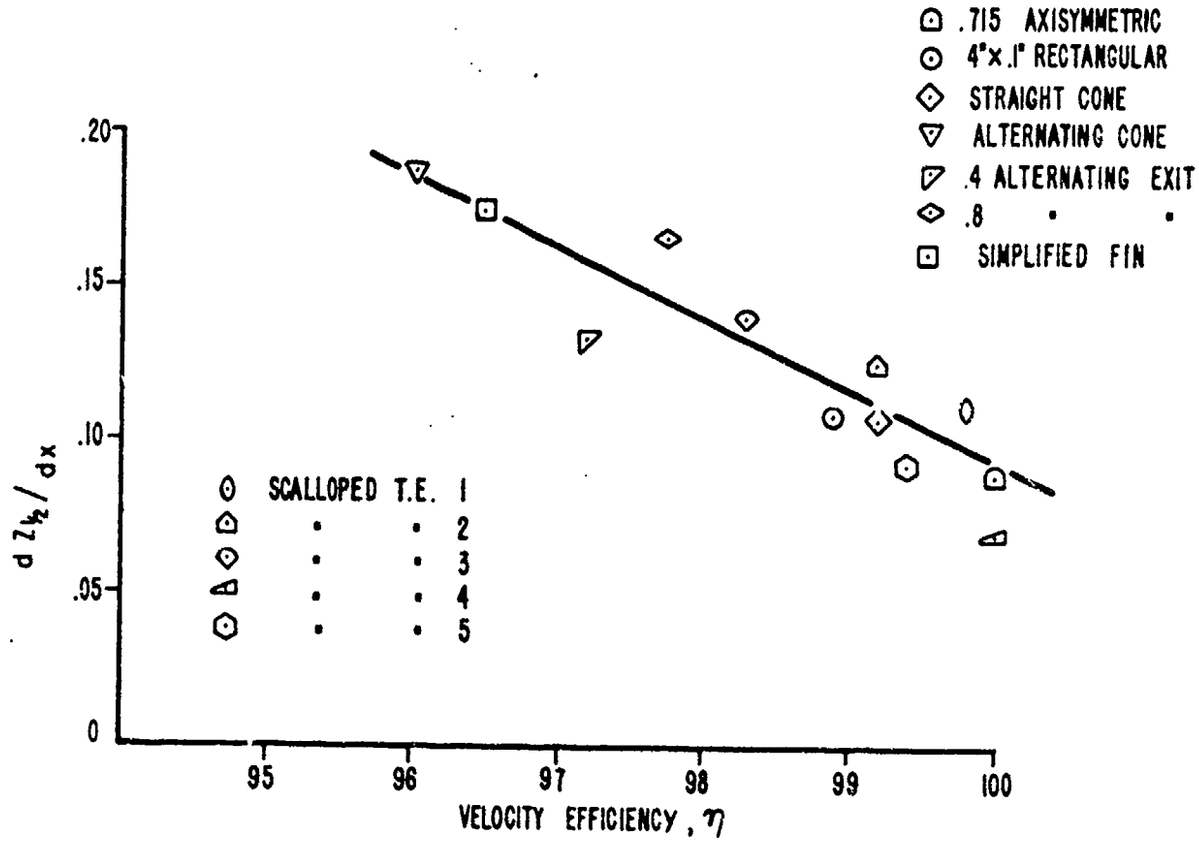

Figure 39. Tradeoff between the spreading rate and nozzle efficiency[46]

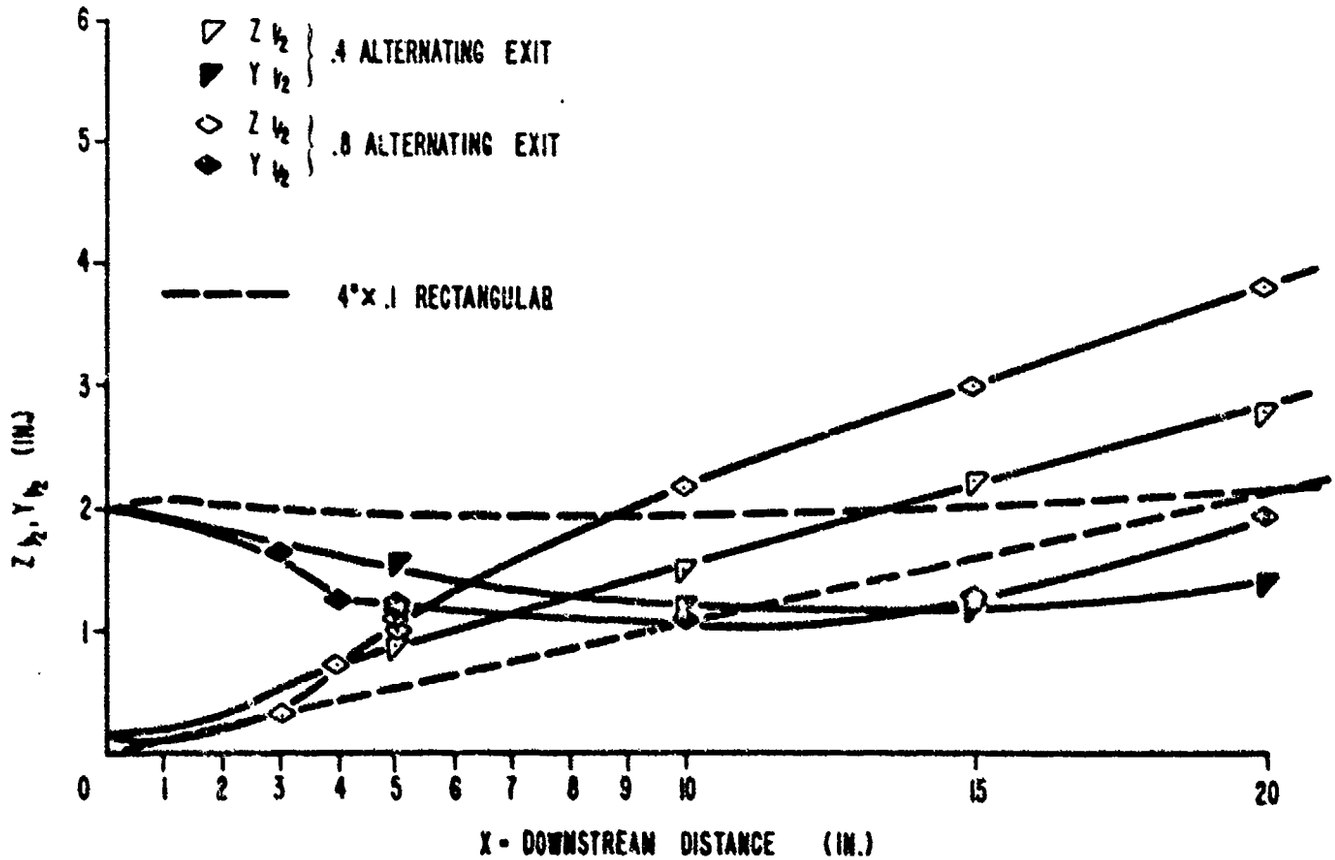

Figure 40. Comparison of halfwidth growths of hypermixing and rectangular slot nozzles[46]

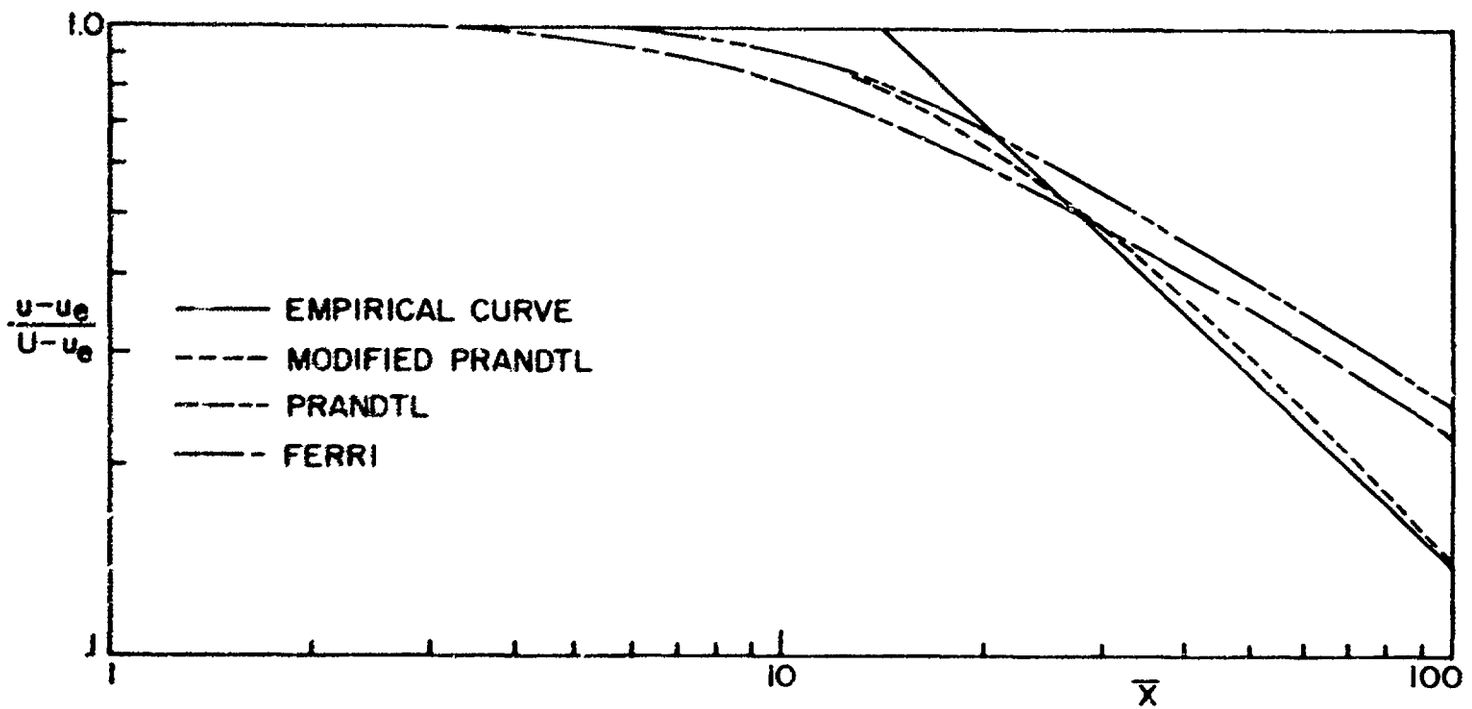

Figure 41. Axial velocity decay predictions of several eddy viscosity models[55]

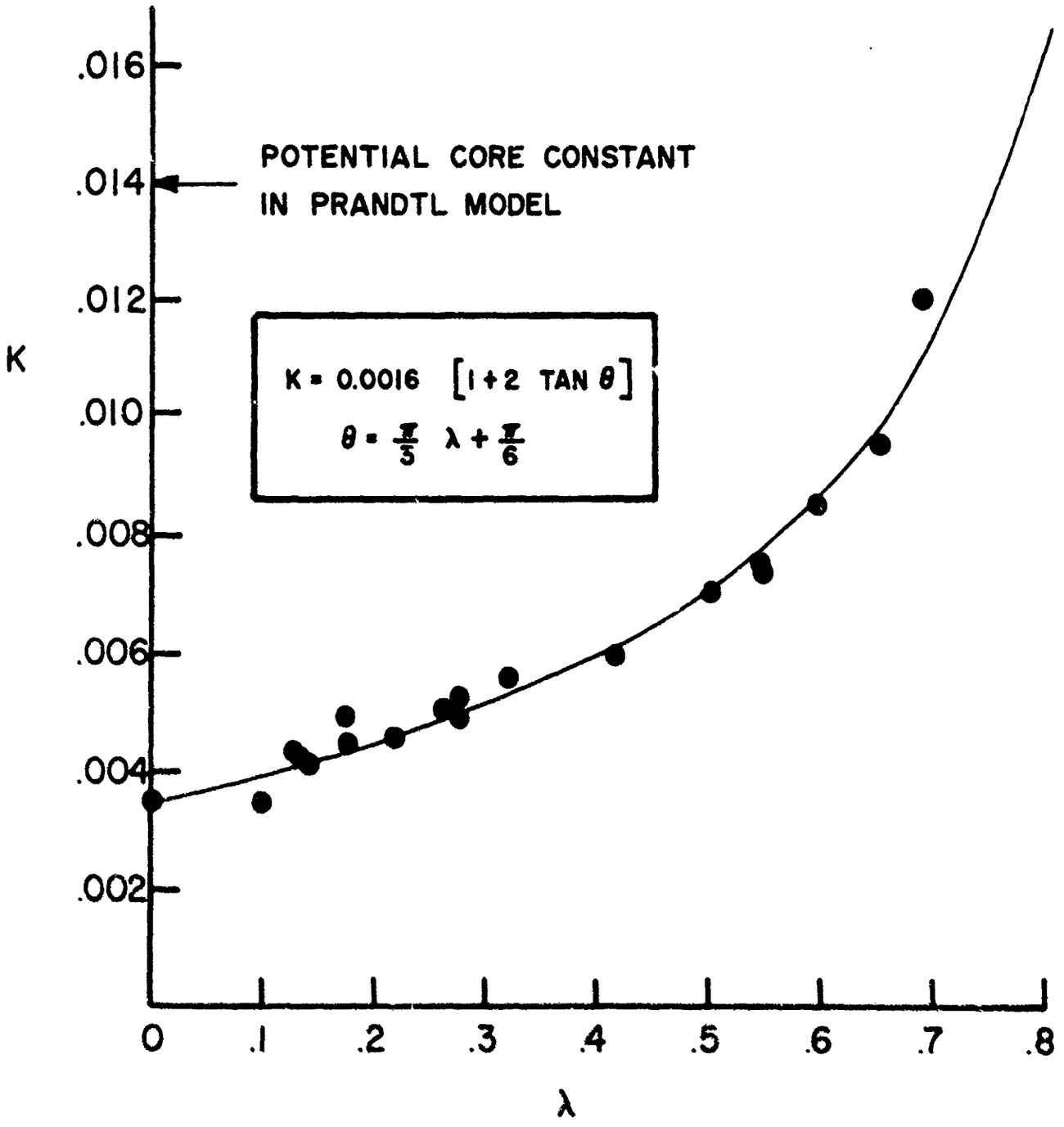

Figure 42. Variation of constant within the potential core of the compressible modified Prandtl model[57]

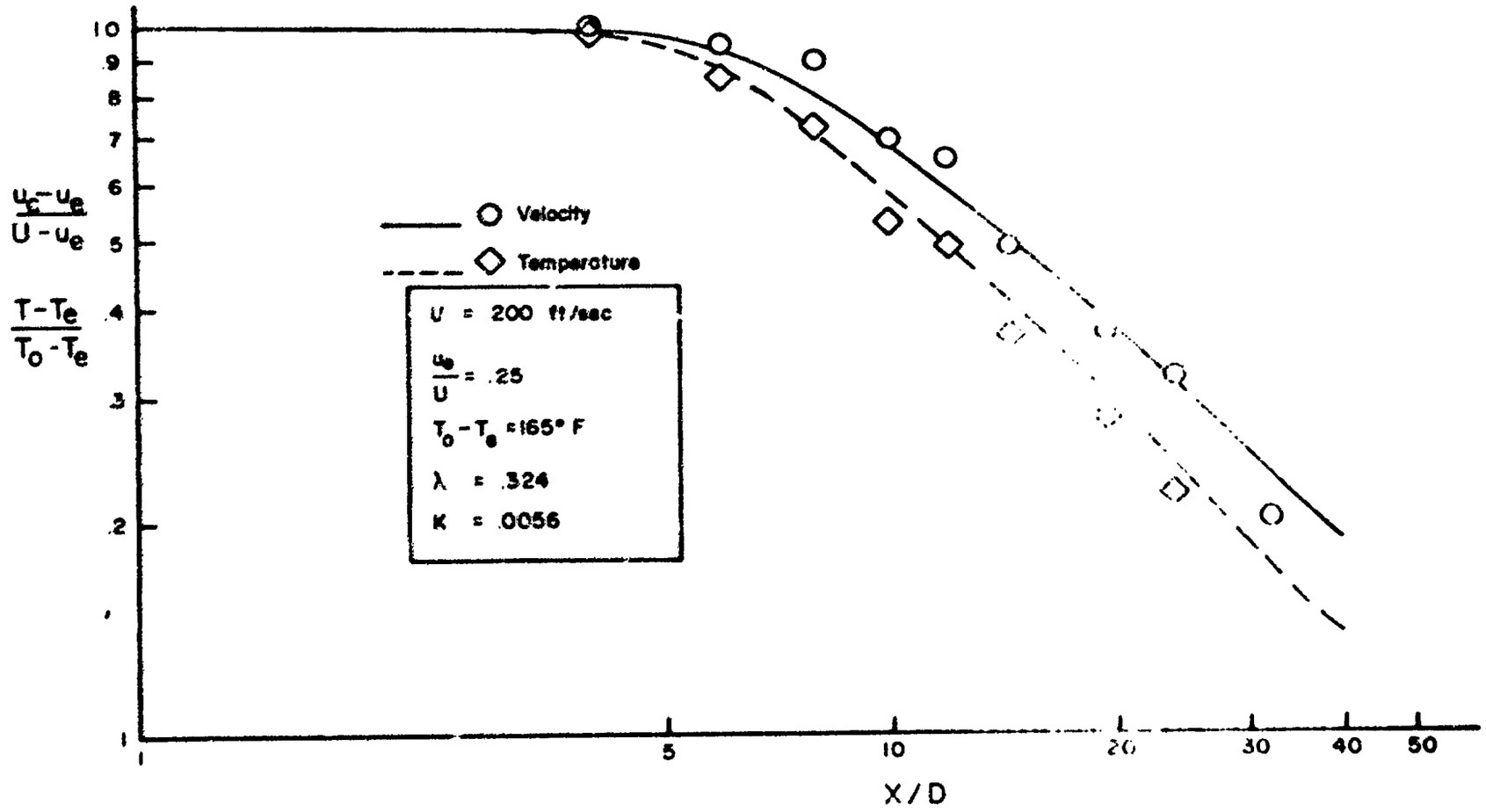

Figure 43. Comparison of compressible Prandtl model predictions with heated jet data

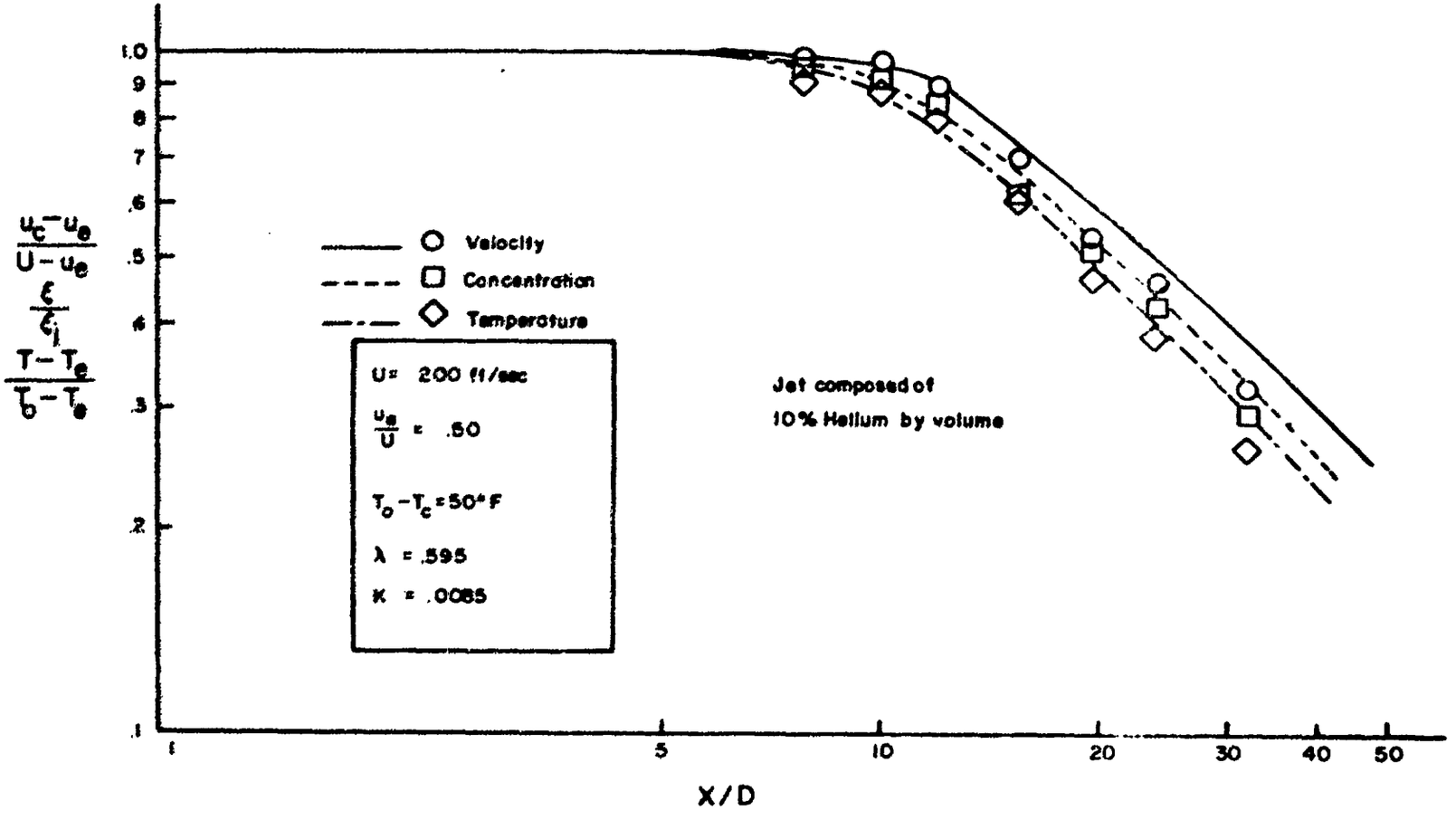

Figure 44. Comparison of compressible Prandtl model predictions with heated jet of diverse composition[57]

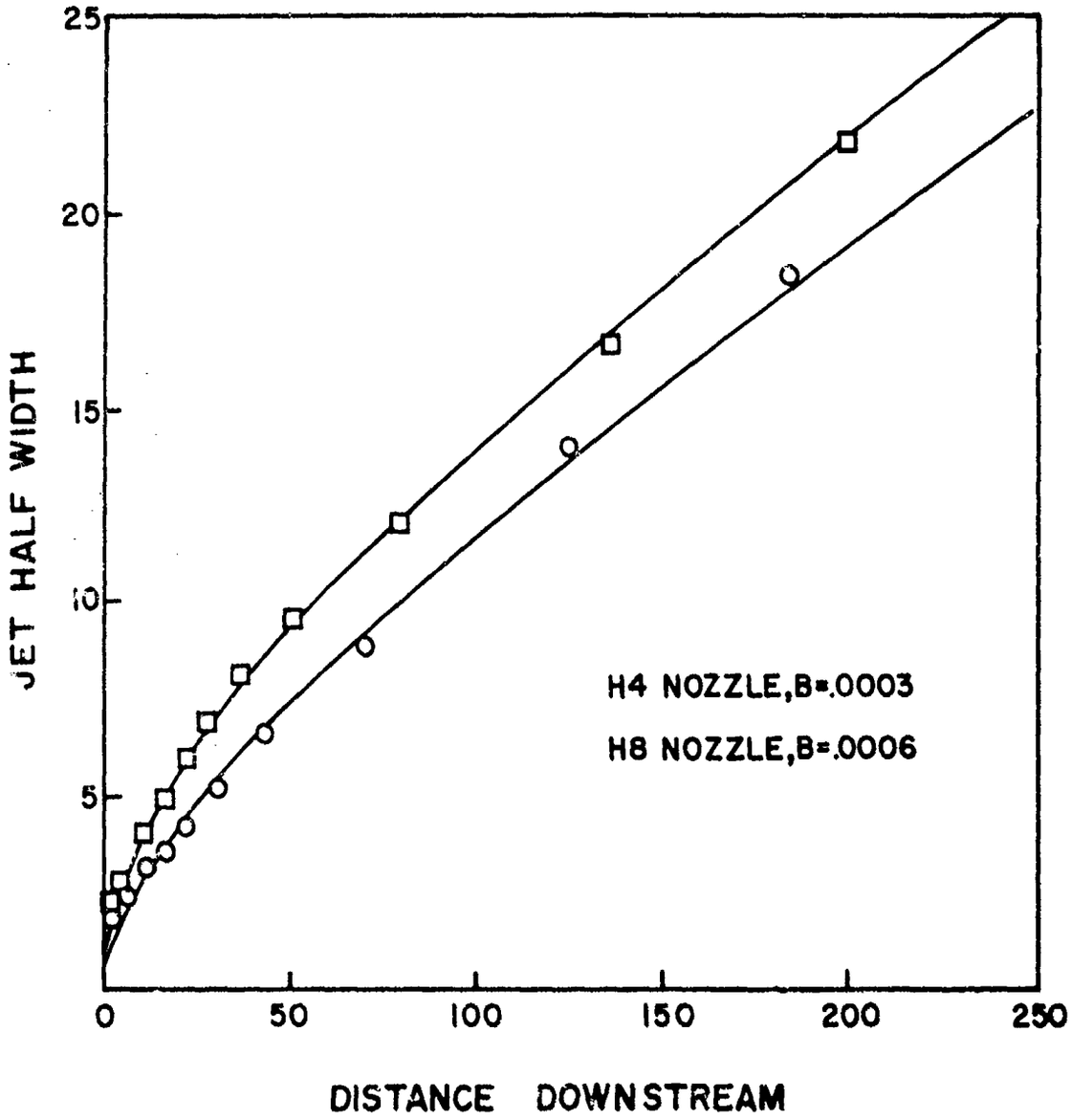

Figure 45. Comparison of predictions of hypermixing model with experiment[22]

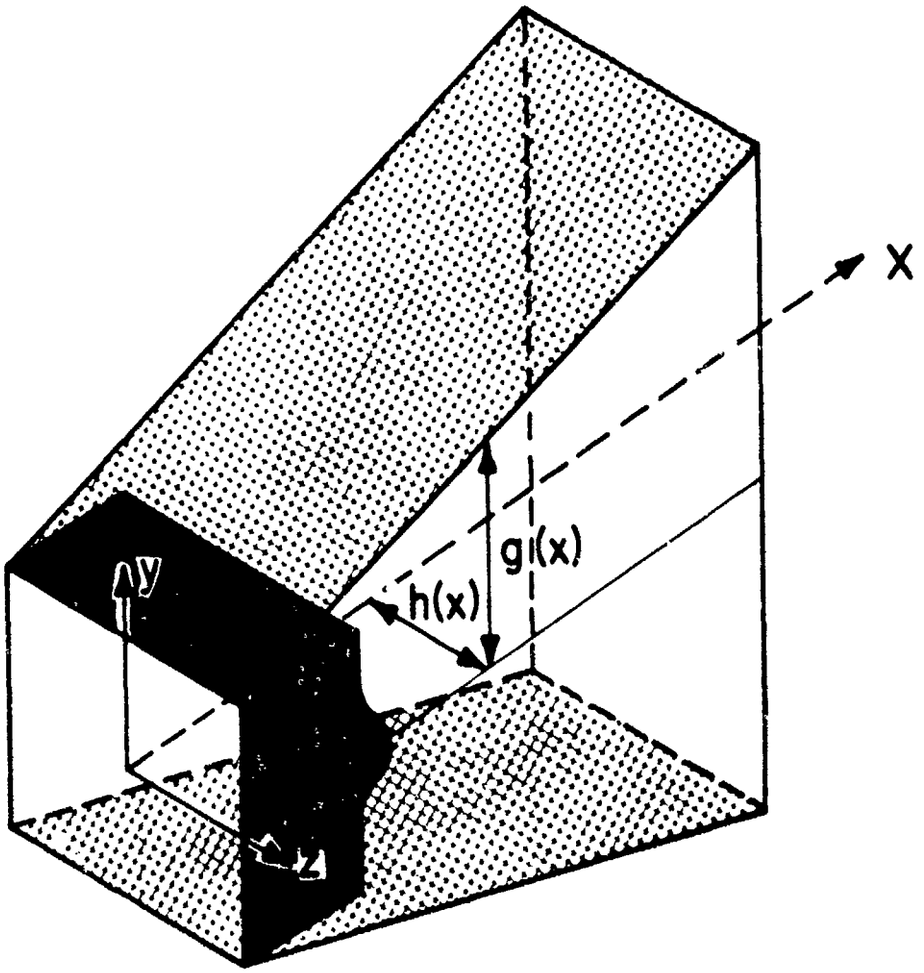

Figure 46. A traditional manner of diffusion[63]

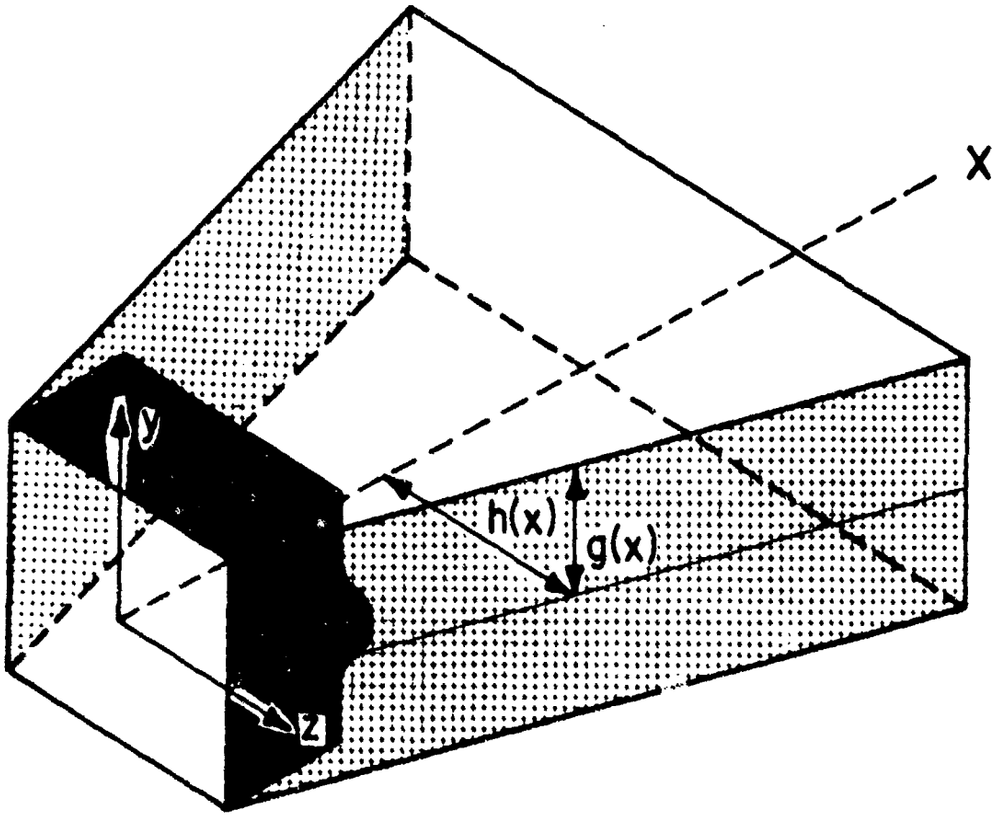

Figure 47. Diffusion out of the plane of the velocity profile[63]

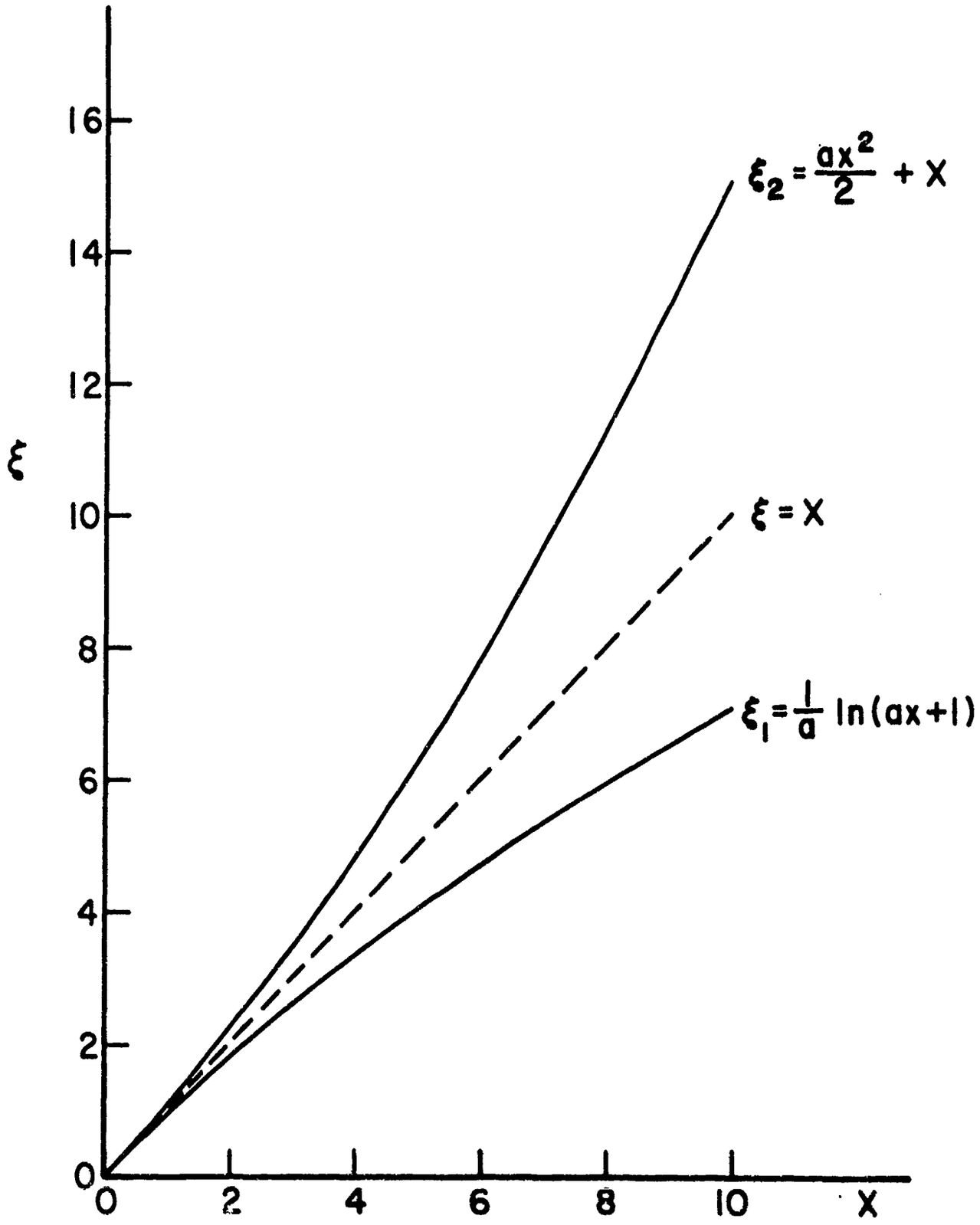

Figure 48. Effect of direction on the transformation of the linearized diffuser problem[63]

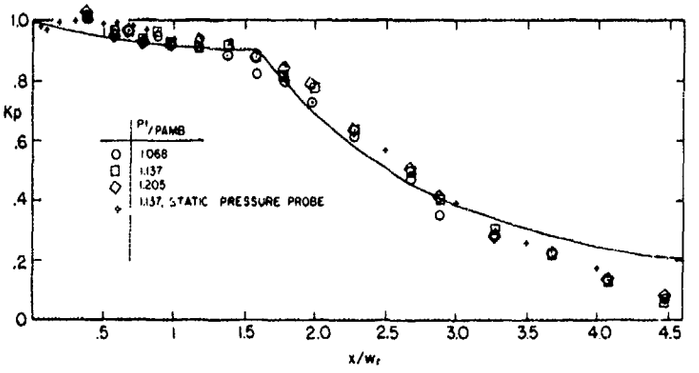

Pressure rise through the ejector. Configuration II, θ = 8.36 deg, V_1/V_0 = 0.338.

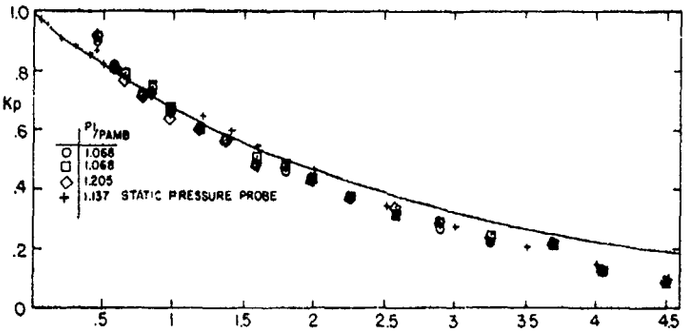

Pressure rise through the ejector. Configuration I, θ = 2.44 deg. V_1/V_0 = 0.258.

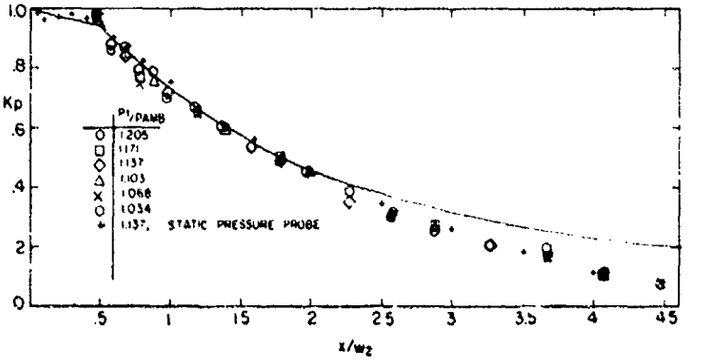

Pressure rise through the ejector. Configuration I, θ = 6.33 deg. V_1/V_0 = 0.345.

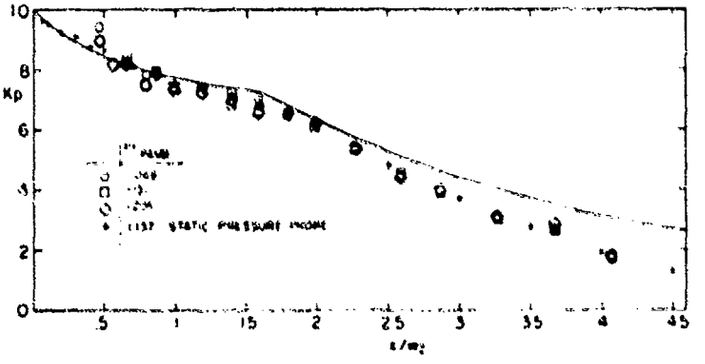

Pressure rise through the ejector. Configuration II, θ = 3.34 deg. V_1/V_0 = 0.261

Figure 49. Comparison of predicted pressure coefficient and experiment for highly skewed flow in ducts

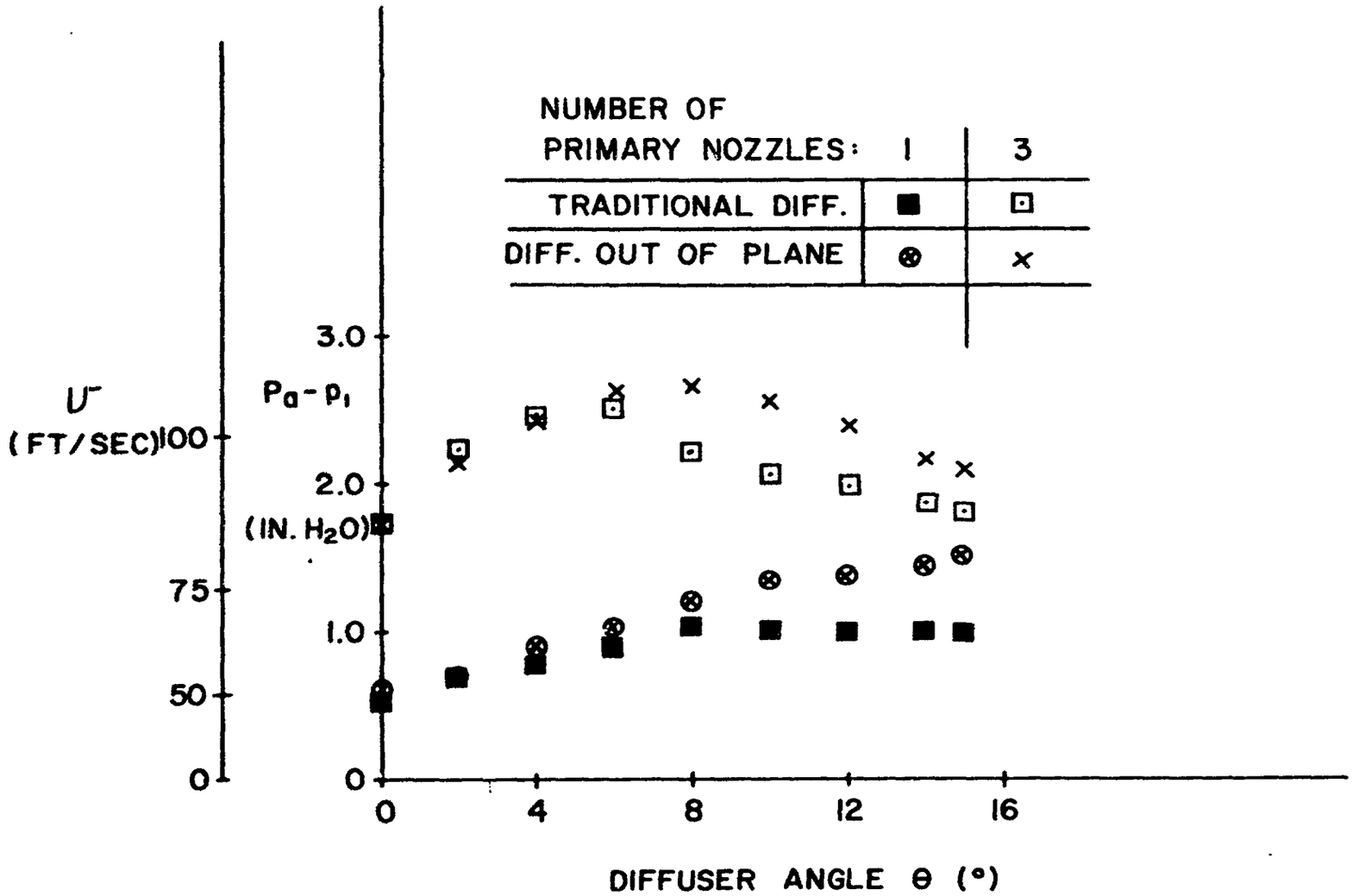

Figure 50. Effect of the diffusion direction on the secondary flow entrained into an experimental diffuser[67]

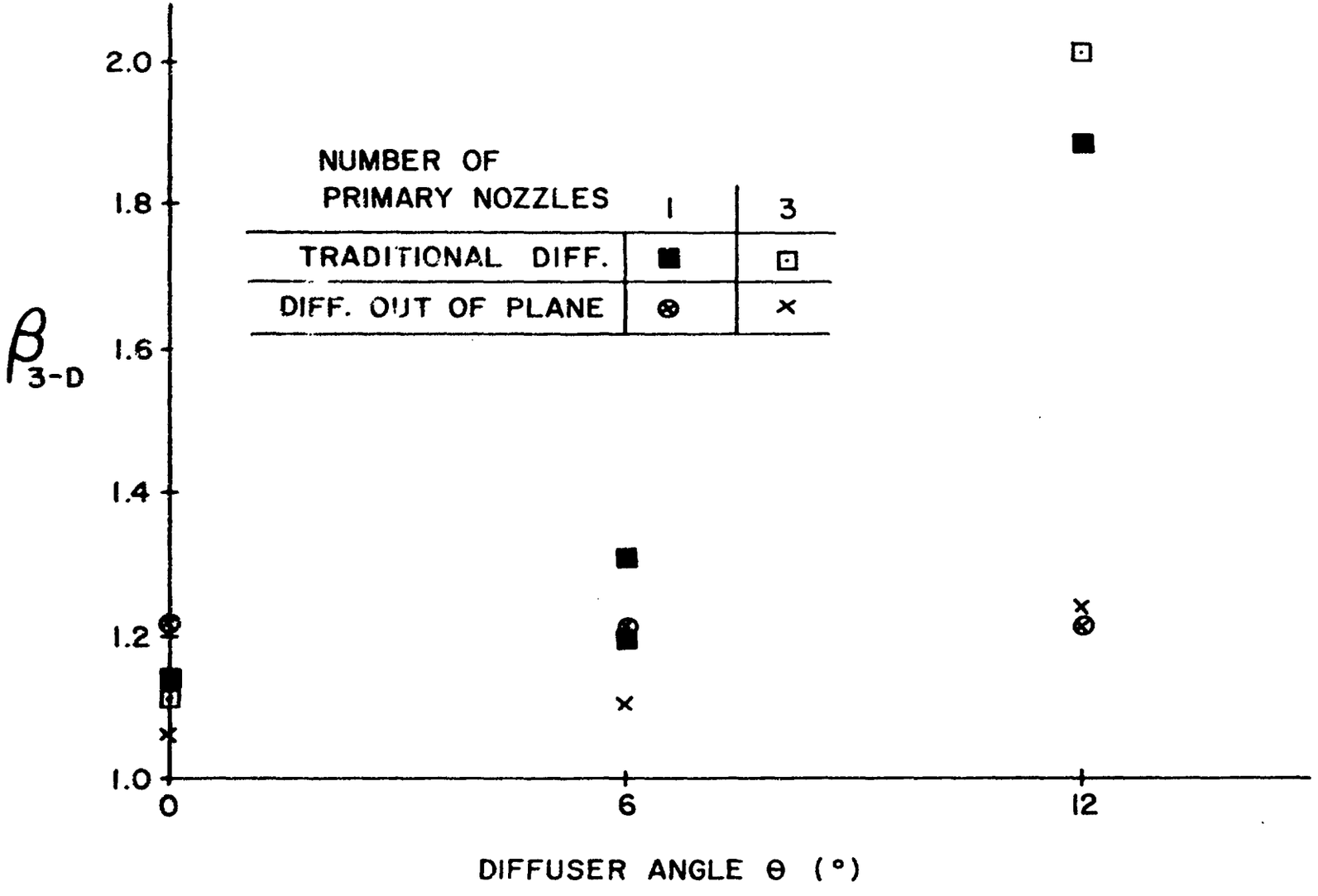

Figure 51. Effect of diffusion direction on the skewness of the exit profile[67]

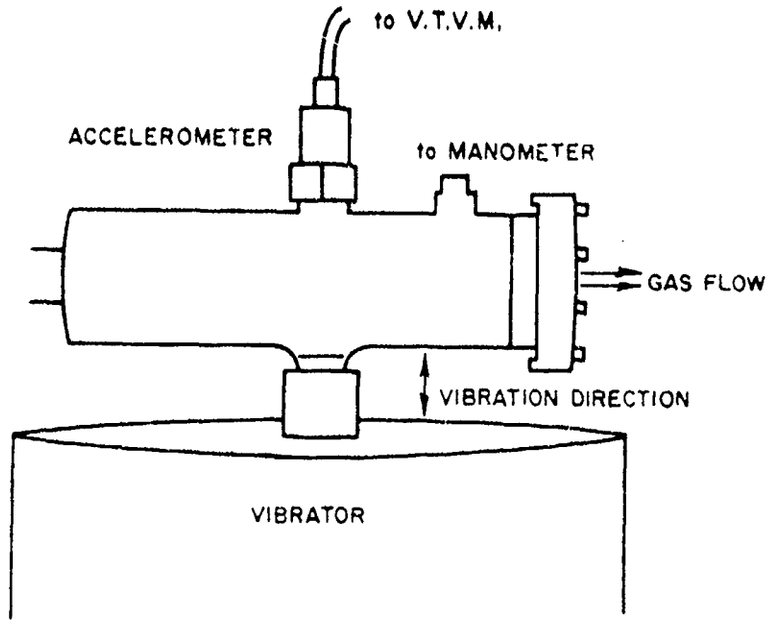

Figure 52. Schematic of vibrating jet flow[71]

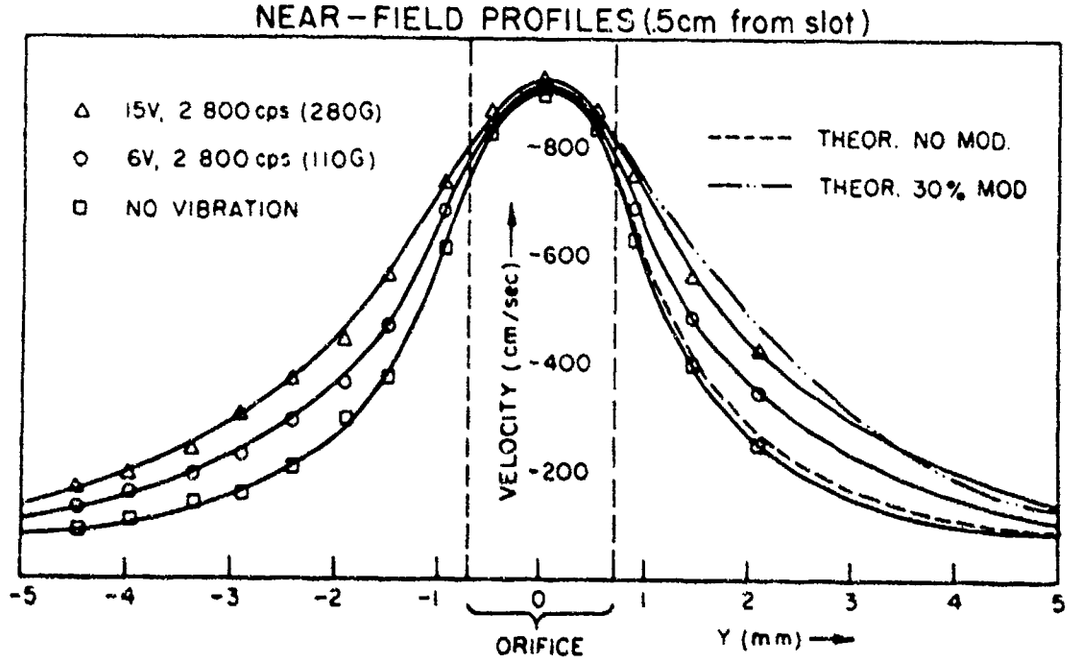

Figure 53. Near field profiles in the vibrating jet[71]

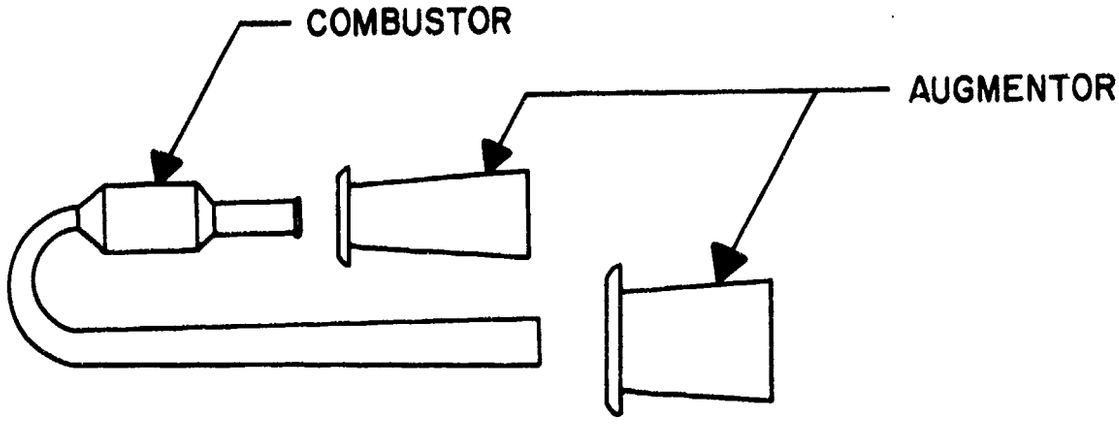

Figure 54. Schematic of a Pulse Jet[73]

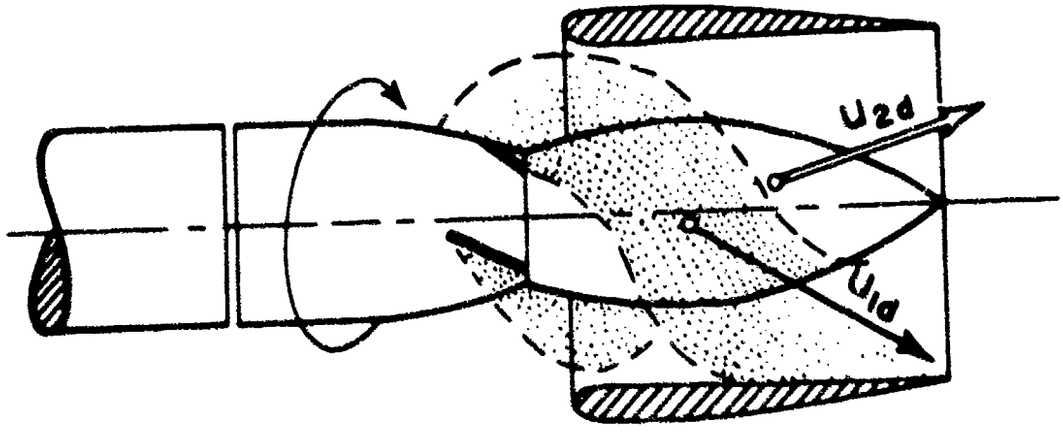

Figure 55. Schematic of the Foa concept axial flow interaction[75]

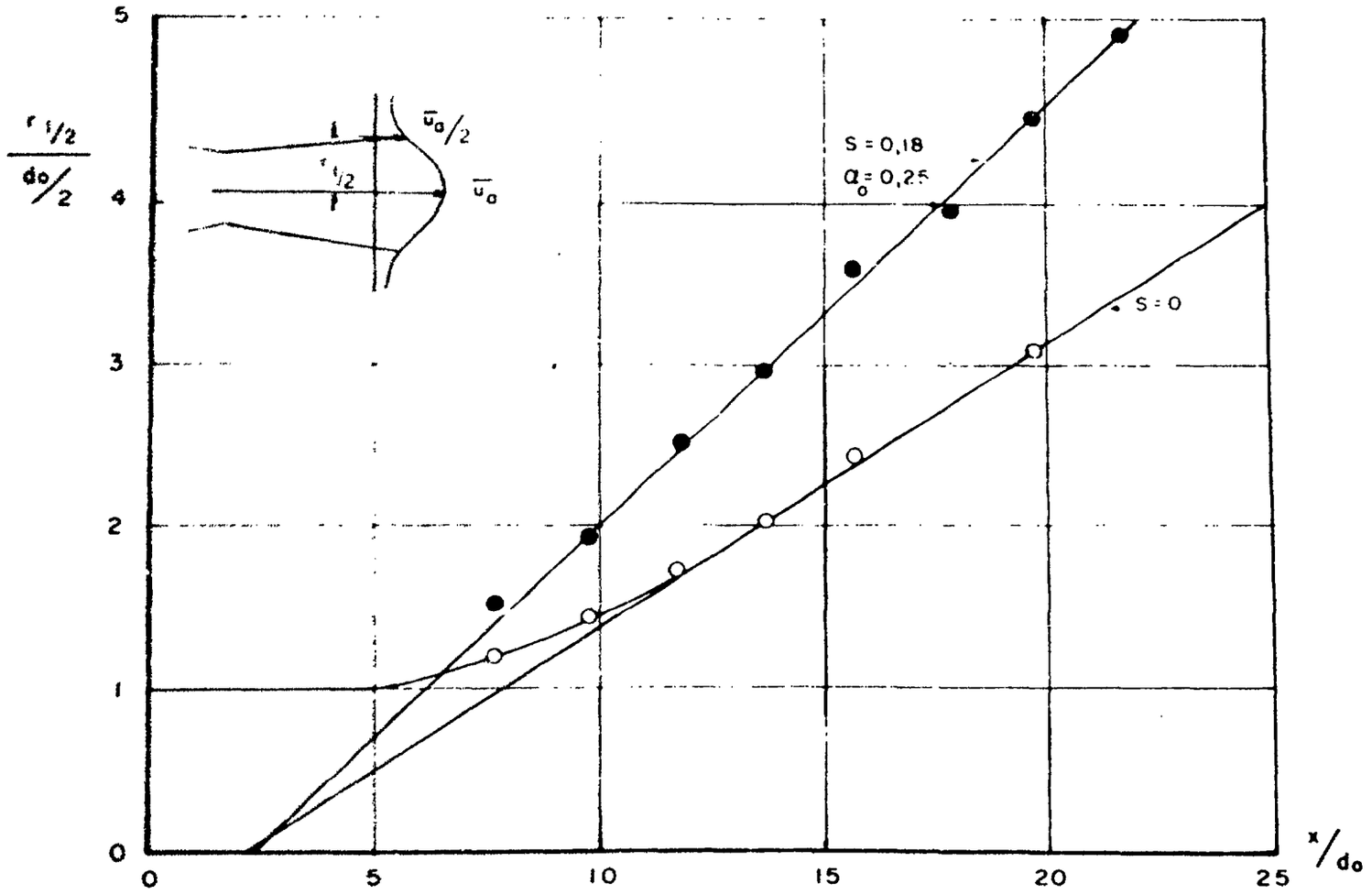

Figure 56. Halfwidth growth of a steady and unsteady axisymmetric primary jet[16]

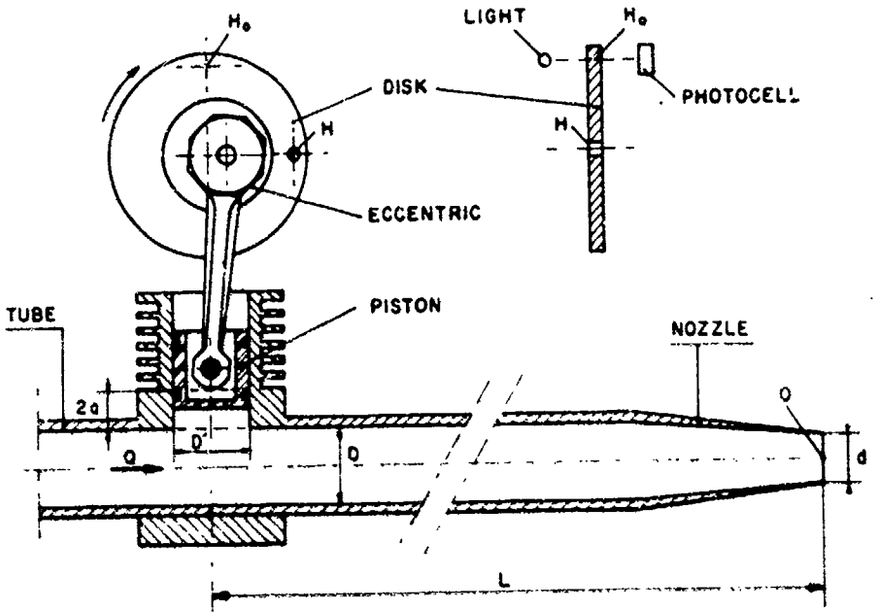

Figure 57. Schematic of piston driven unsteady jet[80]

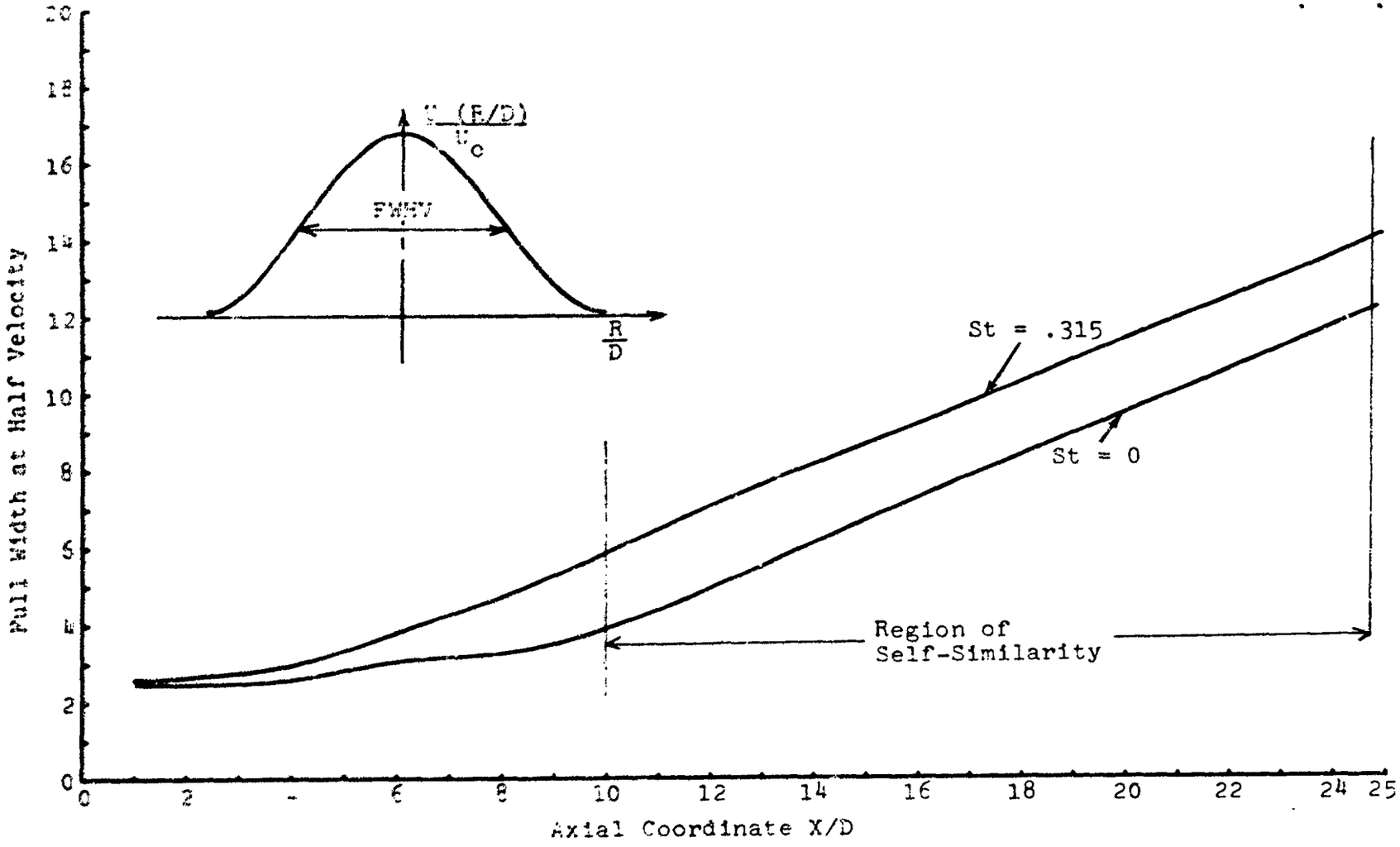

Figure 58. Effect of unsteady flow on the full width (=twice the halfwidth) growth of an unsteady jet[81]

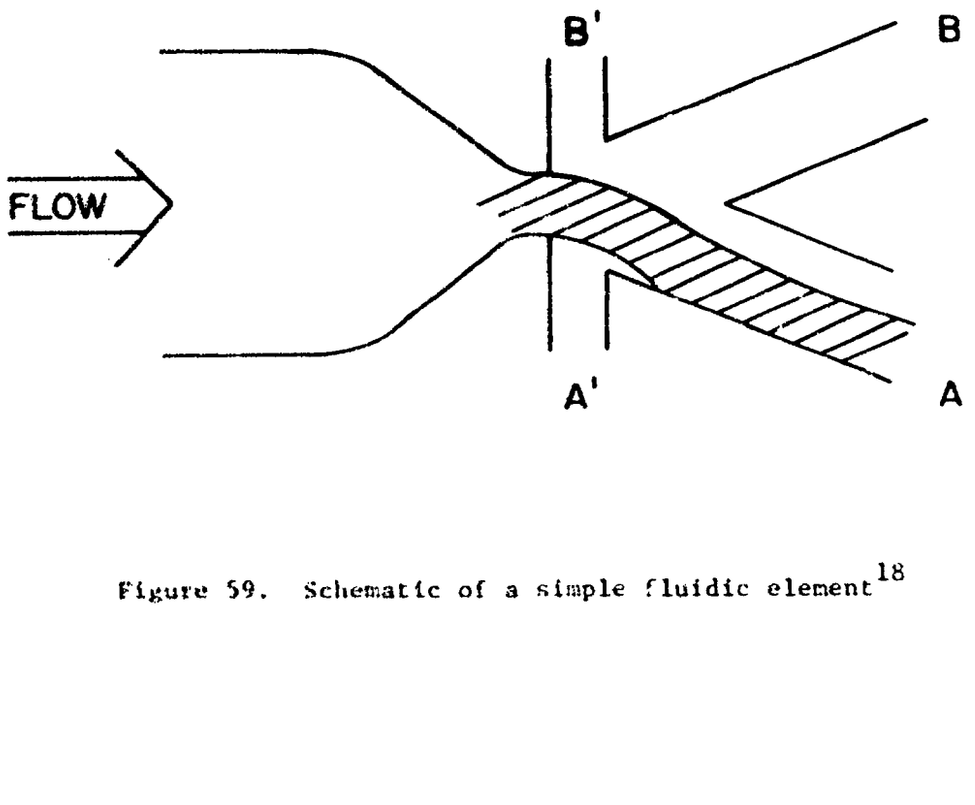

Figure 59. Schematic of a simple fluidic element[18]

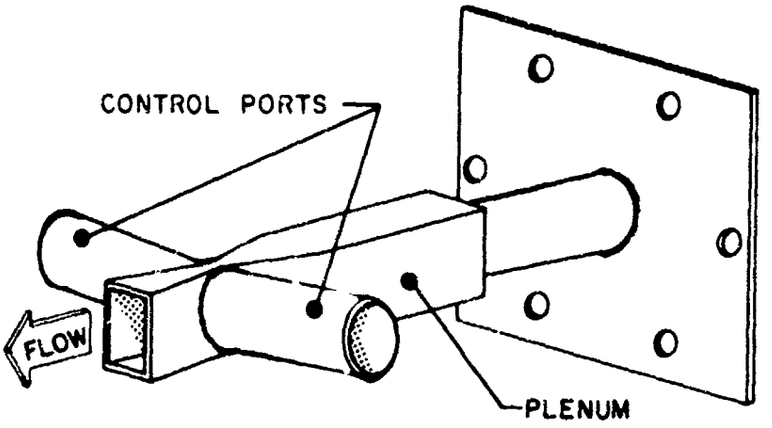

NOZZLE No. 1 SHOWN FOR GENERAL CONFIGURATION

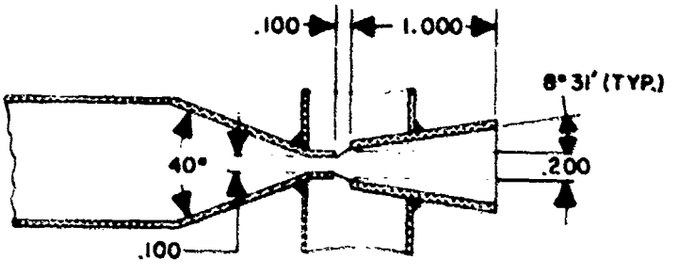

NOZZLE No. 1

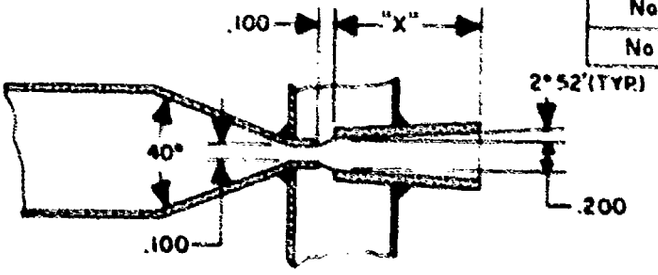

NOZZLE	"X" DIM
No 2	1.000
No 2A	.500

NOZZLE SERIES No. 2

Figure 60. Details of small scale nozzle tested[18]

NOZZLE	"X" DIM.
No. 3	1.000
No. 3A	.750
No. 3B	.562
No. 3C	.562
No. 3D	.312

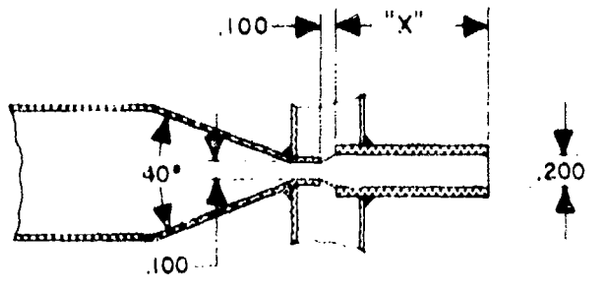

NOTE:
NOZZLE No. 3C ONLY
Cylindrical Oscillating Ports Were Replaced With 1.00" Rectangular Waveguide.

NOZZLE SERIES No. 3

NOZZLE	"X" DIM.
No. 4	.500
No. 4A	.375
No. 4B	.250
No. 4C	.100
No. 4D	0.0

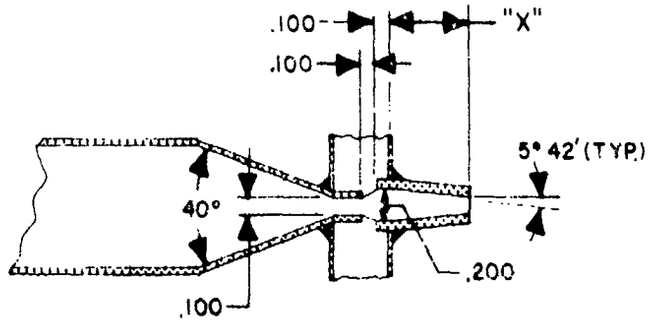

NOZZLE SERIES No. 4

NOZZLE	"X" DIM.
No. 5	.250
No. 5A	200

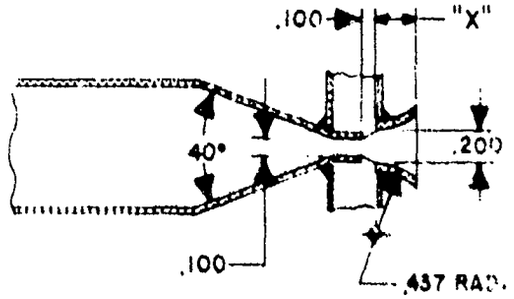

NOZZLE SERIES No. 5

Figure 60. Details of small scale nozzle tests[18] (Continued)

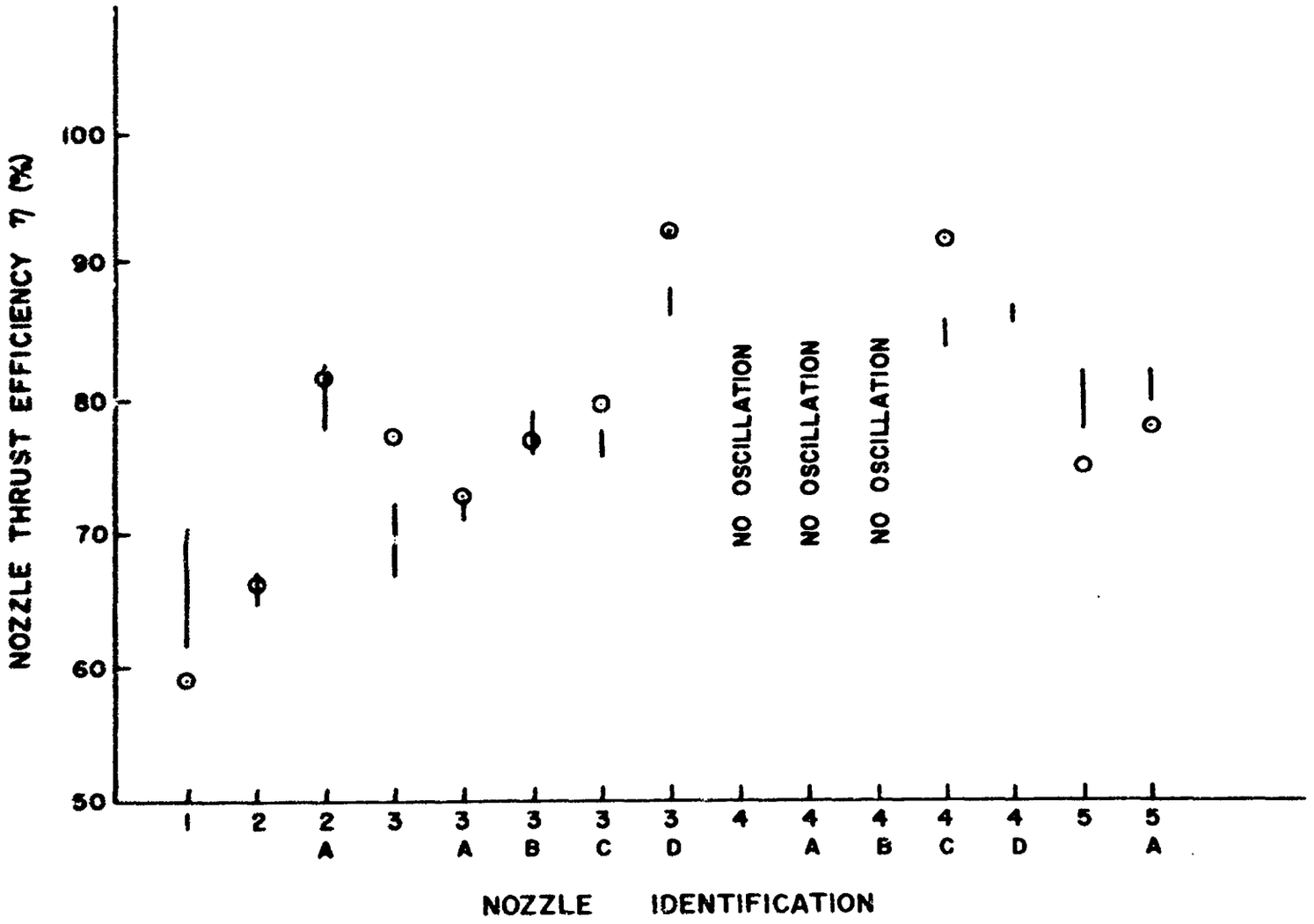

Figure 61. Nozzle thrust efficiencies for small scale test nozzles[18]

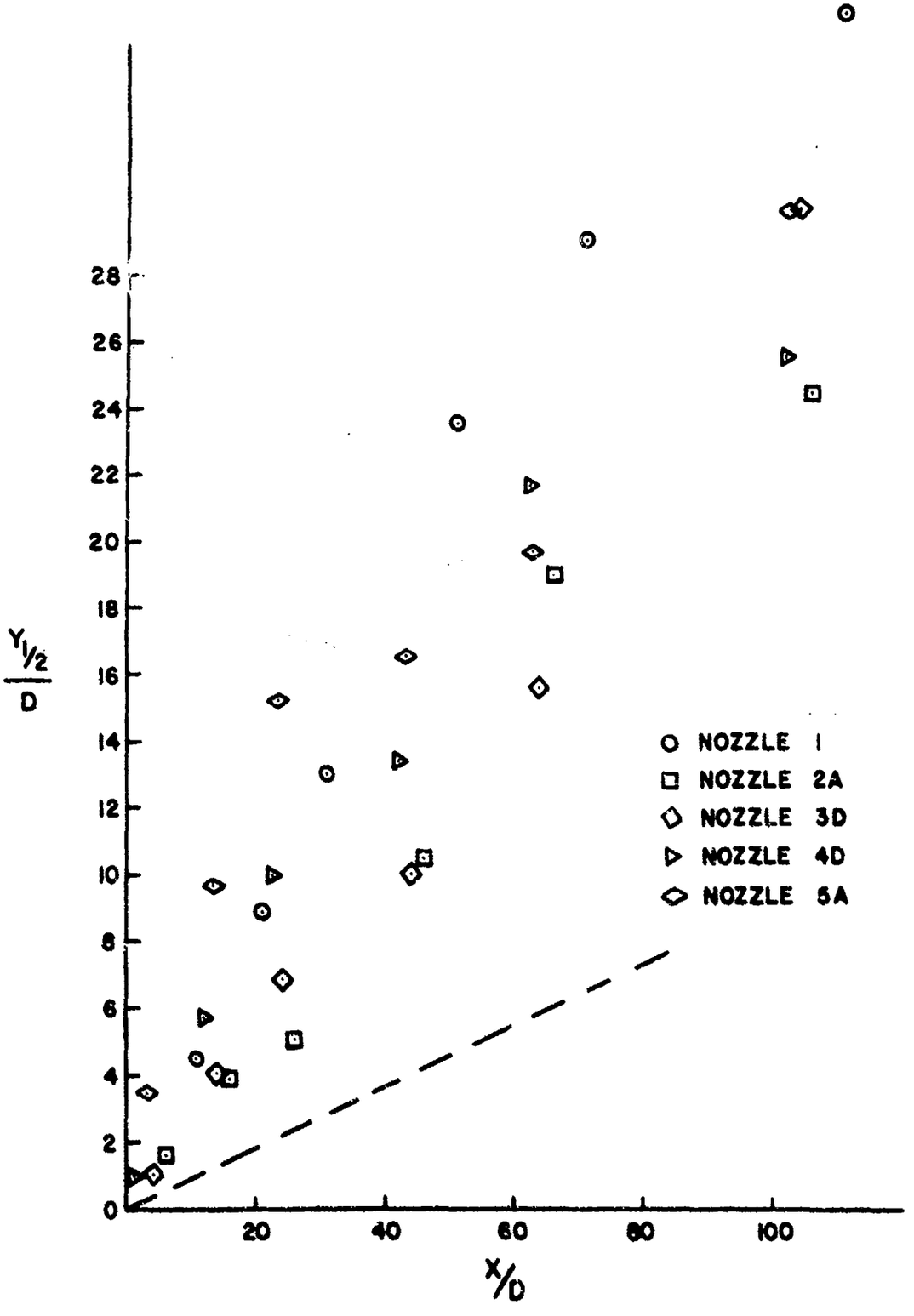

Figure 62. Halfwidth growths for small scale test nozzles. Dashed line represents growth of slot nozzle[18]

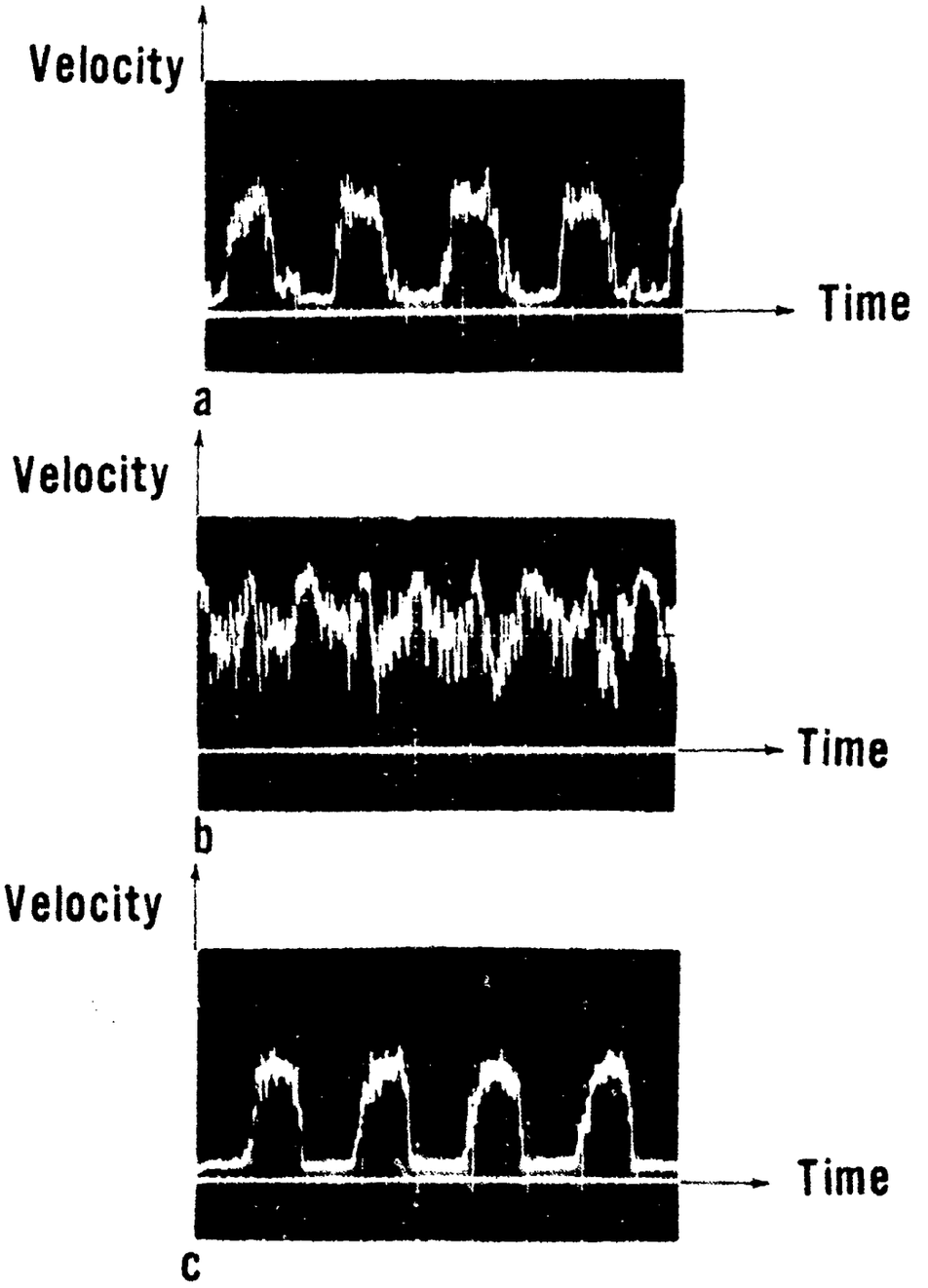

Figure 63. Time dependent velocities for small scale test nozzles[18]

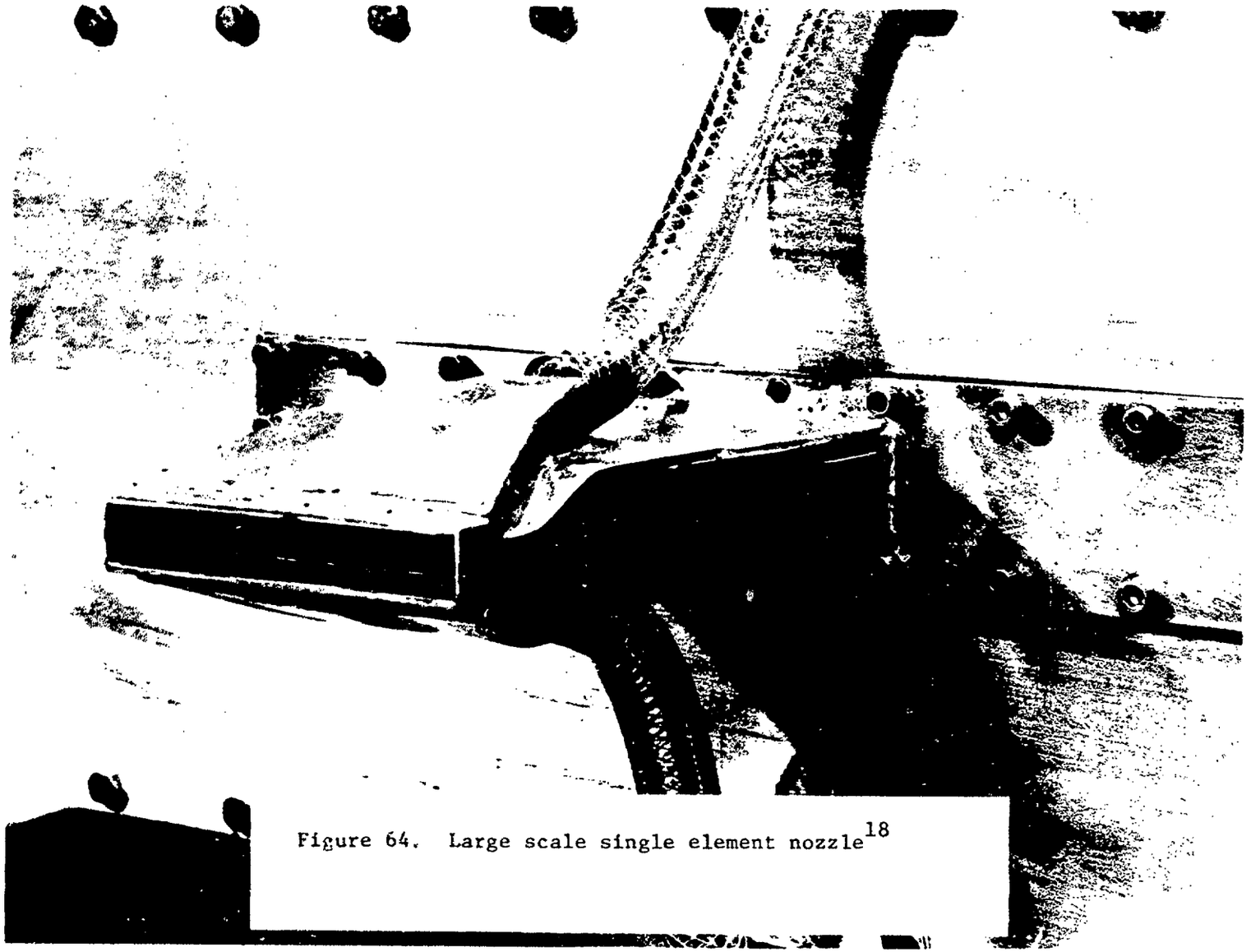

Figure 64. Large scale single element nozzle[18]

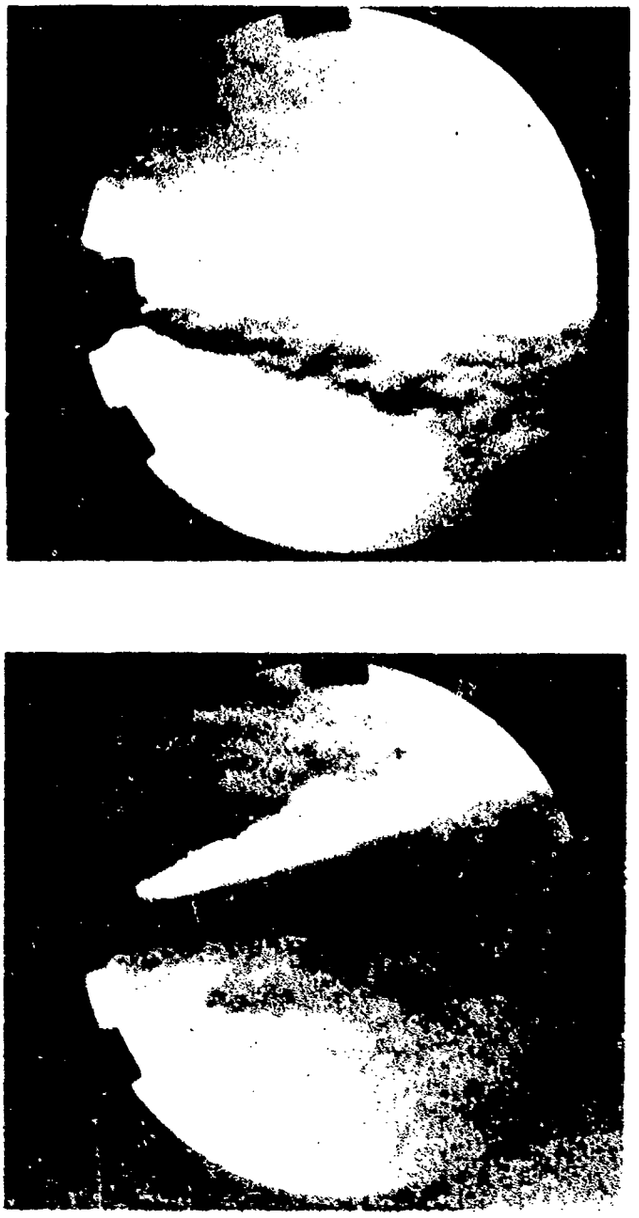

Figure 65. Schlieren photographs of oscillating jet flow field[18]

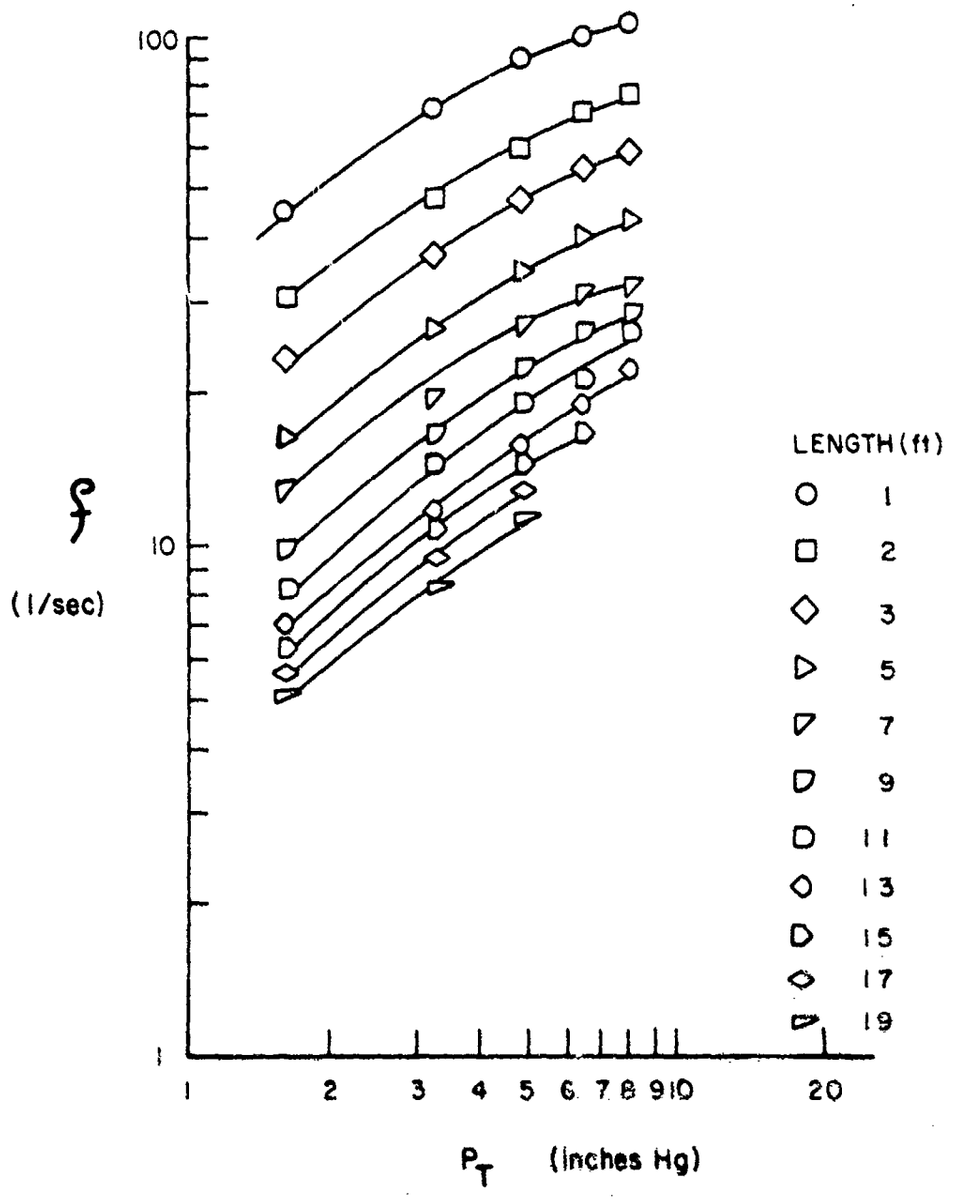

Figure 66. Variation of oscillation frequency with nozzle stagnation pressure[18]

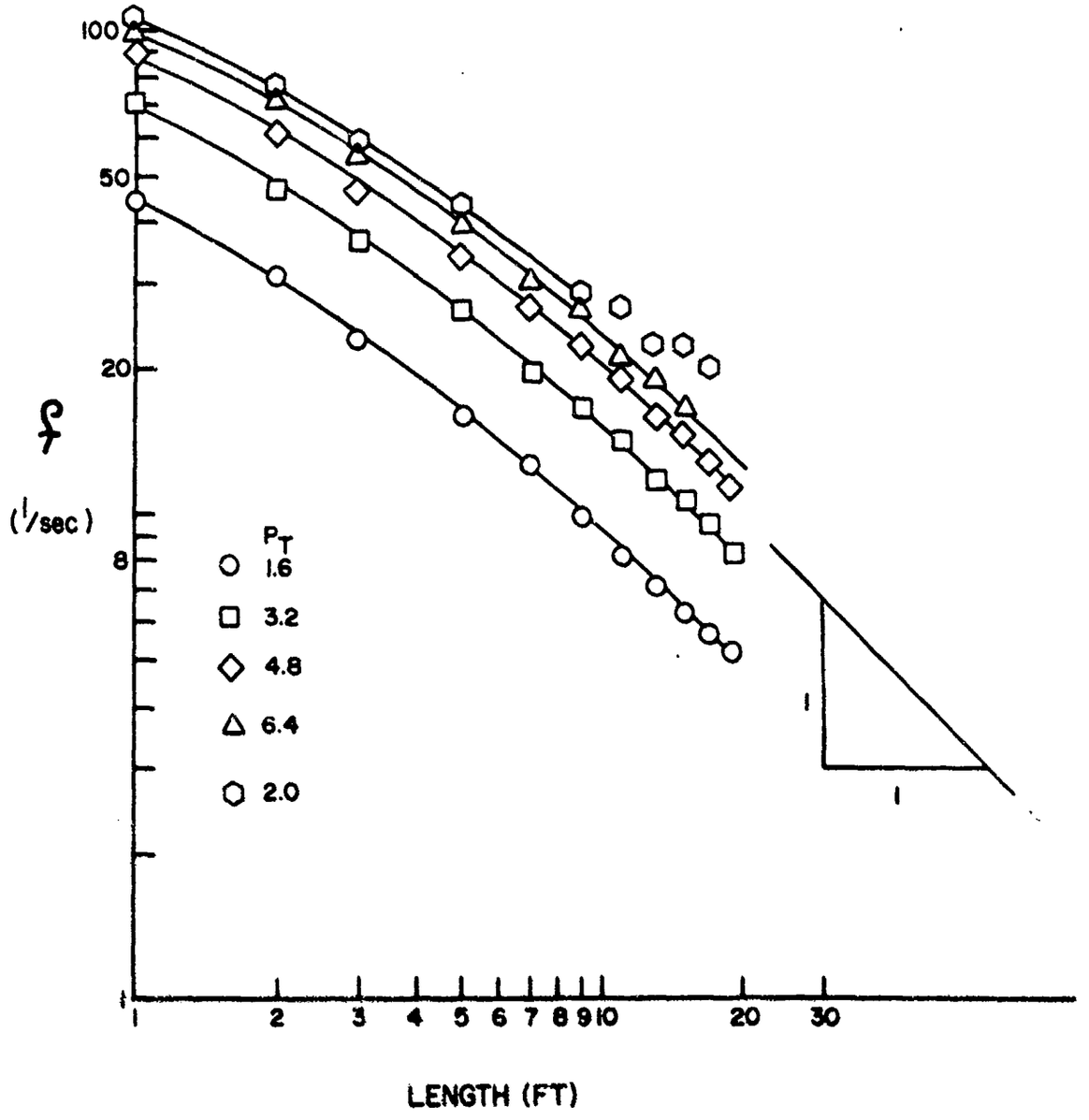

Figure 67. Variation of oscillation frequency with nozzle fluidic feedback length[18]

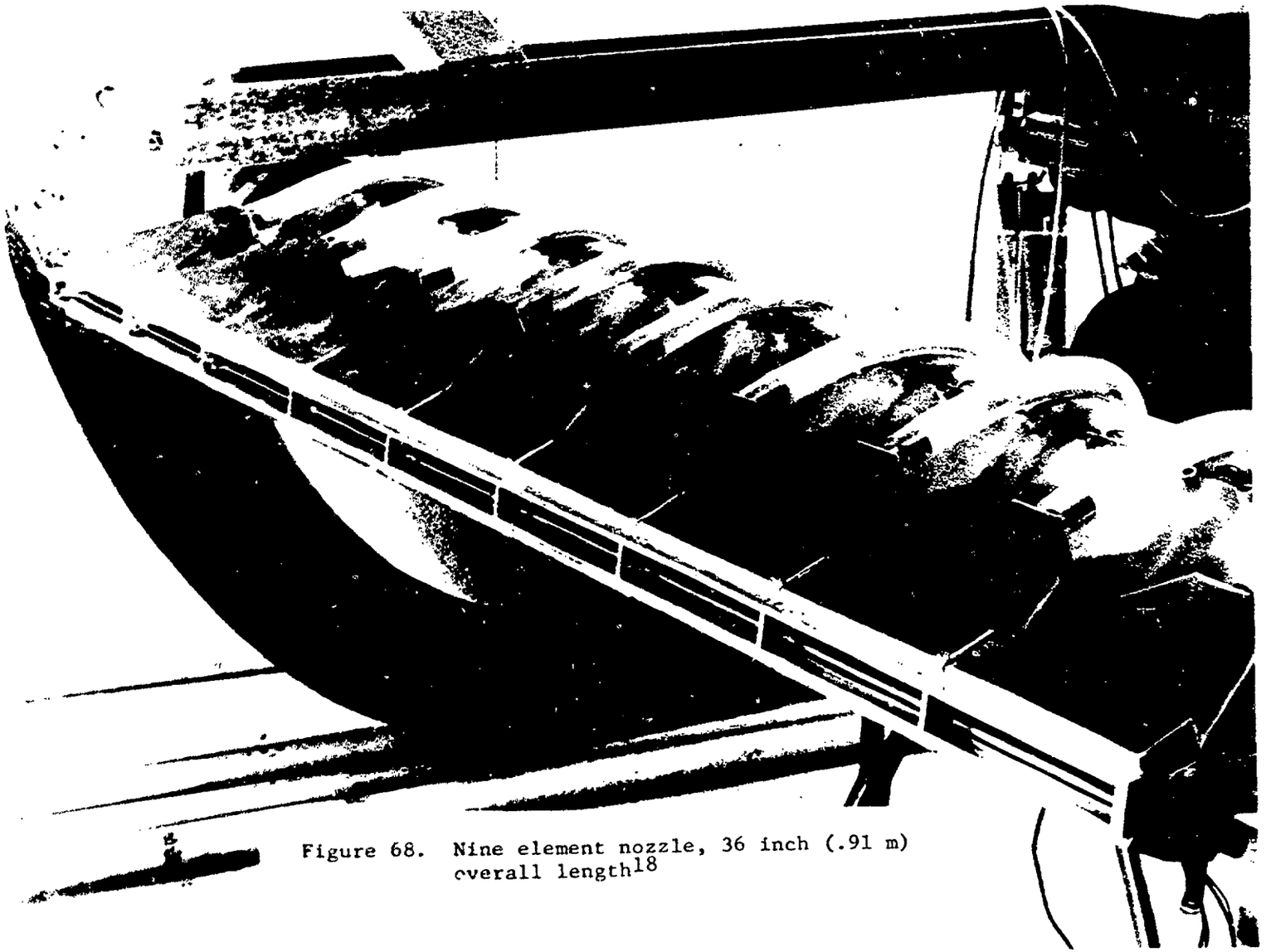

Figure 68. Nine element nozzle, 36 inch (.91 m) overall length[18]

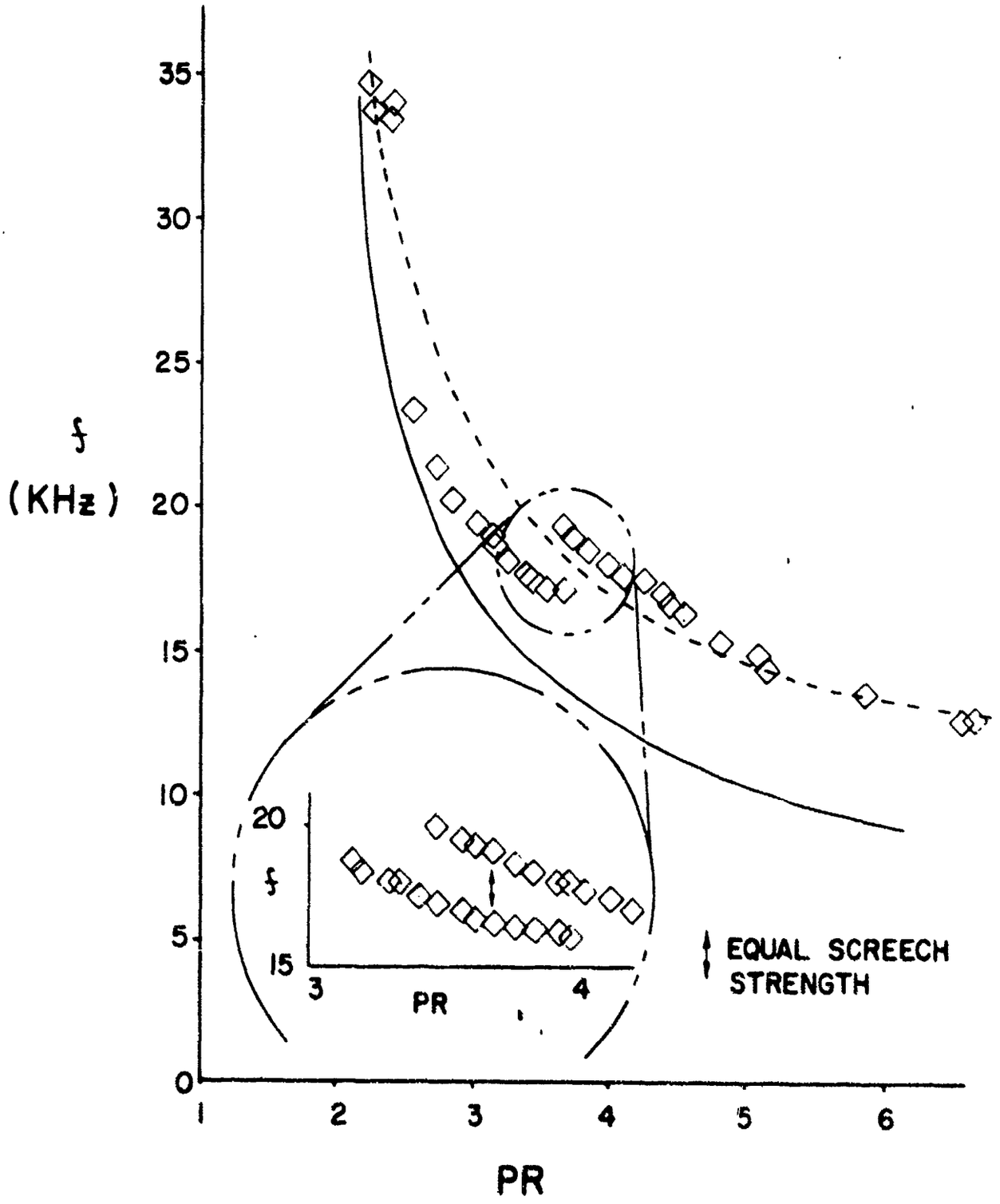

Figure 69. Experimentally determined screech frequency versus primary nozzle pressure ratio[100]

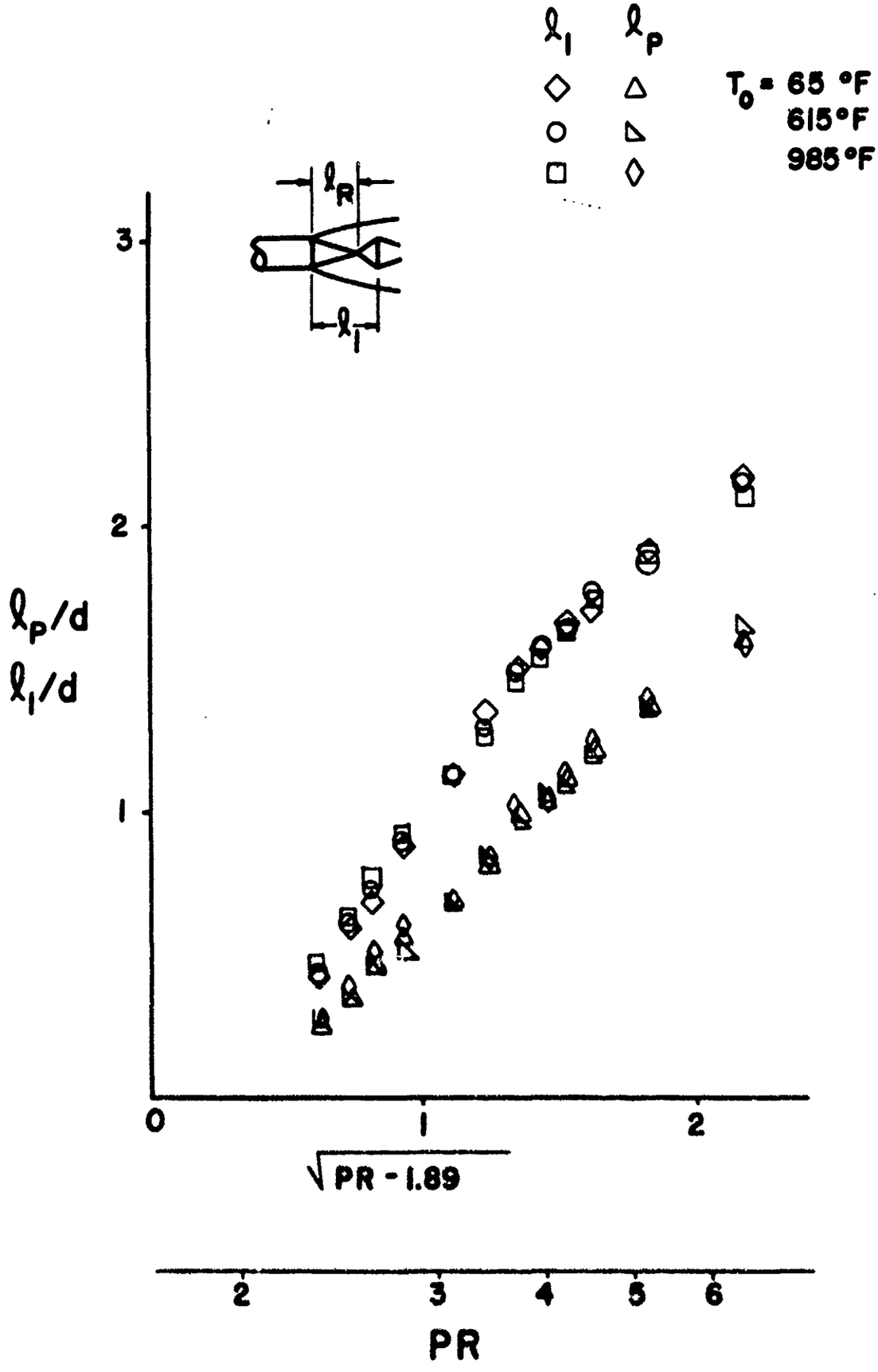

Figure 70. Dependence of the cellular flow structure on jet total temperature[100]

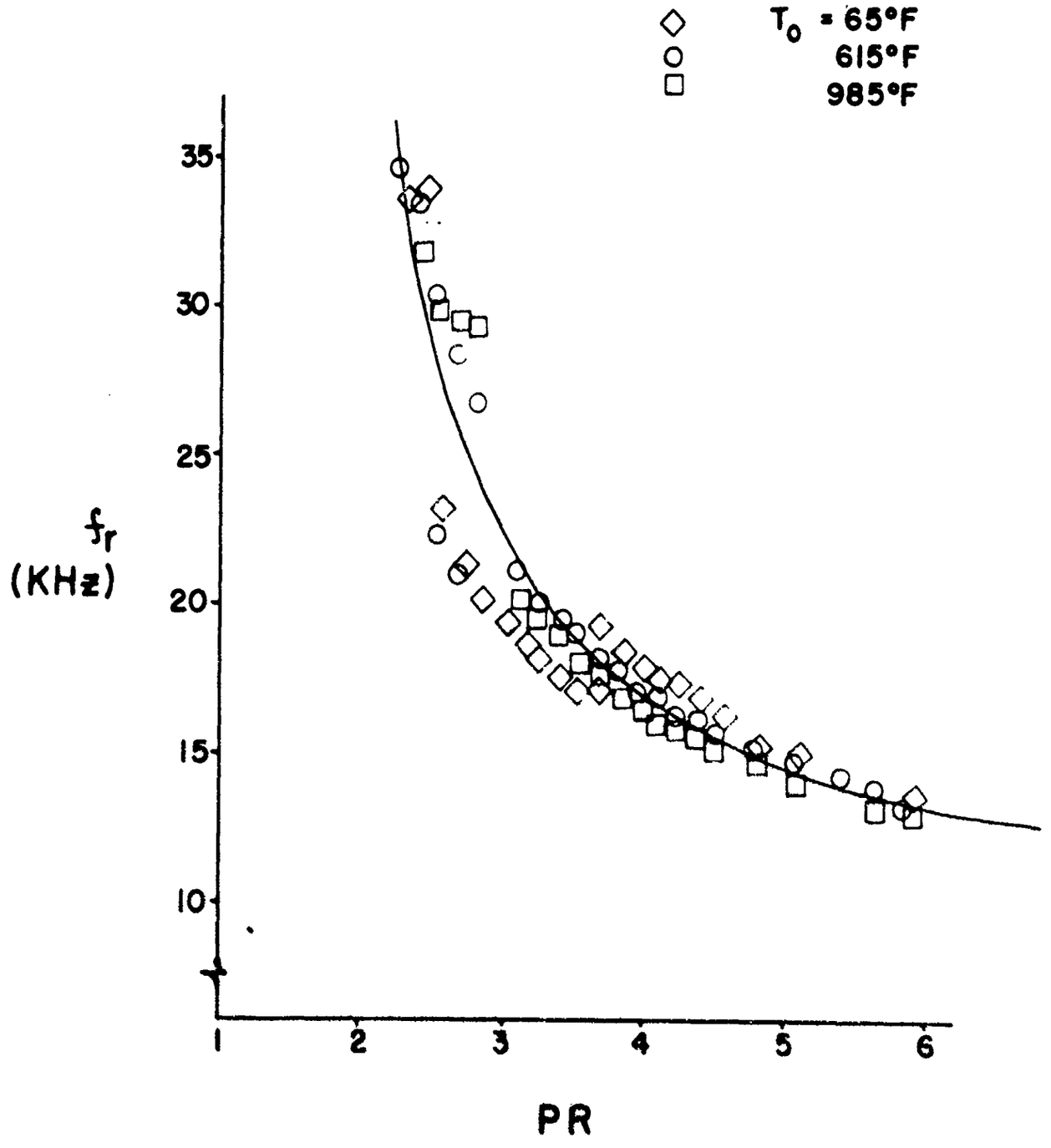

Figure 71. Reduced screech frequency[100]

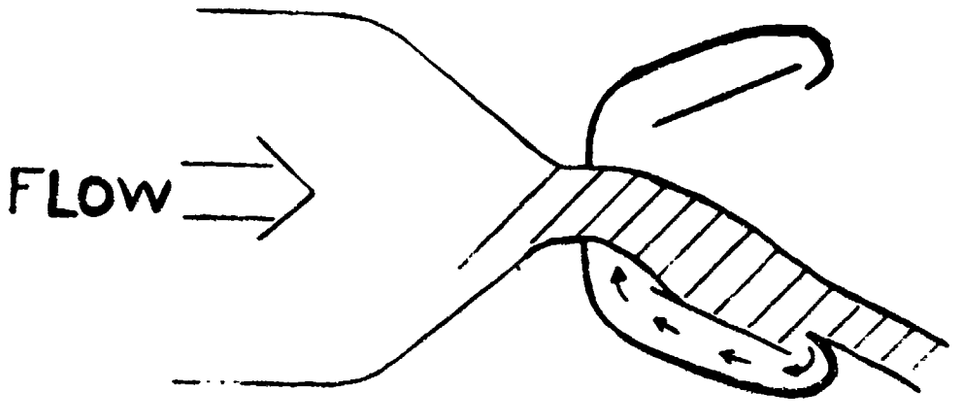

Figure 72. Schematic of the positive scoop flip-flop jet flowfield[102]

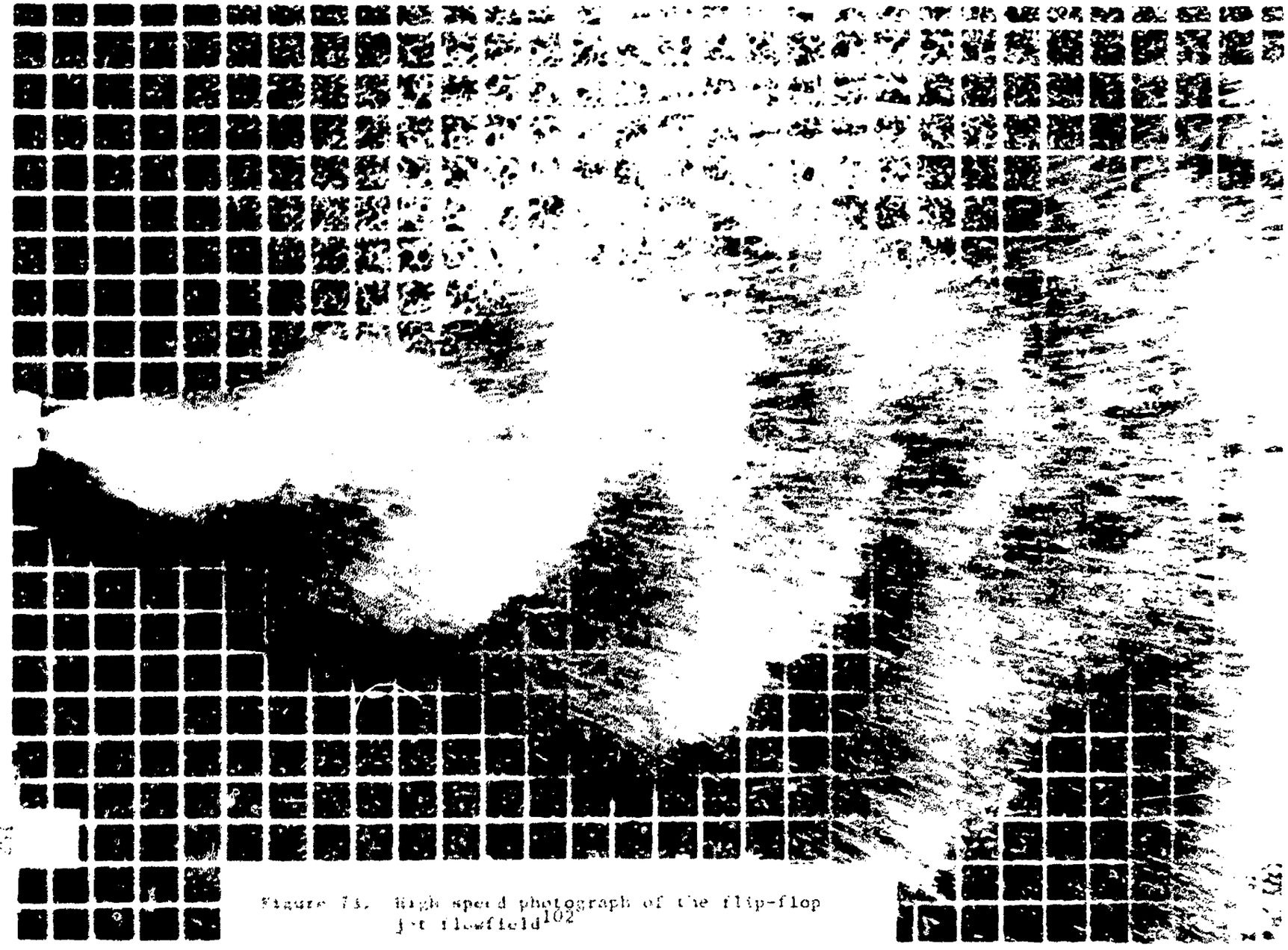

Figure 13. High speed photograph of the flip-flop jet flowfield[102]

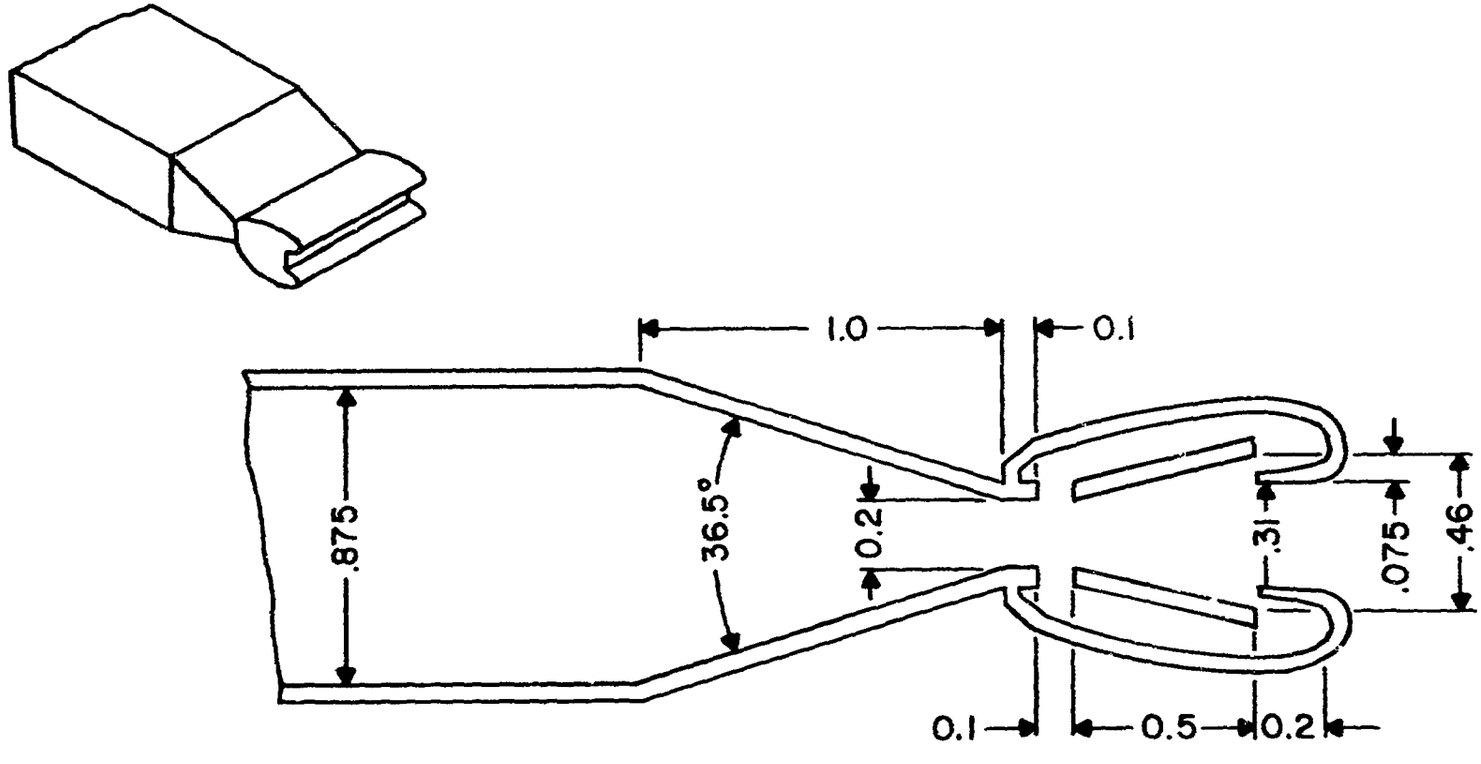

Figure 74. Short feedback loop geometry of the flip-flop nozzle[102]

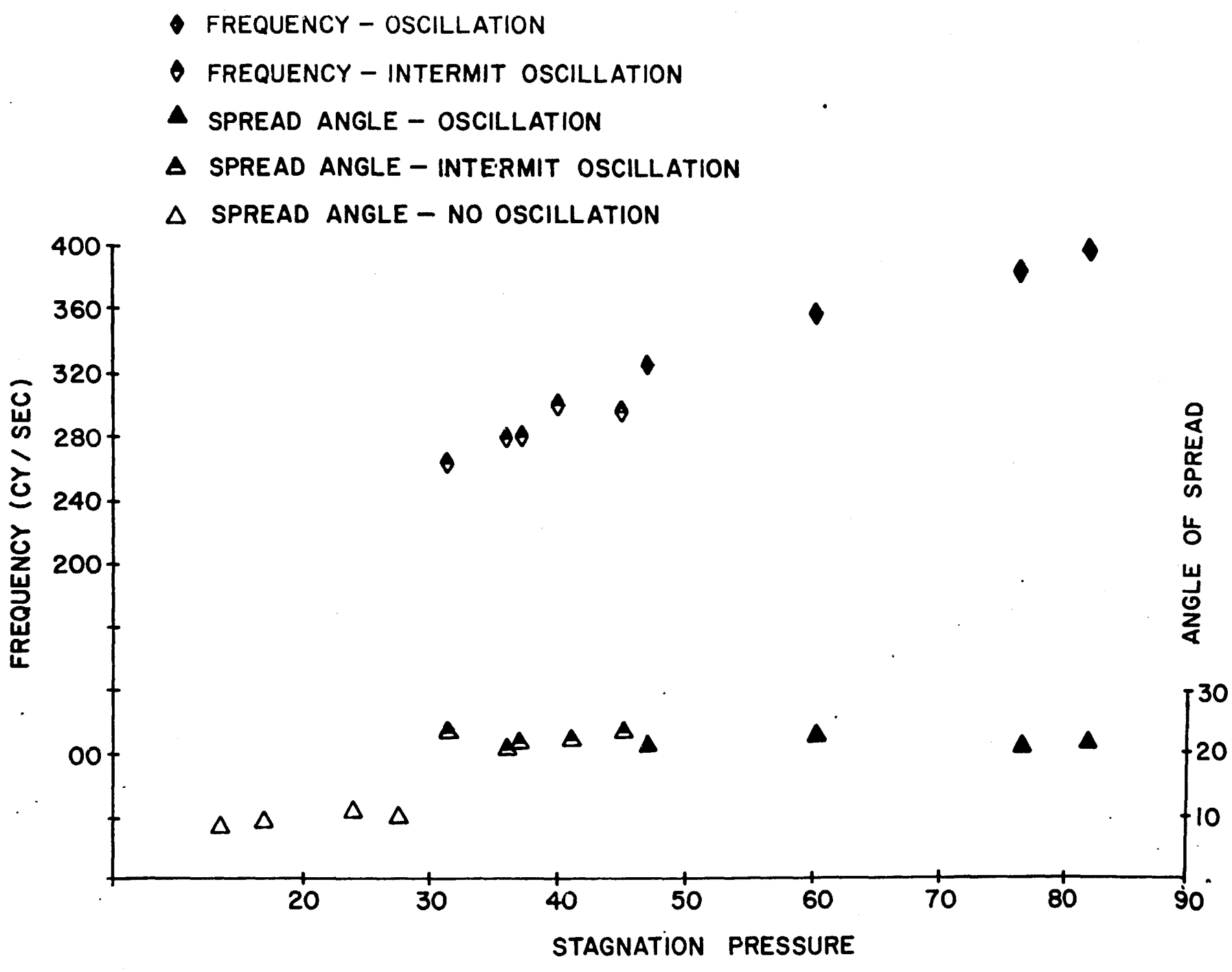

Figure 75. Performance of short feedback nozzle[102]

Figure 75. Performance of short feedback nozzle[102]

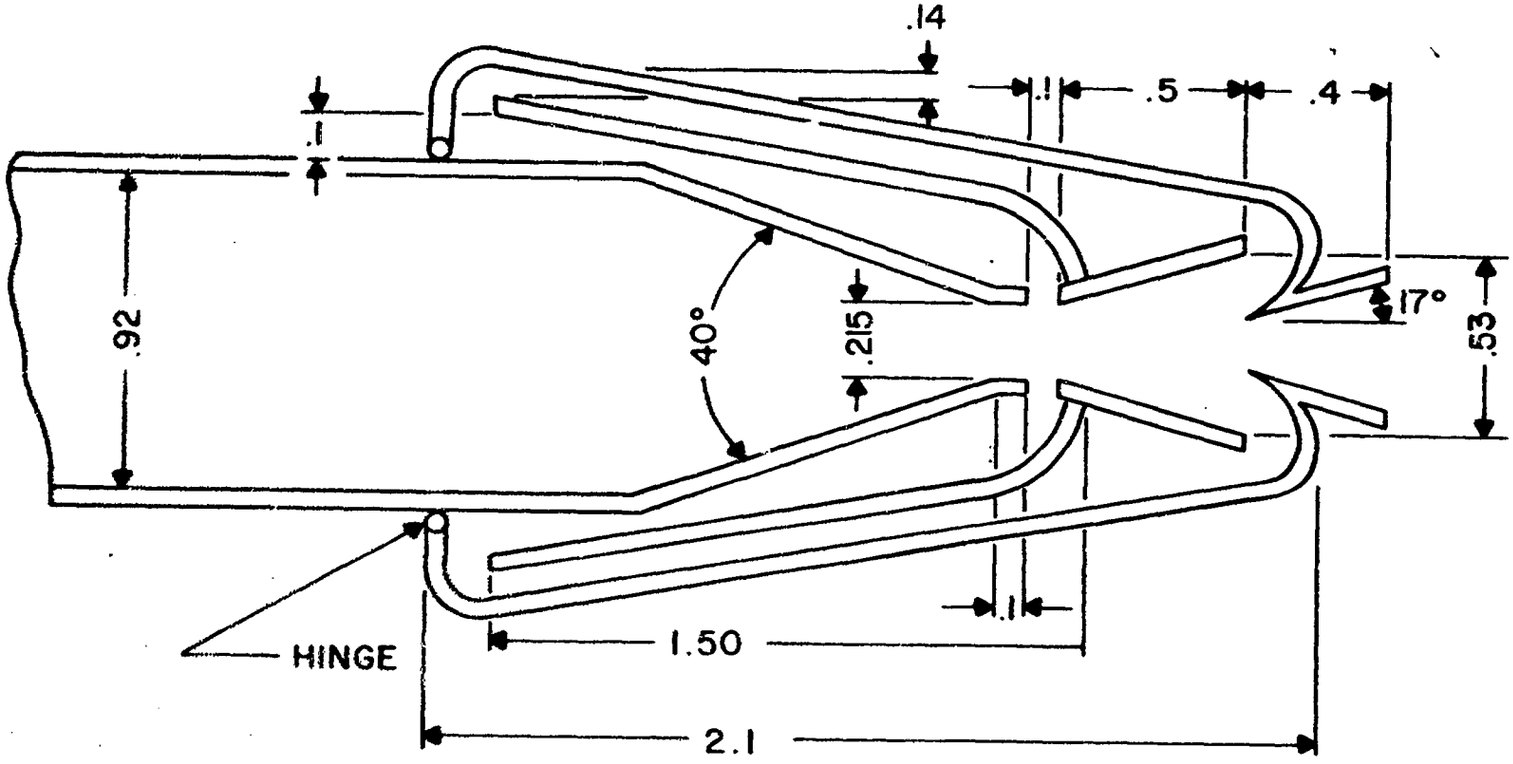

Figure 76. Long feedback nozzle with exit lips[102]

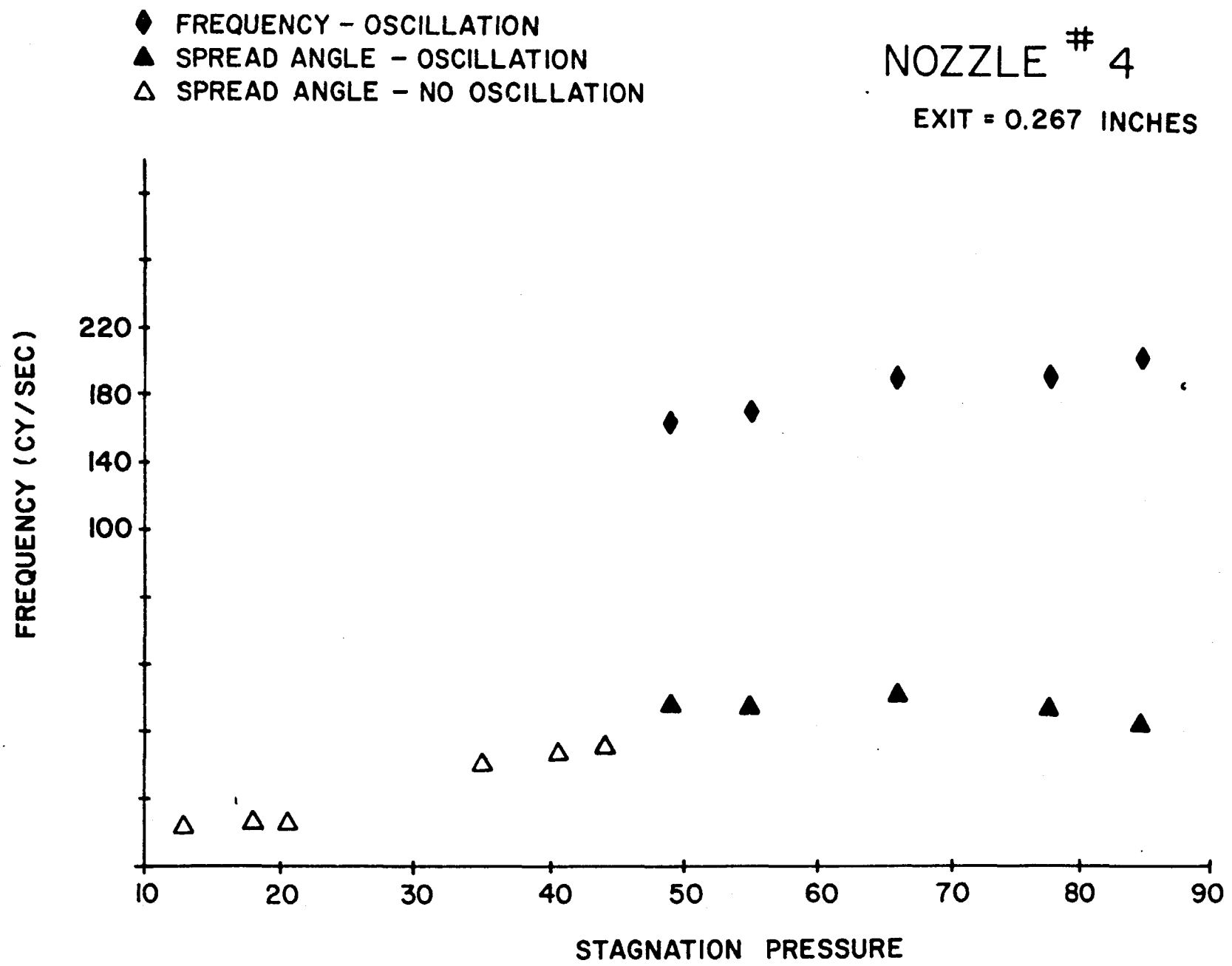

Figure 77. Performance of the variable scoop nozzle, scoop = 122% of throat

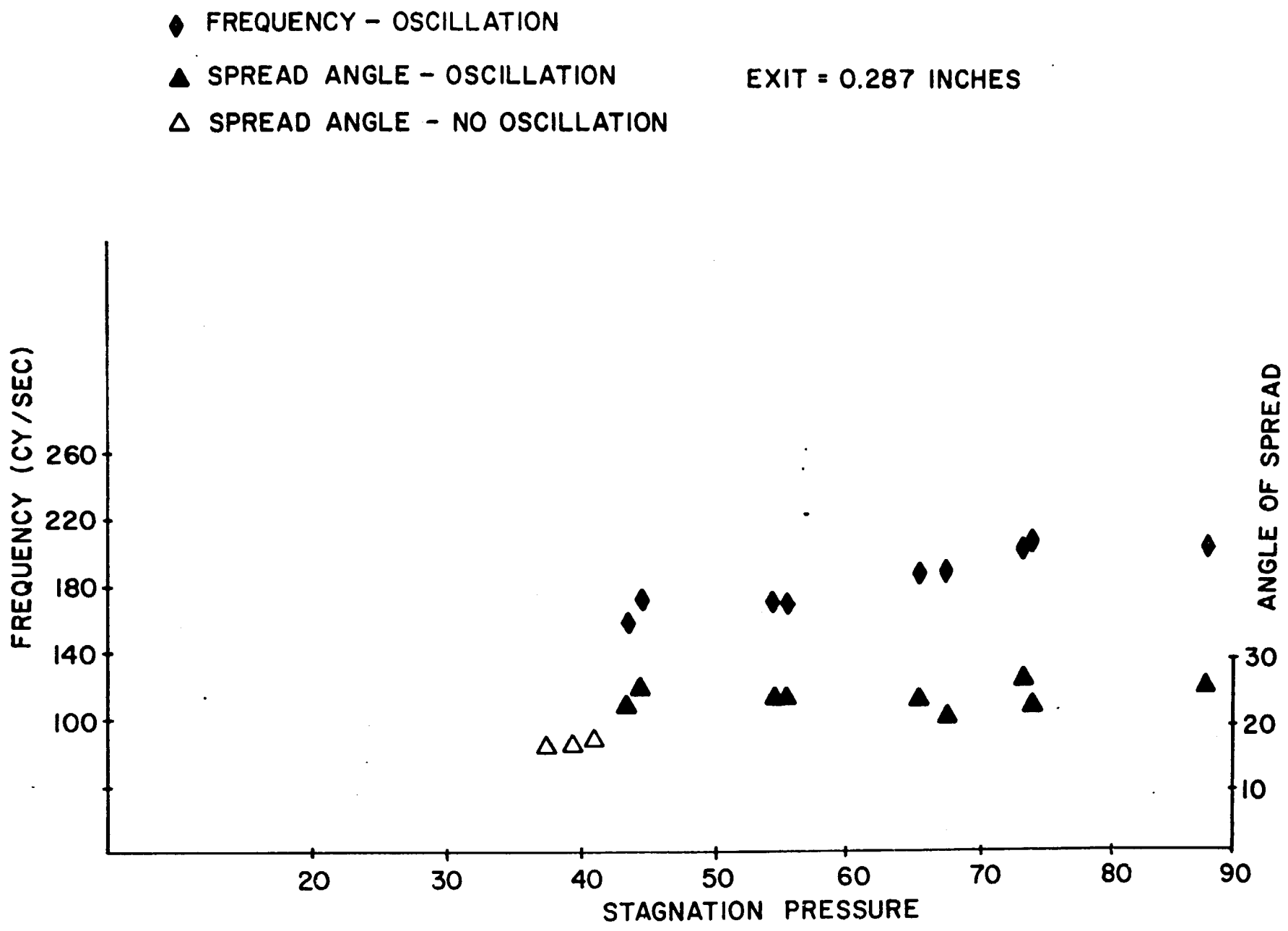

Figure 78. Performance of the variable scoop nozzle, scoop = 113% of throat

scoop = 113% of throat

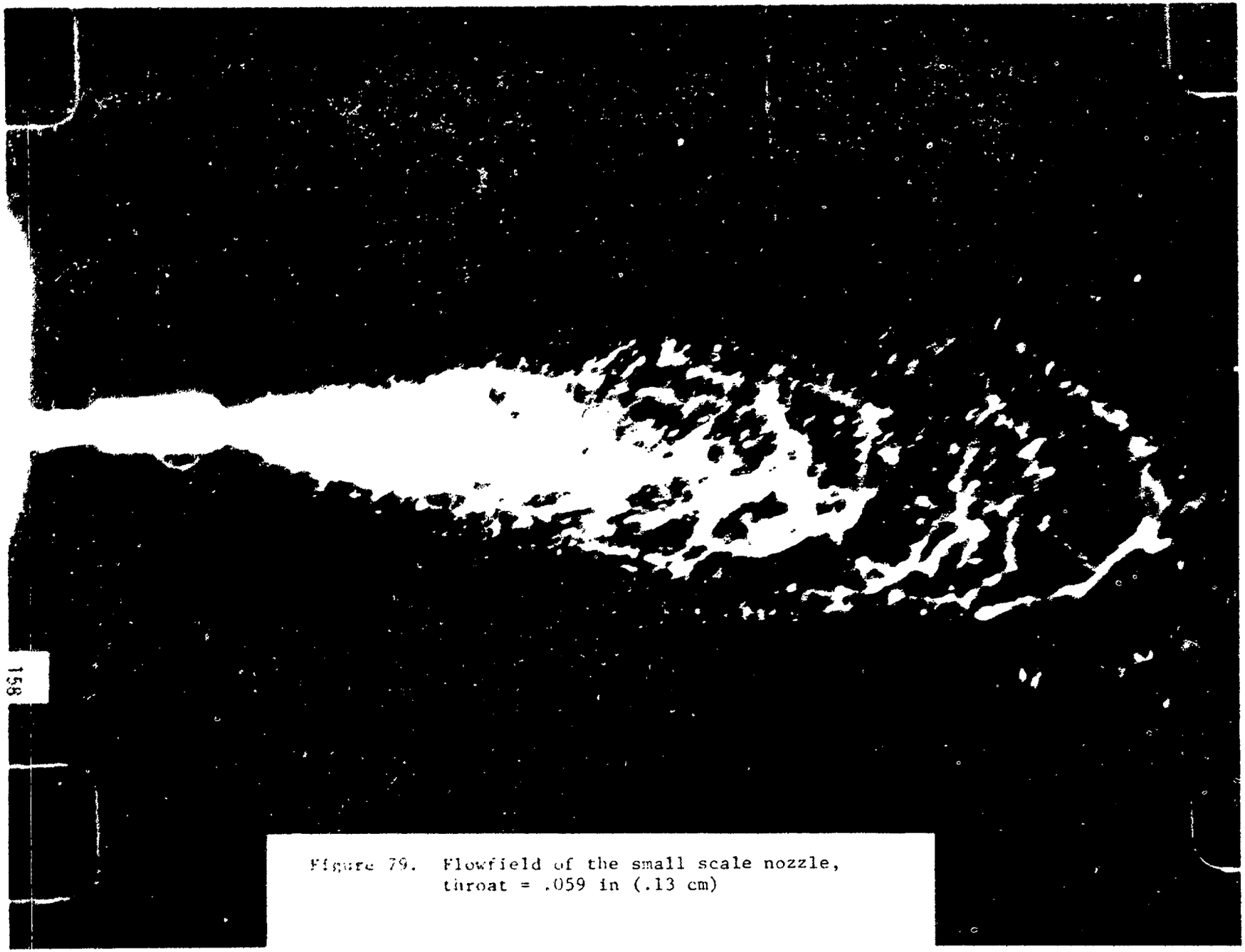

Figure 79. Flowfield of the small scale nozzle, throat = .059 in (.13 cm)

APPLICATIONS

V/STOL EJECTOR WING

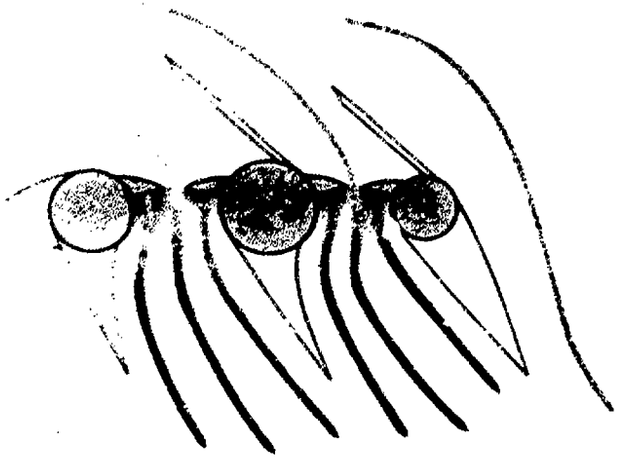

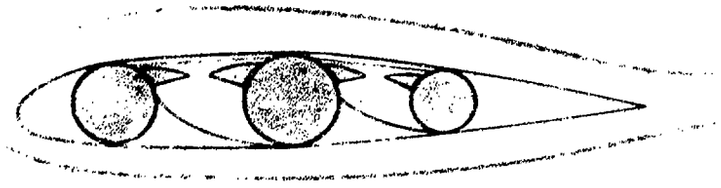

LIGHT INTRATHEATER TRANSPORT

SEARCH & RESCUE

COIN FIGHTER

STOL EJECTOR FLAP

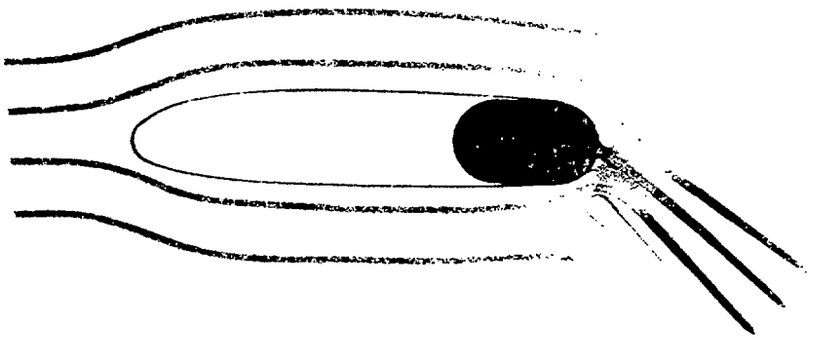

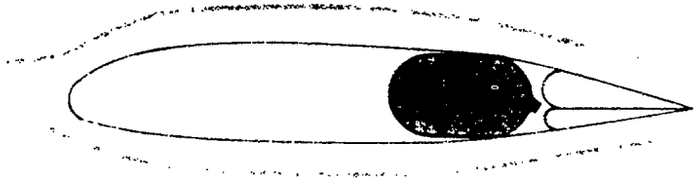

MEDIUM RANGE STOL TRANSPORT

Figure 80. Aircraft applications for thrust augmenting ejectors

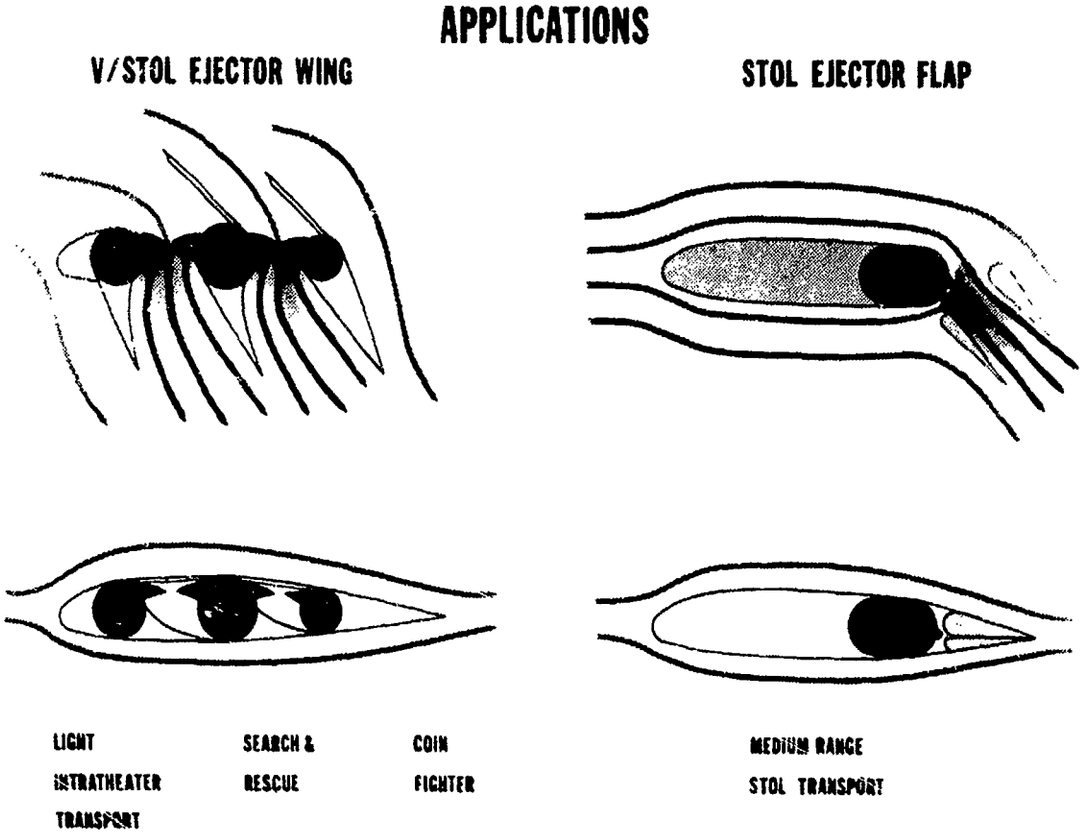

Figure 80. Aircraft applications for thrust augmenting ejectors

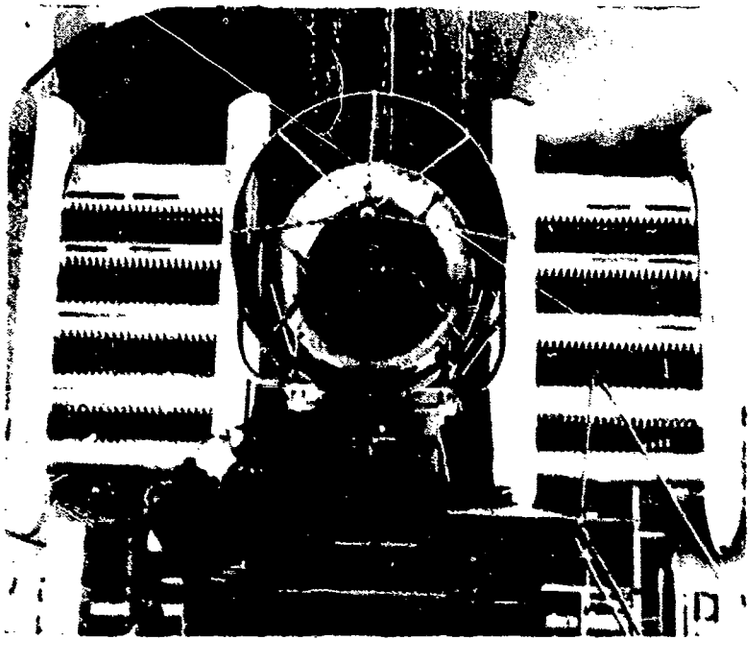

Figure 81. Full scale multi-channel ejector. Frontal view of engine and upper surface of wing with inlet doors removed[104]

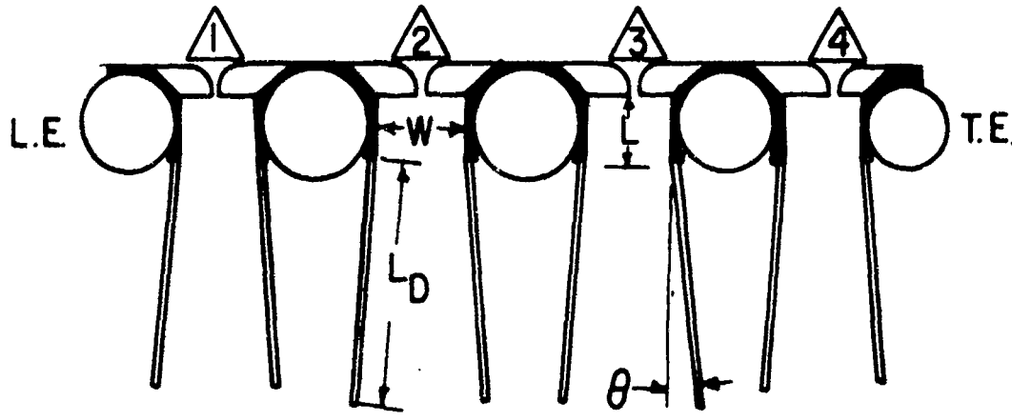

CHANNEL NO	1	2	3	4
W	8"	10"	10"	8"
L	10"	10"	10"	10"
L_D	28"	30"	30"	28"
DIFFUSER AREA RATIOS (A_3/A_2)	1.0	1.0	1.0	1.0
	1.2	1.2	1.2	1.2
	1.4	1.4	1.4	1.4
	1.7	1.7	1.7	1.7
	2.0	2.0	2.0	2.0
DIFFUSER HALF ANGLES (θ)	1.6°	1.9°	1.9°	1.6°
	3.3°	3.8°	3.8	3.3°
	5.7°	6.7°	6.7°	5.7°
	8.2°	9.6°	9.6°	8.2°
	0°	0°	0°	0°

Figure 82. Ejector dimensions and available diffuser positions[104]

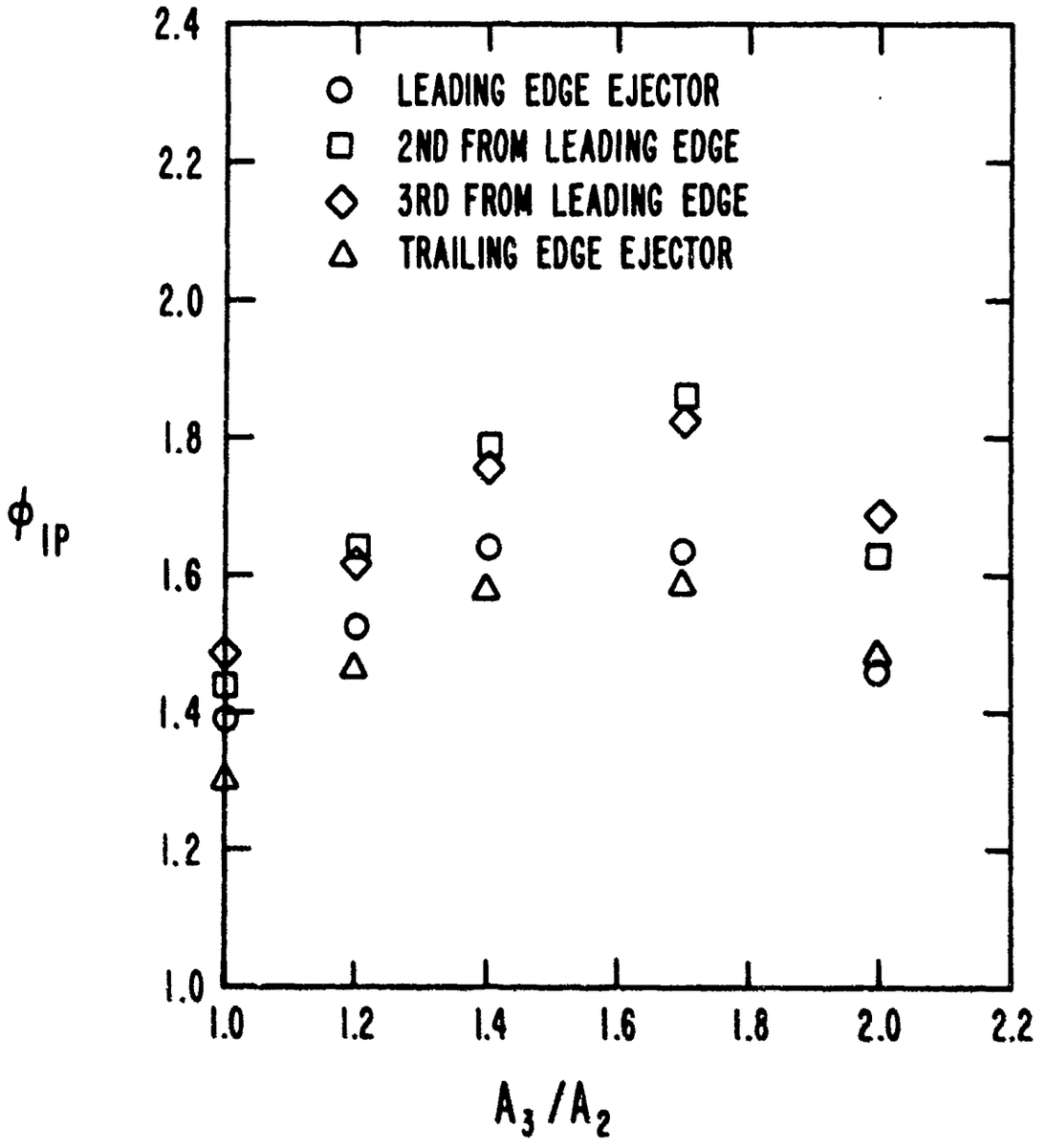

Figure 83. Chordwise distribution of augmentation level[104]

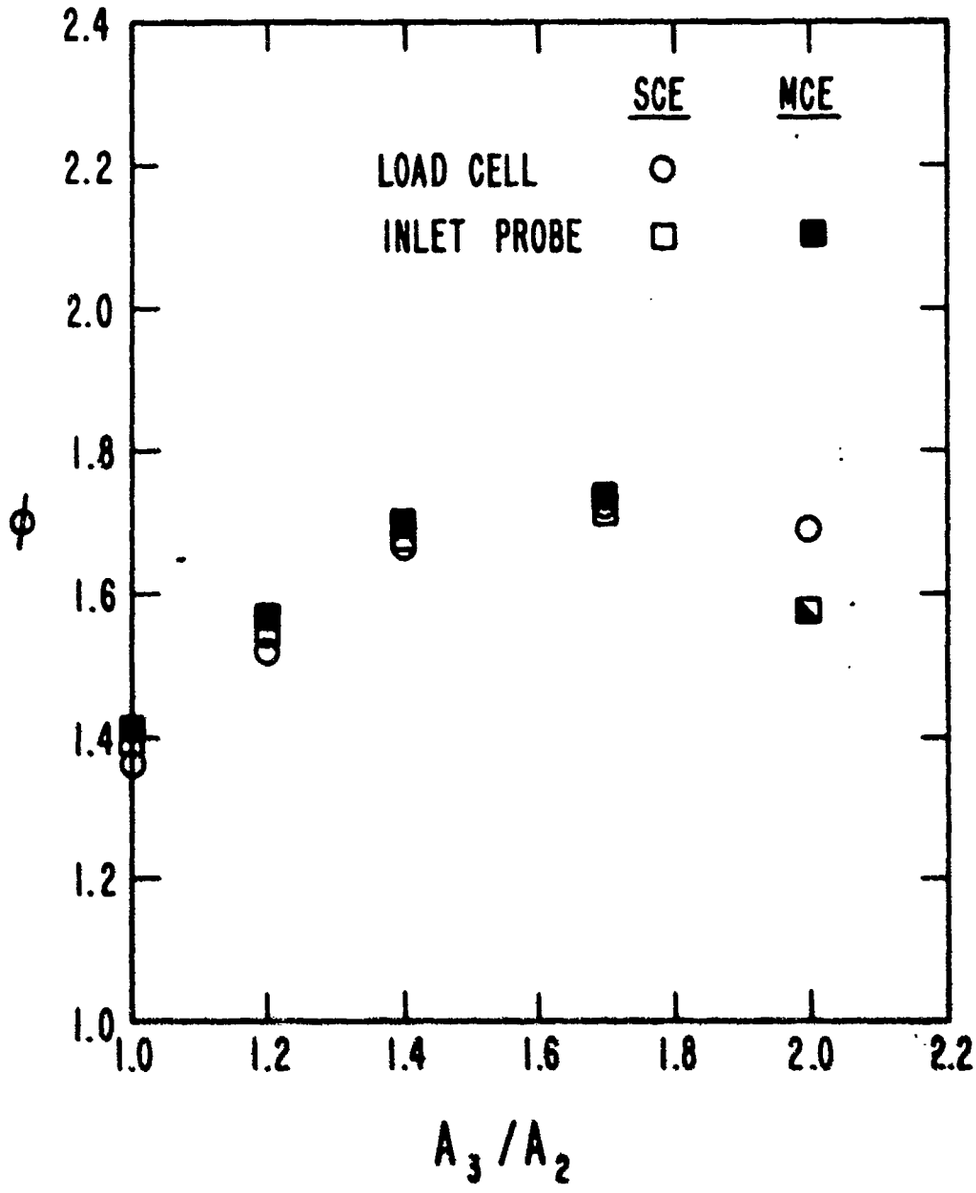

Figure 84. Correlation of the multi-channel (MCE) ejector and single channel (SCE) ejector test results

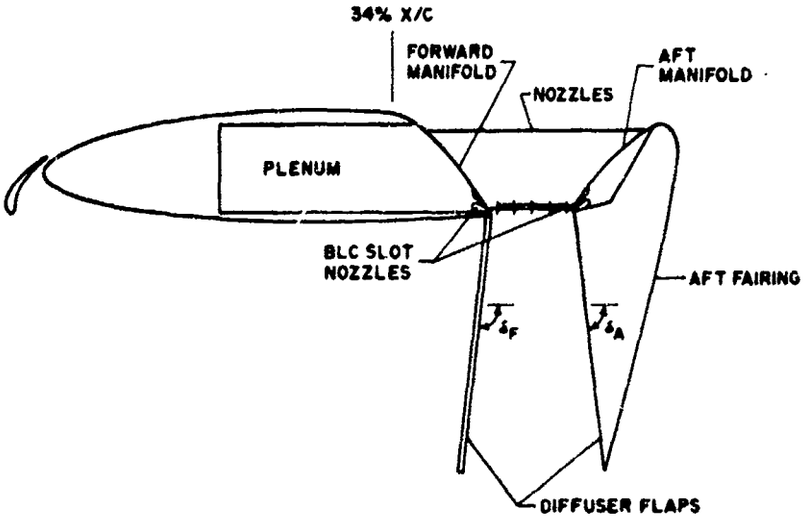

Figure 85. VTOL augmentor wing cross section[105]

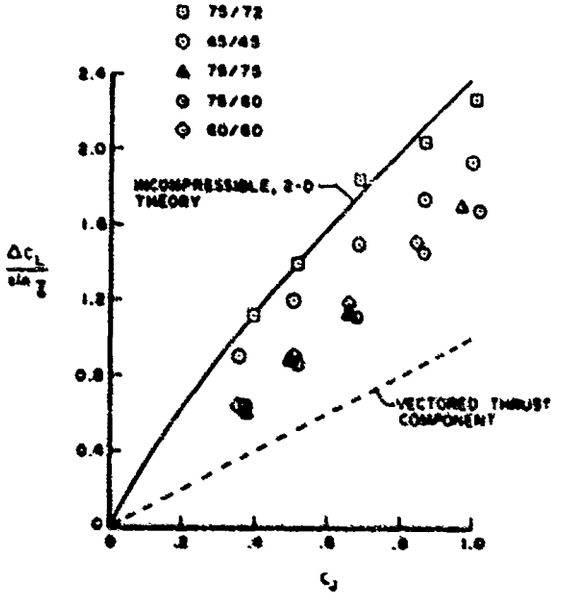

Figure 86. Lift increment due to blowing[105]

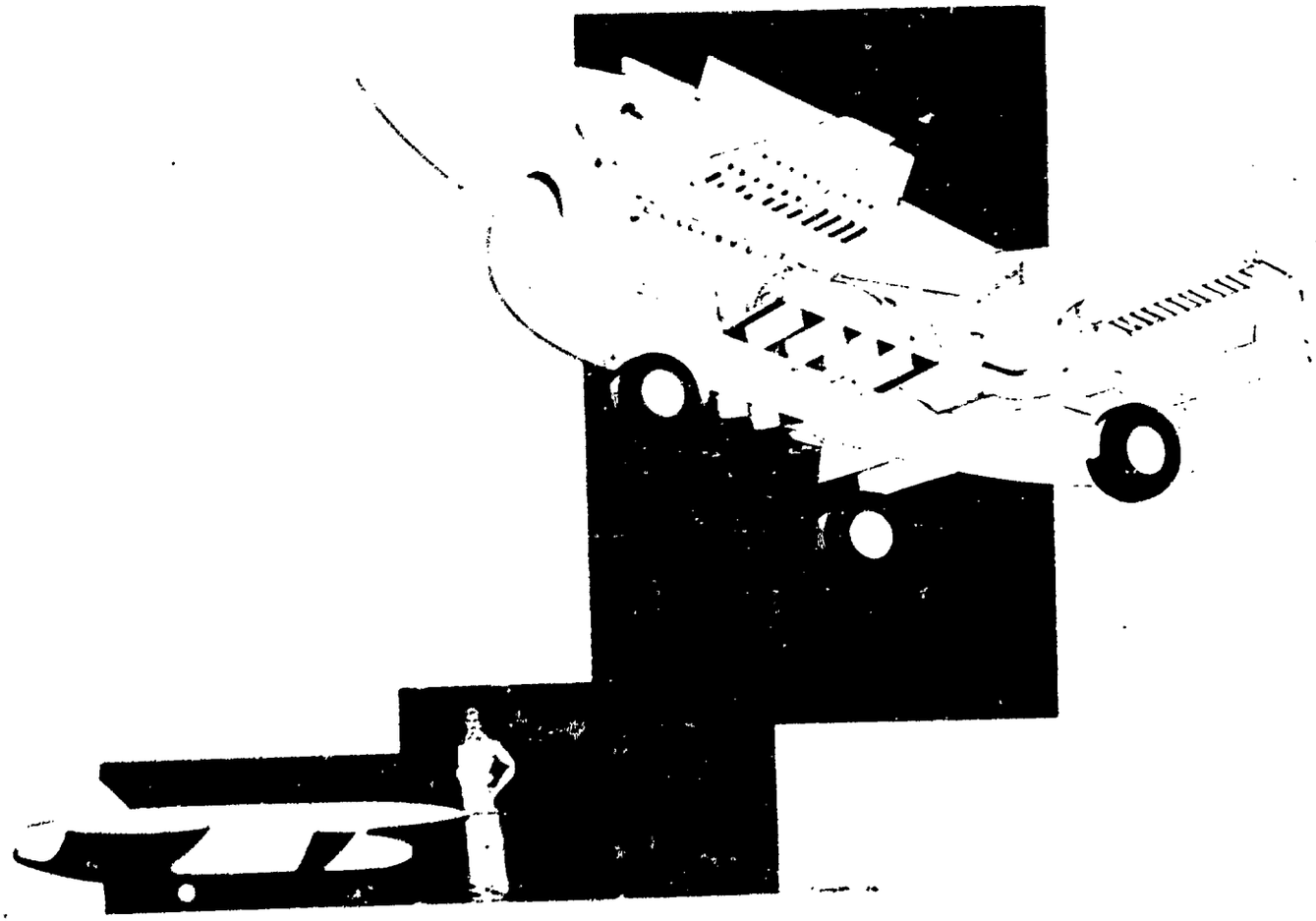

Figure 87. V/STOL demonstrator vehicle for ejector thrust augmentation technology

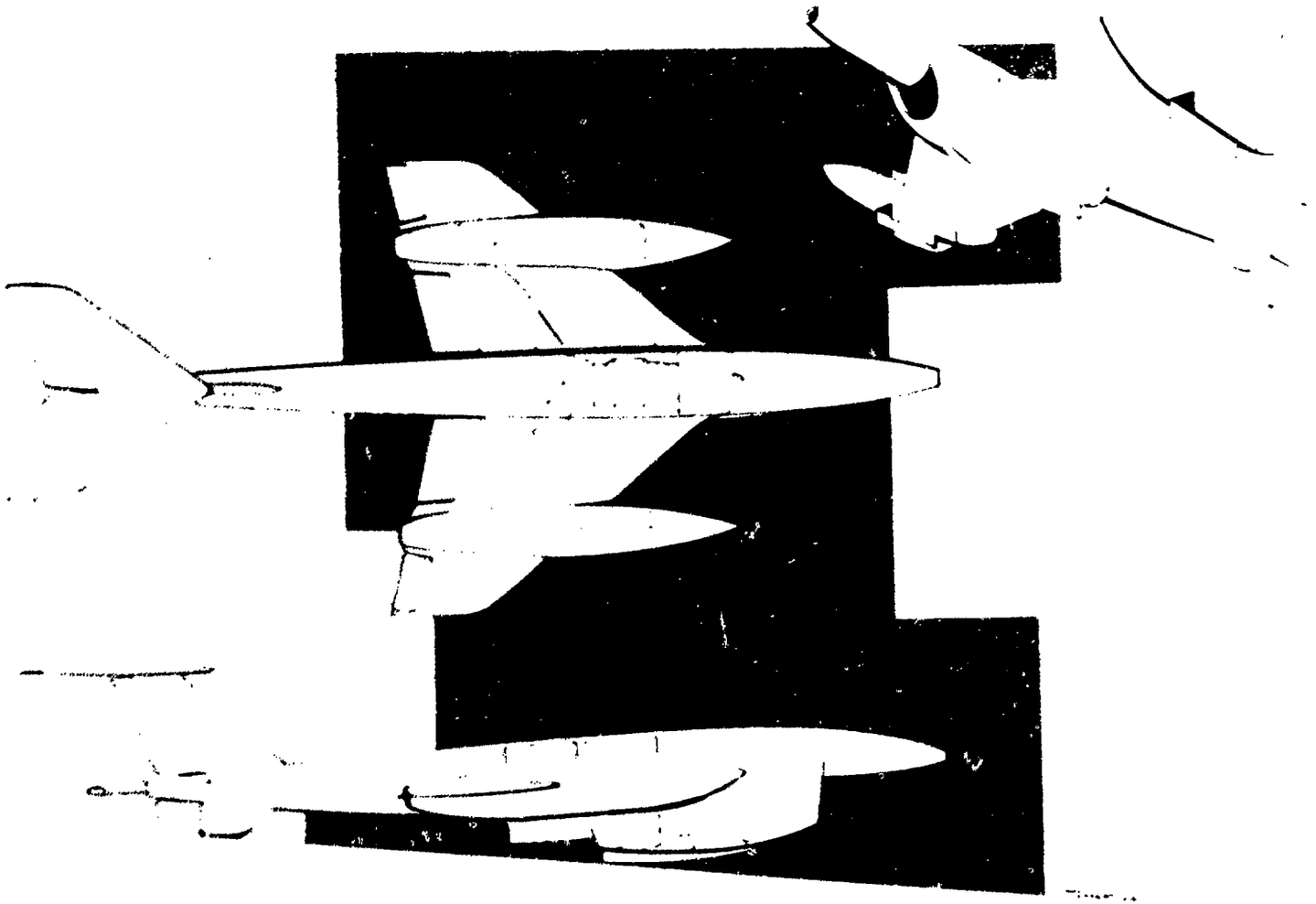

Figure 88. V/STOL RPV cold thrust augmentation concept

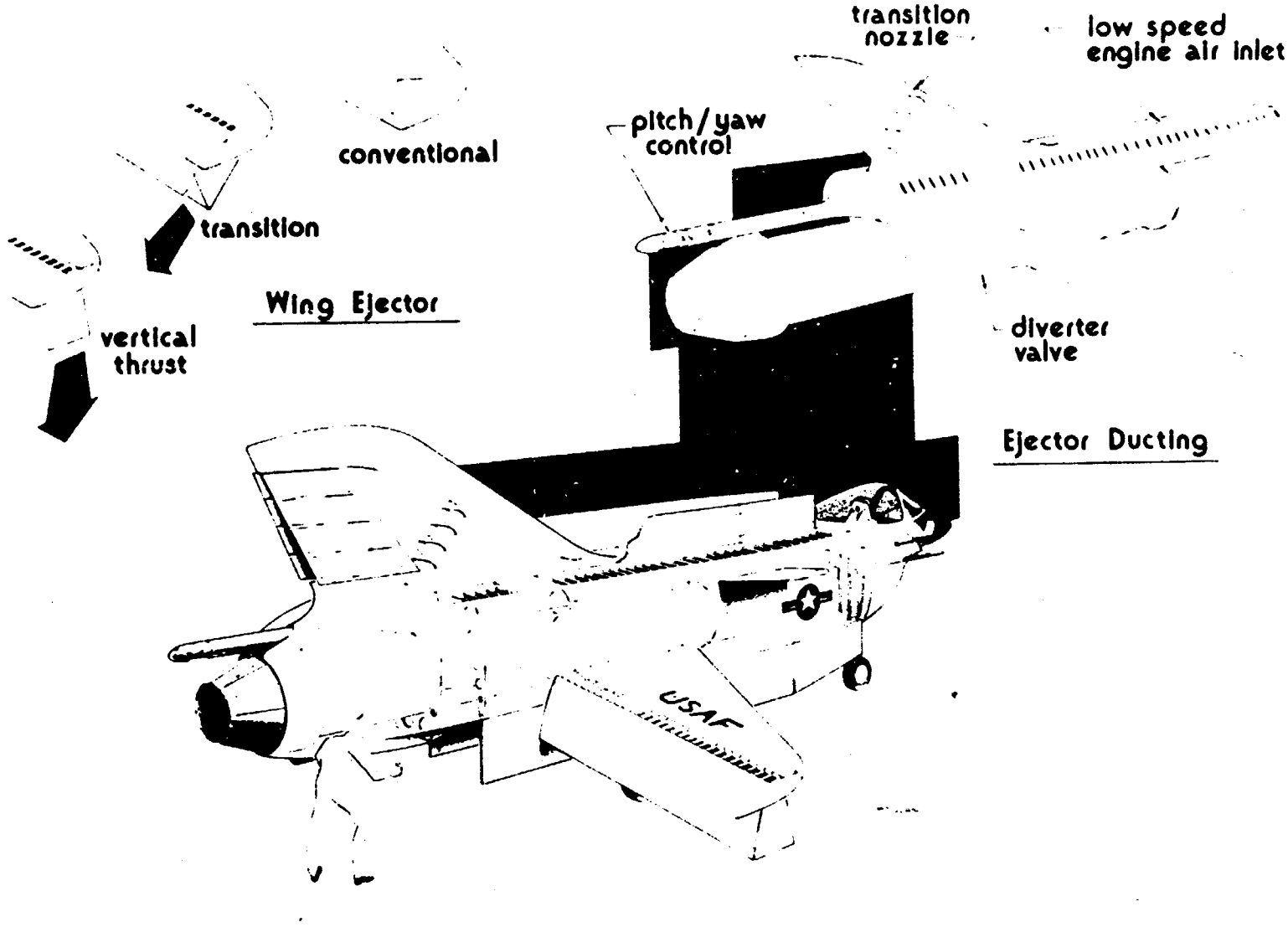

Figure 89. V/STOL Attack Aircraft; USAF Flight Dynamics Lab preliminary design

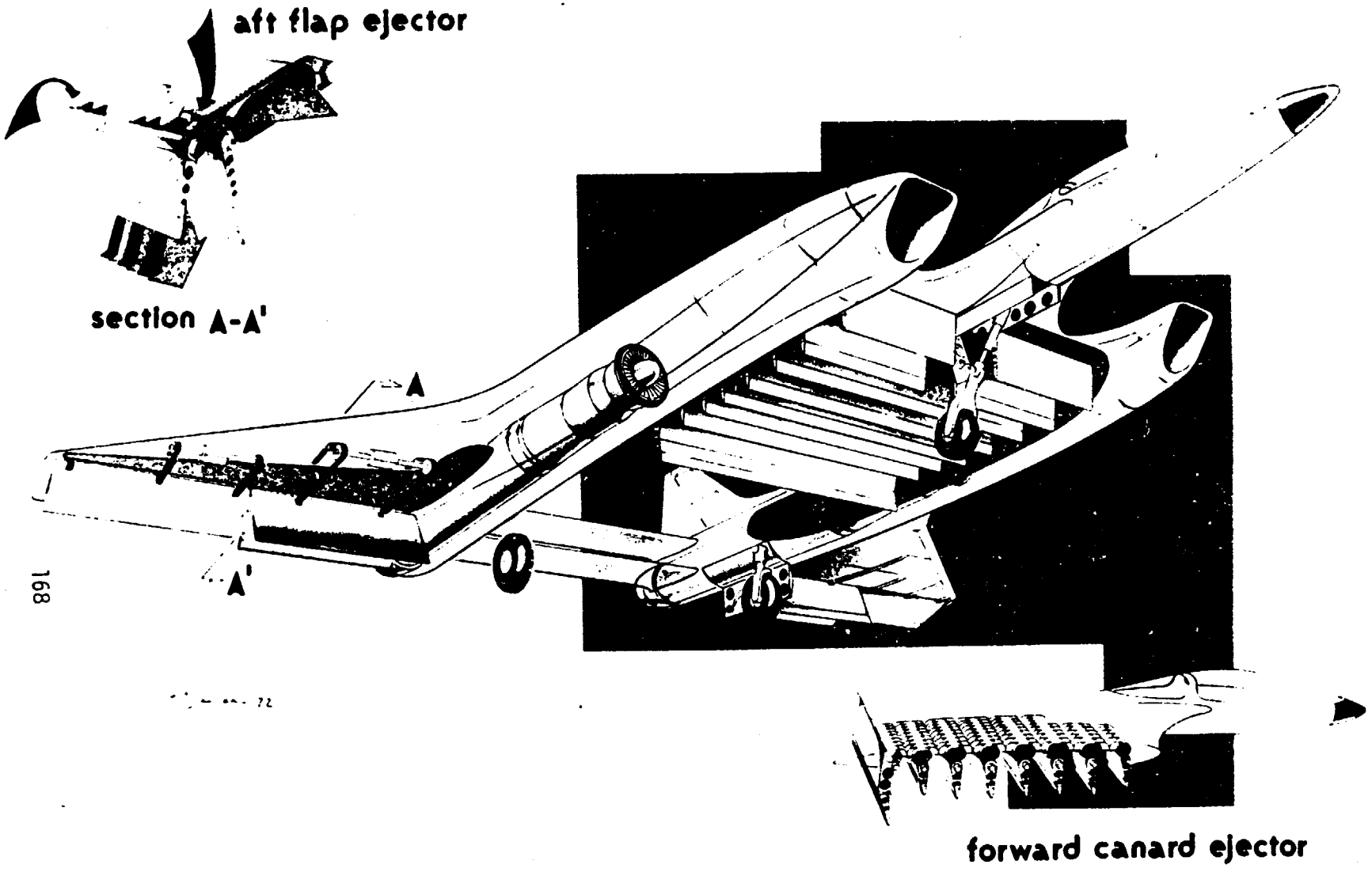

Figure 90. V/STOL Attack Aircraft; USAF Flight Dynamics Lab preliminary design

Dynamics Lab preliminary design

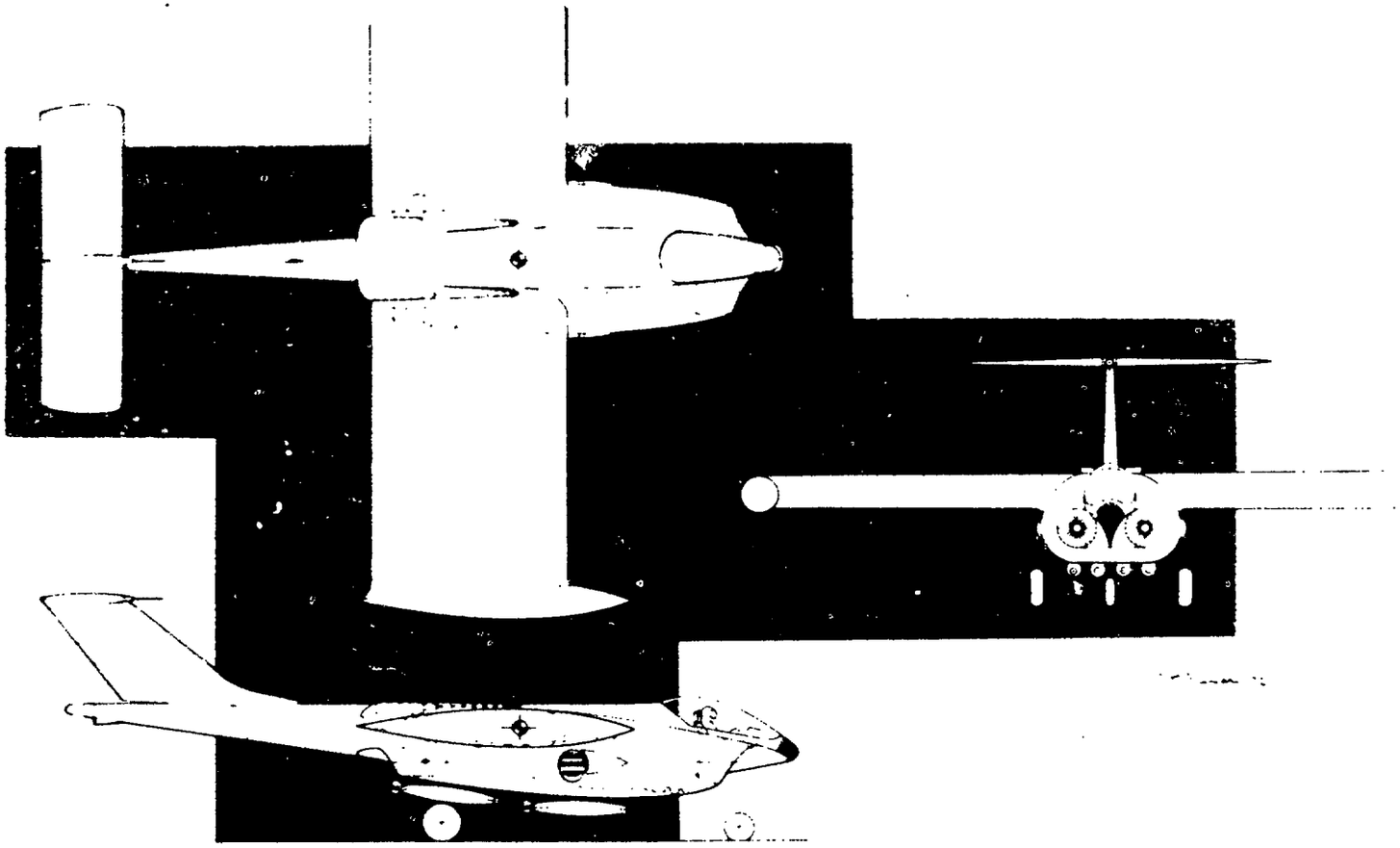

Figure 91. V/STOL Attack Aircraft; USAF Flight Dynamics Lab preliminary design

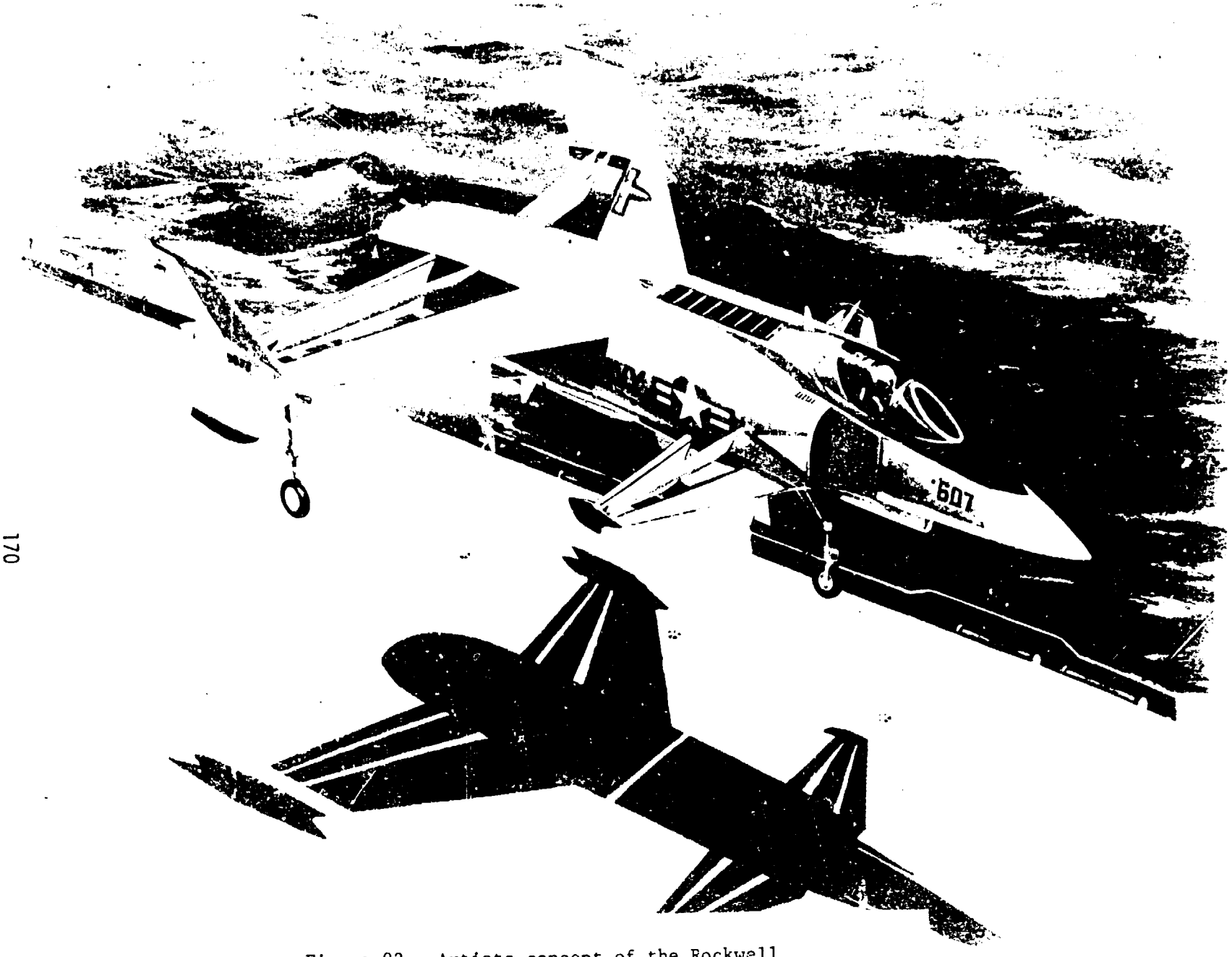

Figure 92. Artists concept of the Rockwell International XFV-12A

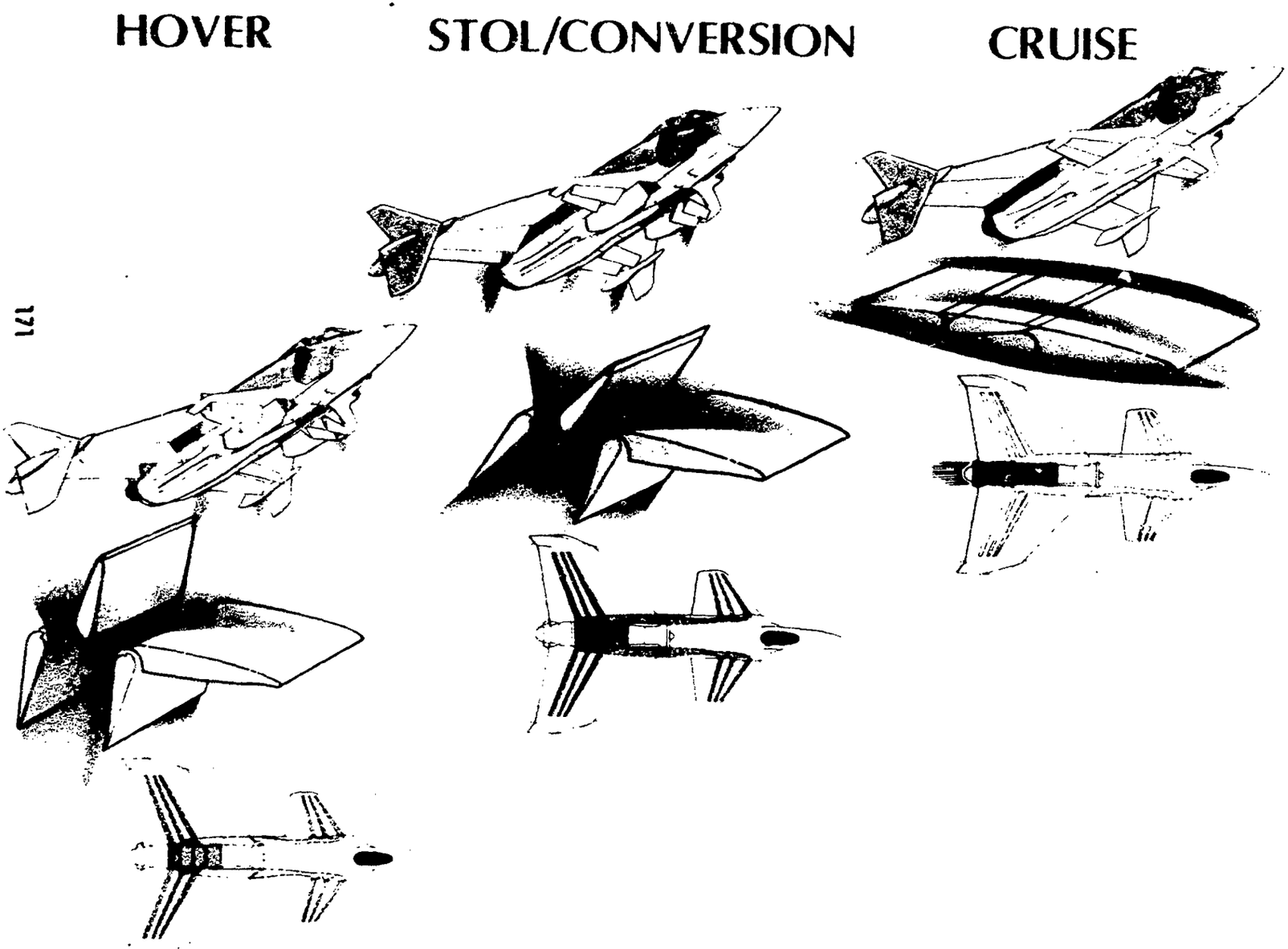

Figure 93. Typical VTOL flight sequence for the XFV-12A

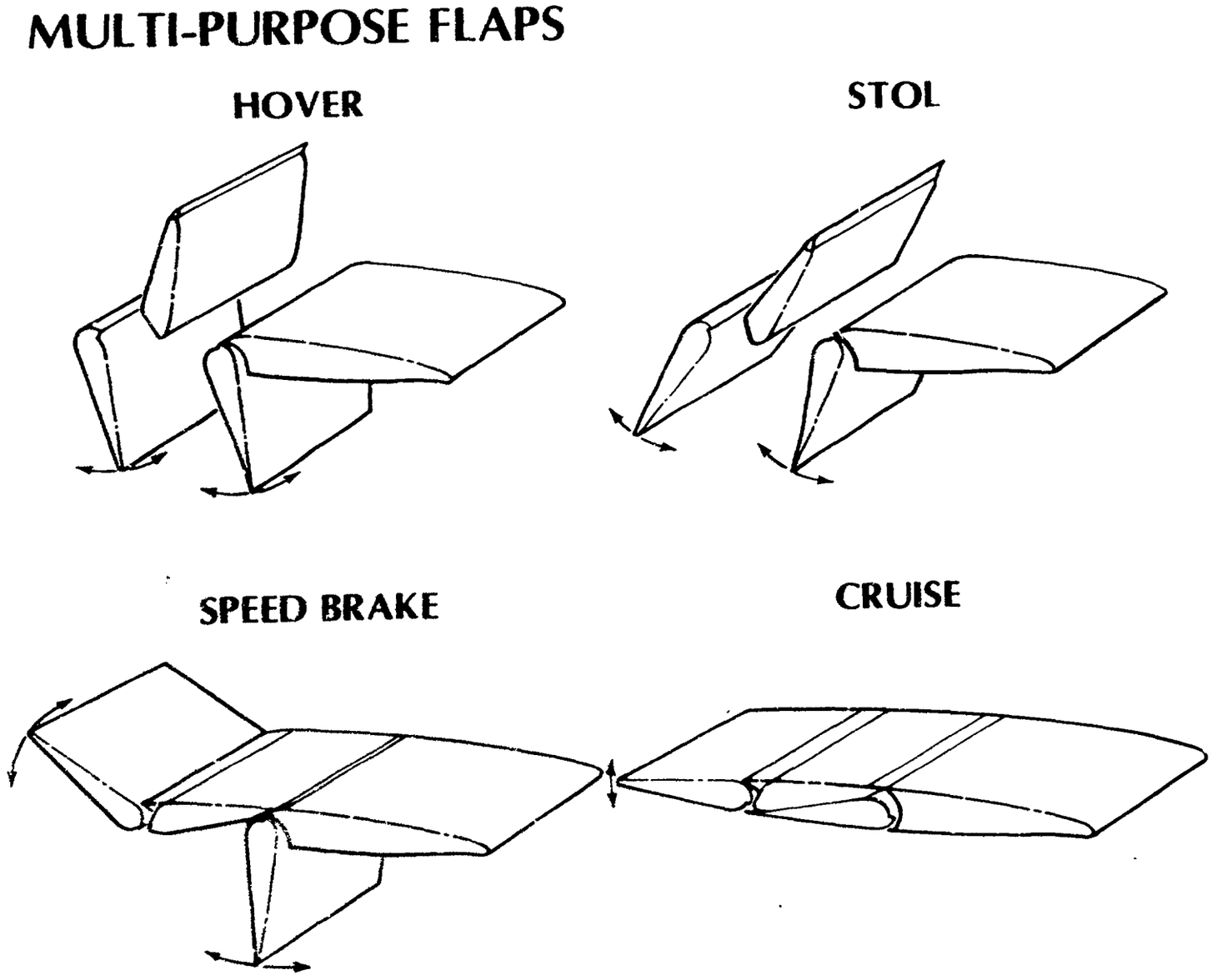

Figure 94. Multi-purpose flaps on the XFV-12A

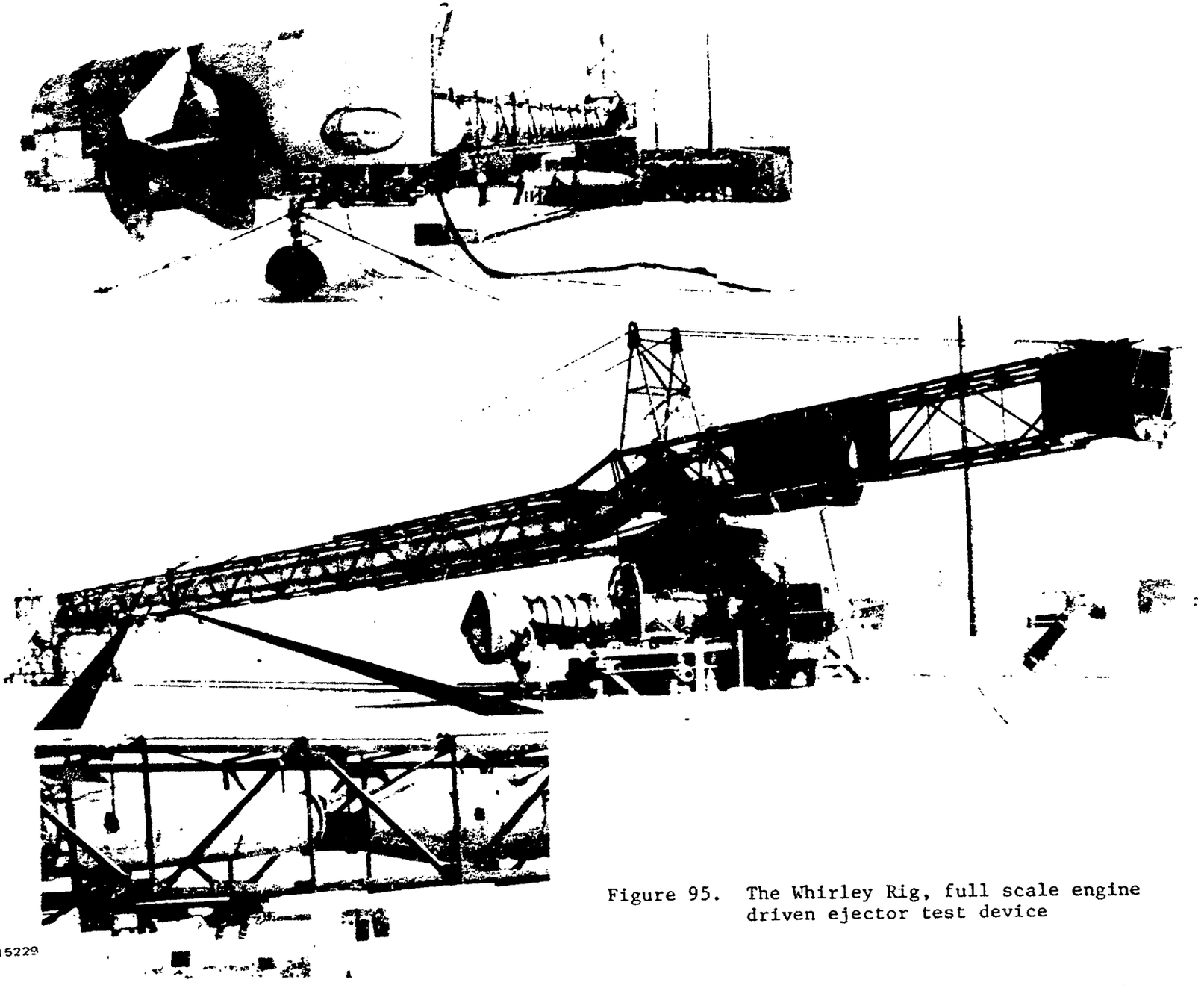

GR 15229

Figure 95. The Whirley Rig, full scale engine driven ejector test device

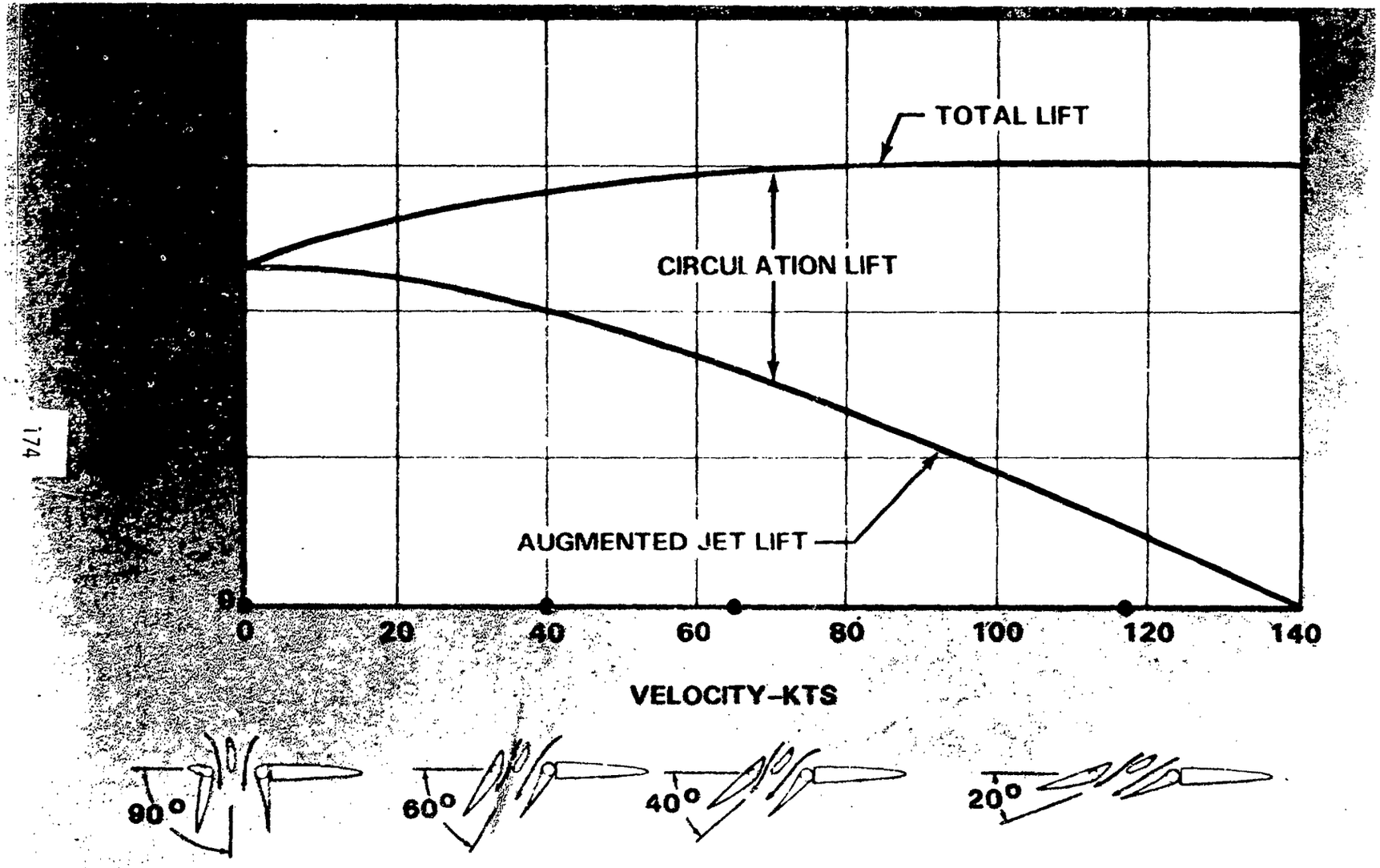

Figure 96. Lift variation with forward speed - supercirculation

REFERENCES

1. Quinn, B., "Compact Thrust Augmentors for V/STOL Aircraft", AGARD Conference Pre-print No. 135 on V/STOL Propulsion Systems, 1973.

2. Fancher, R. B., "Why Ejectors for Aircraft Propulsion-Lift Systems and Where We Stand", Aerospace Research Labs Report TR 71-0140, August 1971.

3. Quinn, B., "Compact Ejector Thrust Augmentation", J. Aircraft, Vol 10, No. 8, August 1973, pp. 481-486.

4. Quinn, B., "Recent Developments in Large Area Ration Thrust Augmentors", AIAA Paper 72-1174, New Orleans, La., 1972.

5. von Karman, T., "Theoretical Remarks on Thrust Augmentation", Reissner Anniversary Volume Contributions to Applied Mechanics, J. W. Edwards, Ann Arbor, Michigan, 1949.

6. Campbell, W. S. and von Ohain, H. J. P., "Thrust Augmentation for V/STOL", Aerospace Research Laboratories Report 67-0065, April 1967.

7. Thornhill, W. J., "A Wind Tunnel Study of Force Generated by an Ejector in a Free Stream", M. S. Thesis, Air Force Institute of Technology, 1969.

8. O'Keefe, J. V. and Kelly, G. S., "Design Integration and Noise Studies for Jet STOL Aircraft", Vol. 1, Final Report NASA CR-114283, May 1972.

9. Harris, G. L., "Steady State Ejector Thrust Augmentation", VKI Ejector Short Course, 22-26 April, 1968.

10. Scott, W. J., "Experimental Thrust Augmentation of a Variable Geometry, Two Dimensional Coanda Wall Jet Ejector", National Research Council of Canada, Aero Rept LR-394 (NRC No. 7898), January 1964.

11. Throndson, L. W., "Compound Ejector Thrust Augmentor Development", ASME Paper 73-GT-67.

12. Haight, C. H. and O'Donnell, R. M., "Experimental Mating of Trapped Vortex Diffusers with Large Area Ratio Thrust Augmentors", Aerospace Research Laboratories Report TR 74-0115, September 1974.

13. Alperin, M., "A Coanda Inlet/Jet Flap Diffuser Ejector", AF Flight Dynamics Lab Report TR-72-106, August 1972.

14. Morrison, R., "Jet Ejectors and Augmentation", NACA CR 6428, September 1942.

15. Nagaraja, K. S., Hammond, D. L. and Graetch, J. E., "One Dimensional Compressible Ejector Flows", AIAA Paper 73-1184, 1973.

16. Binder, G. and Favre-Marinet, M., "Mixing Improvement in Pulsating Turbulent Jets", Symposium on Fluid Mechanics of Mixing, ASME, 1973.

17. Foa, J. V., "A Method of Energy Exchange", Amer. Rocket Soc. J., Vol. 32, No. 9, 1962, pp 1396-8.

18. Viets, H., "Oscillating Jet Nozzles for V/STOL Application", AIAA Paper No. 74-1189, October 1974 (to appear in AIAA Journal).

19. Quinn, B. and Toms, H. L. Jr., "Experimental Evaluation of the Performance of a High Temperature, High Pressure Mass Augmentor", to be published.

20. Rosfjord, T. and Toms, H. L. Jr., "Recent Observations Including Temperature Dependence on Axisymmetric Jet Screech", to be published.

21. Bevilaqua, P. M. and Toms, H. L. Jr., "A Comparison Test of the Hypermixing Nozzle", Aerospace Research Laboratories Report TR 74-0006, January 1974.

22. Bevilaqua, P. M., "An Analytic Description of Hypermixing and Test of an Improved Nozzle", AIAA Paper No. 74-1190, October 1974.

23. Fancher, R. B., "Low Area Ratio, Thrust-Augmenting Ejectors", J. Aircraft, Vol. 9, No. 3, 1972, pp 243-248 (see also AIAA Paper 71-576, June 1971).

24. Bevilaqua, P. M., "Evaluation of Hypermixing for Thrust Augmenting Ejectors", J. Aircraft, Vol. 11, No. 6, 1974, pp 348-354.

25. Quinn, B., "A Simple Estimate of the Effect of Ejector Length on Thrust Augmentation", J. Aircraft, Vol. 10, No. 5, May 1973, pp. 313-314.

26. Fejer, A. A.; Torda, T. P.; Boehman, L. I.; Gia, K. N. and Hermann, W. G., "Research on Mixing of Coaxial Streams", Aerospace Research Laboratories Report ARL 67-0058, March 1967.

27. Fejer, A.; Lavan, Z. and Wolf, L. Jr., "Study of Swirling Fluid Flows". Aerospace Research Laboratories Report ARL 68-0173, October 1968.

28. Fejer, A. A.; Hermann, W. G. and Torda, T. P., "Factors that Enhance Jet Mixing", Aerospace Research Laboratories Report ARL 69-0175, October 1969.

29. Corrsin, S. and Uberoi, M. S., "Further Experiments on the Flow and Heat Transfer in a Heated Turbulent Jet", NACA Report 998, 1950.

30. Szablewski, W., "The Diffusion of a Hot Air Jet in Air in Motion", NACA TM 1288, December 1950.

31. Hinze, J. O. and Van der Hegge Zijnen, B. G., "Transfer of Heat and Matter in the Turbulent Mixing Zone of an Axially Symmetrical Jet", Appl Sci Res, A-1, 1949, p435.

32. Pabst, O., "Die Ausbreitung heisser gasstrahlen in bewegter Luft", Luftahrt Tech, Vol 6, 1960, p. 271.

33. Landis, F. and Shapiro, A. H., "The Turbulent Mixing of Co-axial Gas Jets" Proc. Heat Trans and Fluid Mech Inst, 1951, p 133.

34. Forstall, W. Jr. and Shapiro, A. H., "Momentum and Mass Transfer in Coaxial Gas Jets", J. Appl Mech, Vol 17, No. 4, 1950, pp 399-408.

35. Rose, W. G., "A Swirling Round Turbulent Jet", J. Appl Mech Vol. 29, No. 4, December 1962, pp 615-625.

36. Hill, W. and Jenkins, R.; Grumman Aircraft Corporation Report under contract to the Aerospace Research Labs (to be issued).

37. Sforza, P. M.; Steiger, M. H. and Trentacoste, N., "Studies on Three-Dimensional Viscous Jets", AIAA J., Vol 4, No. 5, May 1966, p. 800.

38. Trentacoste, N. and Sforza, P., "Further Experimental Results for Three-Dimensional Free Jets", AIAA J., Vol. 5, No. 5, May 1967, p 885.

39. Trentacoste, N. and Sforza, P., "Some Remarks on 3-D Wakes and Jets", AIAA J., Vol. 6, No. 12, December 1968.

40. Quinn, B., "Experiments with Hypermixing Nozzles in an Area Ratio 23 Ejector", Aerospace Research Laboratories Report ARL 72-0084, June 1972.

41. Viets, H., "The Three-Dimensional Laminar Elliptical Jet in a Coflowing Stream", Aerospace Research Laboratories Report ARL 72-0052.

42. Foss, J. F. and Jones, J. B., "Secondary Flow Effects in a Bounded Rectangular Jet", J. Basic Eng, Vol. 90, No. 2, June 1968, p 241.

43. Eastlake, C. N. II, "Velocity Measurements in Partially Confined Rectangular Jets", Aerospace Research Laboratories Report ARL 72-121, September 1972.

44. Van der Hegge Zijnen, B. G., "Measurements of the Velocity Distribution in a Plane Turbulent Jet of Air", Appl Sci Res, Sec A, Vol. 7, 1957-58.

45. Viets, H. and Sforza, P. M., "Dynamics of Bilaterally Symmetric Vortex Rings", Phys Fluids, Vol. 15, No. 2, February 1972, pp 230-240.

46. Eastlake, C. N. II, "The Macroscopic Characteristics of Some Subsonic Nozzles and the Three-Dimensional Turbulent Jets They Produce", Aerospace Research Laboratories Report ARL 71-0058, March 1971.

47. Bevilaqua, P. M., and Lykoudis, P. S., "Entrainment and the Large Eddy Structure", AIAA Paper No. 75-115, 1975.

48. Papailou, D. D. and Lykoudis, P. S., "Turbulent Vortex Streets and the Entrainment Mechanism of the Turbulent Wake", J. F. M., Vol. 62, 1974, pp 11-31.

49. Brown, G. L., and Roshko, A., "Effect of Density Difference on the Turbulent Mixing Layer", AGARD Conference Proc No. 93 on Turbulent Shear Flows, 1971.

50. Lau, J. C., Fisher, M. J., and Fuchs, H. V., "The Intrinsic Structure of Turbulent Jets", J. Sound Vib, Vol. 22, 1972, pp 329-406.

51. Bevilaqua, P. M., to be published.

52. Harsha, P. T., "Free Turbulent Mixing - A Critical Evaluation of Theory and Experiment", Arnold Engineering Development Center, Arnold AF Station, Tenn., TR 71-36, February 1971.

53. Prandtl, L., "Bemerkungen zur Theorie der Freien Turbulenz", ZAMM, Vol. 22, October 1942, pp 241-243.

54. Ferri, A., Libby, P. A., Zakkay, V., "Theoretical and Experimental Investigations of Supersonic Combustion", PIBAL 713, September 1962, Polytechnic Institute of Brooklyn, Farmingdale, NY.

55. Viets, H., "Prandtl Eddy Viscosity Model for Coaxial Jets", AIAA J., Vol. 10, No. 12, December 1972, pp 1684-1685.

56. Maczynski, J. F. J., "A Round Jet in an Ambient Coaxial Stream", J.F.M., Vol 13, 1962, p 597.

57. Boyle, R. E. Jr. and Viets, H., "Eddy Viscosity for Variable Density Coflowing Streams", J. Aircraft, Vol. 11, No. 12, December 1974, pp 721-22.

58. Ricou, F. P. and Spalding, D. B., "Measurements of Entrainment by Axisymmetrical Turbulent Jets", J. F. M., Vol. 11, p 21, 1961.

59. Gal, G., "Self Preservation in Fully Expanded Turbulent Coflowing Jets", AIAA J., Vol. 8, No. 4, 1970, p 814.

60. Landis, F. and Shapiro, A. H., "The Turbulent Mixing of Co-axial Gas Jets", Proc. Heat Trans, and Fluid Mech, Inst., 1951, p 133.

61. Prandtl, L., "A Steady Air Stream in Wind Tunnels", NACA TM 726, reprint from Handbuch der Experimentalphysik, Vol. IV, Part 2, pp 65-106.

62. Viets, H., "Directional Effects in 3-D Diffusers", Proc. of the 2nd Int. Symp. on Airbreathing Engines, Sheffield, England, March 1974.

63. Pai, S. I. and Hsieh, T. Y., "Linearized Theory of Three-Dimensional Jet Mixing with and Without Walls", J. Basic Eng., Vol. 92, No. 1, March 1970, pp 3-100.

64. Quinn, B. "The Decay of Highly Skewed Flows in Ducts", J. Eng. Power, Vol. 77, No. 1, January 1975, p 85.

65. Keffer, J. F., "The Uniform Distortion of a Turbulent Wake", J. Fluid Mech, Vol. 22, 1965, pp 135-159.

66. Keffer, J. F., "A Note on the Expansion of Turbulent Wakes", J. Fluid Mech., Vol. 28, 1967, pp 183-193.

67. Viets, H. and Quinn, B., "Concurrent Mixing and Diffusion in Three-Dimensions", AIAA Paper No. 75-873, June 1975.

68. Fishenden, C. R. and Stevens, S. J., "The Performance of Annular Combustor-Dump Diffusers", AIAA Paper No. 74-1097, Oct 1974.

69. Lin, C. C., "Motion in the Boundary Layer with a Rapidly Oscillating External Flow", Proc. Ninth Int. Cong. App. Mech. Vol. 4, Elsevier Publ Co., Inc., Amsterdam, 1957, p 155.

70. Lighthill, M. J., "Response of Laminar Skin Friction and Heat Transfer to Fluctuations in Free Stream Velocity", Proc. Roy. Soc., Vol. 224, 1954, pp 1-23.

71. McCormack, P. D.; Cochran, D. and Crane, L., "Periodic Vorticity and its Effect on Jet Mixing", Phys. Fluids, Vol. 9, No. 8, August 1966, pp 1555-60.

72. Johnson, W. S. and Yang, T., "A Mathematical Model for the Prediction of the Induced Flow in a Pulsejet Ejector with Experimental Verification", ASME Paper WA/FE-33, 1968.

73. Lockwood, R. M. "Investigation of the Process of Energy Transfer from an Intermittent Jet to a Secondary Fluid in an Ejector-Type Thrust Augmenter", Hiller Aircraft Corp Report No. APR-64-4, March 1964.

74. Foa, J. V., "A Vaneless Turbopump", AIAA Journal, Vol. 1, No. 2, February 1963, pp 466-7.

75. Foa, J. V., "A Pressure Exchanger for Marine Propulsion", SAE Transactions, Vol. 79, 1970, pp 346-52.

76. Hohenemser, K. H., "Flow Induction by Rotary Je..", J. Aircraft, Vol. 3, No. 1, 1966, pp 18-24.

77. Hohenemser, K. H., and Porter, J. L., "Contribution to the Theory of Rotary Jet Flow Induction", J. Aircraft, Vol. 3, No. 4, 1966, pp 339-46.

78. Maise, G. and Dunn, G., "Jet Temperature Effects on Performance of Rotary-Flow Augmentors", Grumman Aerospace Corp Report PXP-001-33, February 1974.

79. Maise, G., "Effects of Shroud Design on the Performance of Rotary-Flow Augmentors" Grumman Aerospace Corp, Report PXP-001-38, June 1974.

80. Curtet, R. M. and Girard, J. P., "Visualization of a Pulsating Jet", Symposium on Fluid Mechanics of Mixing, ASME, 1973.

81. Williams, J. R., Ambrosiani, J. P. and Palmer, W. E., "Analysis of a Pulsating Wall Jet", Columbus Aircraft Div/Rockwell Int. Report No. NR72H-325, October 1972.

82. Hill, W. C. Jr. and Greena, P. R., "Self Existed Superturbulence: The Whistler Nozzle", Grumman Aircraft Corp Research Dept Report RE-488, October 1974.

83. Brown, G. B., "On Vortex Motion in Gaseous Jets and the Origin of Their Sensitivity to Sound, Proc. Phys Soc. Vol. 47, 1935, pp 703-732.

84. Johansen, F.C., "Flow Through Pipe Orifices at Low Reynolds Numbers", Proc. Roy. Soc., Series A., Vol. 126, 1929, pp. 231-245.

85. Becker, H.A. and Massaro, T.A., "Vortex Evolution in a Round Jet", JFM, Vol. 31, 1968, pp. 435-448.

86. Roffman, G.L. and Toda, K., "A Discussion of the Effects of Sound on Jets and Flueric Devices", ASME Paper No. 69-Vibr-3.

87. Vlasoc, Y.V. and Ginevskiy, A.S., "Acoustic Effect on Aerodynamic Characteristics of a Turbulent Jet", USAF Systems Command Foreign Technology Division, FTD-MT-24-232-68.

88. Abstracts from the Colloquium on Coherent Structures in Turbulence, 25th-29th March, 1974, University of South Hampton, England, including:

a. Birch, S.F., "A Vortex Model for Unsteady Free Shear Flows".

b. Browand, F.K. and Weidman, P.D., "Large Scale Structure in the Turbulent Mixing Layer".

c. Curtet, R.M. and Patural, R., "Visualization of Flapping Jets".

d. Grant, A.J., "The Time Dependent Structure of Turbulent Jet Flows".

e. Lilley, G.M., "A Mathematical Model of the Large Scale Structure of Turbulent Shear Flows".

89. Simcox, C.D., and Hoglund, R.F., "Acoustic Interactions with Turbulent Jets", ASME J. Basic Eng., Vol. 93, No. 1, March 1971, pp. 42-46.

90. Crow, S.C. and Champagne, F.H., "Orderly Structure in Jet Turbulence", J.F.M., Vol. 48, Part 3, 1971, pp. 547-591.

91. Viets, H., "Development of a Time Dependent Nozzle", Aerospace Research Laboratories Report ARL 74-0113, July 1974.

92. Morris, N.M., "An Introduction to Fluid Logic", McGraw-Hill (United Kingdom) Limited, London, 1973.

93. Warren, R.W., "Some Parameters Affecting the Design of Bistable Fluid Amplifiers", Fluid Jet Control Devices, ASME, 1962.

94. Spyropoulos, C.E., " A Sonic Oscillator", Proceedings of the Fluid Amplification Symposium, Harry Diamond Laboratories, Washington, D.C., May 1964.

95. Platzer, M.F., Deal, L.J. and Johnson, W.S., "Experimental Investigations of Oscillatory Jet-Flow Effects", Symposium on Unsteady Aerodymanics, U. of Arizona, March 1975.

96. Powell, A., "On the Noise Emanating from a Two-Dimensional Jet Above Critical Pressure", the Aero Quart, Vol. 4, Feb 1953, pp. 103-122.

97. Powell, A., "On the Mechanism of Choked Jet Noise", Proc. Phys. Soc. Vol. B66, Dec 1953, pp. 1039-1056.

98. Morse, P.M., Vibration and Sound, 2nd Ed., McGraw-Hill, 1948.

99. Merle, M., "Ondes Sonores Emises par un Jet d'air", Acad. Des Sci., Comp. Rend., Vol. 240, May 1955, pp. 2055-2057.

100. Rosfjord, T.J. and Toms, H.L., Jr., "Recent Observations Including Temperature Dependence of Axisymmetric Jet Screech", to be published.

101. Viets, H., Toms, H.L., Jr., and Balster, D., "A Two Phase Unsteady Jet", presented at the 14th Midwestern Mechanics Conference, Norman, Okla., March 1975.

102. Viets, H., Toms, H.L. Jr., and Balster, D., "Time Dependent Fuel Injectors", to be published.

103. Platzer, M.F., Private Communication, Naval Post Graduate School, Monteray, Calif.

104. Campbell, D.R. and Quinn, B., "Test Results of a VTOL Propulsion Concept Utilizing a Turbofan Powered Augmentor", J. Aircraft, Vol. 11, No. 8, 1974, pp. 467-471.

105. Brown, S.L. and Murphy, R.D., "Design and Test of Ejector Thrust Augmentation Configurations", AGARD Conference Proceedings No. 143.

106. Spence, D.A., "The Lift on a Thin Airfoil with a Jet-Augmented Flap", Aero. Quart., Aug 1958, pp. 287-299.

107. Byrnes, J.M., Murphy, R.D., Ball, R.F., Nagavaja, K.S., Hammond, D.L., Langlehen, E.A. and English, R.B., "V/STOL Demonstrator Vehicle for Thrust Augmentation Technology", AIAA Paper No. 74-995, Aug. 1974.

108. Robinson, C.A. Jr., "XFV-12 May Spur Navy VTOL Family", Aviation Week and Space Tech., April 16, 1973.

109. Swavely, C E., "Engine Flow Diverter System for the XFV-12A Prototype Aircraft", AIAA Paper No. 74-1194, Oct. 1974.